Title
The Cascading Effects of Novelty: How adaptation to a novel niche affects behavior, morphology, and genomics

Author
St. John, Michelle Emilie

Publication Date
2022

Peer reviewed|Thesis/dissertation

The Cascading Effects of Novelty: How adaptation to a novel niche affects behavior, morphology, and genomics

By

Michelle E. St. John

A dissertation submitted in partial satisfaction of the

requirements for the degree of

Doctor of Philosophy

in

Integrative Biology

in the

Graduate Division

of the

University of California, Berkeley

Committee in charge:

Professor Christopher H. Martin, Chair
Professor Eileen A. Lacey
Professor Damian O. Elias

Summer 2022

Abstract

The Cascading Effects of Novelty: How adaptation to a novel niche affects behavior, morphology, and genomics

by

Michelle E. St. John

Doctor of Philosophy in Integrative Biology

University of California, Berkeley

Professor Christopher H. Martin, Chair

Evolutionary novelty may be an important driver of diversification, yet theory does not agree on the circumstances or processes that may lead to novelty in the first place. Current theory may be insufficient for explaining observed natural patterns because it does not consider the multivariate nature of novelty and instead makes predictions assuming that evolution occurs along a single axis. Furthermore, it is challenging to measure variation across many biological levels in a single focal organism, and there is consequently a lack of empirical data to inform new hypotheses. Here, I investigate evolutionary novelty within an adaptive radiation of Cyprinodon pupfish endemic to San Salvador Island, Bahamas. This radiation contains two fantastic examples of novelty in in the snail-eating (*C. brontotheroides*) and scale-eating pupfish (*C. desquamator*), and contains a third generalist pupfish (C. *variegatus*) similar to outgroup populations.

In chapter one I investigate if shifts in behavior are associated with novelty in pupfish. I specifically test the aggression hypothesis, which suggests that scale-eating arose due to the incidental ingestion of scales during aggressive interactions and predicts that scale-eating pupfish should have the highest levels of aggression compared to all other species. I empirically tested this prediction and found that both scale- and snail-eating pupfish are more behaviorally aggressive than algae-eating or outgroup species and show differential expression in the same aggression related pathways compared to the generalist pupfish species. These results suggest that behavioral shifts are indeed associated with the evolution of novelty and may be adaptive for dietary specialization.

In chapters two and three I investigate the contributions of morphological and behavioral adaptations to scale- and snail-feeding performance. I developed a new method for measuring bite size (a proxy for scale-feeding performance) across pupfish species and found that scale-eating pupfish have a unique, behaviorally mediated, kinematic profile adaptive for taking large bites. The kinematic profiles of F1 scale-eating hybrids from this study were dissimilar to those of purebred scale-eaters—even for traits that are behaviorally mediated—suggesting that shifts in morphology and behavior are likely necessary for high performance in this niche. I also measured snail-eating performance between pupfish species, to determine if the novel nasal protrusion (morphology) of the

snail-eating pupfish is adaptive for snail consumption. I found that snail-eaters, snail-eating hybrids, and generalist pupfish all exhibit similar levels of performance and observed no relationship between nasal protrusion size and performance. These chapters suggest that shifts along a single axis (e.g., behavior) may be sufficient to produce some instances of novelty, but that others may require shifts along several axes in order to be successful.

In chapter four I investigated the genetic underpinnings of adaptive behavioral and morphological traits for both snail- and scale-feeding, with the goal of identifying if unique genomic regions, alleles, or SNPs were associated with each instance of novelty. I investigated the genetic basis of 31 adaptive traits for scale- and snail-feeding using a QTL mapping approach in two pupfish populations. I found that the similar genomic regions were associated with craniofacial traits, but that many of these shared regions affected different, but highly correlated traits. I also found evidence of increased levels of adaptive introgression within shared QTL regions, suggesting that: 1) there is a surprising amount of genetic flexibility when adapting to a novel niche, and 2) introgression may be important for this transition.

Ultimately, this dissertation research provides a new framework for studying the multivariate nature of novelty. By quantifying variation across behavioral, morphological, and genomic axes I documented that scale-feeding may require shifts along multiple axes while snail-feeding may only require behavioral shifts. This is one of the first studies to empirically document variation across multiple biological levels in the context of novelty and the patterns described above further emphasizes that hypotheses considering shifts along only a single axis are not sufficient for fully understanding evolutionary novelty.

Table of Contents

Dedication

I did it for the devilment.

Acknowledgements

The first person I would like to acknowledge is myself. I start with this because I don't think we give ourselves enough credit for the hard work we do when pursuing research and graduate school. To that end, this is my public declaration that I am very proud of my research and accomplishments, and I am also proud of everyone pursuing their own endeavors.

Next, I'd like to acknowledge the support, care, and love that I have received from my family, leading up to and during the process of getting a Ph.D. Each of my family members including my grandparents, parents, brother and in-laws have provided me with emotional support during this process. Having a family that you know you can fall back on made this process significantly less scary. I must also offer a specific thank you to my family for letting me talk about fish for so many years – I don't anticipate a slowdown on that topic in the near future, but I appreciate it nonetheless.

I'd like to acknowledge all my furry family members including Tulip, Alfalfa, Tomatillo and Mamie. I know you will never read this, but many biologists get their first experience with appreciating animals from their family pets, and I am no exception to that. Thank you for being a continued source of joy and love in my life.

Thank you to my husband Matthew Kmet. Thank you for moving not just once for my Ph.D. but twice! Thank you for helping me with fish care, field work, and proofreading. Thank you for listening to my many practices talks and presentations over the years and thank you for all the other tangible forms of support you've provided. While I am eternally grateful for all these helpful acts, the thing I am most thankful for is that I never felt that I was doing this Ph.D. alone. This process was quite scary for me but knowing that you would always be with me made me feel like I could handle it. Thank you for making me a braver and stronger person, and I can't wait for us to continue this journey together.

I'd like to express my gratitude for the research experiences I had before pursuing my Ph.D. Specifically, I'd like to thank everyone who was present and supportive during my master's degree:

To my master's advisor, Becky Fuller—Thank you for teaching me about fish, to code in R, and most importantly thank you for making me feel like I could be a successful scientist. I don't think I'd be pursuing academia and research as a career if it were not for you.

To Liza Mitchem and Rachel Moran— Thank you both for being exceptional labmates and friends. You showed me how collaborative and supportive the scientific community can be, and I am a better scientist having developed alongside each of you.

Finally, to the UIUC IB community including Sam Primer, Laura Stein, Erin Welsh, Erin Allman-Updyke Sara Johnson, Miles Bensky, and Rhiannon Peery—The community that you all provided sincerely shaped who I am as a person and scientist, and I appreciate your continued support.

When I started my Ph.D., the lab was located at the University of North Carolina-Chapel Hill, and I'd like to acknowledge the support and acceptance that the UNC community afforded me at the beginning of my career. I'd like to thank my friends and members of my cohort including Kate Gould, Kemal Ozalp, Meggan Alston, Catherine Chen, Kayla Goforth, and Aimee Deconinck. You are all amazing scientists and friends, and I am thankful that I got to start my Ph.D. journey with you.

Thank you to the Integrative Biology and the Museum of Vertebrate Zoology communities at the University of California—Berkeley for showing warmth and welcome when I showed up halfway through my Ph.D. Starting over in a new research community was daunting, and the inclusion and acceptance over the past several years has been integral to my success as a scientist and as a person. In particular, I'd like to thank Sylvia Durkin, Jackie Galvez, and Daisy Horr. Thank you for including me in the new graduate student community when I first arrived and for your continued support and friendship. Thank you to Mallory Ballinger and Molly Womack for including me in the *established* graduate student community and for providing me with a new space to develop scientifically and personally. I am so grateful that the life twist of moving mid-Ph.D. resulted in lifelong friends.

I'd like to extend my gratitude and thanks to the past and present members of the Animal Behavior Group at UCB. This has been my favorite working group and class that I've participated in here at Berkeley. Your feedback has made my science better, and your kindness and humanity has made me a better person.

Thank you to Eileen Lacey and Damian Elias who are not only members of my committee but are also the faculty leaders of Animal Behavior Group. I attribute the community's supportive, kind, and insightful nature to your outstanding leadership and example. You have not only fostered a great community but have also both provided me with valuable feedback and recommendations regarding my academic work and progress and I am extremely thankful to have had you on my committee.

To my current and past labmates including Joe McGirr, Joe Heras, Austin Patton, Feña Palominos and David Tian. Thank you for being there with me. Having caring, knowledgeable, and fun labmates has made this experience infinitely better. I have learned so much from each of you and am excited work with you all in the future.

I'd specifically like to acknowledge all the undergraduate researchers that I have worked with over the years. Especially Kristi Dixon Yow and Julia Dunker. I am truly a better scientist and mentor having worked with you.

I'd like to acknowledge and thank my advisor, Chris Martin. Thank you for deciding to do research on the pupfish— I really enjoy this system and am grateful to have had the opportunity to work with them. Thank you for accepting me into your lab. I'm not sure if you saw it as a risky move but having someone give you the opportunity to pursue research is a big deal—thank you for giving me a shot. Thank you for taking me with to Berkeley and for financially supporting me. Lastly, thank you for helping me become an independent, inventive scientist and an overall expansive thinker. The lab environment that you've created is truly integrative, and I appreciate how much knowledge I've gained by simply being a member. I look forward to working with you in the future and am excited to see what new things we learn about pupfishes!

Finally, I'd like to acknowledge my best friend and lab mate—Emilie Richards.
It is extremely difficult to express how large of an impact you have made on me as a scientist and as a friend. One of the primary reasons I decided to join this lab was because you hosted me during interview weekend. You were (and still are) such a kind, funny, and personable human that it gave me confidence in the fact that I would have a least one friend when I started graduate school. Your presence in my life throughout graduate school has enriched my growth as a scientist in more ways than I can describe here.

For anyone reading through this dissertation in its entirety, you can trace how Emilie's enthusiasm for genomics and variation has seeped into my own research questions and helped me form many lines of inquiry that I am excited about to this day. Having a friend who is equally as excited and inquisitive about the same research topics as yourself is truly transformative as you're forming research ideas and carrying out experiments.

Brainstorming sessions, discussions, and research with you is one of the largest and most important influences I've had during this Ph.D. You are one of the kindest, most empathetic, and understanding people that I have ever known and having you alongside me during this whole process was frankly probably one of the only reasons I made it through.

Thank you for being a great scientist and greater friend.

Dissertation Introduction

Novel traits and innovations are thought to be drivers of diversification; however, we lack a clear understanding of the processes that lead to the ecological and evolutionary success and persistence of these traits. One idea is that ecological opportunity plays a significant role in determining the success of novelty—suggesting that available niche space may be a primary constraint (Simpson 1953; Mayr 1960). This connection between resource use, diversification, and novelty is supported by the many examples of adaptive radiations including the Galapagos finches, Caribbean Anolis, and the East African Cichlids (Grant and Grant 2002; Seehausen 2006; Harmon et al. 2010). Yet the appearance of novel traits in the fossil record often precede new ecological opportunities highlighting that evolutionary novelty can persist without a specific ecological niche (Strömberg 2005; Labandeira 2007; Erwin et al. 2011).

Other frameworks suggest that novelty and innovation are limited by genetic or developmental processes (Erwin 2015, 2019, 2021), especially if changes across multiple genes or developmental pathways are necessary to produce a novel phenotype. This build-up of genetic or developmental changes leading up to novelty, is often referred to as the process of potentiation. Currently, our ability to detect potentiation is greatly limited by 1) our ability to detect accumulating variation and 2) to functionally connect each variant to the novel phenotype of interest. This limitation means that we have mostly observed potentiation in simple model organisms, subjected to the uniform environment of the laboratory (Lenski and Travisano 1994; Stern 2011; Sebé-Pedrós et al. 2018), and we still lack critical information about how populations accumulate the necessary variation (i.e., do changes accumulate primarily via mutation, or can gene flow or gene transfer introduce this variation?) or a full understanding of the fitness effects of intermediate types as the necessary variation accumulates.

Still others argue that novelty is defined by transitions to new adaptive peaks on the fitness landscape using variation that is not present in the ancestral group (Hallgrímsson et al. 2012). This framework argues that novelty is primarily constrained by the formation of new peaks on the landscape that specifically allow selection to move phenotypic means “uphill” (Arnold 1983, 2003). This thought process assumes that for novel phenotypes to evolve several steps must occur: First, it assumes that a new peak must appear on the fitness peak indicating a change in environment. Second, the new fitness peak must be so close to the ancestral peak that there is no valley between the two. This proximity is often referred to as a ridge and implies that the new peak is of the same or greater height as the ancestral peak allowing groups to move between the two without incurring a fitness cost. Finally, this explanation often suggests that the environmental context changes again to increase the distance between the new and ancestral peak, providing an explanation for any observed fitness valleys. Recent empirical studies, however, suggest that there are many additional mechanisms that allow organisms to move between fitness peaks that do not necessitate the elimination of fitness valleys or reduced fitness of the ancestral type (Schluter and Grant 1984; Benkman 2003; Martin and Wainwright 2013b; Patton et al. 2022).

While each of the above hypotheses adds valuable insight to our understanding of novelty, none provide a sufficient explanation for what we observe in nature. One potential reason for this knowledge gap, is that many examples of novelty involve changes across many biological levels. For example, novelties that allow organisms to occupy new ecological niches may involve harmonious changes in behaviors (Bowman and Billeb 1965; Tebbich et al. 2010; Curry and Anderson 2012), morphologies (Ferry-Graham et al. 2001; Ferry-Graham 2002; Hata et al. 2011; Davis et al. 2018), and feeding kinematics (Janovetz 2005a; Patek et al. 2006; Cullen et al. 2013; McGee et al. 2013). Yet, few studies investigate shifts across multiple biological levels in the same species, thus limiting the amount of empirical data available to critically assess current theory on the origins of novelty. In this dissertation, I aim to address this gap by examining novelty across the biological levels of behavior, morphology, and genomics using the San Salvador Island pupfish radiation (*Cyprinodon*).

The pupfish radiation on San Salvador Island is a powerful system for exploring the many biological levels involved in evolutionary novelty. The radiation contains a generalist pupfish species (*C. variegatus*), and two specialist species— the snail-eating pupfish (*C. brontotheroides*) and the scale-eating pupfish (*C. desquamator;* Martin and Wainwright 2013a). The generalist pupfish species is fairly widespread, and populations can be found across the Atlantic coast of North America, throughout the Caribbean, and in areas of Venezuela (TURNER et al. 2008). The specialist species, however, are endemic to the hypersaline lakes of San Salvador Island, Bahamas, where they can be found in sympatry with the generalist pupfish species. Phylogenetic evidence supports that the ancestor of the radiation most likely occupied an ecological niche similar to the generalist pupfish (Martin and Wainwright 2011; Martin and Feinstein 2014; Martin 2016), indicating that both specialists in this radiation have adapted to novel ecological niches. Geological evidence further suggests that the hypersaline lakes on San Salvador Island were dry during the last glacial maximum indicating that this unique radiation is no more than 6-20K years old (Hagey and Mylroie 1995; TURNER et al. 2008; Clark et al. 2009). The abundance of generalist populations available for comparison, the young age of the radiation, and the occupation of novel ecological niches all make the San Salvador Island pupfish radiation, and specifically the snail-eating and scale-eating pupfish species, outstanding focal groups to explore the multivariate nature of novelty and to test the predictions of current hypotheses regarding the origins of novelty.

In chapter one I explicitly investigate the role of behavior for dietary specialization in the pupfish system and connect potentially adaptive behavioral shifts to differences in gene expression. In chapters two and three, I investigate how shifts in behavior interact with variation in morphological traits to produce adaptive phenotypes for snail- and scale-feeding. Finally, in chapter four I investigate the genetic basis of morphological and behavioral variation between snail- and scale-eating pupfish. Together, these chapters represent empirical tests of several current hypotheses on the origins of novelty and are some of the first studies to investigate how shifts in behavior, morphology, and genomics interact to form adaptive phenotypes when organisms adapt to new ecological niches.

Chapter 1: The behavioral origins of novelty: did increased aggression lead to scale-eating in pupfishes?

This chapter has been previously published and is reproduced here in accordance with the journal's article sharing policy:

St. John, M. E., McGirr, J. A., & Martin, C. H. (2019). The behavioral origins of novelty: did increased aggression lead to scale-eating in pupfishes? *Behavioral Ecology, 30(2),* 557–569. doi: 10.1093/beheco/ary196

Abstract

Behavioral changes in a new environment are often assumed to precede the origins of evolutionary novelties. Here, we examined whether an increase in aggression is associated with a novel scale-eating trophic niche within a recent radiation of *Cyprinodon* pupfishes endemic to San Salvador Island, Bahamas. We measured aggression using multiple behavioral assays and used transcriptomic analyses to identify differentially expressed genes in aggression and other behavioral pathways across three sympatric species in the San Salvador radiation (generalist, snail-eating specialist, and scale-eating specialist) and two generalist outgroups. Surprisingly, we found increased behavioral aggression and differential expression of aggression-related pathways in both the scale-eating and snail-eating specialists, despite their independent evolutionary origins. Increased behavioral aggression varied across both sex and stimulus context in both species. Our results indicate that aggression is not unique to scale-eating specialists. Instead, selection may increase aggression in other contexts such as niche specialization in general or mate competition. Alternatively, increased aggression may result from indirect selection on craniofacial traits, pigmentation, or metabolism—all traits which are highly divergent, exhibit signs of selective sweeps, and are affected by aggression-related genetic pathways which are differentially expressed in this system. In conclusion, the evolution of a novel predatory trophic niche within a recent adaptive radiation does not have clear-cut behavioral origins as previously assumed, highlighting the multivariate nature of adaptation and the complex integration of behavior with other phenotypic traits.

Introduction

Evolutionary novelties, such as novel morphological traits or behaviors, allow organisms to perform new functions within new ecological niches, however, their origins are still poorly understood (Pigliucci 2008). For example, in the case of novel resource use, both new behaviors and morphologies are often necessary for organisms to perform new functions. However, the relative importance of behavior and morphology to this new function, and the order in which they evolve is still unknown. Changes in behavior may precede the evolution of novel morphologies, as they can expose organisms to novel environments and selective pressures (Huey et al. 2003; Losos 2010). Investigations of novelty, however, overwhelmingly ignore this possibility (although see: Huey et al. 2003; Losos et al. 2004; Duckworth 2006). Instead, previous studies have focused on novel

adaptive morphologies or on how environmental changes expose organisms to new selective pressures (Liem 1973; Barton and Partridge 2000; Janovetz 2005b; Hulsey et al. 2008). Changes in behavior may be a plausible origin for novel phenotypes, but to document this we must first understand its variation within and among taxa.

One outstanding example of novelty is lepidophagy (scale-eating) in fishes. Scale-eating has been documented in at least 10 freshwater and seven saltwater families of fishes and has independently evolved at least 19 times (Sazima 1983; Janovetz 2005b; Martin and Feinstein 2014; Nelson et al. 2016; Kolmann et al. 2018). Scale-eating includes both novel morphologies and behaviors. For example, some scale-eaters have premaxillary external teeth for scraping scales (Novakowski et al. 2004), some use aggressive mimicry to secure their prey (Boileau et al. 2015), others sneak scales from fish that they are cleaning (Losey 1979), and still others use ambush tactics to obtain scales (Nshombo et al. 1985). Even though scale-eating is an outstanding example of the convergent evolution of novel trophic ecology across disparate environments and taxa and scale-eaters display a wide variety of morphologies and behaviors, the evolutionary origins of lepidophagy are still largely unknown.

There are currently three hypothesized behavioral origins for scale-eating. First, the algae-grazer hypothesis predicts that scale-eating arises from the incidental ingestion of scales during algae scraping (Fryer et al. 1955; Greenwood 1965; Sazima 1983). Indeed, many scale-eaters are closely related to algae-grazers. For example, many Malawi cichlids are algae-scrapers (Greenwood 1965; Fryer and Iles 1972; Ribbink et al. 1983); however, the radiation also includes two sister species of scale-eaters (*Corematodus shiranus* and *Corematodus taeniatus*) and a second independent origin of scale-eating in *Genyochromis mento* (Trewavas 1947; Greenwood 1965) within the predominantly rock-dwelling and algae-scraping mbuna cichlids (Fryer and Iles 1972). Similarly, the extinct Lake Victorian scale-eater *Haplochromis welcommei* was nested within rock-dwelling algae scrapers (Greenwood 1965). This hypothesis, however, does not address why algae-grazing fish would seek food on the surface of other fish (Greenwood 1965). The second hypothesis, termed the cleaner hypothesis, tries to address this gap by arguing that scale-eating arose from the incidental ingestion of scales during the consumption of ectoparasites from the surface of other fishes (Greenwood 1965; Sazima 1983). One line of evidence supporting this hypothesis is that cleaner fish, who primarily consume ectoparasites, sometimes eat scales. For example, the Hawaiian cleaner wrasse (*Labroides phthirophagus*) and two species of juvenile sea chub (*Hermosilla azurea* and *Girella nigricans*) consume both ectoparasites and scales (Demartini and Coyer 1981; Sazima 1983; Losey 1972). The reverse scenario—primarily scale-eating fish who also consume ectoparasites—is less common. In fact, few scale-eating fishes are even closely related to cleaner fish. One of the only examples of this is the spotted piranha (*Sarrasalmus marginatus*), which was observed cleaning fish-lice from larger species of piranha. Even this example, however, is based only on the observations of two individuals (Sazima and Machado 1990). Finally, the aggression hypothesis predicts that scale-eating evolved due to the incidental ingestion of scales during inter- or intra-species aggression (Sazima 1983). This hypothesis is supported by the fact that two characid species of scale-eaters (*Probolodus heterostomus* and *Exodon paradoxus*) are closely related to the aggressive

Astyanax tetras (Sazima 1983; Kolmann et al. 2018*);* a similar argument can be made for the scale-eating piranha (*Catoprion mento*) (Janovetz 2005*).* Furthermore, *Roeboides* species facultatively ingest scales in low-water seasons when competition for insects is high (Peterson and Winemiller 1997; Peterson and McIntyre 1998). It is thus also possible that increased competition for food resources led to increased aggression and lepidophagy.

The scale-eating pupfish, *Cyprinodon desquamator,* is an excellent species for investigating the origins of scale-eating because it is, by far, the youngest scale-eating specialist known. The species is nested within a sympatric adaptive radiation of pupfishes endemic to the hypersaline lakes of San Salvador island, Bahamas (Martin and Wainwright 2011; Martin and Wainwright 2013a). Geological evidence suggests that these hypersaline lakes — and thus the radiation containing the scale-eater — are less than 10 thousand years old (Hagey and Mylroie 1995; Martin and Wainwright 2013a; Martin and Wainwright 2013b). In addition to the scale-eating pupfish, the radiation also includes a widespread generalist (*C. variegatus)* and an endemic snail-eating specialist (*C. brontotheroides).* Other generalist pupfish lineages (*C. variegatus)* are also distributed across the Caribbean and western Atlantic Ocean. Despite their shared taxonomy with the San Salvador generalist species, phylogenetic evidence suggests that these generalist populations are outgroups to the San Salvador clade (Martin and Feinstein 2014; Martin 2016; Richards and Martin 2017). Phylogenies based on RADseq data also indicate that scale-eaters form a monophyletic group among lake populations on San Salvador (Figure. 1), indicating that the scale-eaters' most recent common ancestor was most likely an algae-eater (Martin and Feinstein 2014; Lencer et al. 2017). In contrast, snail-eaters clustered with generalists within the same lake, consistent with multiple origins of the snail-eating specialist or extensive introgression with generalists (Martin and Feinstein 2014; Martin 2016). Further evidence of introgression of adaptive alleles fixed in the snail-eating specialist across lakes is consistent with the latter scenario: generalists and snail-eaters are most closely related to each other genome-wide whereas a small number of alleles underlying the snail-eater phenotype have spread among lakes (Figure 1; Richards and Martin 2017; McGirr and Martin 2017). Phylogenies based on RADseq loci and whole-genome data also support a sister relationship between San Salvador generalist populations and snail-eaters across most of the genome. These species are in turn sister to scale-eaters and the San Salvador radiation forms a clade relative to outgroup generalist populations on neighboring islands (Richards and Martin 2017).

Here, we investigated the behavioral origins of novelty by examining whether an increase in aggression is associated with the evolution of the scale-eating pupfish. We compared measures of aggression using both behavioral and gene expression data among all three sympatric species within the San Salvador clade plus behavioral data for two additional generalist outgroups. If the aggression hypothesis is true, we expected to find increased levels of aggressive behavior in scale-eating pupfish, and lower levels of aggressive behavior in snail-eaters, generalists, and outgroups. Similarly, we expected to find differential gene expression in aggression-related pathways between scale-eaters vs generalists, but not between snail-eaters vs generalists. Surprisingly, we found that scale-eaters and snail-eaters both displayed

high levels of aggression and exhibited differential expression in several aggression-related pathways during early development.

Methods

Sampling

Generalist, snail-eating, and scale-eating pupfish were collected by seine from Crescent Pond, Great Lake, Little Lake, Osprey Lake, and Oyster Pond on San Salvador Island, Bahamas in July, 2016 and April, 2018. Generalist outgroups were also collected from Lake Cunningham, New Providence Island (Nassau), Bahamas (hereafter referred to as NAS) and from the coast of North Carolina (Fort Fisher, Cape Fear river drainage; hereafter referred to as NC) in April 2018 and June 2017, respectively. Fishes were housed in 40 – 80 liter tanks in mixed-sex groups at 5-10 ppt salinity in temperatures ranging from 23℃- 30℃. Fish were fed a diet of frozen blood worms, frozen mysis shrimp, or commercial pellet food daily. Wild-caught fish used for assays were held in the laboratory for at least two weeks before use in behavioral trials. We only used sexually mature adult fish for behavioral assays as pupfish can be visually sexed at this stage. Furthermore, all fish were in reproductive condition; pupfish mate and lay eggs daily and continually throughout the year after they mature.

Behavioral assays

We used three types of behavioral assays to quantify levels of aggression: A mirror assay, a paired aggression assay, and a boldness assay. While mirror assays measured a fish's level of aggression towards its mirror image, paired aggression assays measured levels of aggression toward another fish. Many species of fish use size as a proxy for aggression, and the mirror assay helps control for this, as the stimulus is the exact same size as the focal individual (Rowland 1989; Buston and Cant 2006). Mirror assays, however, may not accurately detect aggression in some cases (Balzarini et al. 2014). For example, some species use lateral displays of aggression which primarily occur head to tail—a maneuver that is impossible with a mirror image. Additional studies also indicate that mirror tests may not accurately predict aggressive display frequency, duration, or orientation (Elwood et al. 2014; Arnott et al. 2016). We therefore also measured aggression using paired aggression assays which allowed focal fish to display aggression in a more natural fashion. Boldness assays, on the other hand, measured a fish's willingness to explore a new environment. While this was not a direct measure of aggression per se, many studies have documented a correlation between aggression and boldness so we chose to include this measure in our study (Fraser et al. 2001; Rehage and Sih 2004; Sih et al. 2004; Gruber et al. 2017). All available adult wild-caught fish were sampled for the mirror assay (n = 198), but only a subset were randomly sampled for the paired aggression assay (n = 40) and the boldness assay (n = 51).

Mirror assay

We quantified levels of aggression for each pupfish species and sex using mirror tests (Vøllestad and Quinn 2003; Francis 2010). To control for individual size and motivation, we incited aggression using a compact mirror (10 cm X 14 cm) placed in a 2-liter trial tank (25 cm X 16 cm X 17 cm). We randomly chose adult fish and isolated each one in 2-liter tanks that contained a single bottom synthetic yarn mop for cover and opaque barriers between adjacent tanks. We gave fish at least 12 hours to acclimate to their new environment before performing an assay.

During a 5-minute focal observation period, we measured three metrics as a proxy for aggression: latency to approach mirror image, latency to attack mirror image, and total number of attacks toward the mirror image. A trial began as soon as the mirror was securely lowered into the tank. We measured latency to approach as the time elapsed before an individual approached the mirror to within one-body length. Similarly, we measured latency to attack as the time elapsed before an individual attacked their mirror image for the first time. Finally, we counted the total number of attacks an individual performed during the entirety of the trial. We also measured the standard length of each fish after the trial. To determine the repeatability of this assay, we measured aggression two separate times in a subset of our fishes (n = 21). We found significant repeatability for latency to attack and total number of attacks (latency to approach, r^2= 0.02, P= 0.50; latency to attack, r^2= 0.18, P= 0.045; total number of attacks, r^2= 0.36, P= 0.0026). As a control, we also measured latency to approach, latency to attack, and the total number of attacks performed towards the non-reflective side of the mirror (n = 51). We used the same methods as above, but inserted the mirror so that its reverse, non-reflective side faced the fish.

Paired aggression assay

We used a paired aggression assay as a second measurement of aggression for a subset of San Salvador generalists, snail-eaters, and scale-eaters (n = 40; Katzir 1981; Pauers et al. 2008). Paired aggression assays quantified levels of aggression for each species and sex using a conspecific of the same sex, conspecific of the opposite sex, and a heterospecific of the same sex as a stimulus fish. We randomly chose and isolated fish in the same manner as the mirror assay. Fish were again given at least 12 hours to acclimate to their new environment before performing an assay. Before an assay, a plastic mesh box (10 cm X 10 cm X 10 cm) with mesh size of 0.5 cm was lowered into the tank, and a stimulus fish was placed inside the box, after which the assay began. During the 5-minute focal observation period we measured the focal fish's latency to approach the stimulus fish (within one-body length), their latency to attack the stimulus fish, and the total number of attacks performed toward the stimulus fish. Each focal fish was given four paired aggression assays: 1) stimulus fish was a conspecific of the same sex, 2) stimulus fish was a conspecific of the opposite sex, 3) stimulus fish was a heterospecific of the same sex, and 4) a control with an empty box. Specialists were always given a generalist as the heterospecific stimuli, but generalists were randomly assigned either a snail-eater or a scale-eater. All fish were tested in the same order and were given at least 12 hours of rest between assays. We also measured the standard length of each stimulus and focal fish.

Boldness assay

Finally, we conducted a boldness assay to determine the relationship between boldness and aggression in pupfishes (Budaev 1997; Brown et al. 2005; Wilson and Godin 2009). We used a random subset of individuals from the mirror assay for this test (n = 51). Before a trial, a PVC cylinder start box was placed into a 2-liter trial tank (25 cm X 16 cm X 17 cm). The start box was 12 cm in diameter with a removable screw top and contained a single drilled 3 cm hole for the fish to emerge from (which was blocked with a cork at the start of the trial). At the start of the trial the top of the start box was removed, and a focal fish was gently placed inside. The top was then secured on the box, and the fish was given one minute to acclimate. After the acclimation time, the 3 cm hole was unplugged (allowing the fish to emerge from the start box) and the 5-minute assay began. We measured the latency of the fish's head to emerge from the hole, a preliminary behavioral inspection of the outside environment, and the latency of the fish's tail (i.e. the entire fish) to emerge from the hole as proxies for boldness.

Statistical analyses

We used time-to-event analyses to determine if species and sex were associated with 1) latency to approach mirror image, 2) latency to attack mirror image, and 3) latency to emerge from the start box. We used time-to-event models for time metrics since it allows for right censored data i.e. individuals who did not approach, attack, or emerge within the 5-minute time window are not excluded from the dataset and contributed to Kaplan-Meier estimates (Rich et al. 2010). We used Cox proportional hazards models to analyze time metrics for the boldness assay, paired aggression assays, and the mirror control assay (Survival Package; Therneau 2015). We used a mixed-effects Cox proportional hazards model (coxme package; Therneau 2016) for the mirror assay as the individuals from this assay originated from multiple populations. For each of the above models we included species and sex as fixed effects and lake population as a random effect for the mirror assay models. Using AICc (Burnham and Anderson 2002; stats package), we compared models to equivalent models that also included the interaction between species and sex as a fixed effect, the size of the focal individual (log-transformed) as a covariate, and—where applicable—the size of the stimulus individual (log-transformed) as a covariate. The interaction between species and sex was significant for: 1) the latency to emerge (head) in the boldness assay, 2) the latency to approach in the mirror assay, 3) the latency to approach in the heterospecific assay, and 4) the latency to attack in the same sex conspecific assay and was therefore retained in those final models. Additionally, the focal fish's size was a significant covariate for the latency to approach model for the heterospecific assay and the latency to attack model for the mirror assay and was also retained in those models. We used Wald and likelihood ratio tests to determine if species, sex, or their interaction were associated with fishes' latency to approach, attack, or emerge depending on the assay (Table 1).

We used generalized linear models (GLM) or generalized linear mixed models (GLMM) to analyze the total number of attacks performed for each assay. For the 1) same sex conspecific assay, 2) opposite sex conspecific assay, and 3) heterospecific

assay, we used GLMs with a negative binomial distribution to analyze the total number of attacks. We modeled species and sex as fixed effects for these models. For the mirror assay, however, we used a GLMM with a negative binomial distribution. Here, we modeled species and sex as fixed effects and population as a random effect. We modeled the total number of attacks during controls for 1) the mirror assays and 2) the paired aggression assay, using GLMs with a Poisson distribution, and included species and sex as fixed effects. Using AICc, we compared each of these models to equivalent models which also included the interaction between species and sex as a fixed effect, the size of the focal individual (log scale) as a covariate, and—for paired aggression assays—the size of the stimulus individual (log scale) as a covariate. We found models including the interaction between species and sex best explained the data for the: 1) control for the paired aggression assay model, 2) the conspecific of the same sex assay model, and 3) the mirror assay model, and were thus retained in the final models. Additionally, models including size of the focal individual significantly improved the fit of the paired aggression assay model and the mirror assay model and were thus retained in the final models. We used Wald and likelihood ratio tests to determine if species, sex, or their interaction significantly affected the total number of attacks performed during assays (Table 1).

One caveat is that we did not correct for phylogeny in any of these models. While correcting for phylogeny is important when hierarchical species relationships exist (Felsenstein 1985), this is not the case for the recently diverged San Salvador clade which is best explained by a network of interconnected populations with extensive gene flow. Indeed, numerous admixture events in addition to the maximum likelihood phylogeny were supported by *Treemix* (Pickrell and Pritchard 2012) population admixture graphs (Martin 2016); similarly, only 82% of the genome supported a monophyletic relationship for San Salvador species (Richards and Martin 2017). Importantly, populations of the scale-eating and snail-eating specialists were never most closely related to each other. When so few regions of the genome underlie phenotypic differences, these species can be viewed as a set of populations with substantial evidence for gene flow.

Finally, we made direct comparisons between groups for all time and count metrics using bootstrap resampling methods with replacement (10,000 replicates; boot package; Canty and Ripley 2017) . For right censored time metrics we calculated the median survival time for each group of interest (Bewick et al. 2004). Median survival times represent the timepoint at which 50% of the group experienced an event (i.e. approached, attacked or emerged). Lower medians indicate that the event occurred quickly while a median of > 300 indicates that 50% of the group never experienced the event (and is therefore right censored). For count data (i.e. attacks), we simply calculated the mean for each group. Finally, we calculated the bias-corrected and accelerated bootstrap 95% confidence intervals for each mean and median (Haukoos and Lewis 2005). All analyses were performed in R (R Core Team 2018).

Early developmental genes affecting differences in aggression between species

We searched a previously published dataset of 15 San Salvador pupfish transcriptomes to identify differentially expressed genes between each generalist and specialist pair annotated for behavioral effects (which had not previously been examined (McGirr and

Martin 2018)). Purebred F_1 and F_2 offspring from the three-species found on San Salvador island were raised in a common garden laboratory environment. Larvae were euthanized in an overdose of MS-222 at 8-10 days post fertilization (dpf), immediately preserved in RNAlater (Ambion, Inc.), and stored at -20 C after 24 hours at 4 C. Total mRNA was extracted from whole larvae for: 6 generalists, 6 snail-eaters, and 3 scale-eaters (RNeasy kits, Qiagen). The KAPA stranded mRNA-seq kit (KAPA Biosystems 2016) was used to prepare libraries at the High Throughput Genomic Sequencing Facility at UNC Chapel Hill. Stranded sequencing on an Illumina HiSeq 4000 resulted in 363 million raw reads that were aligned to the *Cyprinodon variegatus* reference genome (NCBI, *C. variegatus* Annotation Release 100, total sequence length =1,035,184,475; number of scaffold=9,259, scaffold N50, =835,301; contig N50=20,803; Lencer et al. 2017). We removed adaptors and low-quality reads (Phred score <20) using Trim Galore (v. 4.4, Babraham Bioinformatics).

Aligned reads were mapped to annotated features using STAR (v. 2.5(33)), with an average read depth of 309× per individual and read counts were generated across annotated features using the featureCounts function from the Rsubread package (Liao et al. 2013). We then used MultiQC to assess mapping and count quality (Ewels et al. 2016). DEseq2 (Love et al. 2014, v. 3.5) was used to normalize counts and to complete pairwise comparisons between snail-eaters *vs* generalists and between scale-eaters *vs* generalists. Genes with fewer than two read counts or low normalized counts (determined by DESeq2) were discarded (Love et al. 2014). Finally, we compared normalized posterior log fold change estimates between groups using a Wald test (Benjamini-Hochberg correction), and found: 1) 1,014 differentially expressed genes between snail-eaters *vs* generalists and 2) 5,982 differentially expressed genes between scale-eaters *vs* generalists (McGirr and Martin 2018).

We performed gene ontology (GO) enrichment analyses for differentially expressed genes using resources from the GO Consortium (geneontology.org; Ashburner et al. 2000; The Gene Ontology Consortium 2017). We identified one-way and reciprocal best hit zebrafish orthologs for genes differentially expressed between 1) snail-eaters vs generalists (n = 722) and 2) scale-eaters vs generalists (n = 3,966) using BlastP (Shah et al. 2019). While a reciprocal best hit method is more powerful for identifying true orthologs, it often misses orthologs in lineages which have experienced genome duplication events, such as teleost fishes (Dalquen and Dessimoz 2013). Hence, we used both approaches to identify possible orthologs.

Animal aggression has previously been categorized, and includes inter-male aggression, maternal aggression, sex-related aggression, and territorial aggression (Moyer 1971; Nelson and Chiavegatto 2001). Furthermore, previous studies have found differential gene expression in the context of inter-male aggression, female-female aggression, and maternal aggression, (Nelson and Trainor 2007). We then compared the reciprocal best hit and one-way best hit zebrafish orthologs to gene ontologies in the similar categories of: aggressive behavior (GO: 0002118), inter-male aggressive behavior (GO: 0002121), maternal aggressive behavior (GO:0002125), maternal care behavior (GO: 0042711), and territorial aggressive behavior (GO: 0002124; AmiGo; Carbon et al. 2009; Ashburner et al. 2000; The Gene Ontology Consortium 2017). Steroid hormones, like vasopressin, androgens, and estradiol, have also been linked to changes in aggression (Nelson and Chiavegatto 2001; Nelson and Trainor 2007), so we

also searched gene ontologies for those three hormone pathways. Thus, we performed an exhaustive and unbiased search of all aggression and parental-care related genes differentially expressed relative to the generalist in any tissue during the early development of each specialist species.

Results

Behavioral assays

Scale-eaters and snail-eaters are more aggressive than generalists

Both scale-eaters and snail-eaters exhibited increased aggression compared to their generalist counterparts. Male scale- and snail-eaters approached their mirror image significantly quicker than NC and San Salvador generalists (Table 1a, Figure 2a), and attacked their mirror image significantly more than NAS generalists (Table 1c, Figure 4a). Female snail-eaters also attacked their mirror image significantly more than generalists from NC and San Salvador (Table 1c, Figure 4a). We saw a similar pattern when fish were presented with conspecific or heterospecific live fish stimuli. Male scale- and snail-eaters approached heterospecific fish significantly more quickly than San Salvador generalists (Table 1a, Figure 2c), and attacked male conspecifics significantly more quickly than did generalists (Table 1b, Figure 3b). Scale- and snail-eaters also attacked heterospecific fish significantly more quickly and performed more total attacks towards heterospecific fish than did generalists (Table 1a & 1c., Figures 2c & 3c).

Aggression is sex dependent, but not consistent across species

We also found that levels of aggression varied across sexes, but that the pattern was not consistent across species. While male scale- and snail-eaters were consistently more aggressive than their female counterparts, female generalists were more aggressive than males. Both male scale- and snail-eaters showed increased aggression during assays in which they faced stimuli similar to themselves (i.e. mirror assays and same sex conspecific assays). Scale-eater males approached their mirror image more quickly and performed more total attacks toward their mirror image than female scale-eaters (Table 1a & 1c, Figures 1a, & 3a). Similarly, male snail-eaters attacked male conspecifics more quickly and performed more total attacks toward male conspecifics than females did toward female conspecifics (Tables 1b & 1c, Figures 2b, & 3b). Generalist females, however, approached their mirror image more quickly than generalist males (Table 1a, Figure 2a), and attacked female conspecifics quicker than males attacked male conspecifics (Table 1b, Figure 3b).

Aggression varies across different behavioral assays

Not only did aggression vary between species and sex, but it also varied across behavioral assays. While female generalists and scale-eaters attacked female conspecifics quicker than snail-eaters (Table 1b, Figure 3b), female snail-eaters performed more total attacks toward their mirror image than either of these groups (Table 1c, Figure 4a). Similarly, male scale-eaters only exhibited increased aggression

compared to snail-eater males when approaching their mirror image or a heterospecific stimulus fish (Table 1a, Figure 2a &1c).

Boldness did not vary across species

Unlike aggression, boldness did not vary across species. Latency for their head to emerge from the start box did not vary by sex, species, nor their interaction (Table 1d). Further, the latency for the tail to emerge also did not vary by species (Table 1e). It did, however, significantly vary by sex (Table 1e), with male fish fully emerging from the start box about six times quicker than female fish (median male time: 42.23 (17.33,131.67); median female time: 253.05 (112.06, 288.28)). Propensity to approach or attack novel objects also did not vary by species, sex, or their interaction in both our control mirror and control paired aggression assays (Table 1a,1b, &1c).

Gene expression

3,966 genes were differentially expressed between scale-eaters *vs* generalists and 722 genes were differentially expressed between snail-eaters *vs* generalists. We found differentially expressed genes within ontologies for maternal care behavior, the estradiol hormone pathway, and the androgen hormone pathway (Table 2). None of these ontologies were significantly over-represented in either species comparison, which were instead enriched for cranial skeleton, metabolism, and pigmentation genes (McGirr and Martin 2018).

Despite over one thousand differentially expressed genes from whole larvae at this developmental stage, only two genes were associated with aggression-related ontologies in the snail-eater vs generalist comparison (Table 2a) and only 7 genes were associated with aggression-related ontologies in the scale-eater vs generalist comparison (Table 2b) using one-way best hits. Furthermore, these comparisons shared two genes in common: a transcriptional co-activator which interacts with androgen receptors (rnf14) and a DNA binding transcription factor involved in glucocorticoid receptor regulation (crebrf) (Kang et al. 1999; Martyn et al. 2012). While both specialists showed differential expression in androgen and maternal care-related pathways when compared to the generalist, scale-eaters additionally showed differential expression in the estradiol hormone pathway. When using a reciprocal best hits approach, only a single gene, hdac6, was associated with aggression-related ontologies in the scale-eater vs generalist comparison. However, the primary function of this gene is histone deacetylation, and it is conserved across flies and mammals, which could explain why it was the sole result of the conservative reciprocal best hits approach (Perry et al. 2017).

Discussion

The origins of novelty have overwhelmingly been examined from a morphological perspective, often ignoring behavior's potential role (but see: Sol and Lefebvre 2000; Duckworth 2006; Zuk et al. 2006). Here, we used both behavioral and gene expression data to investigate whether increased aggression contributed to the origin of scale-

eating in Caribbean pupfishes. We expected to find increased levels of aggression in scale-eaters compared to generalist and snail-eating pupfish species. Contrary to these predictions, however, both snail-eaters and scale-eaters showed increased levels of aggression compared to generalist species. Our gene expression data supported these findings; both scale-eaters and snail-eaters showed differential expression of genes involved in several aggression-related pathways during larval development. We also found that aggression varied between and within sexes and contexts. Our data therefore does not support the aggression hypothesis as the sole origin of scale-eating in pupfish. Instead, selection may have favored increased levels of aggression in other contexts, such as mate competition or trophic specialization in general. Increased levels of aggression could have also arisen indirectly due to selection for other behaviors or traits, including several differentially expressed genes involved in both aggression and craniofacial morphology (e.g. *med12*).

Only a few previous studies have directly investigated the behavioral origins of novelty. The Pacific field cricket (*Teleogryllus oceanicus*)—which exhibits a novel silent morph—is one of the few examples of evolutionary novelty with a behavioral origin (Zuk et al. 2006; Tinghitella and Zuk 2009; Bailey et al. 2010). Increased brain size in birds has also been linked to behavioral shifts and novelty. Birds that display innovative feeding behaviors have larger brains and are more successful at invading novel environments (Nicolakakis and Lefebvre 2000; Sol and Lefebvre 2000; Overington et al. 2009). Likewise, the role of behavior in evolutionary novelty has also been explored in western bluebirds *(Sialia mexicana;* Duckworth 2006) and *Anolis* lizards (Losos et al. 2004, 2006). Despite the growing empirical evidence of behavior's role in evolutionary innovation, a consensus has not yet been reached on whether behavior ultimately drives or inhibits novelty. Furthermore, studies that investigate behavioral origins of novelty rarely do so using both behavioral and genetic approaches. In this study, however, we were able to leverage our gene expression data to gain some mechanistic insight into the divergent origins of increased behavioral aggression in each specialist species.

While both our behavioral and transcriptomic analyses provided evidence of increased aggression in both trophic specialist species, contrary to our expectations, there are a few caveats. First, aggression and aggression-related pathways were not enriched terms in our GO analysis. Instead, we found enrichment for cranial skeleton, metabolism, and pigmentation terms (McGirr and Martin 2018). However, gene expression differences are biologically relevant even if they are not enriched among all processes. Here, we used whole-larval tissue at a timepoint of 8-10dpf to detect several genes and pathways that were differentially expressed between pupfish species within the San Salvador radiation. This sampling timepoint provides valuable insight which other methods may not afford. For example, gene expression differences (especially in behavioral pathways) are often transient in adults and can be attributed to factors such as diet, sex, dominance status reproductive state, or mood (McGraw et al. 2003; Aubin-Horth et al. 2007; Rosvall 2013). Instead, by examining early larval stages our gene expression analyses provide insight into species-specific differences in aggression-related genetic pathways established during an early developmental timepoint. Second, while we used one-way and reciprocal best hits to determine potential orthology between pupfish and zebrafish many studies have found neofunctionalization of paralogs—

meaning that functions may not always be retained (Braasch et al. 2006; Douard et al. 2008; Cortesi et al. 2015). Nonetheless, we found surprising congruence between our behavioral and transcriptomic data supporting the conclusions of increased aggression in both San Salvador specialists due to different aggression-related genetic pathways.

New hypotheses for varying levels of aggression within a sympatric radiation of pupfishes

1. Increased aggression due to specialization

If increased levels of aggression are not associated with scale-eating, then what explains this variation between species? One possibility is that selection may have directly favored increased aggression in the context of dietary specialization. Aggression may be positively correlated with traits associated with specialization (Genner et al. 1999; Peiman and Robinson 2010; Blowes et al. 2013), suggesting that specialists should show increased levels of aggression compared to generalists. Increased levels of aggression have been documented in specialist butterflyfishes (chaetodontids*;* Blowes et al. 2013), a specialist surfperch (*Embiotoca lateralis*; Holbrook and Schmitt 1992), and even observed in game-theoretic simulation models (Chubaty et al. 2014).

Alternatively, aggression may be increased in specialists due to competition for food. For example, species of Roeboides turn to scale-eating during low-water seasons when competition for insects rises (Peterson and Winemiller 1997; Peterson and McIntyre 1998). However, pupfish inhabit hypersaline lakes connected to the ocean which do not experience seasonal fluctuations in water levels (Hagey and Mylroie 1995). Instead, variation in abundance of pupfish over the year could lead to increased competition for food (Martin and Wainwright 2013a; Martin and Wainwright 2013b, Martin and Wainwright 2013c). Competition for food may also explain increased aggression in snail-eaters. Although snail-eating pupfish consume the largest proportion of snails in their diet (22-30%; Martin and Wainwright 2013a), generalist pupfish also consume snails in low quantities (.03-4%; Martin and Wainwright 2013c). Furthermore, generalists comprise 92-94% of the pupfish population (Martin and Wainwright 2013c), indicating that snail-eaters may compete with generalists for food items regularly. It is possible that snail-eaters developed increased aggression to protect their food source from generalists.

Another possibility is that increased aggression may be associated with colonizing a novel niche. Aggression is often tightly correlated with boldness in a phenomenon termed the aggressiveness-boldness syndrome (Sih et al. 2004). Many studies have shown that increased boldness in species such as cane toads, mosquitofish, and Trinidadian killifish leads to increased dispersal into novel habitats or niches (Fraser et al. 2001; Rehage and Sih 2004; Gruber et al. 2017). This relationship indicates that increased aggression may be an incidental effect of selection for increased boldness and occupation of a novel niche. However, our measures of boldness did not show any variation across species, and instead indicated that males were bolder than females.

This relationship between aggression and specialization is also supported by our transcriptomic data. First, both genes differentially expressed in our snail-eater vs generalist analysis were also differentially expressed in our scale-eater vs generalist

analysis (rnf14 and crebrf). Second, rnf14, a co-activator of androgen receptors, is also associated with metabolism suggesting that it may be the specialized diets of snail- and scale-eaters which led to their increased aggression (Michael et al. 2011). This is consistent with the significant amount of parallel expression in both specialists in genetic pathways associated with metabolism and the increased nitrogen consumption and enrichment in both specialists (McGirr and Martin 2017). While increased aggression may be important for a specialized diet or occupying a novel niche neither of these hypotheses explain the variation in aggression between sexes.

2. Increased aggression due to mating system

Increased aggression may be favored in the context of courtship or mate competition. It is well documented across multiple taxa that the sex with the higher potential reproductive rate should have increased levels of aggression as they must compete more heavily for access to mates (Clutton-Brock and Parker 1992; Andersson 1994; Jennions and Petrie 2007). Normally, males have higher potential reproductive rates since mating is energetically cheap for them (Trivers 1972). *Cyprinodon* pupfishes follow this pattern since they mate in a lekking system and do not provide parental care (Gumm 2012). Our behavioral measures of aggression support this; both male scale- and snail-eaters showed increased levels of aggression compared to their female counterparts.

We also found some support for this in our gene expression data. In our scale-eater *vs* generalist comparison, we found differential gene expression of the *esr1* gene which encodes an estrogen receptor. Differential expression of this gene has been linked to aggression, territoriality, mate-seeking behavior, and even parental care (Tuttle 2003; Horton et al. 2013, 2014; Hashikawa et al. 2016). However, differential expression of *esr1* was only observed in the scale-eater *vs* generalist comparison and not between snail-eaters *vs* generalists. *Crebrf,* a regulatory factor which is differentially expressed in both scale- and snail-eaters *vs* generalists, has also been associated with lack of maternal care in mice (Martyn et al. 2012). Although all three species exhibit a lekking mating system, there may be quantitative differences in male competition and degree of lekking among species and lake populations (CHM pers. obs.).

3. Increased aggression due to indirect selection

Alternatively, aggression may have increased via selection on other traits. For example, melanin production and aggression are physiologically linked via the melanocortin system (Cone 2005; Price et al. 2008). This association has been documented across a wide array of vertebrates and suggests that selection for increased melanin pigmentation in other contexts (e.g. mate choice or camouflage) may incidentally increase aggression (McGraw et al. 2003; Ducrest et al. 2008; Price et al. 2008). Indeed, territorial male scale-eating pupfish exhibit jet black breeding coloration, unique among *Cyprinodon*, and snail-eating pupfish exhibit the lightest male breeding coloration of any *Cyprinodon* species (Martin and Wainwright 2013a). Similarly, selection for morphological traits may also indirectly increase aggression. We found differential gene expression between scale-eater vs generalist pupfish in the med12 gene, which is annotated for the androgen pathway (Table 2B). Med12 is a mediator complex subunit which codes for a thyroid hormone receptor associated protein.

Mutations in this gene have not only been linked to craniofacial defects, but also to a slender body shape (Philibert and Madan 2007; Risheg et al. 2007; Ding et al. 2008; Vulto-Van Silfhout et al. 2013). *C. desquamator* show extreme craniofacial features, including enlarged oral jaws and a fusiform body that may be beneficial for scale-eating with an estimated four moderate-effect quantitative trait loci all increasing oral jaw size, consistent with directional selection on this trait (Martin et al. 2017). Thus, it is intriguing that selection for increased jaw size or body elongation may have indirectly selected for increased aggression in this species. Given the enlarged oral jaws of most scale-eating species, this may be a general mechanism indirectly contributing to increased aggression in scale-eaters depending on how frequently this genetic pathway is modified.

Multimodal signals for aggression

An additional finding of this study is that pupfish aggression varies not only across species and sex, but also across context. This was especially surprising when comparing the results of our mirror assay to the results of the conspecifics of the same sex assays. These assays are arguably the most similar (i.e. stimuli are conspecifics of the same sex), and we expected that the results should also be similar. However, this was not true for female snail- or scale-eaters. Female snail-eaters had very low rates of approaching and attacking female conspecifics (Figures 1b, 2b, & 3b), but they readily approached and attacked their mirror image (Figures 1a, 2a, &3a). This could suggest that snail-eaters need more than visual cues to identify conspecifics. Female snail-eaters also approached and attacked their mirror image at the same rates as heterospecific stimulus fish (Figures 1c, 2c, & 3c), suggesting that they misidentified their mirror image as a heterospecific fish. Female scale-eaters, on the other hand, attacked conspecific stimuli significantly quicker and more often than their mirror image (Figures 2a, b; & 3a, b), and they approached and attacked heterospecifics at the same rate and frequency as conspecifics. This could suggest that, like snail-eaters, female scale-eaters also need multiple signals to determine potential competition or prey. Multiple studies have documented that the use of multiple cues leads to greater accuracy in con- and heterospecific identification (Rand and Williams 1970; Hankison and Morris 2003; Ward and Mehner 2010). Höjesjö et al. (2015) also found that the use of multiple cues was additive for females, but not for males. However, many of these studies focus on identification in the context of mating—not in the context of aggression.

Conclusion

Our study surprisingly suggests that the aggression hypothesis is not a sufficient explanation for the origins of an exceptional trophic innovation, scale-eating in pupfish. Instead, increased aggression in both specialists indicates that aggression may perform a more general function in dietary specialization or occupation of a novel niche. Alternatively, increased aggression may be an indirect effect of selection on other ecological or sexual traits. Specifically, the aggression-boldness syndrome, the melanocortin system, increased protein metabolism, or selection for oral jaw size could all have indirectly increased aggression. Future studies should investigate whether aggression is adaptive for scale- and snail-eating in pupfishes.

Acknowledgements

This research was kindly funded by NSF CAREER 1749764 and NIH R01 1R01DE027052-01A1 grants to CHM. We thank the BEST commission and the Ministry of Agriculture of the Commonwealth of the Bahamas for permission to conduct this research and export specimens; E. Tibbetts for helpful comments on the manuscript; the Gerace Research Centre and Troy Dexter for logistical support during fieldwork; and the Vincent J. Coates Genomics Sequencing Laboratory and Functional Genomics Laboratory at UC Berkeley, supported by NIH S10 OD018174 Instrumentation Grant, for performing RNAseq library preparation and sequencing. All laboratory behavioral and sampling protocols were approved by the University of North Carolina at Chapel Hill IACUC (protocol# 15-179.0).

Data Accessibility

Analyses reported in this article can be reproduced using the data provided by St. John, McGirr, and Martin (2018). Genomic and transcriptomic raw sequence reads are deposited at the NCBI BioProject database (Title: Craniofacial divergence in Caribbean Pupfishes. Accession: PRJNA391309).

Author Contributions

MES and CHM conceptualized the project, MES and JAM collected data and performed all analyses, MES wrote the original draft, and MES, JAM, and CHM reviewed and edited drafts, and CHM provided funding.

Tables

Table 1. Results of 1) mixed-effect Cox proportional hazards models 2) Cox proportional hazards models 3) GLMMs, and 4) GLMs describing aggression related behaviors. Significant predictors are indicated in bold.

metric	**assay**	**predictor**	***df***	χ^2	***p***
a) latency to approach	mirror	species	4	6.02	0.2
		sex	1	0.01	0.91
		species:sex	4	9.67	**0.046**
	conspecific same sex	species	2	1.87	0.39
		sex	1	1.83	0.18
	conspecific opposite sex	species	2	0.55	0.76
		sex	1	0.14	0.71
	heterospecific	species	2	0.05	0.98
		sex	1	1.3	0.25
		size	1	5.02	**0.025**
		species:sex	2	8.26	**0.016**
	mirror control	species	4	2.67	0.61
		sex	1	3.33	0.07
	paired aggression control	species	2	1.58	0.45
		sex	1	0.37	0.55
b) latency to attack	mirror	species	4	5.18	0.27
		sex	1	3.37	0.07
		size	1	6.22	**0.01**
	conspecific same sex	species	2	3.49	0.18
		sex	1	1.77	0.18
		species:sex	2	7.37	**0.025**
	conspecific opposite sex	species	2	2.45	0.29
		sex	1	0.13	0.72
	heterospecific	**species**	2	7.34	**0.026**
		sex	1	6.86	**0.009**
	mirror control	species	4	3.89	0.42
		sex	1	0.81	0.37
	paired aggression control	species	2	2.6	0.27
		sex	1	0.02	0.9
c) total number of attacks	mirror	**species**	4	12.96	**0.01**
		sex	1	7.73	**0.005**

		size	1	3.8	0.051
		species:sex	4	14.37	**0.006**
	conspecific same sex	**species**	2	6.6	**0.037**
		sex	1	4.53	**0.033**
		species:sex	2	6.19	**0.045**
	conspecific opposite sex	species	2	3.52	0.17
		sex	1	0.08	0.78
	heterospecific	**species**	2	13.46	**0.001**
		sex	1	0.68	0.41
	mirror control	species	4	7.78	0.1
		sex	1	1.62	0.2
	paired aggression control	species	2	0	1
		sex	1	0	1
		size	1	0.23	0.64
		species:sex	2	0	1
d) latency to emerge (head)	boldness	species	4	0.48	0.98
		sex	1	0.28	0.6
		species:sex	4	7.02	0.14
e) latency to emerge (tail)	boldness	species	4	5.1	0.28
		sex	1	6.33	**0.01**

Table 2. List of all differentially expressed genes in aggression and parental-care pathways at 8-10 dpf between: a) snail-eaters *vs* generalists and b) scale-eaters *vs* generalists. The two genes differentially expressed in both specialists compared to generalists are highlighted in bold. Asterisks indicate genes which were differentially expressed using both one-way and reciprocal best hits approaches. All remaining genes were identified using one-way best hits.

species comparison	gene	log2 fold change	GO pathway
a) snail-eater *vs* generalist			
	rnf14	-0.53	androgen
	crebrf	-0.7	maternal care
b) scale-eater *vs* generalist			
	*hdac6**	-0.84	androgen
	med12	-0.98	androgen
	med16	1.24	androgen
	ncoa1	1.27	androgen
	rnf14	-1.07	androgen
	crebrf	-1.41	maternal care
	esr1	-0.95	estradiol

Figures

Figure 1.

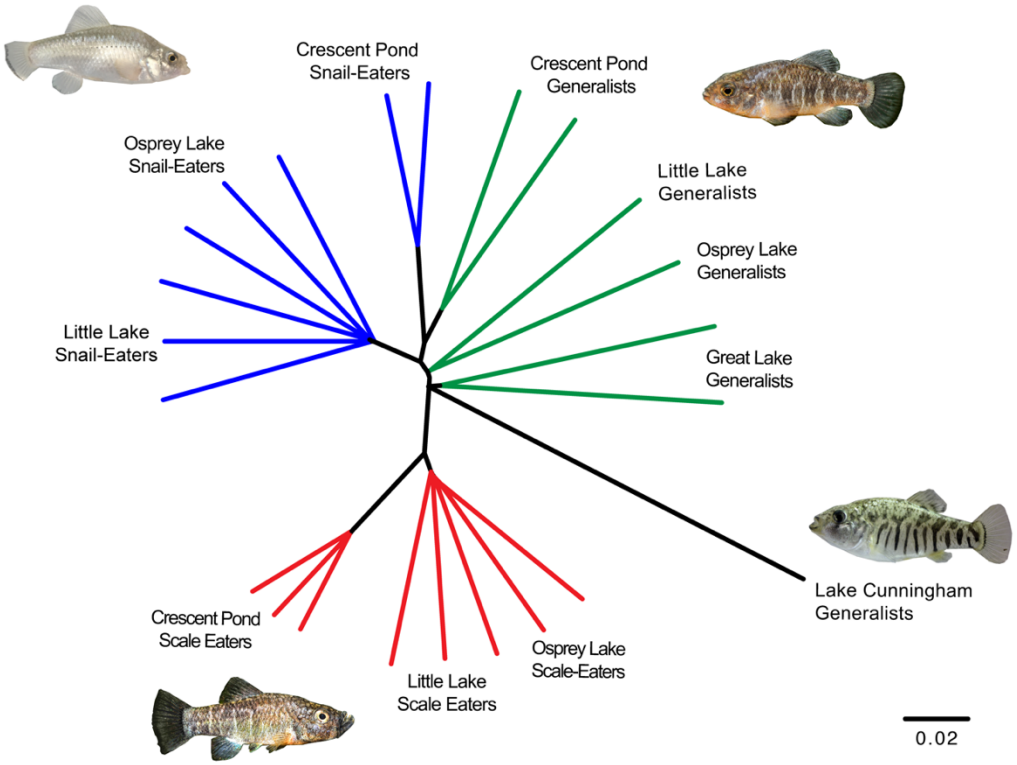

Figure 1. Neighbor joining tree illustrating the relationships between San Salvador Island species and a Caribbean Island outgroup. Predominant topology from a *Saguaro* analysis (Zamani et al. 2013) which represents 64% of the genome of generalists (green), snail-eaters (blue), scale-eaters (red), and the Lake Cunningham generalist outgroup (black). Branch lengths represent average number of substitutions per base pair. Figure modified from Richards and Martin 2017.

Figure 2.

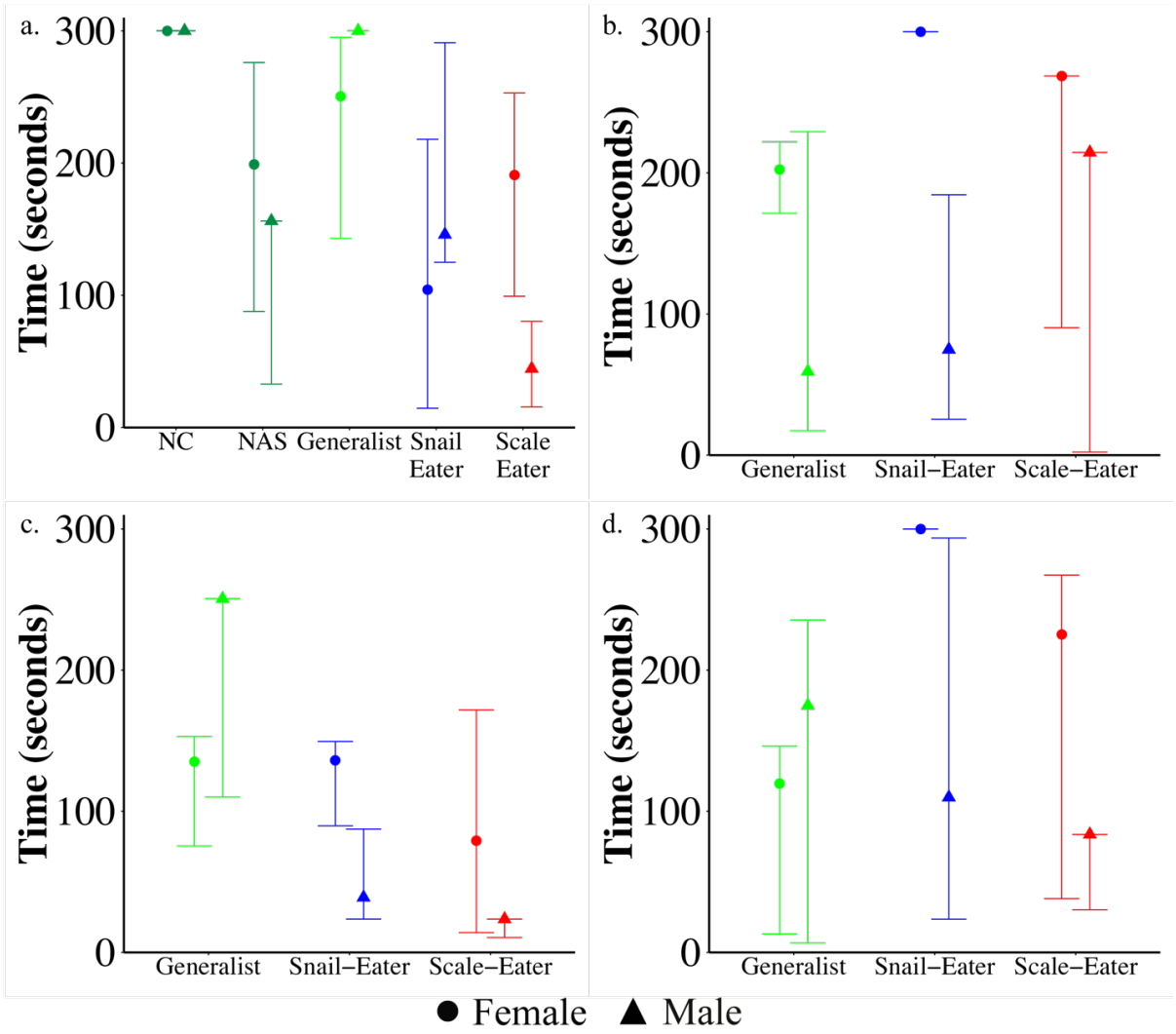

Figure 2. Median and 95% CI's (BCa) for latency to approach: A) mirror image, B) same-sex conspecific, C) heterospecifics, or D) opposite sex conspecific.

Figure 3.

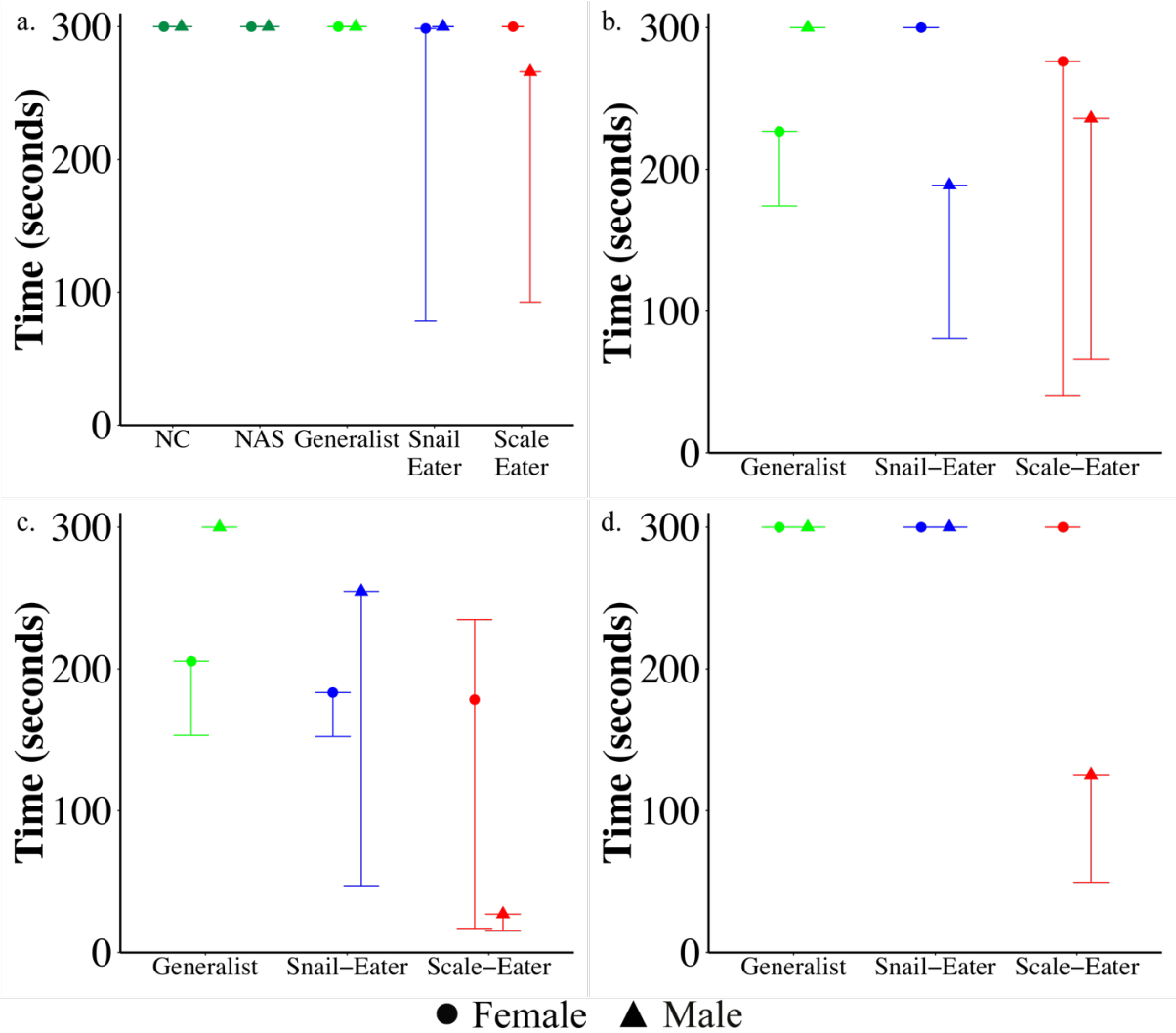

Figure 3. Median survival times and 95% CI's (BCa) for latency to attack: A) mirror image, B) same-sex conspecific, C) heterospecifics, or D) opposite sex conspecific.

Figure 4.

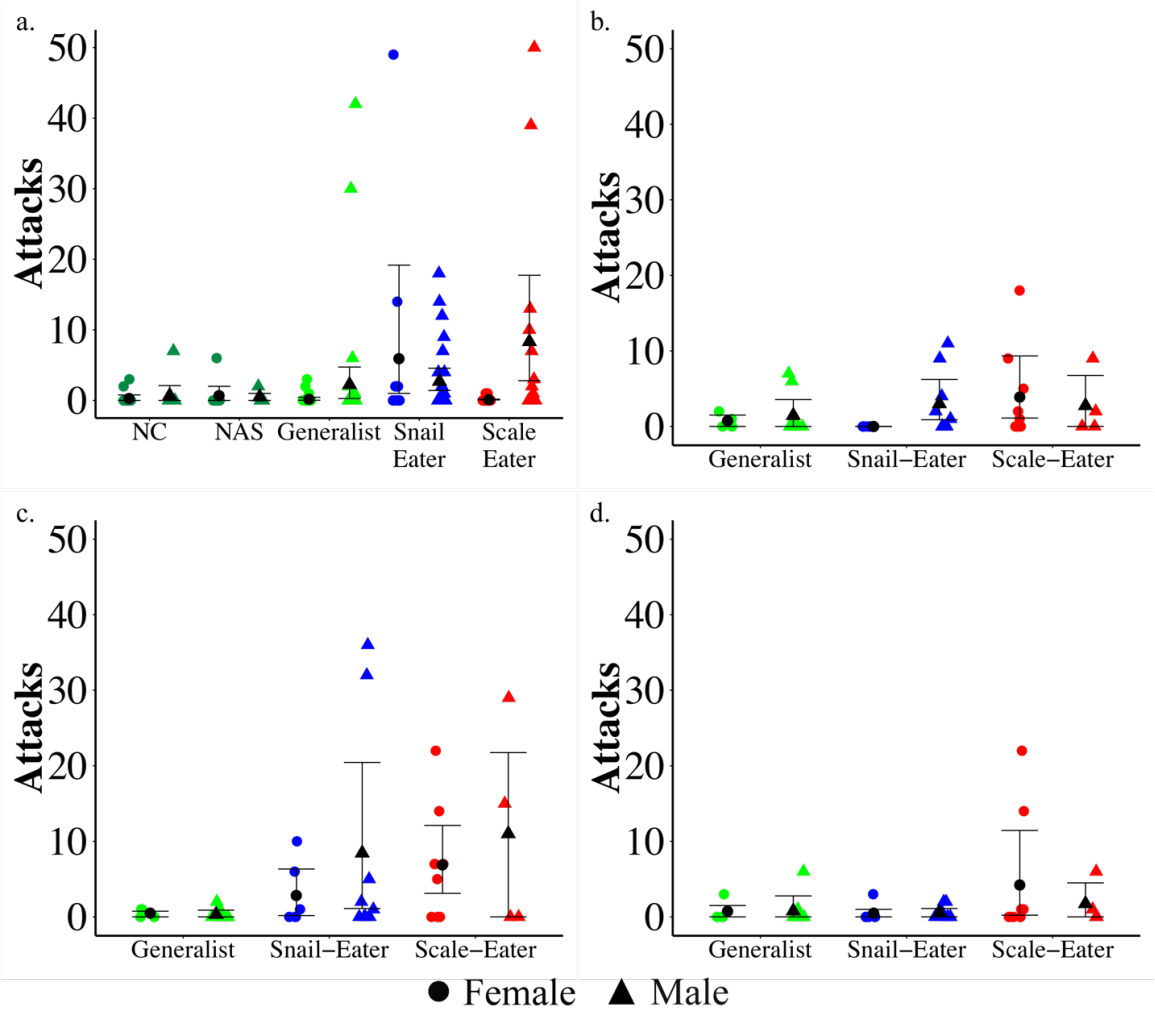

Figure 4. Mean number and 95% CI's (BCa) for attacks performed towards: A) mirror image, B) same-sex conspecific, C) heterospecifics, or D) opposite sex conspecific.

Inter-chapter Transition

In chapter one, I found evidence of increased behavioral aggression in both specialist pupfish species, and that similar aggression pathways were differentially expressed in specialist species compared to generalist species. This pattern suggests that aggression may be associated with specialization in general but is not sufficient as the sole origin of scale-eating in the San Salvador Island pupfish radiation. Instead, it may be that shifts in behavior, kinematics, morphology, or a combination of many different factors is responsible for the evolution of scale-eating in this system. In chapter two, I explore the adaptive contributions of morphology and feeding kinematics to the evolution of scale-eating and find that scale-eating pupfish behaviorally mediate their feeding profile in order to produce large bites that may be adaptive for scale-feeding.

Chapter 2: Rapid adaptive evolution of scale-eating kinematics to a novel ecological niche

This chapter has been previously published and is reproduced here in accordance with the journal's article sharing policy:

St. John, M. E., Holzman, R., & Martin, C. H. (2020). Rapid adaptive evolution of scale-eating kinematics to a novel ecological niche. *The Journal of Experimental Biology*, jeb.217570. doi: 10.1242/jeb.217570

Abstract

The origins of novel trophic specialization, in which organisms begin to exploit novel resources for the first time, may be explained by shifts in behavior such as foraging preferences or feeding kinematics. One way to investigate the behavioral mechanisms underlying ecological novelty is by comparing prey capture kinematics between species. In this study, we investigated the contribution of kinematics to the origins of a novel ecological niche for scale-eating within a microendemic adaptive radiation of pupfishes on San Salvador Island, Bahamas. We compared prey capture kinematics across three species of pupfish while consuming shrimp and scales in the lab, and found that scale-eating pupfish exhibited peak gape sizes that were twice as large as all other species, but also attacked prey with a more obtuse angle between their lower jaw and suspensorium. We then investigated how this variation in feeding kinematics could explain scale-biting performance by measuring bite size (surface area removed) from standardized gelatin cubes. We found that a combination of larger peak gape and more obtuse lower jaw and suspensorium angles resulted in approximately 40% more surface area removed per strike, indicating that scale-eaters may reside on a performance optimum for scale-biting. To test whether feeding performance could contribute to reproductive isolation between species, we also measured feeding kinematics of F1 hybrids and found that their kinematics and performance more closely resembled those of generalists, suggesting that F1 hybrids may have low fitness in the scale-eating niche. Ultimately, our results suggest that the evolution of strike kinematics in this radiation is an adaptation to the novel niche of scale-eating.

Introduction

Determining how organisms use resources for the first time and occupy novel niches is an outstanding question in evolutionary ecology. Many changes accompany adaptation to a novel niche, and previous studies have investigated how shifts in behaviors (Bowman and Billeb 1965; Tebbich et al. 2010; Curry and Anderson 2012), morphologies (Ferry-Graham et al. 2001; Ferry-Graham 2002; Hata et al. 2011; Davis et al. 2018), physiologies (Arias-Rodriguez et al. 2011; Tobler et al. 2015, 2018), and kinematics (Janovetz 2005a; Patek et al. 2006; Cullen et al. 2013; McGee et al. 2013) can all facilitate this transition.

Studying shifts in kinematic traits—particularly those which affect prey capture and feeding—is especially promising, because they can provide biomechanical insights

into the origins of novel trophic niches. For example, the wimple piranha (*Catoprion mento*) uses a ram attack coupled with a uniquely large gape angle to knock scales free from its prey (Janovetz 2005a); syngnathiform fishes specialize on evasive prey items using power-amplified jaws (Longo et al. 2018); and the Pacific leaping blenny (*Alticus arnoldorum)* is able to feed and reproduce on land by using unique axial tail twisting to improve propulsion and stability for greater jumping performance (Hsieh 2010).

Differences in prey capture kinematics between species may also contribute to postzygotic extrinsic reproductive isolation by reducing hybrid feeding performance (Higham et al. 2016), which may lead to speciation (Henning et al. 2017; Matthews and Albertson 2017). For example, McGee et al. (2015) measured prey capture kinematics and performance in two sunfish species (Centrarchidae) and their naturally occurring hybrids. Hybrid sunfish displayed intermediate gape size compared to parental types and initiated strikes from an intermediate distance, yet their actual suction-feeding performance was less than predicted from these additive traits. Hybrid Lake Victoria cichlids (produced by crossing thick-lipped *Haplochromis chilotes* and thin-lipped *Pundamilia nyererei* parents) also exhibited lower foraging performance at removing prey from crevices compared to parental species, most likely due to antagonistic pleiotropy and genetic correlations between head and lip morphology (Henning et al. 2017). Despite these findings, few studies investigate how hybrid kinematics affect the evolution of ecological novelty or explicitly relate kinematics to performance consequences.

Scale-eating (lepidophagy) provides an excellent opportunity for connecting a mechanistic understanding of feeding kinematics with adaptation to a novel trophic niche. It is a rare trophic niche which has convergently evolved at least 20 times in approximately 100 fish species out of over 35,000 (Sazima 1983; Martin and Wainwright 2013a; Kolmann et al. 2018). Current hypotheses for the origins of scale-eating vary, but they all propose that it may be related to shifts in behaviors related to foraging, such as shifts in aggression, shifts from algae-grazing to scale-eating, and even shifts from removing epibionts or ectoparasites to scale-eating (Fryer et al. 1955; Greenwood 1965; Sazima 1983; St. John et al. 2019). This suggests that shifts in kinematics during feeding strikes may accompany the origins of scale-eating. However, only a few studies have investigated the feeding kinematics and performance of scale-eating fishes. Janovetz (2005) measured feeding kinematics of *C. mento* while consuming: 1) free floating scales, 2) whole fish, and 3) scales off the sides of fish, and found that scale-eating kinematics were different from those used during suction-feeding or biting. Interestingly, scale-eating attacks produced gape angles that ranged from 30-100% larger than those produced from consuming free-floating scales or whole fish respectively— suggesting that a larger gape is necessary for scale-eating. Furthermore, this variation in gape angle across food items was documented within individuals, indicating that scale-eating kinematics may be behaviorally mediated (Janovetz 2005). Other studies have also documented a significant interaction between kinematic traits, behavior, and morphology. For example, the Lake Tanganyikan scale-eating cichlids (*Perissodus microlepis)*, which possess an antisymmetric mouth morphology, are able to perform more successful scale-eating strikes using their dominant side (Takeuchi et al. 2012; Takeuchi and Oda 2017), and a similar behavioral laterality has been documented in a scale-eating characiform (*Exodon paradoxus;* Hata et al. 2011). While

these studies provide valuable insights into scale-eating kinematics and performance, the lack of comparative data on the kinematics of closely related non-scale-eating species or hybrids has so far limited further investigations of the origins of scale-eating.

The aim of our study was to fill the following knowledge gaps and shed light on the relationship between kinematic traits and occupation of a novel niche: First, comparisons of scale-eating kinematics across scale-eating and closely related non-scale-eating outgroup species is necessary for investigating the origins of ecological novelty. Without the comparative method it is impossible to determine which kinematic variables are unique or important for scale-eating. Second, very few kinematic studies investigate hybrid kinematics despite the fact that hybridization is quite common, especially among species that diverged recently (Hubbs 1955; Mayr 1963; Arnold 1992; Richards et al. 2019). Understanding hybrid kinematics, especially in the context of ecological novelty, is informative because 1) impaired performance in hybrids is a form of extrinsic postzygotic isolation between species (McGee et al. 2015; Higham et al. 2016) and 2) it can allow the decoupling of morphology, behavior, and kinematics making it easier to identify causative traits underlying performance (Holzman and Hulsey 2017). Finally, few studies connect observed variation in kinematics to variation in whole organism feeding performance (but see: Svanbäck et al. 2002; Takeuchi et al. 2012; China et al. 2017; Sommerfeld and Holzman 2019; Whitford et al. 2019). Making this connection is important because it can identify kinematic traits associated with performance tasks relevant to evolutionary fitness rather than simply describing phenotypic variation in kinematic traits, most of which may not be relevant to performance or fitness (Arnold 1983; Hu et al. 2017).

The scale-eating pupfish (*Cyprinodon desquamator*) is an excellent organism to investigate the interaction of kinematics and ecological novelty for several reasons. First, the scale-eating pupfish evolved within a recent sympatric radiation of pupfishes on San Salvador Island, Bahamas. This radiation is endemic to a few hypersaline lakes on the island (Martin and Wainwright 2013a; Martin et al. 2019), which were most likely dry during the last glacial maximum 10-15 kya (Hagey and Mylroie 1995). Second, the radiation provides closely related sister taxa for kinematic comparison including: 1) the scale-eating pupfish, 2) a generalist pupfish (*C. variegatus*), and 3) the snail-eating pupfish (*C. brontotheroides*). Phylogenetic evidence suggests that scale-eating pupfish form a clade across all lakes where they are found on San Salvador and that this clade is sister to a clade containing generalists and snail-eaters (Martin and Feinstein 2014; Lencer et al. 2017), although gene flow is still ongoing among all three species (Richards and Martin 2017; Richards et al. unpublished data). All three pupfish species can be crossed in the lab to measure the kinematics and performance of hybrid phenotypes.

The morphological similarities and differences between San Salvador pupfishes have also previously been described. Specifically, 1) like all cyprinodontiforms, pupfish species exhibit a vestigial ascending process of the premaxilla allowing for independent movement of the upper and lower jaws during jaw protrusion (Hernandez et al. 2009, 2018), and 2) scale-eating pupfish have two-fold larger, supra-terminal oral jaws compared to the smaller, terminal jaws of the generalist or snail-eating pupfish (Martin and Wainwright 2011, 2013a; Martin 2016). Their divergent morphology, along with Janovetz's (2005) finding that scale-eating strikes by the lepidophagous piranha (*C.*

mento) were associated with larger peak gapes, lead us to predict that scale-eating pupfish should have larger gapes during scale-eating strikes compared to closely related species, and that this increased peak gape should result from a larger angle between the anterior tip of the premaxilla, the quadrate-articular joint, and the anterior tip of the dentary.

We investigated the interaction between kinematics and ecological novelty in pupfishes using high-speed videos of the feeding strikes of San Salvador generalist, snail-eating, and scale-eating pupfishes, along with F1 hybrids. If shifts in kinematics are an evolutionary adaptation for the ecological novelty in this system, then scale-eaters may have divergent feeding kinematics compared to other species and may have greater feeding performance on scales. We tested this by: 1) comparing the feeding kinematics of scale-eating pupfish to other species during scale-eating and suction-feeding strikes, 2) investigating whether variation in kinematics was associated with bite performance (i.e. bite size), and 3) determining if F1 hybrid feeding kinematics differed from parental species.

Ultimately, we found that the feeding kinematics of scale-eating pupfish diverged from all other species and were not solely due to their increased oral jaw size. Instead, scale-eaters may be behaviorally mediating their feeding kinematics to optimize the surface area removed per strike, suggesting that scale-eater kinematics are a recent adaptation to scale-eating.

Methods

Collection and husbandry

We used seine nets to collect generalist, snail-eating, and scale-eating pupfishes from Crescent Pond, Little Lake, and Osprey Lake on San Salvador Island, Bahamas in July, 2017 and March, 2018. Wild-caught fish were maintained in 37-75L mixed-sex stock tanks at a salinity of 5-10 ppt and temperatures of 23-27℃. While in stock tanks, fish were fed a diet of frozen bloodworms, frozen mysis shrimp, and commercial pellet foods daily. In the lab, we crossed generalist and scale-eating pupfishes from both Little Lake and Crescent Pond to produce F1 hybrid offspring. Prior to filming, pupfishes were isolated in 2L tanks to maintain individual IDs throughout the study.

Feeding kinematics

We recorded pupfishes feeding on three different food items: frozen mysis shrimp (Mysida, Hikari Inc.), scales, and standardized gelatin cubes (dimensions: 1.5 cm x 1.5cm x 1.5 cm x 1.5 cm cube; Repashy Superfoods, Community Plus Omnivore Gel Premix; prepared following manufacturer's instructions). We measured feeding kinematics while fish consumed both shrimp and scales because it allowed us to ask whether 1) scale-eating pupfish differed in their feeding kinematics compared to other groups, 2) if the kinematics of scale-eating strikes differ from those used during suction feeding (e.g. shrimp), and 3) if F1 hybrid feeding kinematics differed from their parental species. We explicitly examined F1 hybrid kinematics in this study because lowered hybrid feeding performance may contribute to reproductive isolation between species and may shed light on rapid adaptive diversification of this clade. We additionally

measured feeding kinematics across all groups while fish consumed gelatin cubes to ask whether variation in kinematic traits affected feeding performance (i.e. bite size).

In the lab, fish freely consumed mysis shrimp, but we had to train all species to feed on scales from the sides of euthanized zebrafish (*Danio rerio*; stored frozen) and to feed from gelatin cubes (stored at 4℃). For training, we isolated each fish in a 2-liter plastic tank and presented a given food item (either euthanized zebrafish or gelatin cube) daily. If a pupfish began feeding on the item, it was left in the tank until the pupfish stopped feeding. If a pupfish did not begin feeding within one minute, the food item was removed from the tank. Any pupfish that did not feed received a supplemental feeding of commercial pellet food (New Life Spectrum Thera-A, medium sinking pellets). If an individual did not feed on a training item for more than two days, we reduced supplemental feedings to once every two days to ensure that the fish was sufficiently motivated. Once pupfish reliably began feeding on either scales or gelatin cubes, we proceeded to film their feeding behaviors according to the filming protocol below. Fish were never trained on more than one item at a time, and we instead ensured that all filming was completed for a single food item before proceeding to train for the next item.

For all three food items, we used a Sony Cyber-shot DSC-RX10 III or Sony Cyber-shot DSC-RX100 IV 20.1 MP to obtain high-speed videos (480 frames per second) of foraging strikes. Illumination was provided by a dimmable bi-color 480 LED light (Neewer) positioned approximately 0.3 m from the filming tank. Pupfish were allowed to acclimate to the lighting before feeding commenced. Fish were considered acclimated when they moved around their tank freely (usually after ~5 minutes). For scale-eating we used forceps to hold a euthanized zebrafish horizontally in the water column and perpendicular to the front of an individual. For mysis shrimp and gelatin cubes, we dropped the food item a few inches in front of an individual. All videos were taken from a lateral perspective. Once filming for one food item was completed, the process was repeated until we filmed each individual consuming all three food items.

Kinematic analyses

Videos were converted to image stacks and analyzed using the image processing software ImageJ (FIJI; Schindelin et al. 2012). To quantify feeding performance, we measured 10 kinematic trait metrics including 1) peak jaw protrusion, defined as the distance (mm) from the center of the orbit to the anterior tip of the premaxilla. 2) Time to peak jaw protrusion, defined as the time (s) from the start of an attack (defined as 20% of peak gape) to peak protrusion. 3) Peak gape, defined as the distance (mm) from the anterior tip of the premaxilla to the anterior tip of the dentary. 4) Time to peak gape, defined as the time (s) from the start of an attack at 20% of peak gape to peak gape. 5) Gape angle was the angle (degrees) produced at peak gape between the anterior tip of the premaxilla, the quadrate-articular joint, and the anterior tip of the dentary. 6) Lower jaw angle was the angle produced at peak gape between the lower jaw, the quadrate-articular joint, and the ventral surface of the fish beneath the suspensorium (Figure 1&2). 7) Time to impact was the time (s) from the start of an attack (20% peak gape) to first contact of oral jaws with the prey item. 8) Time from peak gape to impact was the difference between the time to impact (s) and the time to peak gape (s). 9) Starting distance from prey was the distance (mm) from the center of the orbit at the start of an attack to the center of the orbit at impact with prey item. Finally, 10) ram speed was the

starting distance from prey at 20% of peak gape (m) divided by the time to impact (s). In addition to our kinematic metrics, we also measured body length and lower jaw length (Table S1) using images from the video. We calibrated each video using a grid, positioned at the back of the filming tank.

Measuring bite size

In order to relate variation in feeding kinematics to variation in bite size we recorded high-speed strikes on gelatin meal replacement for fish in the shape of a 1.5 x 1.5 x 1.5 cm cube. Upon filming a feeding strike on a single cube, we immediately removed the cube from the tank. The gel cube retains its shape in water and therefore allowed us to precisely photograph and measure the area removed by each bite. We used an Olympus Tough TG-5 camera to take photos of each lateral surface of the cube – ensuring that we had photographed the entire bite—and measured the total surface area removed (pixels^2) from the cube (Figure 3B). We then standardized bite sizes across photos by calculating bite area as a proportion relative to a standardized grid present in each photo, and converting this proportional data into area (mm^2) by multiplying the proportion times the area of the grid (573.12 mm^2). One caveat is we did not measure the depth of the bite, which may be affected by additional kinematic variables during the strike. However, scale-eating attacks observed in the lab and field do not typically produce deep wounds in which bite depth would be relevant, thus we expect that surface area is the best proxy for scale-biting performance in this system. Although bites were removed from both the lateral surface and edge of the gelatin cubes during strikes, there was no significant difference in surface area removed (*t*-test, $P = 0.12$).

Statistical analyses

Comparing strike kinematics

We collected and analyzed 101 feeding strikes from 31 individuals striking both shrimp and scales (7 generalists; 7 snail-eaters; 9 scale-eaters; 8 F1 hybrids). We used linear mixed models (LMMs) in the lme4 package (Bates et al. 2014) in R (R Core Team 2018) to determine if any of our kinematic metrics varied between species or food item. A mixed model approach is appropriate for these data, because it accounts for errors due to repeated measures (Holzman et al. 2008; Holzman and Wainwright 2009). In each model we included: 1) the kinematic metric as the response variable, 2) species designation, food item, and their interaction as fixed effects, 3) individual fish IDs and population nested within species as random effects, and 3) log body size as a covariate (Table 1). Although we compared kinematic data across multiple species, very few genetic variants are fixed between species (<1,000 SNPs out of 12 million) and generalists and molluscivores cluster by lake rather than by species (McGirr and Martin 2017; Richards and Martin 2017; McGirr and Martin unpublished data; Richards et al. unpublished data). Thus, it is appropriate to analyze species differences at these recent timescales as population-scale data using mixed model analyses of independent populations (e.g. Hatfield and Schluter 1999; McGee et al. 2013), rather than phylogenetic comparative methods.

We also performed a linear discriminant analysis (LDA) on the combined shrimp and scales kinematic data to reduce dimensionality and identify which kinematic metrics

contributed most to differences between species (Table 2, Figure 1A). We used a MANOVA and Wilks' ƛ to assess the significance of the LDA. We did not have enough degrees of freedom to perform these analyses with all of our kinematic variables, so we excluded time to peak protrusion and time to impact as they were highly correlated with time to peak gape (Table S2, $r^2 > 0.85$), and also excluded distance from prey as it was highly correlated with ram speed (Table S2, $r^2 = 0.90$). Our MANOVA ultimately included 1) peak protrusion, peak gape, time to peak gape, gape angle, lower jaw angle, time from peak gape to impact, and ram speed as response variables, 2) species designation as a predictor variable, and 3) individual ID as a random effect.

Determining how kinematic variables affect bite performance

We collected and analyzed 31 strikes on cubes across all three species and F1 hybrids. We used generalized additive models (GAMs) from the mgcv package (Wood 2011) in R to investigate how peak gape, peak protrusion, gape angle and lower jaw angle affected bite size. We used GAMs for this analysis because they do not assume a linear relationship between performance (i.e. bite size) and our given kinematic variables, but instead can fit smoothing splines to the data to test for nonlinear associations. We used AIC scores to select our optimal model (Table 3). We started with the most complete model which included 1) bite size as the response variable 2) a spline modeling the interaction between two of our predictor variables, and 3) a single fixed effect. There were insufficient degrees of freedom to test all four terms at once in this model, therefore we tested all combinations of this model with our four predictor variables (Table 3A). We also tested all nested versions of this complex model by 1) removing the interaction term, but maintaining two splines and a fixed effect (Table 3B), 2) removing one spline and including three fixed effects (Table 3C), and finally 3) by testing the model with all four variables as only fixed effects (Table 3D). Ultimately, our best supported model included bite size as the response variable, a thin-plate spline of the interaction between peak gape and gape angle, and lower jaw angle as a fixed effect (ΔAIC of next best fitting model =32.56).

Finally, we predicted the bite size for each fish from their peak gape and gape angle kinematic measurements using a machine-learning algorithm from the caret package (Kuhn 2008) using a spline-based method. Using predictive modeling allowed us to address two problems from our original cube dataset and analysis: First, cubes are an ideal food item for connecting variation in kinematics to bite size (something that was very difficult to do with shrimp and zebrafish), but are ultimately an unnatural food item for fish, and their feeding strikes on cubes may not reflect feeding on natural prey. Predictive modeling allowed us to use strikes performed on zebrafish and shrimp and estimate bite sizes for each relevant prey item. Second, the cube dataset and analysis did not look for variation across species, and instead, explicitly connected variation in feeding kinematics (regardless of species) to bite size. Applying our predictive model to the shrimp and zebrafish dataset allowed us to gain additional insight into differences between species (Figure 4).

We used a GAM model, estimating the effect of gape size and gape angle on the area removed from gelatin cubes, to predict bite performance (bite size) from the 101 feeding strikes on scales and mysis shrimp used in our previous analyses. Although we would not realistically expect suction feeding strikes on mysis shrimp to result in a bite

per se, we found no difference in any kinematic traits between food items and therefore used strikes on both scales and shrimp for this analysis.

Ideally, we would have used our best-fitting GAM model, which also included lower jaw angle as a fixed effect. However, the caret package currently only accepts two fixed effects, and lower jaw angle ultimately did not affect bite size (P = 0.219). We trained the model using all strikes observed on gelatin cubes (31 strikes across all three species and F1 hybrids) and 10-fold cross-validations with three repeats as the resampling scheme. We tested the accuracy of this model by comparing fitted values from the model to observed values from the data set and found that our model was able to predict 46% of the variance in the gelatin-strike dataset (df=1, F= 25.06 , P=2.5x10^{-5}, R^2=0.46). We then used this model to predict bite size from each scale-biting and suction-feeding strike based on the kinematic measurements alone. We used bootstrap resampling (10,000 iterations) to calculate mean bite size and 95% confidence intervals for each species.

Determining if hybrid kinematics match additive predictions

We calculated the predicted values for peak gape, lower jaw angle, and bite size for the scale-eater x generalist F1 hybrids under the hypothesis that these kinematic traits would be additive and therefore intermediate between generalist and scale-eater values. We used a one sample t-test to test whether the observed values of the three traits (peak gape, lower jaw angle, predicted bite sizes) for F1 hybrids deviated from additive predictions.

Results

Scale-eaters exhibited divergent feeding kinematics compared to other pupfishes

Scale-eaters exhibited divergent feeding kinematics, while consuming both shrimp and scales, compared to other groups (Figure 1A). A MANOVA supported the significance of this discriminant analysis and found that species designation was a significant predictor of kinematics (Wilks' ƛ = 0.13; F = 3.05; df = 3; P= 0.00036). Species significantly varied in their peak gape and lower jaw angles during feeding strikes—regardless of the food item— in a linear mixed model controlling for individual ID and body length (Table 1). This pattern was driven by scale-eaters who had peak gapes that were twice as large as other species, but also had lower jaw angles with their suspensorium that were 14% more obtuse than other species (Figure 1B, C). Importantly, the scale-eaters' more acute angle of the jaw complex with respect to their body, along with their greatly enlarged oral jaws, allows them to have increased peak gape while maintaining the same gape angle as other species (Figure 2). This may allow their upper jaws to more effectively 'rake' scales from the prey surface. Ram speed was the only kinematic variable that marginally varied between food items: strikes on shrimp were approximately 16% faster than those on scales (Table 1, Figure S1; P = 0.053).

Variation in strike kinematics affected bite size performance

GAM modeling indicated that the thin-plate spline of the interaction between peak gape and gape angle was significantly associated with bite size (edf=22.85, F=3.27, P= 0.0391). However, the fixed effect of lower jaw angle was not significant (t=-1.37,

P=0.219). Ultimately this model explained 94.6% of the observed deviance in bite size, and suggests that large gapes of about 4-5mm paired with gape angles of 80° are associated with larger bites (Figure 3).

F1 hybrid kinematics are not strictly additive and more closely resemble generalist kinematics

F1 hybrid feeding kinematics differed from scale-eater kinematics (Tukey HSD, peak gape: $P = 1.2x10^{-6}$, lower jaw angle: $P = 0.0090$), but were not significantly different from generalist kinematics (Tukey's HSD, peak gape: $P = 0.21$, lower jaw angle: $P = 0.37$). Mean hybrid peak gape was 39% smaller than scale-eater peak gape and 32% larger than generalist peak gape (Figure 1B). Similarly, mean hybrid lower jaw angle was 9.5% more acute than scale-eater peak lower jaw angle, and 5.6% more obtuse than the mean generalist lower jaw angle (Figure 1C). F1 hybrids failed to match additive predictions of intermediate kinematics (i.e. the mean of the two parental species) for peak gape (t-test, μ= 3.035, mean= 2.52 mm, $P = 0.013$), but did meet these predictions for lower jaw angle (t-test, μ= 136.5, mean= 133.92 degrees, $P = 0.18$). Our machine learning model also predicted that scale-eater kinematics would result in bite sizes that are approximately 40% larger than the predicted bites of the other species (Figure 4). Estimates for F1 hybrid bite sizes were approximately 5% smaller than expected based on additive predictions (*t*-test, predicted= 6.40 mm^2, observed= 6.08 mm^2, $P = 0.49$).

Discussion

Scale-eating pupfish have divergent feeding kinematics

Scale-eating pupfish exhibited peak gapes that were twice as large as other groups, but simultaneously displayed gape angles that were not different from other groups, and lower jaw angles that were 12% more obtuse. Thus, scale-eaters kept their jaws more closed during strikes compared to other species, resulting in smaller gape sizes than the maximum achievable gape given their morphology. These counterintuitive results only partially support our prediction that scale-eaters should have larger peak gapes, similar to the findings of Janovetz (2005) for the scale-eating piranha. Increased gape size in scale-eating pupfish was not due to an increased gape angle as we predicted. Instead, scale-eaters appear to maintain the same gape angle of their oral jaws as in other species (~80°) and increased their lower jaw angle resulting in more closure of their jaws during strikes. Morphologically, it appears that scale-eaters are not physically constrained from depressing their lower jaw much more than the observed 150° during strikes (Figure 2D), indicating that their obtuse lower jaw angles are decreasing their physically obtainable maximum peak gape (Figure 2). For example, if a scale-eater were to adopt a generalist lower jaw angle of 130°, they could increase their peak gape by about 8%. One possibility is that this more obtuse lower jaw angle is an artifact of filming scale-eating strikes in the lab. To investigate this, we analyzed four scale-eating strikes performed by wild scale-eaters observed in Crescent Pond, San Salvador Island, Bahamas (filmed using a Chronos camera (Kron Technologies, model 1.4, 16 GB memory, Color image sensor) with an f1.4 zoom lens in a custom underwater housing (Salty Surf, Inc. Krontech Chronos 1.4 housing with M80 flat port) and compared their

jaw angles to those seen in the lab. Wild strikes had an even more obtuse mean lower jaw angle of 168° whereas scale-eating strikes in the lab had a mean lower jaw angle of 153°, suggesting that an obtuse lower jaw angle is also used during natural scale-eating strikes in hypersaline lakes on San Salvador Island.

Strike kinematics did not vary across prey items (Table 1), contrary to Janovetz (2005). In fact, the only kinematic variable that remotely varied between prey items was ram speed (Table 1, Figure S1), but this may simply be due to the fact that sinking frozen shrimp were a moving target during feeding trials while euthanized zebrafish were held stationary with forceps for scale-eating strikes. Alternatively, phenotypic plasticity due to rearing environment could produce a similar pattern; however, we did not observe any differences in strike kinematics between wild caught and lab-reared fish.

Is jaw morphology solely responsible for kinematic variation?

The kinematic variables that varied the most between scale-eating and non-scale-eating pupfishes were peak gape and lower jaw angle—both related to the size of the oral jaws. Previous work has documented that the oral jaws of scale-eating pupfish are two-fold larger than their sister species (Holtmeier 2001; Martin and Wainwright 2013a; Martin 2016) and may be controlled by four moderate-effect QTL with all positive effects on jaw size, consistent with directional selection on this trait (Martin et al. 2017). It may be that increased oral jaw size is sufficient to create variation in feeding kinematics without an accompanying shift in behavior. Previous studies have documented how changes in morphology alone can alter feeding kinematics. For example, kinematic studies have found that the scaling of the lower jaw in bluegill (Wainwright and Shaw 1999) and body size in largemouth bass (*Micropterus salmoides;* Richard and Wainwright 1995) both significantly affected prey capture kinematics. Furthermore, Ferry-Graham et al. (2010) used the pike killifish (*Belonesox belizanus*) to show that simply doubling the length of the jaws significantly affected key kinematic variables such as peak gape size—even while keeping lower jaw angle constant. Simply stated, the key adaptation necessary for scale-eating may be enlarged, supra-terminal jaws. If this hypothesis were true, we would expect that peak gape would increase with jaw size and that gape angle would increase with the shift from terminal to supra-terminal jaws, but all other kinematics variables would remain constant across species. Our results reject this hypothesis. Instead, scale-eaters maintain the gape angle observed in other species and increase their lower jaw angle with the suspensorium by 12 degrees resulting in a reduction in their potential peak gape size (Figure 2). This suggests that scale-eaters have evolved more obtuse lower jaw angles during strikes to increase feeding performance (Figures 3&4). Another explanation for the obtuse lower jaw angles observed in scale-eaters may be related to the position of the lower jaw joint. In scale-eaters, the lower jaw joint is more ventral than it is in generalists and snail-eaters due to the supra-terminal position of the mouth. This positioning may physically constrain how acute the lower jaw angle can be, preventing scale-eaters from depressing their lower jaws past an angle of ~150°. However, this is highly unlikely because the lower jaws of cleared and alizarin-stained scale-eating pupfish specimens can be depressed to angles as small as ~100° with the suspensorium (Figure 2B). The jaws of cleared and stained generalists can be depressed to a similar angle (Figure 2D).

This strongly suggests that scale-eater morphology does not physically constrain them from opening their jaws even larger than observed during strikes.

Scale-eating performance optimum

Scale-eaters may have reduced their lower jaw angles relative to other species in order to remain on a performance optimum for scale-eating. Our models of bite size supported this: peak gapes larger than approximately 4.5 mm counterintuitively resulted in smaller bite sizes (Figure 3A&C). An enlarged lower jaw angle in scale-eating pupfish results in a lower jaw that points directly towards the prey during strikes – possibly resulting in greater stability for biting scales while retaining a large gape (Figure 2). This large gape and unique jaw alignment may allow scale-eaters to attack prey from a roughly perpendicular angle (as frequently observed during field observations) — appearing to wrap their large lower jaw under prey items and subsequently scraping scales from their sides using their independently protrusible upper jaws (also observed in a scale-eating characin: Hata et al. 2011). Interestingly, perpendicular angles of attack and large gapes are associated with scraping in benthic feeding fish (Van Wassenbergh et al. 2008; O'Neill and Gibb 2013). In fact, two prominent hypotheses for the origins of scale-eating are that it arose from 1) an algae-scraping ancestor or 2) an ancestor specializing on scraping parasites from other fish (Sazima 1983).

One caveat for this hypothesis, however, is that our current performance estimates do not include all possible combinations of peak gape and lower jaw angle and few observations of the largest peak gape sizes. Future work should estimate performance across multiple performance axes (e.g. Stayton 2019, Keren et al. 2018, Dickson and Pierce 2019), ideally using F2 hybrids. F2 hybrids are a useful tool for this type of experiment, as they are the first generation of offspring in which recombination among parental alleles can produce new combinations of kinematic, morphological, and behavioral traits not observed in the F0 or F1 generations. Identifying and measuring other traits that may be important for scale-eating, such as bite force, bite depth, or endurance (which may affect prey acquisition), would also be informative.

Non-additive F1 hybrid feeding kinematics may contribute to reproductive isolation of scale-eaters

It is well documented that complex performance traits, such as feeding kinematics, are most likely controlled by numerous loci (i.e. polygenic), and can mostly be described as additive (reviewed in Sella and Barton 2019). We therefore expected F1 hybrids to exhibit intermediate kinematics and performance relative to both parental species. Instead, we found that F1 hybrid kinematics more closely resembled generalists (Table 1; Figure 1) suggesting that F1 hybrids may have higher performance in a generalist trophic niche.

Current evidence from field fitness experiments supports the idea that hybrid pupfish exhibit better performance in the generalist ecological niche compared to their performance in the scale-eater niche. One field experiment in these lakes measured hybrid fitness in the wild and found high mortality and low growth rates for hybrids most closely resembling the scale-eating phenotype (Martin and Wainwright 2013b). Furthermore, for the few hybrids resembling scale-eaters which did survive, only 36% had recently consumed any scales compared to 92% of wild-caught scale-eaters

(Martin and Wainwright 2013a,b). Impaired hybrid performance in the scale-eating niche may contribute to extrinsic postzygotic isolation between species (McGhee et al. 2007; McGee et al. 2013; Higham et al. 2016). Reproductive isolation may also evolve more quickly in species that occupy a more distant fitness peak with a larger fitness valley such as the scale-eating pupfish due to stronger selection against hybrids and reinforced pre-mating isolation (Martin and Feinstein 2014). Thus, impaired hybrid scale-eating performance could also contribute to increased diversification rates through the mechanism of a wider fitness valley.

Low hybrid performance may also be due to the morphological differences between scale-eaters and generalists. As mentioned above, it is possible that a shift in morphology – such as enlarged oral jaws in scale-eaters—may be sufficient to change kinematic profiles alone. F1 hybrid kinematics clearly differed from scale-eater kinematics, but their jaw lengths were also significantly smaller than the jaws of scale-eaters (Tukey's HSD, $P = 5.21 \times 10^{-5}$). Furthermore, previous work has shown that F1 hybrid pupfish offspring (produced from generalist x scale-eater crosses) tend to develop along a more similar trajectory to their maternal parent (Holtmeier 2001). This could indicate that F1 hybrid pupfish with scale-eating mothers are more likely to develop jaws resembling a purebred scale-eater, but may also retain their generalist-like kinematics. The resulting mismatch between morphology, kinematic traits, and ecological niche may be driving low hybrid survival in the scale-eating niche and contributing to reproductive isolation between generalist and scale-eating pupfish species.

Conclusion

In conclusion, this study explicitly takes advantage of an adaptive radiation of *Cyprinodon* pupfishes to make comparisons of scale-eating kinematics across multiple species. This comparative approach allowed us to pinpoint traits that are important for scale-eating. Our results suggest that shifts in key kinematic traits may have preceded or facilitated the origin of scale-eating in *Cyprinodon* pupfishes. Scale-eating pupfish exhibited peak gapes that were twice as large as other pupfish species, but simultaneously had lower jaw angles that were significantly larger. We also directly connected variation in kinematic traits to feeding performance—a step that is rarely taken in kinematic studies. Surprisingly, we found that this unique combination of scale-eater kinematics may reside on a performance optimum, as large peak gapes and large lower jaw angles resulted in larger bite sizes. Impaired F1 hybrid kinematics and performance in the scale-eating niche also suggests that kinematic traits contribute to reproductive isolation of the scale-eating pupfish and the evolution of ecological novelty. Future work should investigate if other performance optima exist on the kinematic landscape and whether F2 hybrid fitness in the wild is reduced due to a mismatch between morphology and feeding kinematics.

Data Accessibility

All analyses reported in this article can be reproduced using the data provided by St. John and Martin (2019). Raw data will be deposited in Dryad.

Acknowledgements

We thank the University of California, Berkeley, University of North Carolina at Chapel Hill, NSF CAREER 1749764, NIH 5R01DE027052-02, and BSF 2016136 for funding to CHM and the UNC Quality Enhancement Plan for course-based undergraduate research (CURE) funding to CHM. The Bahamas Environmental Science and Technology Commission and the Ministry of Agriculture kindly provided permission to export fish and conduct this research. Rochelle Hanna, Velda Knowles, Troy Day, and the Gerace Research Centre provided logistical assistance in the field; Kristi Dixon, Casey Charbonneau, Gabriel Harris, Amelia Ward, Delaney O'Connell, and the undergraduate students of BIO221L 'Evolution of Extraordinary Adaptations' assisted with high-speed videography and kinematic analysis. All animal care protocols were approved by the University of California, Berkeley and the University of North Carolina at Chapel Hill Animal Care and Use Committees.

Tables

Table 1. Results of linear mixed models investigating if strike kinematic variables vary between 1) species (generalists, snail-eaters, scale-eaters, or hybrids), 2) food item (shrimp or scales), or 3) the interaction between the two. Significant predictors are indicted in bold.

Response	Predictors	χ^2	*df*	*P*
Peak Protrusion (mm)				
	Species	4.01	3	0.26
	Food Item	1.10	1	0.29
	log(Body Length)	3.01	1	0.082
	Species:Food Item	2.03	3	0.57
Time to Peak Protrusion (s)				
	Species	3.80	3	0.27
	Food Item	0.73	1	0.39
	log(Body Length)	1.02	1	0.31
	Species:Food Item	4.03	3	0.26
Peak Gape (mm)				
	Species	**23.13**	**3**	**3.8×10^{-5}**
	Food Item	0.71	1	0.40
	log(Body Length)	1.24	1	0.27
	Species:Food Item	0.65	3	0.88
Time to Peak Gape (s)				
	Species	2.43	3	0.49
	Food Item	0.57	1	0.45
	log(Body Length)	2.80	1	0.17
	Species:Food Item	1.87	3	0.60
Gape Angle (degrees)				
	Species	3.28	3	0.35
	Food Item	0.032	1	0.86
	log(Body Length)	1.01	1	0.32
	Species:Food Item	3.43	3	0.33
Lower Jaw Angle (degrees)				
	Species	**18.62**	**3**	**0.00033**
	Food Item	0.0031	1	0.96
	log(Body Length)	3.53	1	0.060
	Species:Food Item	3.56	3	0.31
Time to Impact (s)				
	Species	2.55	3	0.47
	Food Item	2.05	1	0.15
	log(Body Length)	1.40	1	0.24
	Species:Food Item	4.69	3	0.20

Time from Peak Gape to Impact (s)				
	Species	2.44	3	0.48
	Food Item	0.97	1	0.32
	log(Body Length)	0.57	1	0.45
	Species:Food Item	1.39	3	0.71
Starting Distance from prey (mm)				
	Species	0.43	3	0.93
	Food Item	1.99	1	0.16
	log(Body Length)	2.77	1	0.10
	Species:Food Item	0.80	3	0.85
Ram speed (m/s)				
	Species	3.25	3	0.35
	Food Item	3.75	1	0.053
	log(Body Length)	1.55	1	0.21
	Species:Food Item	2.02	3	0.57

Table 2. Results of a linear discriminant analysis for kinematic variables for strikes on shrimp and scales.

Kinematic Metrics	LD1	LD2	LD3
Peak Jaw Protrusion (mm)	-0.082	-0.49	-0.065
Peak Gape (mm)	1.55	0.39	-0.56
Time To Peak Gape (s)	-8.00	12.16	10.24
Gape Angle (degrees)	-0.032	-0.012	-0.033
Lower Jaw Angle (degrees)	0.069	0.0029	0.022
Time to Impact (s)	-9.85	31.32	-33.03
Ram speed (m/s)	-7.98	17.27	10.67
Proportion of Trace	0.92	0.056	0.028

Table 3. Results of GAM model comparisons using AIC score. The best-fitting model is indicated in bold.

	Model		ΔAIC
A	1	Area~s(Peak Gape, Peak Protrusion, bs="ts")+(Lower Jaw Angle)	38.76
	2	Area~s(Peak Gape, Peak Protrusion, bs="ts")+(Gape Angle)	39.81
	3	**Area~s(Peak Gape, Gape Angle, bs="ts")+(Lower Jaw Angle)**	**0**
	4	Area~s(Peak Gape, Gape Angle, bs="ts")+(Peak Protrusion)	44
	5	Area~s(Peak Gape, Lower Jaw Angle, bs="ts")+(Peak Protrusion)	42.86
	6	Area~s(Peak Gape, Lower Jaw Angle, bs="ts")+(Gape Angle)	43.97
	7	Area~s(Peak Protrusion, Lower Jaw Angle, bs="ts")+(Peak Gape)	41.75
	8	Area~s(Peak Protrusion, Lower Jaw Angle, bs="ts")+(Gape Angle)	44.55
	9	Area~s(Peak Protrusion, Gape Angle, bs="ts")+(Peak Gape)	36.93
	10	Area~s(Peak Protrusion, Gape Angle, bs="ts")+(Lower Jaw Angle)	44.29
	11	Area~s(Gape Angle,Lower Jaw Angle, bs="ts")+(Peak Gape)	41.75
	12	Area~s(Gape Angle,Lower Jaw Angle, bs="ts")+(Peak Protrusion)	44.87
B	13	Area~s(Peak Gape)+ s(Peak Protrusion)+(Lower Jaw Angle)	32.56
	14	Area~s(Peak Gape)+ s(Peak Protrusion)+(Gape Angle)	34.64
	15	Area~s(Peak Gape)+ s(Gape Angle)+(Lower Jaw Angle)	37.35
	16	Area~s(Peak Gape)+ s(Gape Angle)+(Peak Protrusion)	34.64
	17	Area~s(Peak Gape)+ s(Lower Jaw Angle)+(Peak Protrusion)	32.56
	18	Area~s(Peak Gape)+ s(Lower Jaw Angle)+(Gape Angle)	34.88
	19	Area~s(Peak Protrusion)+s(Lower Jaw Angle)+(Peak Gape)	43.45
	20	Area~s(Peak Protrusion)+s(Lower Jaw Angle)+(Gape Angle)	47.74
	21	Area~s(Peak Protrusion)+s(Gape Angle)+(Peak Gape)	44.15
	22	Area~s(Peak Protrusion)+s(Gape Angle)+(Lower Jaw Angle)	47.97
	23	Area~s(Gape Angle)+s(Lower Jaw Angle)+(Peak Gape)	45.07
	24	Area~s(Gape Angle)+s(Lower Jaw Angle)+(Peak Protrusion)	47.74
C	25	Area~s(Peak Gape)+Peak Protrusion+Lower Jaw Angle+Gape Angle	33.8
	26	Area~s(Peak Protrusion)+Peak Gape+Lower Jaw Angle+Gape Angle	45.45
	27	Area~s(Lower Jaw Angle)+Peak Protrusion+Peak Gape+Gape Angle	45.45
	28	Area~s(Gape Angle)+Peak Protrusion+Peak Gape+Lower Jaw Angle	45.45
D	29	Area~Peak Gape+Peak Protrusion+Lower Jaw Angle+Gape Angle	45.45

Figures

Figure 1.

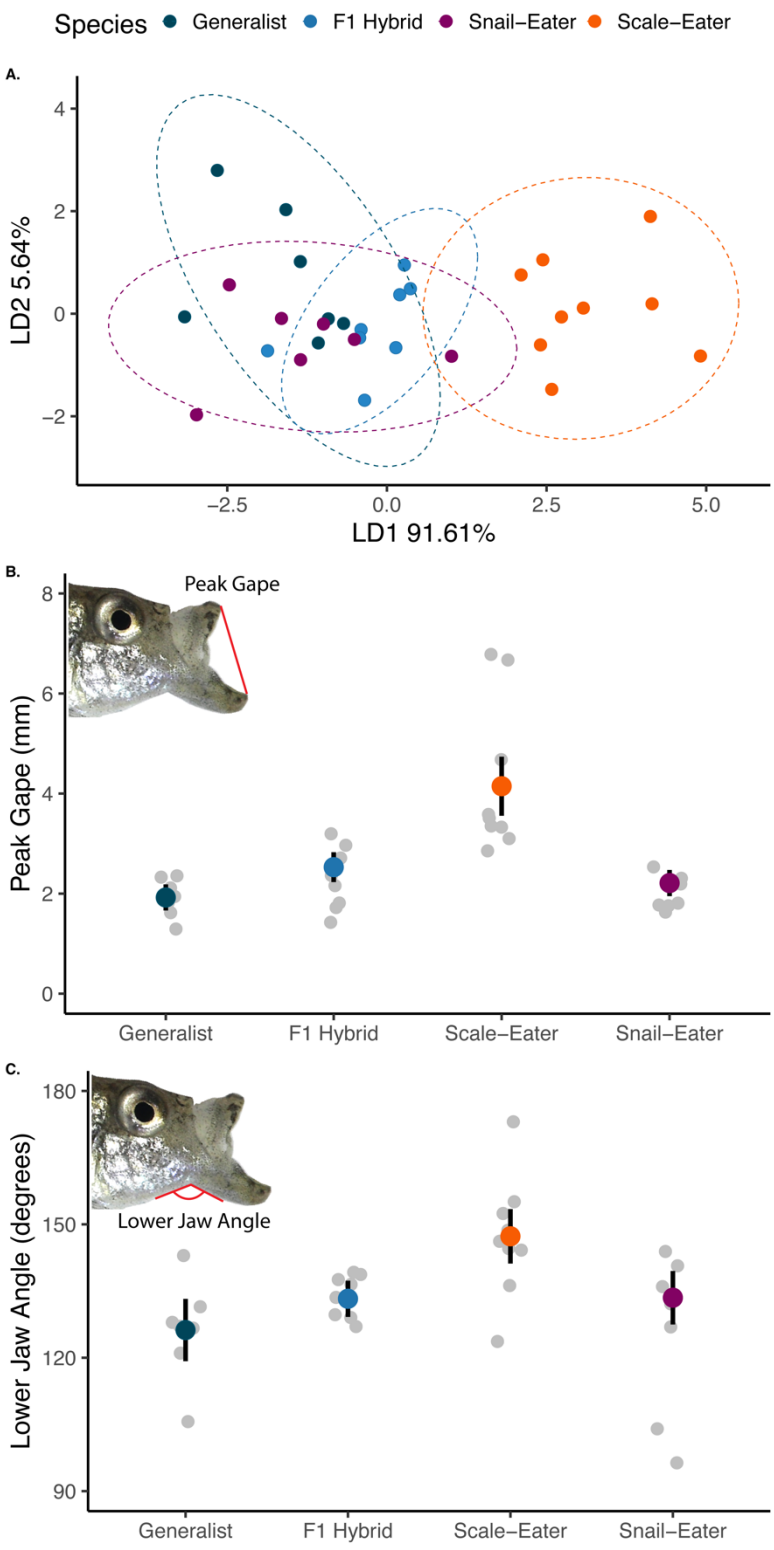

Figure 1. Divergent feeding kinematics in scale-eaters. A) Biplot of discriminant axes 1 (LD1) and 2 (LD2) describing overall kinematic differences among pupfish groups (generalists, snail-eaters, scale-eaters, or F1 hybrids). Ellipses represent 95% CIs. B) Mean peak gape (mm) for each species with ± 95% CIs calculated via bootstrapping (10,000 iterations). C) Mean lower jaw angle at peak gape (mm) for each species with ± 95% CIs calculated via bootstrapping (10,000 iterations).

Figure 2.

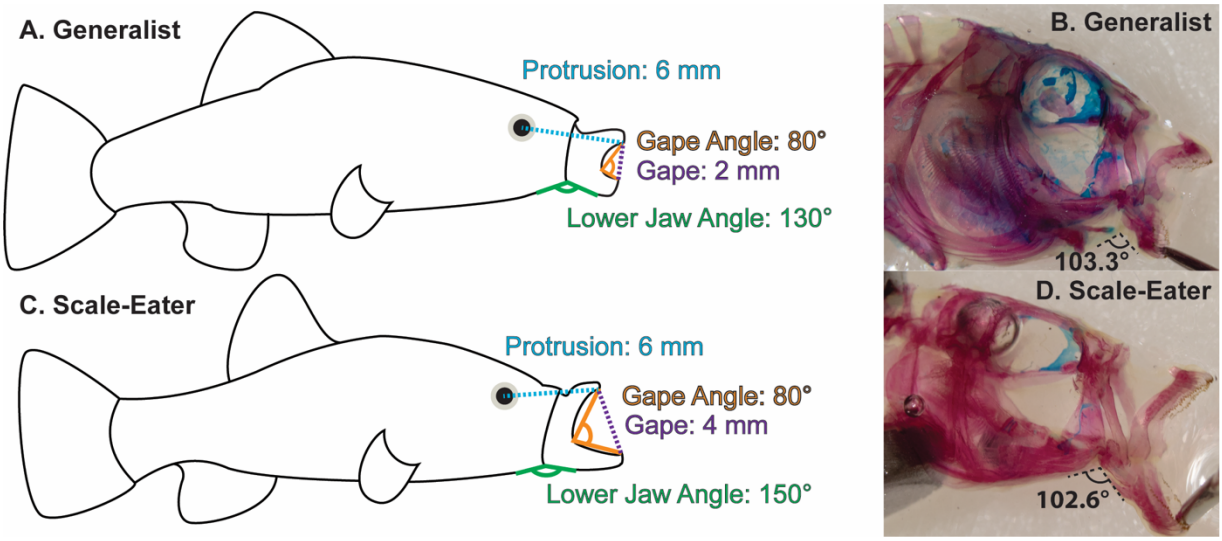

Figure 2. The large jaws of scale-eating pupfish allow them to double their gape size and increase the angle between their lower jaw and suspensorium (lower jaw angle) while maintaining the same gape angle as other species during feeding strikes. A) Hypothetical measurements of a generalist's protrusion distance, peak gape, and lower jaw angle if they strike a food item with an 80° gape angle. B) Lower jaw angle produced by maximum depression of a generalist's lower jaw on a cleared and alizarin/alcian blue double-stained specimen. C) Hypothetical measurements of a scale-eater's protrusion distance, peak gape, and lower jaw angle if they strike a food item with an 80° gape angle. D) Lower jaw angle produced by maximum depression of a scale-eater's lower jaw.

Figure 3.

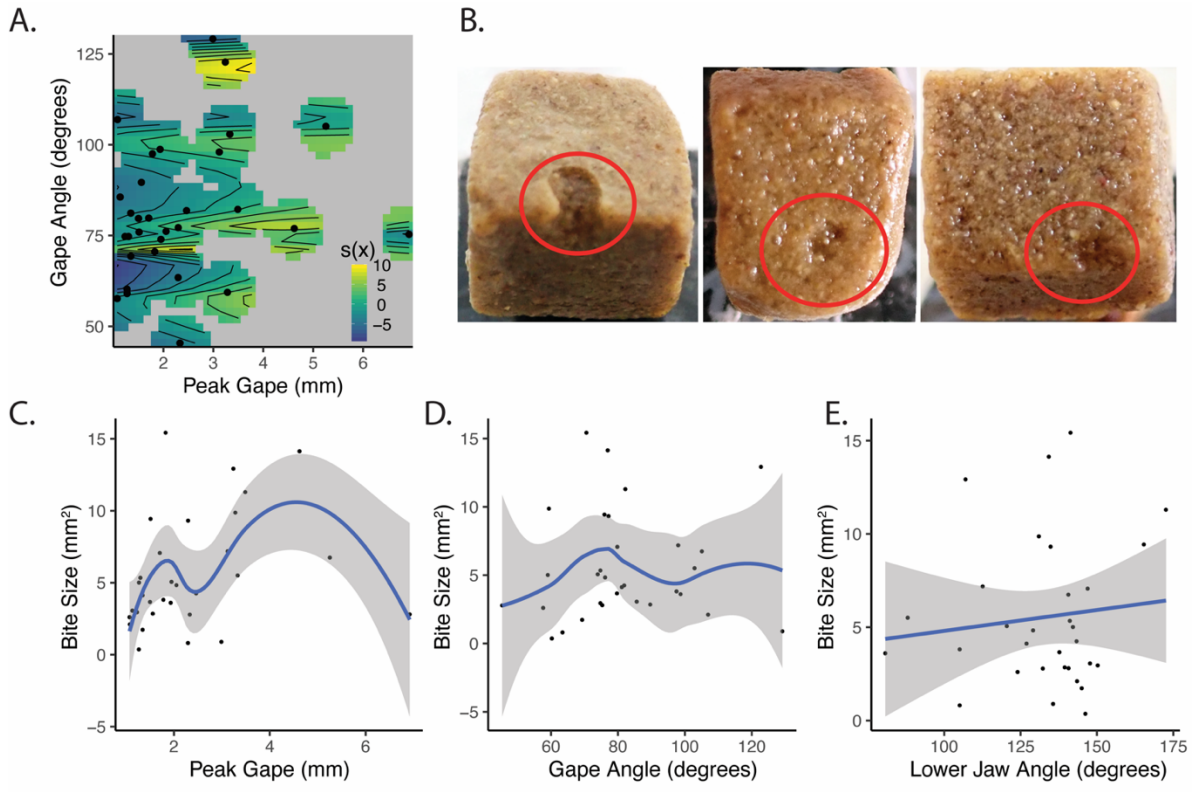

Figure 3. The interaction of peak gape and gape angle may result in a performance optimum for scale-biting. A) Visualization of the two-way thin-plate spline from the best fitting GAM model. Points represent raw data and colors represent relative bite sizes from a thin-plate spline fit to peak gape (mm) and gape angle (degrees). Estimates of the surface by the GAM model are only calculated in regions containing data. B) Representative scale-eating bites taken out of gelatin cubes. Visualization of the relationship between bite size (surface area removed from the gelatin cube per strike) and C) peak gape (mm), D) gape angle, and E) lower jaw angle from the best fitting GAM model. Points represent raw data from each strike and lines represent univariate splines (C and D) or a linear regression (E) fit to the data along with 95% CIs in grey.

Figure 4.

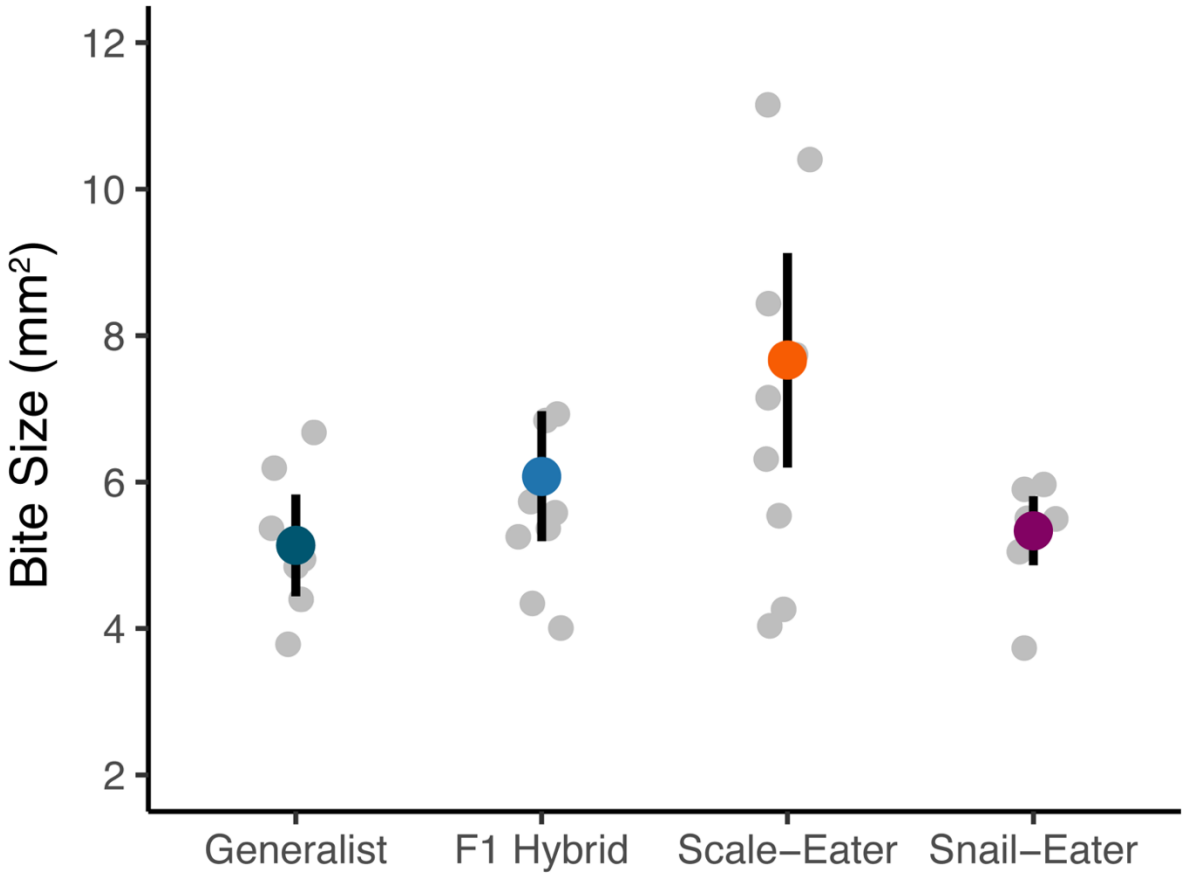

Figure 4. Scale-eaters have larger predicted bite sizes compared to other groups. Predicted bite sizes for all strikes from each species using machine-learning optimization of GAM models. Grey points represent predicted bite sizes for individuals, color points represent means, and bars represent ± 95% CIs calculated via bootstrapping (10,000 iterations).

Supplemental Material

Supplemental tables

Table S1. Jaw length varies between species. Results of linear mixed model investigating if any morphological traits varied between species. Significant predictors are indicated in bold.

Response	Predictors	χ^2	df	*P*
Log Body Length				
	Species	6.36	3	0.095
Log Jaw Length				
	Species	**45.87**	**3**	**6.039×10^{-10}**

Table S2. Correlation matrix describing the relationship between 10 kinematic variables. Variables that are highly correlated ($r^2 > .8$) are indicated in bold

	Peak Protrusion	Time to Peak Protrusion	Peak Gape	Time to Peak Gape	Inner Jaw Angle	Lower Jaw Angle	Time to Impact	Time from Peak Gape to Impact	Distance from prey	Ram Speed
Peak Protrusion	**1**	0.37	0.54	0.38	-0.14	0.17	0.26	-0.33	0.22	0.08
Time to Peak Protrusion	0.37	**1**	0.43	**0.91**	0.14	-0.04	**0.86**	-0.25	0.42	0.06
Peak Gape	0.54	0.43	**1**	0.43	0.24	0.13	0.29	-0.37	0.13	-0.01
Time to Peak Gape	0.38	**0.91**	0.43	**1**	0.16	0.01	0.91	-0.36	0.41	0.03
Inner Jaw Angle	-0.14	0.14	0.24	0.16	**1**	-0.11	0.1	-0.16	0.08	0.04
Lower Jaw Angle	0.17	-0.04	0.13	0.01	-0.11	**1**	-0.03	-0.09	-0.09	-0.08
Time to Impact	0.26	**0.86**	0.29	**0.91**	0.1	-0.03	**1**	0.06	0.37	-0.04
Time from Peak Gape to Impact	-0.33	-0.25	-0.37	-0.36	-0.16	-0.09	0.06	**1**	-0.16	-0.17
Distance from prey	0.22	0.42	0.13	0.41	0.08	-0.09	0.37	-0.16	**1**	**0.9**
Ram Speed	0.08	0.06	-0.01	0.03	0.04	-0.08	-0.04	-0.17	**0.9**	**1**

Supplemental figures

Figure S1.

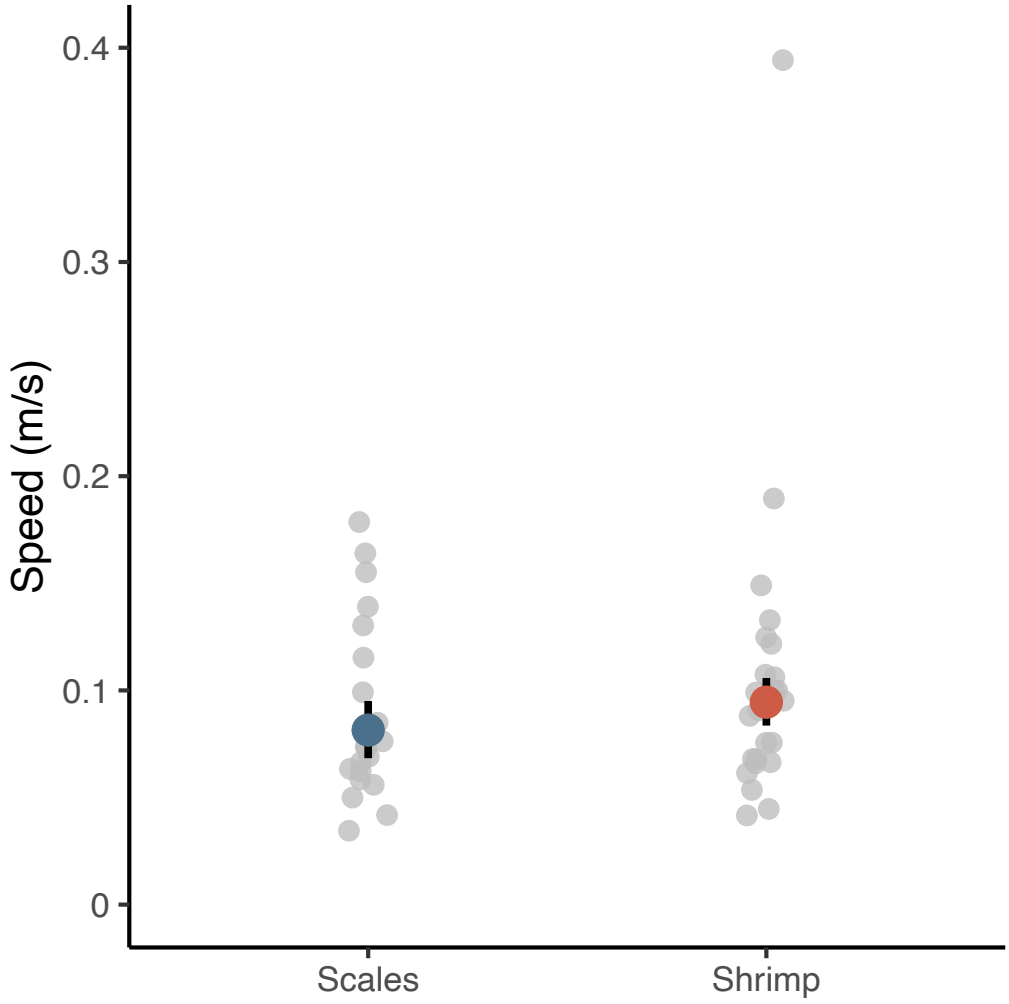

Figure S1. Pupfishes approach shrimp more quickly than they do scales. Colored points represent mean ram speed (m/s) and 95% confidence intervals when consuming shrimp versus scales for all species.

Inter-chapter Transition

In chapter two, I investigated whether scale-eating pupfish 1) exhibited differential feeding kinematic profiles compared to other pupfish species and 2) whether these differences are adaptive for scale-feeding. I found that scale-eaters indeed exhibit differential kinematic profiles while feeding, and that these differences lead to larger bites. These data, however, also indicate that scale-eating pupfish are anatomically capable of taking larger bites but that they behaviorally mediate their feeding kinematics to produce optimal bite kinematics. Findings from this chapter, in conjunction with the findings of chapter one, highlight the importance of investigating the interaction between morphology and behavior, especially when considering complex phenotypes such as feeding performance. Chapter three directly applies these principles to the complex phenotype of snail-feeding in the pupfish system. I directly investigate the relative contribution of morphology *vs* behavior for snail-eating using the natural variation produced from F1 and F2 snail-eating hybrids and find that, in the case of snail-feeding, behavioral adaptation may be sufficient for performing in this unique ecological niche.

Chapter 3: Oral shelling within an adaptive radiation of pupfishes: testing the adaptive function of novel nasal protrusion and behavioral preference

This chapter has been previously published and is reproduced here in accordance with the journal's article sharing policy:

St. John, M. E., Dixon, K., & Martin, C. H. (2020). Oral shelling within an adaptive radiation of pupfishes: testing the adaptive function of novel nasal protrusion and behavioral preference. *Journal of Fish Biology*, (April), 1–9. doi: 10.1111/jfb.14344

Significance Statement

Specialization on hard-shell prey items (i.e. durophagy) is a common dietary niche among fishes. Oral-shelling is a rare technique used by some durophagous fish to consume prey items like snails; however, adaptations for oral-shelling are still unknown. Here, we document the first evidence of oral-shelling in a cyprinodontiform fish, the durophagous pupfish (*Cyprinodon brontotheroides*), and experimentally test whether its novel nasal protrusion is an adaptation for oral-shelling using hybrid feeding trials.

Abstract

Dietary specialization on hard prey items, such as mollusks and crustaceans, is commonly observed in a diverse array of fish species. Many fish consume these types of prey by crushing the shell to consume the soft tissue within, but a few fishes extricate the soft tissue without breaking the shell using a method known as oral-shelling. Oral-shelling involves pulling a mollusk from its shell and may be a way to subvert an otherwise insurmountable shell defense. However, the biomechanical requirements and potential adaptations for oral-shelling are unknown. Here, we test the hypothesis that a novel nasal protrusion is an adaptation for oral-shelling in a durophagous pupfish (*Cyprinodon brontotheroides*). We first demonstrate oral-shelling in this species and then predicted that a larger nasal protrusion would allow pupfish to consume larger snails. Durophagous pupfish are found within an endemic radiation of pupfish on San Salvador Island, Bahamas. We took advantage of closely related sympatric species and outgroups to test: 1) whether durophagous pupfish shell and consume more snails than other species, 2) if F1 and F2 durophagous hybrids consume similar amounts of snails as purebred durophagous pupfish, and 3) to determine if nasal protrusion size in parental and hybrid populations increases the maximum diameter snail consumed. We found that durophagous pupfish and their hybrids consumed the most snails, but did not find a strong association between nasal protrusion size and maximum snail size consumed within the parental or F2 hybrid population, suggesting that the size of their novel nasal protrusion does not provide a major benefit in oral-shelling. Instead, we suggest that nasal protrusion may increase feeding efficiency, act as a sensory organ, or is a sexually selected trait, and that a strong feeding preference may be most important for oral-shelling.

Introduction

Dietary specialization is thought to be one way to reduce competition for a food source or to forage more optimally (Pyke 1984; Futuyman and Moreno 1988; Robinson and Wilson 1998). One form of dietary specialization, especially among fishes, is the increased consumption of hard-shelled prey items, such as mollusks and crustaceans (hereafter referred to as durophagy), and both freshwater and marine fishes include durophagous specialists. There are two main ways that fish consume hard-shelled prey items: First, fish may crush or break the outer shell to consume the soft tissue within. Some fishes, such as black carp (*Mylopharyngodon picesus*), pumpkinseed sunfish (*Lepomis gibbosus*), redear sunfish (*Lepomis microlophus*), black drum (*Pogonias cromis*), Florida pompano (*trachinotus carolinus*), and the black margate (*Anisotremus surinamensis*), use their pharyngeal jaws to crush the shells of snails and other mollusks in order to consume them (Lauder 1983; Grubich 2003; Gidmark et al. 2015). Others, such as the striped burrfish (*Chilomycterus schoepfi*), use their fused oral teeth to manipulate and crush shells (Winterbottom 1974; Ralston and Wainwright 1997). The biomechanical constraints of crushing hard shells is well documented in fish. For example, body mass (g), bite force (N), and pharyngeal jaw gape size are understood to limit the upper size of prey in the Caribbean hogfish (*Lachnolaimus maximus*), where larger fish generally produce both larger gapes and increased crushing force, allowing them to crush larger or thicker shells (Wainwright 1987, 1991). Similarly, the upper prey size consumed by black carp is limited by 1) the amount of force produced by its pharyngeal jaw closing muscle (*medial levator arcus branchialis V*) (Gidmark et al. 2013) and 2) the size of the pharyngeal jaw gape (Gidmark et al. 2015).

An alternative and much rarer method of consuming hard-shelled prey, primarily documented in cichlids endemic to Lake Malawi (*Metriaclima lanisticola*), Lake Victoria (*Hapochromis. xenognathus, H. sauvagei* and *Macropleurodus bicolor*), and Lake Edward *(H. concilians sp. nov., H. erutus sp. nov.* and *H. planus sp. nov*), is to extract the soft tissue of the gastropod from its shell via wrenching or shaking, known as 'oral-shelling' (Slootweg 1987; Madsen et al. 2010; Lundeba et al. 2011; Vranken et al. 2019). It is typically thought that oral-shelling is a way to circumvent the force and pharyngeal gape size requirements for consuming large mollusks because oral-shelling does not require a fish to break a mollusk's shell; however, very few studies have investigated oral-shelling in general (but see: Slootweg 1987; De Visser and Barel 1996) nor have they investigated adaptations for oral-shelling.

One possibility may be that fish use morphological adaptations to create a mechanical advantage during oral-shelling. For example, one hypothesis is that the fleshy snout of *Labeotropheus* cichlids is used as a fulcrum, allowing fish to more easily crop algae from rocks versus the bite-and-twist method observed in other cichlid species (Konings 2007; Conith et al. 2018), and specifically that increased snout depth may help create this mechanical advantage (Conith et al. 2019). A similar method may be used during oral-shelling to amplify force while removing snails from their shells. Thus, we predicted that larger nasal fulcrums should provide greater mechanical advantage for successfully oral-shelling larger prey.

The durophagous pupfish (*Cyprinodon brontotheroides*) is an excellent species for testing whether a novel morphological trait provides a mechanical advantage for oral-shelling. Durophagous pupfish are found within an adaptive radiation of pupfish

endemic to the hypersaline lakes of San Salvador Island, Bahamas, which also includes a generalist pupfish (*C. variegatus*) and a scale-eating pupfish (*C. desquamator;* Martin and Wainwright 2011, 2013*a*). Geological evidence suggests that the hypersaline lakes of San Salvador Island, and thus the radiation itself, are less than 10,000 years old (Hagey and Mylroie 1995; Martin and Wainwright 2013c,a). Phylogenetic evidence also indicates that: 1) generalist pupfish found outside San Salvador Island are outgroups to the entire San Salvador clade, and 2) that durophagous pupfish cluster near generalists from the same lake populations, indicating that there is extensive admixture between these young species (Martin and Feinstein 2014; Martin 2016; Lencer et al. 2017; Richards and Martin 2017). Gut content analyses indicated that durophagous pupfish consume approximately 5.5 times the number of mollusks and crustaceans (specifically ostracods) as generalists and fewer shells, suggesting that durophagous pupfish may be orally shelling their prey (Martin and Wainwright 2013c). In addition to their dietary specialization, durophagous pupfish also possess a novel nasal protrusion not observed in other pupfish species (Martin and Wainwright 2013*a*). This nasal protrusion is an expansion of the maxilla, and extends rostrally over the upper jaws (Hernandez et al. 2018). It is plausible that this nasal protrusion is an adaptation for oral-shelling used by the durophage as a fulcrum.

We investigated oral-shelling behavior in the laboratory and tested if the nasal protrusion of durophagous pupfish is an adaptation for oral-shelling. We measured snail consumption across 6 groups in the laboratory: outgroup generalists, generalists from San Salvador Island, scale-eaters, durophages, and F1 and F2 durophage hybrids (produced by crossing purebred durophages and generalists in the lab). If the novel nasal protrusion is adapted for oral-shelling, we expected that durophages would consume significantly more snails than generalists and scale-eaters. We explicitly took advantage of the ease of hybridization in this system to test predictions about the underlying genetics of the nasal protrusion and snail-eating behavior using F1 and F2 hybrids. If the nasal protrusion or snail-eating behavior is an additive trait, then we expected that F1 hybrids would show intermediate snail consumption and intermediate nasal protrusion size between the parental species, and that F2 hybrids would show greater variation in snail consumption and nasal protrusion size compared to parental species. Finally, we also investigated the relationship between nasal protrusion size and snail-shelling performance, by asking if individuals with larger noses could consume larger snails in lab-reared populations of both durophages and F2 hybrids. Again, we took advantage of F2 hybrids, because we could test a wider variety of nasal protrusion sizes, and because recombination may have broken up the relationship between nasal protrusion size and snail-eating preference in the F2 generation.

Ultimately, we found that, contrary to our predictions, purebred durophages, F1, and F2 hybrids all shelled significantly more snails than other pupfish species and we did not find evidence that larger nasal protrusions allowed durophages to consume larger snails. Instead, we discuss alternative explanations for the novel nasal protrusion such as a putative function in foraging efficiency, sexual selection, olfaction, or increased area for superficial neuromasts.

Methods

Collection and care

During the summer of 2017, we used seine nets to collect generalist, durophage, and scale-eater pupfishes from Crescent Pond (24.113102, -74.458204), Little Lake (24.101137, -74.482333), Osprey Lake (24.111895, -74.465260), and Oyster Pond (24.108591, -74.462730, San Salvador Island, Bahamas). We also collected generalist pupfish from Lake Cunningham (25.060154, -77.405679, Nassau, Bahamas) to use in outgroup comparisons. We transported fish back to the University of North Carolina, Chapel Hill, where they were maintained in mixed-sex stock tanks (37-75 l) in approximately 26° C water at approximately 5-10 ppt salinity (Instant Ocean salt mix). In the lab, we produced F1 and F2 hybrid offspring using snail-eater and generalist parents. Wild caught individuals were also allowed to breed and produced F1-F3 purebred offspring. Hybrid and purebred offspring were used in our feeding assays. We fed all fish a diet of commercial pellet foods, frozen bloodworms, and mysis shrimp daily.

We also maintained a colony of freshwater sinistral snails (*Physella sp.*). We kept snails in a 7-liter stock tank containing the same water used in pupfish tanks. All snails were acclimated to 5-10 ppt salinity for at least 48 hours before being used in a feeding trial. We fed snails a diet of bloodworms every 48 hours. We ran multiple control trials without fish alongside feeding trials to track natural snail mortality rates.

Morphological measurements

We measured standard length of each fish by measuring the distance from the tip of the upper jaw to the posterior end of the hypural plate. We also measured nasal protrusion size for a subset of fish (9 generalists, 50 durophages, 17 F1 hybrids, and 62 F2 hybrids) using image processing software (Schindelin et al. 2012). Scale-eating pupfish do not exhibit even marginal nasal protrusion, and therefore we did not include them in this analysis. We measured fish nasal protrusion size by drawing a tangent line aligning the most anterior dorsal point of the premaxilla with the neurocranium and measuring a perpendicular line at the deepest part of the nasal region (Figure 1C).

Feeding assay

We quantified the number of snails consumed by all three species of pupfish and hybrids using feeding assays. Prior to a feeding assay, fish were removed from stock tanks and isolated in 2L trial tanks which contained one synthetic yarn mop to provide cover for the fish. We allowed fish to acclimate in trial tanks for at least 12 hours before the start of a feeding assay. After the acclimation time, we haphazardly chose 5 snails from our snail stock tank and added them to each feeding assay tank. We added one bloodworm to each tank to ensure that even fish which did not consume any snails had an adequate diet. Fish were allowed to feed freely on snails for 48 hours with no additional food source. At the end of the 48-hour assay period fish were removed from trial tanks, photographed, and placed back into mixed-sex stock tanks. We then recorded the number of snails that were consumed (empty shells remaining) and unconsumed. Finally, we measured the size of each snail shell from the anterior tip of the shell's aperture to farthest tip of the spire (mm) using digital calipers and image processing software. In total, we measured feeding success for 13 outgroup generalists,

20 generalists, 55 durophages, 20 scale-eaters, 25 F1 hybrids, and 63 F2 hybrids. We sampled purebred durophages and F2 hybrids more densely (i.e. testing all available individuals from our lab colony), because we anticipated needing increased power to detect how variation in nasal protrusion size affected snail-consumption compared to the power required to detect differences between species. Out of the 196 trials, only 11 finished the trial period with four snail shells instead of the given five, suggesting that at most 3.5% of snail consumption involved also eating the shell.

Data processing

No differences between fully consumed and partially consumed snails

We noticed that a portion of the snails were only partially consumed (i.e. part of the snail tissue remained in the shell versus a completely empty shell after 48 hours) and therefore used a generalized linear mixed model (GLMM) with a binomial response distribution to determine if partially consumed snails should be analyzed separately from fully consumed snails. We included 1) whether snails were fully or partially consumed as the response variable (binomial data), 2) species designation as a fixed effect, 3) population and fish ID as random effects, and 4) log standard length as a covariate. We found that the pattern of partially and fully consumed snails did not vary across species (χ2= 2.73, *df*=5, *P*=0.74), and therefore included all partially consumed snails in the general "consumed" category for the remainder of our analyses.

Statistical analysis

We used a linear mixed model to investigate the relationship between nasal protrusion distance and species. For this analysis we used a subset of our data which includes: 9 generalists, 50 durophages, 17 F1 hybrids, and 62 F2 hybrids. Our model included 1) log nasal protrusion size as the response variable, 2) species designation, log standard length, and their interaction as fixed effects, and 3) population as a random effect. We also used Tukey's HSD to make *post hoc* comparisons across species.

We used a GLMM with a negative binomial distribution to explore whether the number of snails consumed varied between species. We included 1) whether snails were consumed or unconsumed as the response variable (binomial data), 2) species designation as a fixed effect, 3) population and fish ID as random effects, and 4) log standard length as a covariate. We made additional *post hoc* comparisons between groups using Tukey's HSD.

We used a linear mixed model to determine if the size of snails varied by whether they were consumed or unconsumed and whether that varied between species. We included 1) snail size (mm) as the response variable, 2) whether snails were consumed or unconsumed, species designation, and their interaction as fixed effects, 3) population and fish ID as random effects, and log standard length as a covariate. We made additional *post hoc* comparisons between groups using contrasts and an FDR correction.

Finally, we investigated if nasal protrusion distance affected the maximum size snail an individual could consume as an estimate of snail-shelling performance. For this analysis we only considered purebred durophages and F2 hybrids (separately) as they had the largest observed variance in nasal protrusion size and only included individuals that consumed at least one snail during the feeding trial. For each group, we used a

linear model with 1) the size of the largest consumed snail for each individual as the response variable, 2) log nasal protrusion size, log standard size, and their interaction as fixed effects, and 3) the residuals from a linear model investigating the relationship between snail size and nasal protrusion size as a covariate. We included this additional covariate because we found a strong positive relationship between mean snail size provided during trials and nasal protrusion in both purebred durophages (LM: P=1.72 x 10^{-9}, adjusted R^2 =0.14) and F2 hybrids (LM: P=5.58 x 10^{-10}, adjusted R^2 =0.12), and wanted to account for this variation in the model (Figure S2). This variation reflected our attempt to provide some larger snails in trials with larger fish to better assess performance. We additionally included the random effect of population in our durophage model.

Ethical statement
This study was conducted with the approval of the Animal Care and Use Committee of the University of North Carolina, Chapel Hill, NC (protocol# 15–179.0). All wild fish were collected with a research and export permit from the Bahamas BEST commission, renewed annually since 2011.

Results

Nasal protrusion size does not vary between purebred durophages and hybrids
Our linear mixed model indicated that nasal protrusion size is significantly associated with log standard length (χ2= 27.63, df=1, P=1.47x10^{-7}; Figure S1), but that this relationship does not vary between purebred and hybrid durophages (χ2= 3.22, df=3, P = 0.36). *Post hoc* analysis indicated that generalists had smaller noses than durophages (P < 0.0001) and F1 hybrids (P = 0.016; Figure 1A).

Purebred durophages and their hybrids consume the most snails
We found that species designation was a significant predictor for the number of snails an individual consumed (GLMM; χ2= 35.61, df=5, P= 1.129X10^{-6}). Specifically, we found that durophages, F1 hybrids, and F2 hybrids consumed more snails than the generalist outgroup population (Lake Cunningham, New Providence Island, Bahamas) and scale-eating pupfish (Figure 1B). Durophages, F1 hybrids, and F2 hybrids also consumed twice as many snails as generalists, however this difference was not significant.

Consumed snails were larger than unconsumed snails
In general, we found that the size of snails varied 1) by whether they were consumed (χ2= 4.002, df=1, P=0.045), and 2) across species (χ2= 24.79, df=5, P=0.00015). Specifically, we found that consumed snails were on average 0.12 mm larger in diameter than unconsumed snails (P=0.046). Generalists and scale-eaters received snails that were approximately 17% larger than other groups (generalists: P=0.016; scale-eaters: P=0.02; Figure 1D). Although this was unintentional due to the available size distributions of snails in our colony over the ten month course of the feeding trails, we believe that it did not introduce a significant bias because 1) larger snails were more likely to be consumed (in fact there was only an 8% difference between the mean size

of snail given to generalists and scale-eaters *vs* the mean size of consumed snails) and 2) generalists and scale-eaters were excluded from analyses which examined how nasal protrusion affected a fish's ability to consume snails.

Nasal protrusion size did not significantly increase the maximum snail size consumed
We found no effect of log nasal protrusion size, log standard length, or their interaction on the size of the largest consumed snail for either durophages ($P_{log(nasalprotrusionsize)}$=0.49, $P_{log(standardlength)}$=0.61, $P_{interaction}$=0.56; Figure 2A) or F2 hybrids ($P_{log(nasalprotrusionsize)}$=0.83, $P_{log(standardlength)}$=0.66, $P_{interaction}$=0.91; Figure 2B).

Discussion

We present the first strong evidence in any cyprinodontiform fish that the durophagous pupfish is an oral-sheller, shaking snails free from their shells rather than crushing or ingesting the whole shell. This is consistent with their notably non-molariform pharyngeal jaws relative to generalists and snail-crushing species (Figure 3). We then tested the hypothesis that the durophagous pupfish's novel nasal protrusion is an adaptation for removing snails from their shells, potentially functioning as a fulcrum. We predicted that durophagous pupfish would 1) consume more snails than other groups, and 2) consume larger snails than other groups. We found that both durophages and their F1 and F2 hybrid offspring consumed the most snails compared to other groups (Figure 1B), indicating that any substantial amount of durophagous genetic ancestry increases the number of snails consumed over a 48-hour feeding trial. However, contrary to our expectations, we found no significant evidence that larger nasal protrusions within hybrid or parental durophagous pupfish populations enabled the fish to consume larger snails (Figure 2).

Durophages have a stronger behavioral preference for snails compared to other species
One explanation for the observed pattern is that durophagous pupfish have a stronger preference for snails which is independent from their novel nasal protrusion. We see some support for this within our data. Generalist pupfish from San Salvador Island consumed significantly more snails than generalists found outside of the radiation on New Providence Island, and even consumed statistically similar amounts of snails as purebred durophages despite having much smaller nasal protrusions (Figure 1A&B). It could be that extensive geneflow between generalists and durophages on San Salvador Island spread alleles for snail-eating preference throughout both pupfish species (Martin and Feinstein 2014). Alternatively, the common ancestor of durophages and generalists may have had a strong preference for snails (Martin and Feinstein 2014; Richards and Martin 2017). The increased aggression of both male and female durophages toward conspecifics by potentially alternate genetic pathways to scale-eaters, as shown in a recent study (St. John et al. 2019), could also be associated with their stronger preference for aggressively attacking snails to flip them over before gripping the body of the snail in their oral jaws and shaking them free from their shells.

Liem's hypothesis and subsequent work has long supported the idea that morphological specialization need not coincide with trophic specialization, or *vice versa*. For example, *Tropheops tropheops* and *Metriaclima zebra*, two cichlids from Lake

Malawi that are morphologically specialized for scraping algae often fill a generalist ecological niche, consuming zooplankton, benthic invertebrates, and phytoplankton (Liem 1978, 1980; McKaye and Marsh 1983), particularly during periods of resource abundance (Martin and Genner 2009). An analogous argument can be made for individual dietary specialization within a population (Bolnick et al. 2003). For example, Werner and Sherry (1987) found that individual Cocos Island finches specialize on a wide variety of taxa including crustacea, nectar, fruit, seeds, mollusks, and lizards, and that individual dietary specialization was most likely driven by behavioral differences. Similarly, increased levels of individual specialization in sticklebacks are driven by shifts in forager density or intraspecific competition (Svanbäck and Bolnick 2005, 2007; Araújo et al. 2008). Thus, individual specialization is often driven entirely by differences in behavior, feeding preference, or other external factors and can be divorced from adaptive differences in morphology (Werner and Sherry 1987).

Alternative functions of the novel nasal protrusion

We investigated whether an increase in nasal protrusion size affected the maximum size snail an individual could consume (Figure 2). However, it could be that the novel nasal protrusion is related to feeding efficiency, e.g. in handling time per snail, or is a sensory organ used for locating snails more efficiently with potentially increased numbers of superficial neuromasts (Shibuya et al. 2020). There are several examples of nasal protrusions that are used for this purpose. The unique rostrums of paddlefish (Polydontidae), sturgeon (Acipenseridae), and sawfish (Pristidae) are all used as sensory organs, containing electroreceptors, lateral line canals, and even barbels for detecting prey items (Miller 2006; Wueringer et al. 2012). The novel nasal protrusion of the durophagous pupfish may also be a sensory organ, however, whether the nasal protrusion has an increased number of superficial neuromasts is still unknown.

Alternatively, the novel nasal protrusion may allow durophagous pupfish to orally shell snails more quickly, increasing their feeding efficiency. For example, Schluter (1993) documented that benthic sticklebacks with deep bodies, large mouths, and few, short gill rakers were more efficient at consuming benthic prey items, while limnetic species of stickleback, with slender bodies, small mouths, and many, long gill rakers, were more efficient at consuming limnetic prey items. Interestingly, Schluter (1993, 1995) also found that F1 hybrids had decreased efficiency feeding on both limnetic and benthic prey items which was primarily due to their intermediate phenotypes and suggested that reduced fitness in hybrids helps maintain species boundaries between benthic and limnetic species. It could be that the durophage F1 and F2 hybrids have similar preferences for gastropods, but cannot consume snails as efficiently due to their intermediate phenotype. However, we found no strong evidence suggesting that the nasal protrusion is adapted for oral-shelling (Figure 2). Future work should investigate other traits that may be adaptive for oral-shelling such as the strength of the dorsal head of the maxilla which comprises the skeletal basis of the novel nasal protrusion, structural differences in the mandibular symphysis, coronoid process, or the articular bones which may all provide additional strength or stabilization during biting, or tooth variation in the durophage pharyngeal jaws (Fig. 3). Indeed, there is subtle variation apparent in the pharyngeal teeth and jaws of durophages compared to other pupfish

species (Figure 3) which has not been previously reported, suggesting that pharyngeal jaws may be adapted for processing hard-shelled prey.

The novel nasal protrusion may be a sexually selected trait

Finally, the novel nasal protrusion may be unrelated to oral-shelling and instead may be used in species recognition or mate preference functions. Exaggerated traits, like the novel nasal protrusion in durophage pupfish, commonly arise via sexual selection. For example, forceps size in earwigs (Simmons and Tomkins 1996), major claw size in fiddler crabs (Rosenberg 2002), and the size of the sword tail ornament present in swordtail fish (Rosenthal and Evans 1998) are all thought to be sexually selected traits. Two commonly invoked hallmarks of a sexually selected trait are 1) allometric scaling compared to body size and 2) that the trait is sexually dimorphic (Kodric-Brown and Brown 1984; Kodric-Brown et al. 2006; Shingleton and Frankino 2013). In pupfish, there is a weak positive relationship between standard length and nasal protrusion size observed for generalists (Figure S1A, $generalist_{slope}$= 0.35). Generalist pupfish mostly likely resemble the most recent common ancestor for the radiation, making the observed slope a good null expectation for how nasal protrusion size should scale with body size in pupfish. In durophages, we observe much stronger positive allometry of the nasal protrusion (Figure S1B, $durophage_{slope}$= 0.93), in which large durophage individuals have nasal protrusion sizes more than twice as large as those in large generalists. However, we found no significant difference in nasal protrusion size between male and female durophages when accounting for these size differences (LM, P=0.96).

Conclusion

In conclusion, we did not find evidence to support that the novel nasal protrusion observed in durophagous pupfish is adapted for consuming large snails. Instead, we found that purebred durophages and their F1 and F2 hybrids have stronger preferences for consuming snails than other species. We suggest that the novel nasal protrusion may be adapted for other aspects of oral-shelling such as feeding efficiency, or that variation in other traits, such as the pharyngeal jaws (Figure 3), may play a larger role in oral-shelling. Alternatively, this may be an example of trophic specialization due to behavioral specialization (i.e. feeding preference).

Figures

Figure 1.

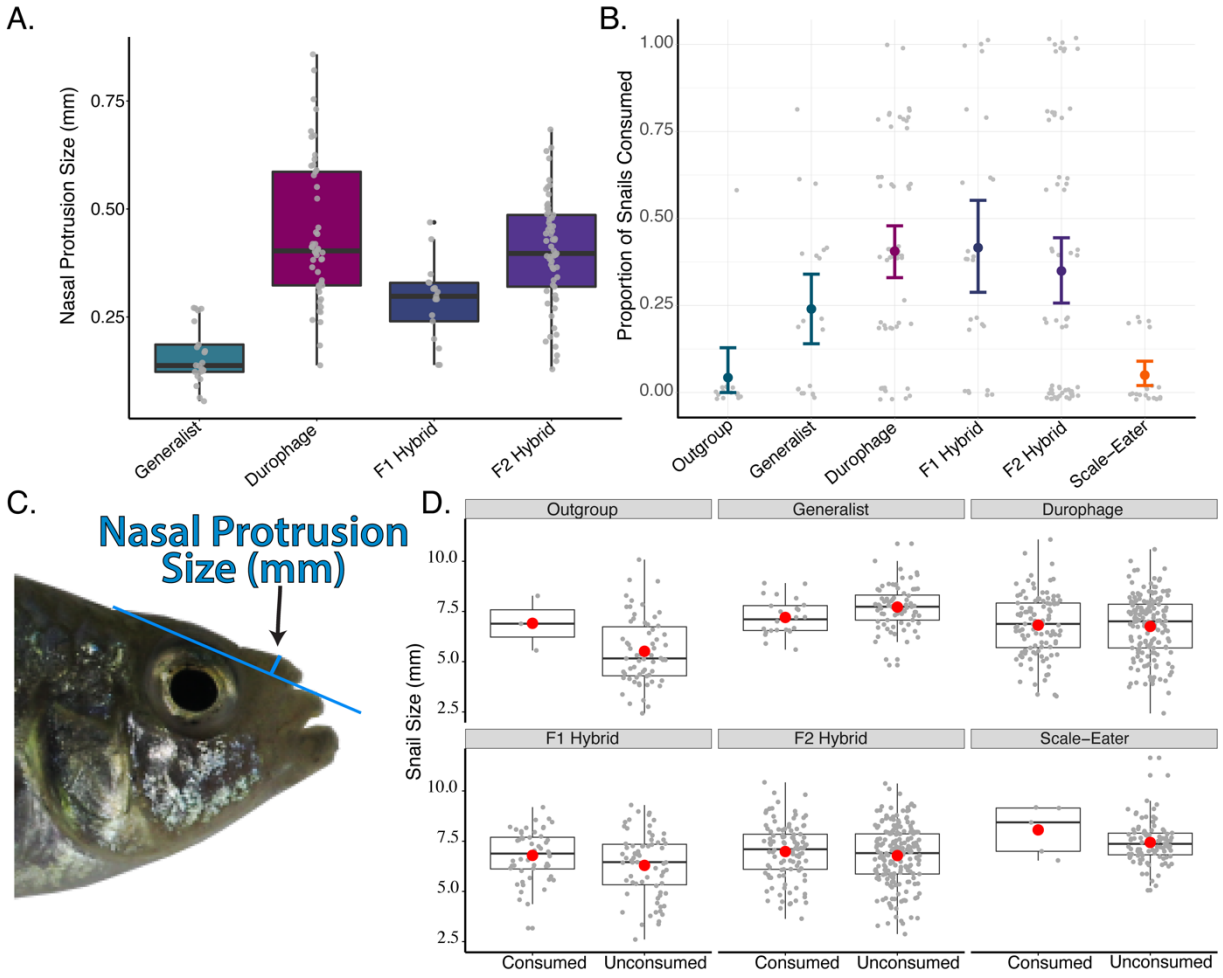

Figure 1. Snail consumption, nasal protrusion size, and snail size by species. A) Variation in nasal protrusion size across pupfish groups. Grey dots represent individual fish. B) Proportion of snails consumed across six groups of pupfish. Colored dots represent mean proportion, and error bars represent 95% confidence intervals (bootstrapping: 1,000 iterations). C) Visualization of how nasal protrusion size was measured (pictured: durophagous pupfish). D) Visualization of the size of consumed and unconsumed snails for each species. Grey dots represent individual snails and red dots represent the mean snail size.

Figure 2.

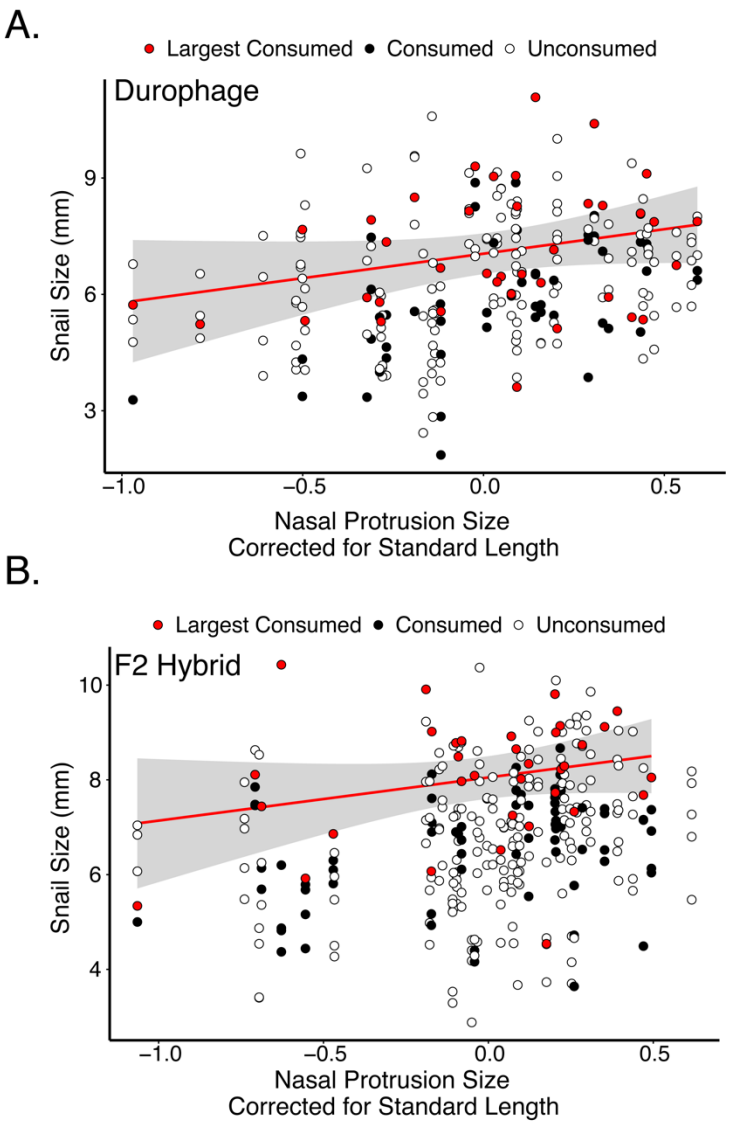

Figure 2. The maximum prey size a pupfish can consume was not affected by nasal protrusion size. The X-axis shows nasal protrusion size corrected for standard length while the Y-axis shows snail size (mm). Red dots show the size of largest consumed snail from each trial, the red line represents the linear model describing the relationship between nasal protrusion size and the largest consumed snails, and the grey area represents 95% CI. Closed circles show the size of other snails that were consumed during trials; open circles show the size of unconsumed snails.

Figure 3.

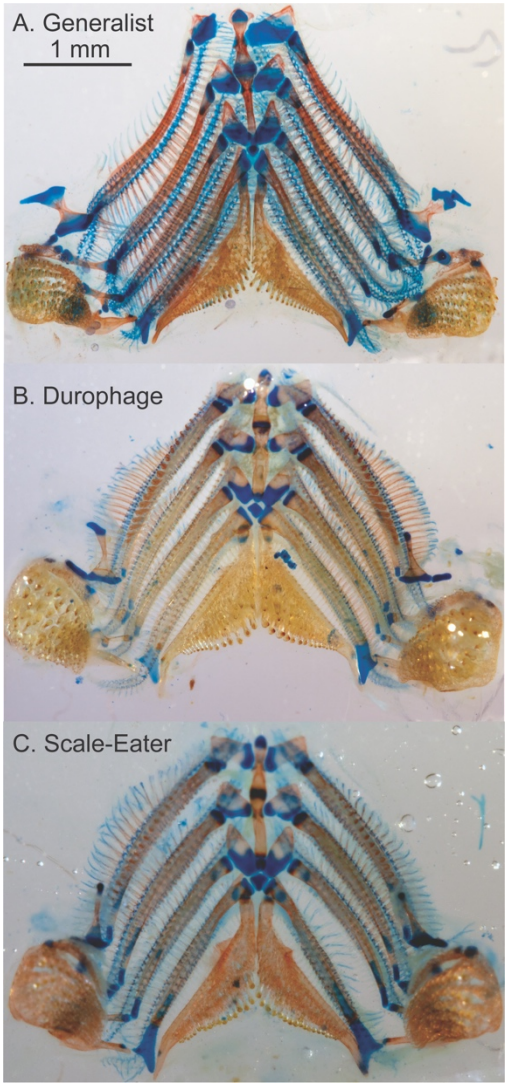

Figure 3. Branchial skeleton and pharyngeal teeth of all three San Salvador Island species. Image of the dissected branchial skeleton and pharyngeal jaws of A) generalist, B) durophage, and C) scale-eater pupfish. Scale (1mm) is shown in Figure A and is consistent across all three photos. From these three individuals, the representative snail-eater has lower pharyngeal teeth that are 50% longer and 75% wider than the generalist or scale-eating individuals.

Supplemental Material
Supplemental figures

Figure S1.

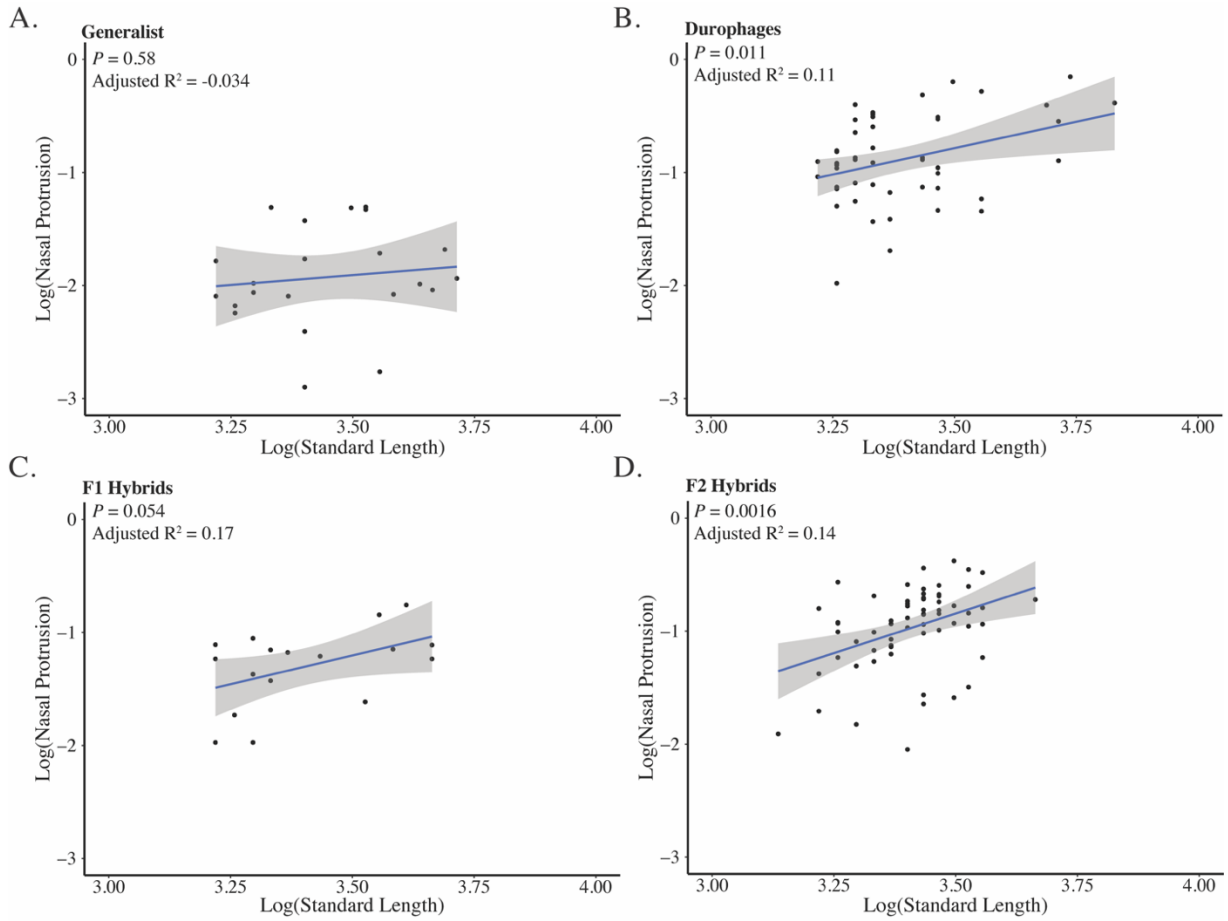

Supplemental Figure 1. There is a positive relationship between standard length and nasal protrusion size for Durophages and F2 Hybrids. Blue lines represent a linear model describing the relationship between log(nasal protrusion size) and log(standard length). Grey bars represent 95% CIs, and black dots represent individuals.

Figure S2.

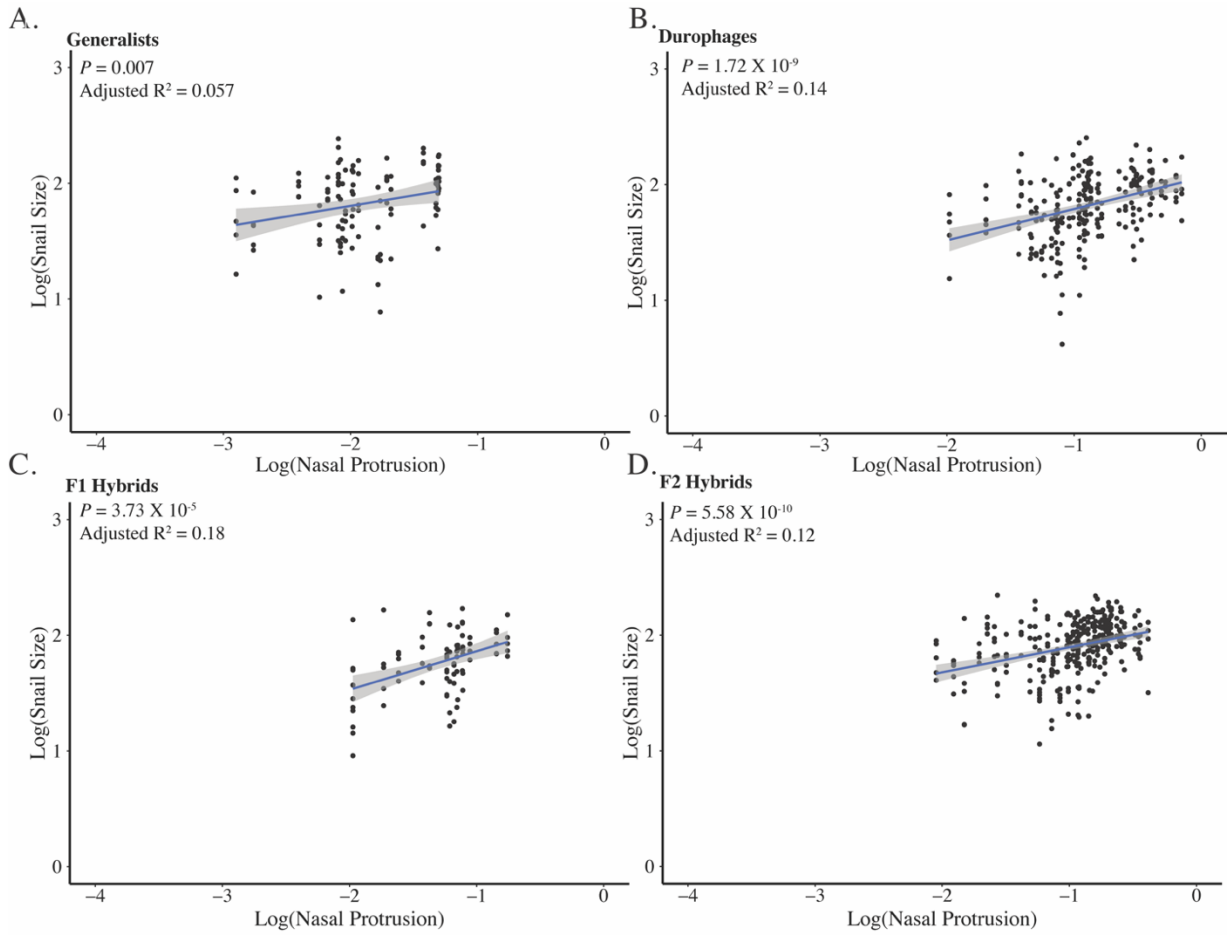

Supplemental Figure 2. There is a positive relationship between nasal protrusion size and snail size for all groups. Blue lines represent a linear model describing the relationship between log(nasal protrusion size) and log(standard length). Grey bars represent 95% CIs, and black dots represent individuals.

Inter-chapter Transition

In chapter three, I found that morphological variation, namely the presence and size of the nasal protrusion, did not strongly correlate with a pupfish's snail-eating performance. Instead, I found evidence that purebred snail-eaters, F1 and F2 snail-eating hybrids, and even generalist pupfish species from San Salvador Island were all able to consume similar numbers of snails. This suggests that behavior may be the primary adaptive trait for snail-eating and that ongoing geneflow between San Salvador Island snail-eaters and generalists has resulted in increased snail-eating performance for generalists on the island. Together, chapters one, two, and three show that complex phenotypes may involve changes in morphology, behavior, and even changes in how these two phenotypes interact. All of these chapters also highlight the need for a deeper understanding of the genetic underpinnings of traits that are adaptive for scale- and snail-eating in the pupfish system. The explicit goal of chapter four is to identify potential regions of the genome that are associated with adaptive traits for scale- and snail-eating in two ponds on San Salvador Island. I find that regions of the genome are reused to produce adaptive traits between ponds, but that these regions are not always associated with the same traits. Ultimately, this chapter provides insight into which regions of the pupfish genome are associated with adaptive morphological and behavior traits for scale- and snail-eating, and sheds light on the evolutionary history of candidate genes that reside within these regions.

Chapter 4: Parallel genetic changes underlie integrated craniofacial traits in an adaptive radiation of trophic specialist pupfishes

Abstract

Many factors such as divergence time, shared standing genetic variation, frequency of introgression, and mutation rates can influence the likelihood of whether populations adapt to similar environments via parallel or non-parallel genetic changes. However, the frequency of parallel *vs* non-parallel genetic changes resulting in parallel phenotypic evolution is still unknown. In this study, we used a QTL mapping approach to investigate the genetic basis of highly divergent craniofacial traits between scale- and snail-eating trophic specialist species across similar hypersaline lake environments in an adaptive radiation of pupfishes endemic to San Salvador Island, Bahamas. We raised F2 intercrosses of scale- and snail-eaters from two different lake populations of sympatric specialists, estimated linkage maps, scanned for significant QTL for 30 skeletal and craniofacial traits, and compared the location of QTL between lakes to quantify parallel and non-parallel genetic changes. We found strong support for parallel genetic changes in both lakes for five traits in which we detected a significant QTL in at least one lake. However, many of these shared QTL affected different, but highly correlated craniofacial traits in each lake, suggesting that pleiotropy and trait integration should not be neglected when estimating rates of parallel evolution. We further observed a 23-52% increase in adaptive introgression within shared QTL, suggesting that introgression may be important for parallel evolution. Overall, our results suggest that the same genomic regions contribute to parallel integrated craniofacial phenotypes across lakes. We also highlight the need for more expansive searches for shared QTL when testing for parallel evolution.

Introduction

Convergent evolution describes the independent evolution of similar phenotypes in response to similar selective pressures and provides strong support for ecological adaptation (Losos 2009; Schluter 2000). This includes both non-parallel genetic changes, such as the evolution of antifreeze glycoproteins in icefishes or the ‘thunniform’ body shape of lamnid sharks and tunas (Chen et al. 1997; Donley et al. 2004), and parallel genetic changes such as tetrodotoxin resistance in snakes and pufferfishes or the evolution of voltage-gated sodium channels in mormyrid and gymnotiform electric fishes (Hopkins 1995; Katz 2006; Jost et al. 2008; Feldman et al. 2009; Zakon et al. 2006). Instances of convergence across independent lineages (i.e., across groups that lack a recent common ancestor and shared genetic backgrounds) provide the strongest evidence for adaptation; however, repeated evolution of similar phenotypes in response to similar selective pressures among lineages derived from the same ancestral population can also provide insight into the process of adaptation. Understanding this process, traditionally known as parallel evolution (Futuyman 1986), is important because it can help to tease apart the contributions of natural selection and shared genetic constraints to similar phenotypes (Schluter et al. 2004; Stuart et al.

2017). Parallel phenotypic evolution can also occur via parallel or non-parallel genetic changes (e.g., Cresko et al. 2004), but even non-parallel genetic changes occurring in the same ancestral genetic background (e.g. Chan et al. 2010; Xie et al. 2019) provide weaker evidence for adaptation than convergence across independent lineages due this shared history. Despite substantial attention, the frequency and likelihood of parallel phenotypic evolution via parallel or non-parallel genetic changes is still relatively unknown (Stern and Orgogozo 2008; Stern 2013; Rosenblum et al. 2014).

Many factors influence whether parallel phenotypic evolution in similar environments is produced by parallel or non-parallel genetic mechanisms. First, recently diverged species exhibit increased probabilities of genetic parallelism when adapting to similar environments. Recently diverged taxa may inhabit similar environments more frequently or they may have similar genetic architectures, similar genetic variance-covariance matrices, or similar genetic backgrounds that produce similar epistatic interactions (Conte et al. 2012; Rosenblum et al. 2014). Second, any mechanism that allows the use of the same adaptive genetic mechanism should increase the likelihood of convergence via parallelism, including the availability of shared standing genetic variation and introgression (Rosenblum et al. 2014). For example, threespine sticklebacks colonized freshwater thousands of times and converged on similar phenotypes largely due to selection on an ancient shared pool of marine standing genetic variation (Jones et al. 2012; Feulner et al. 2013; Nelson and Cresko 2018; Haenel et al. 2019; but see: Chan et al. 2010; Stuart et al. 2017). Similarly, increased adaptive introgression should also make genetic parallelism more likely (Grant et al. 2004; Morjan and Rieseberg 2004; Hedrick 2013; Taylor et al. 2020). Third, adaptive genetic variation with larger effect sizes and fewer pleiotropic effects should be reused more frequently across populations, particularly when a population is far from a new adaptive optimum (Linnen et al., 2013; Orr, 2005; Stern, 2013). Finally, de novo mutations, large mutational target sizes, and polygenic adaptive phenotypes are more likely to result in parallel phenotypic evolution via non-parallel genetic pathways (Wittkopp et al. 2003; Kowalko et al. 2013; Bolnick et al. 2018, but see: Colosimo et al. 2004; Chan et al. 2010; Xie et al. 2019).

Quantitative trait locus (QTL) mapping is often used to infer whether parallel or non-parallel genetic changes underlie parallel phenotypes. However, many QTL studies only investigate a limited number of traits that are controlled by large effect loci, which may bias the literature towards supporting genetic parallelism (Conte et al. 2012). This bias may be exacerbated by the fact that in many QTL studies the genomic regions associated with a parallel phenotype are large, contain many genes, and their effects on phenotypic variance are overestimated in under-powered studies (Beavis 1998). These methodological and experimental limitations reduce confidence in the specific genomic regions associated with a parallel phenotype and, by extension, reduce confidence in whether parallel evolution was due to parallel or non-parallel genetic changes. One possible solution is to compare the genomic regions associated with many different phenotypes across populations (Erickson et al. 2016). In this scenario, shared genomic regions across populations provide strong support for genetic parallelism, except in the likely rare instances of independent de novo mutations within the same region (O'Brown et al. 2015; Xie et al. 2019; Chan et al. 2010).

The San Salvador Island (SSI), Bahamas pupfish radiation is an excellent system for investigating the genetic underpinnings of parallel ecomorph phenotypes because novel trophic specialists occur in sympatry across multiple hypersaline lake populations on the island. The radiation includes three pupfish species: a generalist pupfish (*Cyprinodon variegatus*), a scale-eating (lepidophagous) pupfish (*C. desquamator*), and a snail-eating (durophagous) pupfish (*C. brontotheroides;* Martin and Wainwright 2013). The snail- and scale-eating pupfishes are endemic to SSI and occur in sympatry with one another and the generalist pupfish.

Among lakes, specialists have converged on multivariate phenotypes that are adaptive for their given ecological niche. For example, scale-eaters across all lakes exhibit increased oral jaw size (Martin & Wainwright, 2013; Hernandez et al. 2018) and reduced lower jaw angles during scale-eating strikes which may play a critical role in scale-biting performance during high-speed strikes on their prey (St. John et al. 2020b). Similarly, the snail-eating pupfish exhibits a novel nasal protrusion which may improve oral snail-shelling performance or result from sexual selection (Martin and Wainwright 2013a; St. John et al. 2020a). Furthermore, the nasal protrusion of the snail-eating species varies substantially among lake populations (Martin and Feinstein 2014; Hernandez et al. 2018). Despite the importance of these species characteristics, we still do not understand how their genetic architecture varies across populations.

There is some evidence to suggest that parallel genetic changes underlie specialist phenotypes on SSI. First, the SSI radiation is very young, diverging only about 10 kya (Hagey and Mylroie 1995). Second, previous genomic analyses show that many of the alleles associated with trophic specialization arrived on SSI from Caribbean-wide standing genetic variation within generalist pupfish populations, but there are also some de novo adaptive mutations associated with scale-eating (Richards et al. 2021). Scale-eaters form a monophyletic group, suggesting a shared genetic component to the scale-eating phenotype across lakes (Richards and Martin 2017). In contrast, snail-eaters and generalists often genetically cluster together by lake instead of by species—suggesting that non-parallel genetic changes could underlie parallel snail-eater phenotypes across lakes (Martin and Feinstein 2014; Richards and Martin 2017). Furthermore, previous studies have documented strong genetic divergence between scale-eaters from Crescent Pond and all other populations of scale-eater (Richards & Martin, 2017; Richards et al., 2021).

In this study we mapped the genetic basis of 30 skeletal craniofacial and body traits associated with snail- and scale-eating using lab-reared F2 intercrosses from Crescent Pond and Little Lake. We called variants, estimated linkage maps, and performed QTL analyses independently for each F2 population. We found that only one trait— cranial height—mapped to the same genomic region in both Crescent Pond and Little Lake, but 4 of the 5 remaining significant QTL detected in one lake mapped to the same genomic region as a highly correlated craniofacial trait in the second lake. Ultimately, we conclude that parallel evolution through reuse of introgressed adaptive alleles is acting to produce similar snail- and scale-eating phenotypes across lake populations on SSI.

Methods

Genetic cross

Currently, pupfish species can been found in 12 hypersaline lakes across the island: generalist pupfish are found in allopatry in five lakes, the generalist and snail-eating pupfish are found in sympatry without the scale-eater in two lakes, the generalist and scale-eater are found in sympatry in a single lake, and all three species are found in sympatry in four lakes (Martin and Feinstein 2014). We collected wild-caught scale-eating and snail-eating pupfishes from two different sympatric populations (containing all three species) on SSI – Crescent Pond and Little Lake—during the years of 2011 and 2013-2015 using seine nets. We brought individuals back to the University of California, Davis or the University of California, Berkeley and a single wild-caught scale-eating female from each lake was allowed to breed freely with a single wild-caught snail-eating male from the same lake resulting in two separate genetic crosses (one cross from Crescent Pond and one cross from Little Lake). At least four F1 offspring from each hybrid population were crossed to produce F2 intercrosses, resulting in 354 individuals from Crescent Pond and 287 individuals from Little Lake included in this study. All fish were maintained in 40-L tanks at 5-10ppt salinity at the University of California, Davis or the University of California, Berkeley. We fed fry a diet of newly hatched *Artemia* nauplii for approximately 40 days post fertilization, after which they were switched to the adult diet of frozen and pellet foods. We euthanized fish in an overdose of MS-222 (Finquel, Inc.) according to the approved University of California, Davis Institutional Animal Care and Use Protocol #17455 or University of California, Berkeley IACUC Protocol AUP-2015-01-7053, and stored them in 95% ethanol.

Phenotyping

Sex and mate preferences

For individuals from Crescent Pond, we recorded their sex using their sexually dimorphic body and fin coloration. Male pupfish develop a blue iridescent coloration along their anteriodorsal surface and a black marginal band along their caudal fin (Echelle and Echelle 2020).

Once F2 hybrids reached sexual maturity, we performed mating assays using a subset of the hybrid females from Crescent Pond to estimate mate preferences for snail- or scale-eating mates (N=74). Prior to the mating assays, female fish were isolated for at least twelve hours and conditioned on frozen bloodworms with a 12:12 light:dark cycle. Mating assays occurred in three 1.1 m diameter kiddie pools (5-10ppts salinity). Pools were covered with gravel substrate and divided in half. In each half, we placed three clear plastic 7.5-L Kritter Keepers in a row containing three conspecific males housed individually to avoid aggression. Size-matched scale-eater males were placed on one side of each arena and snail-eating males on the other. Once the males were placed in individually in clear boxes, a female F2 hybrid from Crescent Pond was placed into the center of one of the three kiddie pools, chosen at random. We considered females acclimated to the pool once they had visited both rows of males, after which we started the seven-minute trial period. During each trial we recorded the amount of time a female spent within one body-length of each species. Each female was tested consecutively in all three pools, and we used the mean of her association time (scale-eater association time / total association time during each 7-minute trial)

across all three pools for QTL analysis. Size-matched males were periodically rotated into and among kiddie pools during the 12-month testing period.

Morphological traits

To measure skeletal phenotypes in our F2 intercrosses, we cleared and double-stained each specimen with alizarin red and alcian blue. Before clearing and staining, each fish was skinned and fixed in 95% ethanol. We then fixed specimens in 10% buffered formalin for at least one week and stained batches of individually labeled specimens following Dingerkus and Uhler's (1977) protocol. We suspended cleared and stained specimens in glycerin, and photographed their left lateral side using a Canon EOS 60D digital SLR camera with a 60 mm macro lens. For each individual, we took two types of photographs: first, we took a whole-body photograph to calculate fin and body measurements and second, a lateral skull image to calculate craniofacial measurements (Figure 1). We used DLTdv8 software (Hedrick 2008) to digitize 11 landmarks on each whole body image and 19 landmarks on each lateral skull image following the morphometric methods described in Martin et al. (2017). For individuals from Crescent Pond, we also weighed the adductor mandibulae muscle mass. Each image included a standardized grid background which we used to calibrate and transform our measurements from pixels into millimeters. In total, we measured 354 individuals from Crescent Pond and 287 individuals from Little Lake. We used R to convert the 30 landmarks into linear distances. To reduce measurement error due to the lateral positioning of the specimens, we took the mean distances from the two clearest skull and whole-body photographs for each individual when possible. If an individual did not have two clear photographs for each orientation, we measured the single clearest photograph. Finally, we size-corrected each trait by using the residuals from a linear model including the log-transformed measurement of each trait as the response variable and log-transformed standard length as the predictor variable. We investigated whether size-corrected traits varied between the two populations using a PCA and a MANOVA test, but found no appreciable difference between them (Supplemental Figure 1, num df = 28, approximate F-value= 0.34, P = 1)

Genotyping

We genotyped individuals using three different methods: First, we used whole genome resequencing for the wild-caught F0 parental generation of our Crescent Pond and Little Lake intercrosses. We used DNeasy Blood and Tissue Kits (Qiagen, Inc.) to extract DNA from the muscle tissue of each fish and quantified it on a Qubit 3.0 fluoromether (Thermofisher Scientific, Inc.). Genomic libraries were then prepared at the Vincent J. Coates Genomic Sequencing Center (QB3) using the automated Apollo 324 system (WaterGen Biosystems, Inc.). Samples were fragmented using Covaris sonication and barcoded with Illumina indices. A quality check was also performed on all samples using a Fragment Analyzer (Advanced Analytical Technologies, Inc.). We used 150 paired-end sequencing on an Illumina Hiseq4000 for these four parental samples along with an additional 38 samples that were included in a previous study (Richards and Martin 2017).

Second, in addition to the 190 previously sequenced individuals from Crescent Pond used for a QTL mapping study (Martin et al. 2017), we included an additional 164

F2 individuals from Crescent Pond sequenced using double-digest restriction site associated sequencing (ddRADseq) following similar library prep and sequencing methods described in Martin et al. (2015, 2016, 2017). Briefly, we prepared four indexed libraries each containing 96 barcoded individuals. We sequenced these using 100 single-end high-output mode on two lanes of Illumina Hiseq4000 at the Vincent J. Coates Genomic Sequencing Center (QB3).

Finally, we sequenced all F2 individuals from Little Lake and a subset of previously sequenced, but low-coverage Crescent Pond F2's (N=84), using Nextera-tagmented reductively-amplified DNA (NextRad) sequencing (Russello et al. 2015). We followed the above methods for DNA extraction and sent samples to SNPsaurus (SNPsaurus, LLC) for quality checking, NextRad library preparation, and 150 single-end sequencing on two lanes of Illumina Hiseq4000 at the University of Oregon sequencing core.

Calling variants

We used the following methods to call variants separately for: 1) the Crescent Pond intercross (2 parents and 354 F2 hybrids), and 2) the Little Lake intercross (2 parents and 285 F2 hybrids): First, we inspected raw read quality using FastQC (Babraham Bioinformatics Institute, v0.11.7) and trimmed reads to their appropriate length (100bp for samples sequenced with ddRAD, and 150bp for samples sequenced with NextRAD) using TrimGalore! (v0.6.4). For samples that were sequenced using both ddRAD and NextRad methods, we concatenated trimmed raw reads into a single file. We next used bwa-mem to map reads from all individuals in an intercross, both parents and offspring, to the *Cyprinodon brontotheroides* reference genome (v 1.0; total sequence length = 1,162,855,435 bp; number of scaffolds = 15,698, scaffold N50 = 32 Mbp; (Richards et al. 2021)). We identified duplicate reads using MarkDuplicates and created BAM indices using BuildBamIndex in the Picard package (http://picard.sourceforge.net(v.2.0.1)). Following the best practices guide from the Genome Analysis Toolkit (v 3.5; (Depristo et al. 2011)), we called and refined our single nucleotide polymorphism (SNP) variant data set using the program HaplotypeCaller. Pupfish lack high-quality known alleles because they are a non-model organism; we therefore used the recommended hard filter criteria (QD < 2.0; FS <; 60; MQRankSum < -12.5; ReadPosRankSum < -8; (Depristo et al. 2011; Marsden et al. 2014)) to filter our SNP variant dataset. Ultimately, we detected 13.7 million variants in our Crescent Pond dataset and 14.4 million variants in our Little Lake dataset.

We used the program STACKS to further filter our dataset and convert our vcf files into phenotype and genotype comma-separated values files that could be imported into the Rqtl program. Specifically, we used the populations program to filter out variants that were not present in both the parental and F2 populations, and to filter out variants found in 10% or less of the population. From this filtering step we retained 36,318 variants with 46.5 mean mappable progeny per site in Crescent Pond and 87,579 variants with 85.984 mean mappable progeny per site in Little Lake.

We continued to filter our datasets using the Rqtl (v1.46-2), and ASMap (v1.0-4) packages (Broman et al. 2003; Taylor and Butler 2017). We started filtering by removing individuals that did not contain any filtered variants and any duplicate individuals. This reduced our Crescent Pond data set to 227 individuals, and our Little Lake data set to

281 individuals. Next, we filtered markers that had >0.98 or <0.1 heterozygosity (Crescent Pond: markers =15,247, Little Lake: markers=14,661). This step also filtered out 13 individuals from Crescent Pond which only contained markers with >0.98 or <0.1 heterozygosity. Before constructing our genetic maps, we set aside markers that appeared to suffer from segregation distortion. We used the pullCross() function from the ASmap package to set aside markers in both data sets that were missing in >75% of individuals, departed from Mendelian ratios (1:2:1), or any co-located markers for the initial construction of the linkage maps. This filtering retained more than twice the number of markers for Crescent Pond than Little Lake. We therefore used a stricter filtering threshold for missing data (i.e., removing markers with >72% missing data) for our Crescent Pond dataset to construct linkage maps of comparable sizes for downstream comparative analyses. At the end of this filtering process the Crescent Pond dataset contained 214 individuals and 657 markers and the Little Lake dataset contained 281 individuals with 490 markers.

Linkage map construction

We used the mstmap.cross() function to form initial linkage groups and order markers, using the kosambi method for calculating genetic distances and a clustering threshold of $P = 1 \times 10^{-14}$ for Little Lake and $P = 1 \times 10^{-20}$ for Crescent Pond. After forming these initial linkage groups, we used the pushCross() function from the ASmap package to integrate previously set aside markers back into our map. We pushed markers back based on a segregation ratio of 3:4:3 and we pushed back any markers that had previously been designated as co-located. This increased our map sizes to 817 markers for Crescent Pond and 580 markers for Little Lake. With these additional markers, we re-estimated our linkage map using the est.rf() and formLinkageGroups() functions from the Rqtl package. We used a max recombination fraction of 0.35 and a minimum LOD threshold of 5 to estimate linkage groups for both data sets. We used the droponemarker() command from Rqtl with an error probability of 0.01 to identify and drop problematic markers from the genetic maps, including dropping linkage groups with 3 or fewer markers. Finally, we visually inspected our linkage groups using plotRF() from the Rqtl package, and merged linkage groups which had been incorrectly split up using the mergeCross() function from the ASmap package. Ultimately our final genetic maps included: 1) Crescent Pond: 214 individuals, 743 markers, 24 linkage groups and 2) Little Lake: 281 individuals, 540 markers, and 24 linkage groups (Figure 2).

QTL analyses

We mapped QTL for 29 skeletal traits for both populations, and additional morphological (adductor mandibulae muscle mass) and behavioral traits (mate preference) for Crescent Pond. We used the Rqtl2 package (v0.22-11) to calculate genotype probabilities with a multipoint hidden Markov model using an error probability of 0.0001 and a Kosambi map function. We calculated kinship matrices to account for the relationship among individuals in two ways: 1) overall kinship, which represents the proportion of shared alleles between individuals, and 2) kinship calculated using the leave-one-chromosome-out method (LOCO). We used the scan1() function to perform three separate genome scans using a single-qtl model by: 1) Haley-Knott regression, 2) a linear mixed model using the overall kinship matrix, and 3) a linear mixed model using

the LOCO kinship matrix. For our Crescent Pond data set we also included sex as an additive covariate. We assessed the significance of all three models using two significance thresholds $P < 0.1$ and 0.05 based on 1000 permutations each, using the scan1perm() function. As noted above the scan1() function can use several different methods to determine if a region is significantly associated with a given phenotype (Broman et al., 2019; Haley & Knott, 1992; Yang, Zaitlen, Goddard, Visscher, & Price, 2014; Yu et al., 2006), however, it is clear from previous theoretical work that many of these methods may suffer from type II error depending on the size of an organism's genome, the density of markers in a linkage map, or the complexity of the phenotypic traits being measured (Lander and Botstein 1989; Risch 1990). We therefore relaxed the *P*-value cut off from 0.05 to 0.1 to capture potentially important genomic regions. This relaxation is further supported by the LOD scores associated with regions significant at the $P<0.1$ level because they all exceed the traditional threshold of 3 (Nyholt 2000), the more conservative threshold of ~3.3 (Lander and Kruglyak 1995; Nyholt 2000), the suggestive threshold of 1.86 (Lander and Kruglyak 1995), and are in line with estimates of significant LOD thresholds in previous studies (Erickson et al. 2016). All three of these methods detected similar QTLs and moving forward we only used the Haley-Knott regression method.

For each trait, we calculated the location of the maximum LOD score, and used the fit1() function to re-fit a single-QTL model at this location. We used the newly calculated LOD score to estimate the proportion of variance explained by the QTL and to calculate a *P*-value associated with each significant QTL (x^2-test). We also used the location of the maximum LOD score to calculate 95% Bayes credible intervals using the bayes_int() function from the Rqtl2 package. We note that the maximum LOD score associated with every trait across both ponds exceeded the suggestive threshold of 1.86 (Lander and Kruglyak 1995). We used the find.markerpos() function from Rqtl to determine where markers in each linkage map fell within the reference genome. With this information we were able to determine the scaffolds/positions from the reference genome that fell within the 95% credible intervals for each putative QTL. Finally, we used the maxmarg() function from the Rqtl2 package to find the genotype with the maximum marginal probability at the location of the maximum LOD. We used these genotypes to visualize the relationship between genotype and phenotypes.

Identifying adaptive alleles within QTL regions

For each scaffold that fell within a QTL's credible interval we calculated the minimum and maximum position for that scaffold (that was identified in the putative QTL region) and searched the *C. brontotheroides* reference genome for annotated genes within the region. We then compared this list to a previously published list of genes that 1) contained or were adjacent to (within 20 kbp) fixed or nearly fixed ($Fst > 0.95$) SNPs between specialist species on SSI, and 2) showed significant evidence of a hard selective sweep in both the site frequency spectrum-based method SweeD (Pavlidis et al. 2013) and the linkage-disequilibrium-based method OmegaPlus (Alachiotis et al. 2012). We hereafter refer to these loci as adaptive alleles. We also noted whether adaptive alleles within QTL regions were classified as de novo, introgressed, or as standing genetic variation on SSI (Richards et al. 2021). We used a bootstrap resampling method to determine whether the observed proportions of adaptive alleles

originating from de novo, introgression, or standing genetic variation found within QTL 95% credible intervals were different than the proportions expected when drawn from the genome at random. We used the boot (v. 1.3-25) package (Buckland et al. 1998; Canty and Ripley 2021) to resample our entire adaptive allele dataset (with replacement) 10,000 times. We then used the boot.ci() command from the boot package to calculated the 95% credible intervals around expected proportions of de novo, introgressed, and standing adaptive alleles. We performed these calculations separately for scale-eater and snail-eater adaptive alleles.

Results

Linkage map construction

We identified 24 linkage groups from 743 markers for Crescent Pond, and 24 linkage groups from 540 markers for Little Lake (Figure 2). Previous karyotypes of *Cyprinodon* species estimated 24 diploid chromosomes, matching the linkage groups in this study (Liu & Echelle, 2013; Stevenson, 1981). The total map length for Crescent Pond was 7335 cM and the total map length for Little Lake was 5330; the largest linkage groups for each map were 740 cM and 380 cM, respectively, and inter-marker map distance did not exceed 20cM in either map. To compare our maps and to determine if the same genomic regions were being reused across lakes, we identified where each marker was located in our reference genome. Overall, we found 324 markers in both maps that were within 10 Kbp of one another, indicating that 60% of the Little Lake map was also present in the Crescent Pond map and 44% of the Crescent Pond map was present in the Little Lake map (Figure 3).

Craniofacial QTL

We detected three significant QTL in Crescent Pond and five QTL in Little Lake (Table 1, Table 2). In Crescent Pond, we identified QTL associated with the depth of the dentigerous arm of the premaxilla, cranial height, and adductor mandibulae muscle mass. Cranial height in Crescent Pond mapped to linkage group (LG) 10. Dentigerous arm depth and adductor mandibulae muscle mass both mapped to LG 13, which also contained the max LOD scores for two additional jaw traits (jaw opening in-lever and maxillary head height; Table 2). The 95% credible intervals for all these traits overlapped, suggesting that LG 13 may contain a single pleiotropic locus or many loci that affect all four traits.

In Little Lake, we detected significant QTL associated with jaw closing in-lever (i.e. height of the coronoid process on the articular: LG9), width and depth of the dentigerous arm of the premaxilla (LG3 and LG6), maxillary head protrusion (LG10), and cranial height (LG1; Table 1, Table 2). The 95% credible interval for dentigerous arm width on LG3 also contained the max LOD score for lower jaw length, suggesting that either a single pleiotropic locus or a cluster of loci in this region may be controlling both traits.

Candidate genes and adaptive alleles within QTL regions

Cranial height

Cranial height was the only trait with statistically significant or marginally significant QTL in both lakes (Figure 4, $P < 0.1$). While the QTL occurred on different linkage groups between maps, we found a high degree of synteny between these linkage groups indicating that the QTL is located in the same genomic region in both lakes (Table 2, Figure 3). We also found the same overdominant genetic pattern in both lake crosses: heterozygotes showed increased cranial height relative to homozygous individuals (Figure 5).

We found 44 genes within scaffold 33 that fell partially or fully within the 95% credible intervals of the QTL in both lakes (Table 1, Supplemental Table 1). Only three of these genes contained adaptive alleles within 20 kb: *wdr31*, *bri3bp*, and *gnaq* (Table ***3*** 3). Interestingly, *gnaq* is well known to be associated with craniofacial development (Hall et al. 2007; Shirley et al. 2013) and is differentially expressed between our specialist species in developing larvae (McGirr and Martin 2020).

Dentigerous arm width

We found that regions on scaffolds 58 and 24 were associated with a significant QTL for dentigerous arm width in Little Lake and contained the max LOD scores for maxillary head protrusion and female mate preference in Crescent Pond (Table 1, Table 2). We found 161 genes which fell partially or completely within these shared regions, but only 2 genes, *dysf* and *cyp26b1*, which contained adaptive alleles within 20 kbp (Table 3). The *dysf* gene provides instructions for making a protein called dysferlin, which is found in the sarcolemma membrane that surrounds muscle fibers (Liu et al. 1998). This could indicate a role for muscle development in affecting skeletal development of the maxilla and premaxilla.

Dentigerous arm depth

The QTL for dentigerous arm depth in Little Lake was associated with LG 6, which corresponds to LG 7 in Crescent Pond, however, no traits from Crescent Pond mapped to this linkage group (Table 2, Figure 3). Instead, dentigerous arm depth in Crescent Pond was associated with LG 13 and did not share any similar genomic regions with those associated with dentigerous arm depth in Little Lake. We found 80 genes completely or partially within the 95% credible region for this QTL in Little Lake, but none contained adaptive alleles based on our criteria (Supplemental Table 1). In fact, only a single adaptive allele was found in this QTL region, but it was in an unannotated region of the genome (Table 3).

Maxillary head protrusion

Maxillary head protrusion in Little Lake mapped to a QTL region on LG10 which corresponds to the max LOD scores for both lower jaw length and caudal peduncle height in Crescent Pond (Table 2, Figure 3). Across lakes, all three traits were associated with scaffolds 53, 2336, and 6275. We found 528 genes partially or fully within these shared regions, but only 21 of these genes contained adaptive alleles within 20 kbp (Table 3). One of these genes, *twist1*, contains a non-synonymous substitution fixed in scale-eating pupfish on San Salvador Island, Bahamas (Richards et al. 2021). *Twist1* is a transcription factor and oncogene associated with palate

development and oral jaw size in model organisms (Parsons et al. 2014; Teng et al. 2018).

Jaw closing in-lever
The QTL for jaw closing in-lever was associated with LG 9 in Little Lake, which corresponds to the max LOD scores for orbit diameter and anterior body depth in Crescent Pond (Table 2, Figure 3). Scaffolds 8 and 8020 were associated with all three of these traits. We found 13 genes which partially or completely fell within these shared regions, and only two genes, *map2k6* and *galr2*, which contained adaptive alleles within 20 kbp (Table 3). *Galr2* was also previously detected within a significant QTL for lower jaw length in pupfish (Martin et al. 2017).

Dentigerous arm depth and adductor mandibulae muscle mass
Finally, in Crescent Pond the QTL for dentigerous arm depth and adductor mandibulae muscle mass mapped to the exact same location on LG 13 (95% CI dentigerous arm depth (0, 250), adductor mandibulae muscle mass (0,70). This linkage group corresponds to LG14 in Little Lake, which contains the max LOD scores for both palatine height and suspensorium length (Table 3). We found 52 genes that overlapped between these regions, 18 of which contained adaptive alleles. Furthermore, three of the genes— *ube2w, ncoa2, and prlh*—contained adaptive alleles that introgressed from Laguna Bavaro in the Dominican Republic to snail-eating pupfish (*ube2w*), from Lake Cunningham, New Providence Island to scale-eating pupfish (*ncoa2*), or from North Carolina, USA to scale-eating pupfish (*prlh)*. We also found four genes that contained adaptive alleles within 20 kbp that arose from de novo mutations: *cd226, cmbl, slc51a,* and *zfhx;* however*,* only one adaptive allele in *slc51a* is found within a coding region.

Origins of adaptive alleles
Adaptive alleles originating from standing genetic variation across the Caribbean were most common within shared QTL regions between lakes (86.03% within scale-eater populations, and 53.32% within snail-eating populations; Table 3). However, observed proportions within shared QTL were significantly less than expected by chance (scale-eater expected 95% CI: (88.33%-90.37%), snail-eater expected 95% CI: (62%-67%;10,000 bootstrapped iterations). Instead, we found more introgressed scale-eater and snail-eater adaptive variants in shared QTL regions than expected by chance (Scale-eater observed: 12.13% introgressed, scale-eater expected 95% CI: (7.96%-9.88%); Snail-eater observed: 46.67% introgressed, snail-eater expected 95% CI: (32.22%-37.06%)). Finally, we found that about 1.83% of adaptive alleles within overlapping regions between lakes originated from de novo mutations in scale-eaters, however, this fell within the predicted null range (95% CI: (1.29%-2.17%)).

Discussion

Parallel genetic changes underlie 5 out of 6 of craniofacial QTL
We found evidence supporting both parallel and non-parallel genetic changes in an adaptive radiation of trophic specialist pupfishes. A single significant QTL was associated with cranial height in both lakes and mapped to the same genomic region,

suggesting that parallel genetic changes are responsible for variation in this trait in both lakes. On the other hand, significant QTLs were identified for premaxilla dentigerous arm depth in each lake, but they mapped to different locations, indicating that this trait is associated with non-parallel genetic changes. We found an additional three traits with significant QTLs (dentigerous arm width, jaw closing in-lever, maxillary head protrusion) in the Little Lake population that were not detected in Crescent Pond. However, all genomic regions associated with these traits in Little Lake also mapped to the max LOD score for this same integrated suite of craniofacial traits in Crescent Pond. Therefore, rather than assume independent QTL for each trait, we conservatively conclude that the same genomic regions are being reused in each lake and affect a highly integrated suite of craniofacial traits. Overall, we found that 5 out of the 6 significant QTLs were reused in some way across lakes suggesting that parallel genetic changes underly adaptive phenotypes in the San Salvador Island pupfish radiation.

High level of QTL reuse across ponds

Overall, we found that about 16% (1 out of 6) of the identified QTL regions corresponded to non-parallel changes and 84% (5 out of 6) corresponded to parallel genetic changes—either affecting the same phenotypic trait or a tightly correlated craniofacial trait— across populations. The presence of both non-parallel and parallel genetic changes leading to convergent phenotypes across lakes has been documented previously. For example, Colosimo et al. (2004) investigated the genetic basis of armor plate morphology in two independent threespine stickleback populations and found a single large effect locus on LG 4 in the two populations. However, they also noted a potential difference in the dominance relationships of alleles across ponds at this location, and found additional differences in modifier QTLs between populations, suggesting that both parallel and non-parallel genetic changes could lead to the loss of armor plating. Similarly, Erickson et al. (2016) found evidence for both parallel (43% of QTL regions overlapped between at least two populations) and non-parallel (57% of QTL regions were found in only a single population) evolution in a QTL study investigating the genetic basis of 36 skeletal phenotypes in three independent threespine stickleback populations. However, our findings suggest that pupfish exhibit a much higher proportion of parallel evolution than previously documented in stickleback. In fact, Conte et al. (2012) estimated that the probability of convergence via gene reuse is only 32-55% —which is 1.5 to 2.5 times lower than our current finding— although this may be underestimated (Stern 2013).

Pupfish may have a higher rate of parallel evolution than other model fish speciation systems for a few reasons. First, the pupfish radiation is recent, although comparable in age to glacial stickleback populations, with specialist species diverging less than 10kya (Hagey and Mylroie 1995; Martin and Wainwright 2013a), and parallel evolution is predicted to be more likely when populations or species have recently diverged (Rosenblum et al. 2014). This may be because recently diverged species are more likely to experience similar environments, have access to similar pools of genetic variation (either due to standing genetic variation or introgression), or similar genetic constraints. Second, the genomic basis of pupfish skeletal traits may be primarily controlled by cis-regulatory elements, which evolve more quickly and have less negative pleiotropy which may make them more likely to undergo parallel evolution (Stern and

Orgogozo 2008). However, a previous study of allele-specific expression in the pupfish system found strong evidence that two cis-regulatory alleles were associated with skeletal development, but trans-acting elements predominated overall (McGirr and Martin 2021).

In part, the increased proportion of parallel evolution estimated in this study results from our relaxed thresholds for detecting and categorizing shared QTL regions. Previous QTL studies have typically searched for evidence of parallel evolution by only looking for one-to-one mapping in which the same genomic regions are associated with the same trait across populations at a genome-wide level of significance in each (Colosimo et al. 2004; Conte et al. 2012). While this method provides the most clear-cut examples of parallel evolution, we argue that it vastly underestimates its frequency in nature. For example, this method would not consider reuse of the same genomic regions for integrated morphological traits as parallel evolution, a pattern seen in this study and in Erickson et al. (2016). Furthermore, the strict one-to-one significance method for detecting parallel evolution does not include consideration of the hierarchy and diversity of convergence and parallel evolution, which can span morphological traits, ecotypes, performance, or even fitness (James et al. 2020; Rosenblum et al., 2014; Stern, 2013; Martin and Wainwright 2013). Ultimately, we argue that our method of quantifying parallel evolution provides a more wholistic view of the process and better captures the frequency of reuse of adaptive genetic variation in nature.

Few QTL may affect many highly integrated craniofacial traits

There are several processes that may cause the same genomic regions to be associated with different traits between lakes. First, these genomic regions may be highly pleiotropic and affect several traits simultaneously. For example, Albert et al. (2007) found that that on average a single QTL affected 3.5 phenotypic traits in an analysis of 54 body traits in three-spine stickleback. Wagner et al. (2008) found a similar pattern in QTL analyses of 70 skeletal traits in mice, where a single QTL affected on average 7.8 phenotypic traits (the maximum being 30).

A second possibility is that a single QTL region may contain several tightly linked causative variants that are responsible for variation in many traits. Correlated phenotypic traits are generally assumed to have a shared genetic basis, but it is extremely difficult to determine if this is due to pleiotropy or tight linkage between genomic regions (Lynch and Walsh 1998; Gardner and Latta 2007; Paaby and Rockman 2013; Wright et al. 2010).

Finally, it may be that differences in methodology or sample sizes between lakes enable us to detect significant QTL for some traits in one lake and not the other. For example, our analyses of Little Lake allowed us to detect significant QTL for effect sizes greater than 6.54 PVE at 80% power, but we could only detect significant QTL for effect sizes greater than 8.41 PVE at 80% power in Crescent Pond due to our lower sample size for this cross (Sen et al. 2007). However, this level of power is typical in many non-model QTL studies (Ashton et al. 2017). The ability to detect a significant QTL in one lake but not the other may be further explained by our use of different sequencing methods between populations. However, a critical component of our analyses involved searching for regions within 10 kbp of one another across maps to provide confidence that if we detected a significant QTL in one lake and not the other that it was not simply

because that genomic region was not captured by the sequencing. For example, in Little Lake we detected a significant QTL associated with dentigerous arm depth on LG 6 but did not find any traits associated with this region of the genome in Crescent Pond.

QTL are associated with different craniofacial traits across different lakes

In this study we found an intriguing pattern of different traits mapping to the same region of the genome across lake populations. One potential explanation for this is that there are different relationships between traits in each lake, and we find some evidence of this in our phenotypic data. Supplemental Figure S2 depicts correlation matrices between traits in 1) Little Lake and 2) Crescent Pond, and X^2 comparisons of these two matrices reveals that the relationship between traits varies significantly between lakes (X^2=3135.99, df = 756, P< 3.6e-29). For example, the relationship between maxillary head protrusion and lower jaw length is more than two times stronger in Little Lake compared to Crescent Pond (Pearson's r_{LL}=0.27, Pearson's r_{CP} = 0.12), the relationship between dentigerous arm depth and suspensorium length is 1.8 times stronger in Little Lake than in Crescent Pond (Pearson's r_{LL}=0.45, Pearson's r_{CP} = 0.24), and the relationship between jaw closing in-lever and anterior body depth is more than two times stronger in Crescent Pond than in Little Lake (Pearson's r_{CP} = 0.23, Pearson's r_{LL}=0.11).

This pattern may be explained by different epistatic interactions in each lake. For example, Juenger et al. (2005) detected significant QTL-QTL interactions in one mapping population of *Arabidopsis* but found no evidence of the same interactions in the other population. When we investigated the relationship between phenotype and genotype for cranial height, we found the same overdominance pattern in both lakes (Figure 5). However, the presence of epistatic interactions may also be an obstacle for QTL detection. In a mapping study of body weight in chicken, Carlborg et al. (2006) were only able to detect a single weak QTL despite the extremely divergent phenotypes between parental lines. However, when accounting for epistatic interactions, Carlborg et al. identified several additional significant QTL regions that explained a large amount of variation in body weights.

Finally, our method for searching for putative QTL regions may have led to this pattern. Similar studies have searched for influential genomic regions by first identifying a putative QTL in a single population, and then searching the already identified linkage group in the second population for any signal of a QTL associated with the same phenotype, often using relaxed LOD thresholds closer to the suggestive cut-off (LOD> 1.8, e.g., Erickson et al. 2016). Our approach, however, independently identified the positions of maximum LOD for all traits across the entire linkage map before searching for similar implicated regions between populations. We argue that our approach minimizes bias, because there are no prior expectations about which traits should be associated with a given genomic region within a suite of integrated traits, and reduces false positives because we only examine the maximum LOD position for each trait.

Identifying causative regions within QTL

Multiple mapping populations across lakes may also be particularly useful for identifying candidate causal alleles. We found that one out of our six unique QTL regions mapped to the same genomic location across lakes and was associated with the same

phenotypic trait—cranial height (Figure 4). In Crescent Pond, we found that a region of 110 cM was associated with this trait (LG10, position: 204, 95% CI (130,340)), which contained 426 genes. However, when we compared this region to the region independently identified in our Little Lake analysis, we found that the overlapping region was reduced to 20cM (LG1, position: 259, 95% CI (250-270)) and contained only 44 genes—a reduction of more than 80%. We found a similar pattern in the additional four QTL regions that mapped to the same genomic location across maps but were associated with different phenotypic traits and observed an average 56% reduction in region size. As noted above, Erickson et al. (2016) used a similar method of identifying candidate QTL regions across three hybrid populations of stickleback, and found that 43% of identified QTL regions were shared across two or more populations; however, they did not investigate whether these QTL regions completely or partially overlapped.

We also searched for adaptive alleles within QTL region that were identified in a previous study as 1) nearly fixed between species (F_{st} >0.95) and 2) showed significant evidence of a hard selective sweep (Richards et al. 2021). Overall, we found 789 shared genes within shared QTL regions across lakes, and that 45 of those genes contained adaptive variants (5.7%). This is a six-fold increase from the genome-wide expectation of 0.91% (176 genes associated with at least one adaptive variant / 19304 annotated genic regions), suggesting that these specific regions are important for adaptation to scale- and snail-feeding in wild pupfish. For example, a variant in *twist1* was found within the region associated with maxillary head protrusion in Little Lake (which also overlapped with lower jaw length and caudal peduncle height in Crescent Pond). In model organisms, *twist1* is associated with palate and jaw development (Parsons et al. 2014; Teng et al. 2018), and previous genome-wide association scans in pupfish showed that a region containing *twist1* was significantly associated with oral jaw size in the system (Richards et al. 2021). Similarly, we found that variants associated with *galr2* fell within the QTL region associated with jaw closing in-lever in Little Lake (which also overlapped with regions associated with orbit diameter and anterior body depth in Crescent Pond; scaffolds 8 and 8020), and previous QTL mapping studies, gene expression studies, and genome-wide association analyses have all implicated regions containing *galr2* with oral jaw development in pupfish (McGirr and Martin 2016; Martin et al. 2017; Richards et al. 2021).

Increased use of introgressed adaptive variants in QTL regions

We found that most genetic variation within shared QTL regions was also segregating across outgroup Caribbean generalist populations characterized by Richards et al. (2021; 86.04% within scale-eater populations, and 53.32% within snail-eating populations). Furthermore, we found more introgressed adaptive alleles from both scale-eater (observed: 12.13% introgressed, expected 95% CI: (7.96%-9.88%)) and snail-eater populations in shared QTL regions than expected by chance (observed: 46.67%, expected 95% CI: (32.22%-37.06%)). This supports the prediction that standing genetic variation and introgressed variation should underlie parallel genetic changes (Stern 2013; Thompson et al. 2019). Finally, we found that only 1.83% of adaptive alleles within shared QTL regions across both lakes originated from de novo mutations on San Salvador Island. While this percentage did not differ significantly from

the expected estimates (expected 95% CI: 1.3%-2.17%) it does not eliminate the possibility that de novo mutations play an important adaptive role in pupfish evolution.

Conclusion

In conclusion, we found that a single QTL region was responsible for variation in cranial height in both populations, and an additional four QTL regions were responsible for variation in different craniofacial traits across lakes, suggesting that parallel genetic changes underlie integrated suites of adaptive craniofacial phenotypes on San Salvador Island. Adaptive alleles were more commonly found within these detected QTL regions, and more of these adaptive alleles arrived on SSI via introgression than expected by chance. Finally, we argue that investigating QTL regions across populations in concert with estimation of hard selective sweeps in wild populations is a powerful tool for identifying potential causative regions of the genome affecting adaptive divergence.

Acknowledgements

We thank the University of California, Davis, the University of California, Berkeley, the University of North Carolina at Chapel Hill, NSF CAREER 1749764, NIH 5R01DE027052-02, and BSF 2016136 for funding to CHM. The Bahamas Environmental Science and Technology Commission and the Ministry of Agriculture provided permission to export fish and conduct this research. Rochelle Hanna, Velda Knowles, Troy Day, and the Gerace Research Centre provided logistical assistance in the field. All animal care protocols were approved by the University of California, Davis and the University of California, Berkeley Animal Care

Author Contributions

MESJ and CHM designed research; MESJ, CHM, JCD, and SR performed data collection; MESJ and EJR performed data analysis; MESJ and CHM wrote the paper. CHM provided funding.

Tables

Table 1. Maximum LOD scores for all 29 traits measured in Little Lake and Crescent Pond mapping crosses. A genome scan with a single-QTL model by Haley-Knott regression was used to identify the position with the highest LOD score, 95% Bayesian credible intervals, and the genome-wide significance level for each trait (*P*< 0.1: ·; *P* < 0.05: *). We also report the scaffold numbers of genomic regions that fell within the 95% credible intervals associated with the maximum LOD position for each trait, the number of individuals phenotyped, percent variance explained (PVE) by the max LOD region, and the uncorrected *P*-value associated with each max LOD region.

Trait	Population	Scaffold	Max LOD	Genome-wide sig.	n	PVE	x^2 *P*-Value
Lower Jaw Length	Crescent Pond	53, 7087, 2336, 6275, 26, 7335	2.89		205	6.29	0.0013
	Little Lake	24, 4028, 58, 16	3.30		228	6.45	0.0005
Jaw closing In-Lever	Crescent Pond	31, 4, 451, 19	3.60		204	7.81	0.0002
	Little Lake	8, 9588, 8020	4.11	·	227	7.99	0.0001
Jaw Opening In-Lever	Crescent Pond	6086, 11	2.43		205	5.32	0.0037
	Little Lake	43	2.98		227	5.87	0.0010
Palatine Height	Crescent Pond	34, 22, 6304	2.90		205	6.31	0.0013
	Little Lake	11	2.73		228	5.36	0.0019
Suspen-sorium Length	Crescent Pond	46, 37, 31, 26, 60, 7556, 10198, 22	3.54		204	7.68	0.0003
	Little Lake	11	3.51		227	6.88	0.0003
Dentigerous Arm Width	Crescent Pond	52, 13137, 40	2.19		202	4.87	0.0065
	Little Lake	24, 4028, 58, 16	4.05	·*	228	7.85	0.0001
Maxilla Length	Crescent Pond	27, 593, 4, 31, 451, 19	2.67		204	5.85	0.0021
	Little Lake	56	3.03		228	5.94	0.0009
Dentigerous Arm Base	Crescent Pond	27, 593, 4, 31, 451, 19	2.98		205	6.47	0.0011
	Little Lake	26	3.70		228	7.21	0.0002
Dentigerous Arm Depth	Crescent Pond	6086, 11, 46	4.20	·*	205	9.00	0.0001
	Little Lake	5	3.70	·	217	7.55	0.0002

Ascending Process Length	Crescent Pond	27, 593, 4, 31, 451, 19	2.70		201	6.00	0.0020
	Little Lake	46, 37	3.70		210	7.79	0.0002
Maxillary Head Height	Crescent Pond	6086, 11, 46	2.33		205	5.11	0.0046
	Little Lake	7, 30	2.19		228	4.33	0.0064
Ectopter-ygoid	Crescent Pond	14, 9, 16, 5405, 11419	2.81		205	6.11	0.0016
	Little Lake	9	3.36		228	6.56	0.0004
Maxillary Head Protrusion	Crescent Pond	58, 24, 41, 47	2.70		205	5.88	0.0020
	Little Lake	7431, 53, 6275, 2336, 25	4.03	· *	228	7.82	0.0001
Nasal Tissue Protrusion	Crescent Pond	46, 37, 31, 26, 60, 7556, 10198, 22	2.25		205	4.93	0.0056
	Little Lake	9	3.69		228	7.18	0.0002
Orbit Diameter	Crescent Pond	9588, 8, 8020	2.34		205	5.13	0.0045
	Little Lake	52, 40, 41	2.58		227	5.10	0.0026
Cranial Height	Crescent Pond	33, 39	3.59	·	205	7.74	0.0003
	Little Lake	33	3.94	·	224	7.78	0.0001
Head Depth	Crescent Pond	16, 40	2.98		204	6.51	0.0010
	Little Lake	52, 40, 41	2.71		223	5.45	0.0019
Pelvic Girdle Length	Crescent Pond	31, 18, 15, 11057, 55, 52	2.68		203	5.90	0.0021
	Little Lake	27, 37, 7	2.87		226	5.68	0.0014
Premaxilla Pelvic Girdle	Crescent Pond	37, 46, 7556, 10198	3.15		202	6.92	0.0007
	Little Lake	35, 38, 20, 8508, 10278, 33	2.63		231	5.10	0.0024
Standard Length (mm)	Crescent Pond	14, 9, 16, 5405, 11419	2.90		204	6.34	0.0013
	Little Lake	31, 46, 37	3.48		231	6.69	0.0003
Cranium Dorsal Fin	Crescent Pond	6704, 52, 13137, 40	2.84		205	6.18	0.0014
	Little Lake	37, 22, 7556	3.45		231	6.65	0.0004
Dorsal Fin Width	Crescent Pond	43, 26, 14743	2.18		205	4.78	0.0066

	Little Lake	842, 44, 1074, 6, 30	3.00		230	5.83	0.0010
Dorsal Fin Height	Crescent Pond	18, 31, 15, 11057, 55	2.84		203	6.23	0.0015
	Little Lake	43	3.50		222	7.00	0.0003
Anterior Body Depth	Crescent Pond	8, 8020	2.94		204	6.43	0.0011
	Little Lake	6094, 5, 4	3.33		230	6.45	0.0005
Posterior Body Depth	Crescent Pond	20, 471, 39, 8508, 33	2.86		203	6.27	0.0014
	Little Lake	18, 15	3.02		228	5.92	0.0009
Caudal Peduncle Length	Crescent Pond	31, 18, 15, 11057, 55, 52	2.87		203	6.30	0.0014
	Little Lake	24, 4028, 58, 16	2.16		230	4.23	0.0070
Anal Fin Width	Crescent Pond	18, 15, 11057, 55	2.89		201	6.41	0.0013
	Little Lake	6, 842, 44, 1074, 30	2.40		229	4.71	0.0040
Anal Fin Height	Crescent Pond	43, 26, 14743	2.93		201	6.48	0.0012
	Little Lake	8, 9588, 8020	3.15		229	6.14	0.0007
Caudal Peduncle Height	Crescent Pond	53, 7087, 2336, 6275, 26, 7335	1.97		205	4.32	0.0108
	Little Lake	47, 1962	3.32		230	6.44	0.0005
Adductor	Crescent Pond	6086, 11	3.56	·	170	9.18	0.0003
	Little Lake	-	-	-	-	-	-
Proportion Time Spent Near Scale-Eater Mates	Crescent Pond	58, 24, 41, 47	2.05		74	12.00	0.0089
	Little Lake	-	-	-	-	-	-

Table 2. Position of maximum LOD score and 95% credible intervals for each trait in the Little Lake linkage map and the Crescent Pond linkage map. Colors represent corresponding linkage groups across lakes. Asterisks represent traits that were marginally significant at the $P < 0.1$ level in the genome scan.

Little Lake					Crescent Pond				
Trait	Sig.	LG	Position genomewide Max LOD score	95% CI	Trait	Sig.	LG	Position genomewide Max LOD score	95% CI
Cranial Height	*	1	259	(250,270)	Suspensorium Length		1	566	(20,730)
Premaxilla to Pelvic Girdle		1	146	(0,350)	Nasal Tissue Protrusion		1	570	(0,740)
Cranium to Dorsal Fin		2	303	(160,380)	Premaxilla to Pelvic Girdle		1	568	(310,600)
Lower Jaw Length		3	9	(0,340)	Ectopterygoid		3	272	(0,560)
Dentigerous Arm Width	*	3	9	(0,340)	Standard Length (mm)		3	50	(40,500)
Caudal Peduncle Length		3	168	(0,340)	Dentigerous Arm Width		4	317	(40,510)
Dorsal Find width		4	187	(10,310)	Cranium to Dorsal Fin		4	89	(30,510)
Anal Fin Width		4	14	(0,280)	Lower Jaw Length		5	136	(0,470)
Dentigerous Arm Depth	*	6	79	(20,90)	Caudal Peduncle height		5	381	(0,470)
Anterior Body Depth		6	289	(0,300)	Jaw Closing In-Lever		6	380	(150,410)
Orbit Diameter		8	266	(0,290)	Maxilla Length		6	468	(0,480)
Head Depth		8	206	(0,290)	Dentigerous Arm Base		6	107	(0,480)
Jaw Closing In-Lever	*	9	54	(40,90)	Ascending Proces Length		6	106	(0,470)
Anal Fin Height		9	100	(70,240)	Pelvic Girdle Length		8	370	(20,435)
Maxillary Head Protrusion	*	10	35	(0,260)	Dorsal Fin Height		8	91	(0,380)
Ascending Process Length		12	119	(90,150)	Caudal Peduncle Length		8	258	(30,425)
Standard Length (mm)		12	200	(50,210)	Anal Fin Width		8	190	(110,400)
Ectopterygoid		13	170	(150,180)	Maxillary Head Protrusion		9	300	(0,350)
Nasal Tissue Protrusion		13	193	(20,200)	Proportion Time Spent Near Scale-Eater Males		9	166	(50,340)
Palatine Height		14	147	(110,210)	Cranial Height	*	10	204	(130,340)
Suspensorium Length		14	153	(70,180)	Posterior Body Depth		10	270	(0,330)
Jaw Opening In-Lever		16	58	(40,140)	Palatine Height		11	70	(0,310)
Dorsal Fin Height		16	52	(40,60)	Head Depth		12	111	(100,280)
Pelvic Girdle Length		17	50	(10,160)	Opening In-Lever		13	10	(0,90)
Maxillary Head Height		18	122	(30,160)	Dentigerous Arm Depth	*	13	2	(0,250)
Caudal Peduncle Height		19	44	(20,90)	Maxillary Head Height		13	170	(0,280)
Dentigerous Arm Base		21	74	(0,100)	Adductor Mandibulae Mass	*	13	2	(0,70)
Maxilla Length		22	40	(20,50)	Dorsal Fin Width		14	305	(30,330)
Posterior Body Depth		24	30	(10,30)	Anal Fin Width		14	330	(280,330)
					Orbit Diameter		16	107	(0,190)
					Anterior Body Depth		16	170	(10,220)

Table 3. Number of adaptive alleles and any genes within 20 kbp found in trait QTL with maximum LOD scores for both lakes. Adaptive alleles were categorized as either standing genetic variation (SGV), introgression (Intro.), or de novo mutations, and were estimated independently for snail-eaters and scale-eaters in a previous study (Richards et al. 2021). Asterisks represent traits that were significant at the P < 0.1 level in the genome-wide scan, while crosses show traits that corresponded to the same locations in the alternate lake.

Traits	Gene	Snail-Eater		Scale-Eater		
		SGV	Intro.	SGV	Intro.	de novo
Cranial Height*	*bri3bp*	-	26	28	-	-
	gnaq	9	-	9	-	-
	wdr31	18	2	20	-	-
	Unannotated Regions	1	-	11	-	-
Dentigerous Arm Width*	*cyp26b1*	-	8	8	-	-
	dysf	-	-	1	-	-
Female mate preference† **Maxillary Head Protrusion†**	Unannotated Regions	-	67	216	-	1
Dentigerous Arm Depth*	Unannotated Regions	-	-	1	-	-
Maxillary Head Protrusion* Lower Jaw Length† **Caudal Peduncle Height†**	*cox6b1*	8	-	8	-	-
	cyp21a2	-	-	2	-	-
	eva1b	-	-	2	-	-
	fhod3	-	-	2	-	-
	galnt1	-	-	-	17	-
	glipr2	-	-	3	-	-
	hdac9b	-	-	-	1	-
	mag	-	-	2	-	-
	map7d1	25	-	25	-	-
	mindy3	-	-	8	-	-
	nacad	-	-	2	-	-
	pxn1	-	-	1	-	-
	rasip1	13	-	13	-	-
	slc2a3	15	-	15	-	-
	steap4	-	-	-	26	-
	tbrg4	-	-	2	-	-
	them4	-	-	5	-	-
	tnc	-	-	1	-	-

	twist1	-	-	-	-	1
	zhx2	5	-	6	-	-
	znf628	5	-	6	-	-
	Unannotated Regions	29	68	93	64	-
Jaw closing In-Lever*	*galr2*	-	-	-	2	-
Orbit Diameter†						
Anterior Body Depth†	*map2k6*	-	-	-	3	-
	atp8a2	92	-	92	-	-
	cd226	6	-	6	-	1
	cdk8	-	-	1	-	-
	cmbl	-	-	4	-	7
	crispld1	-	-	7	-	-
	dok6	-	-	50	-	-
	fbxl7	-	-	6	-	-
	hnf4g	-	-	1	-	-
Dentigerous Arm Depth*	*med1*	-	-	26	-	-
Adductor Mandibulae Mass*	*mtrr*	-	-	2	-	-
	ncoa2	7	-	-	4	-
Palatine Height†	*prlh*	-	-	12	6	-
Suspensorium Length†	*rnf6*	-	-	4	-	-
	shisa2	18	-	38	-	-
	slc51a	-	-	22	-	7
	spice1	4	-	2	-	-
	ube2w	-	48	-	-	-
	zfhx4	-	-	-	-	1
	Unannotated Regions	34	34	131	3	1

Figures

Figure 1.

A)

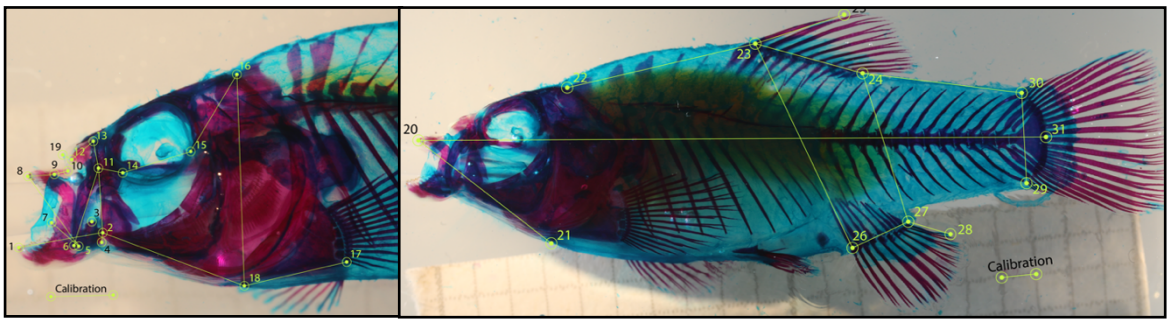

B)

Head			**Body**		
Point 1	Point 2	Trait	Point 1	Point 2	Trait
1	2	Lower Jaw Length	20	21	Premaxilla to Pelvic Girdle
2	3	Jaw closing In-Lever	20	31	Standard Length
2	4	Jaw Opening In-Lever	22	23	Cranium to Dorsal Fin
2	11	Palatine Height	23	24	Dorsal Fin Width
2	18	Suspensorium Length	23	25	Dorsal Fin Height
5	8	Dentigerous Arm Width	23	26	Anterior Body Depth
6	11	Maxilla Length	24	27	Posterior Body Depth
7	5	Dentigerous Arm Base	24	30	Caudal Peduncle Length
8	9	Dentigerous Arm Depth	26	27	Anal Fin Width
9	10	Ascending Process Length	27	28	Anal Fin Height
11	13	Maxillary Head Height	29	30	Caudal Peduncle Height
11	14	Ectopterygoid			
12	13	Maxillary Head Protrusion			
12	19	Nasal Tissue Protrusion			
14	15	Orbit Diameter			
15	16	Cranial Height			
16	18	Head Depth			
17	18	Pelvic Girdle Length			

For the Crescent Pond individuals, we recorded sex and the mass of the adductor mandibulae muscle before clearing and staining each specimen.

Figure 1 A) Representative photographs of F2 intercross cleared and double-stained specimen used for skeletal morphometrics. Points represent landmarks used to measure linear distances between skeletal traits. B) Table containing the two landmarks that correspond to each trait.

Figure 2.

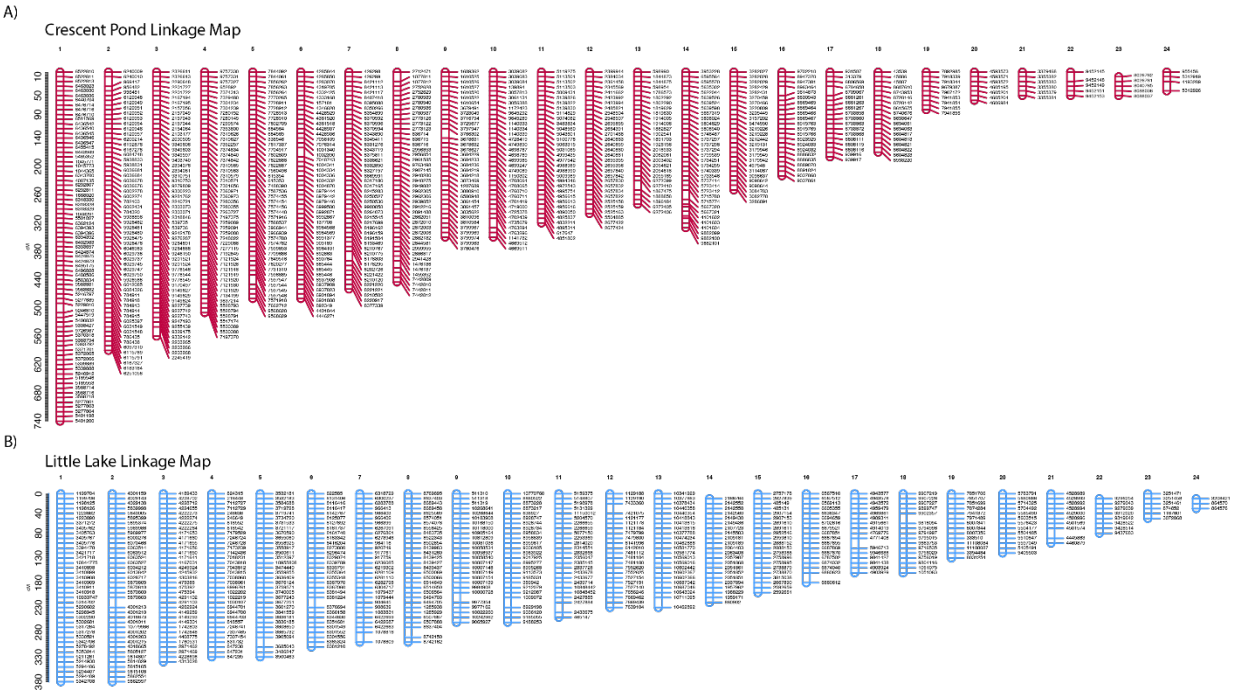

Figure 2 Linkage maps for A) Crescent Pond and B) Little Lake crosses. The Crescent Pond linkage map was estimated from 743 markers and the Little Lake linkage map was estimated from 540 markers. Both maps were generated from crosses between a scale-eater (*C. desquamator*) and snail-eater (*C. brontotheroides*) from the respective lakes.

Figure 3.

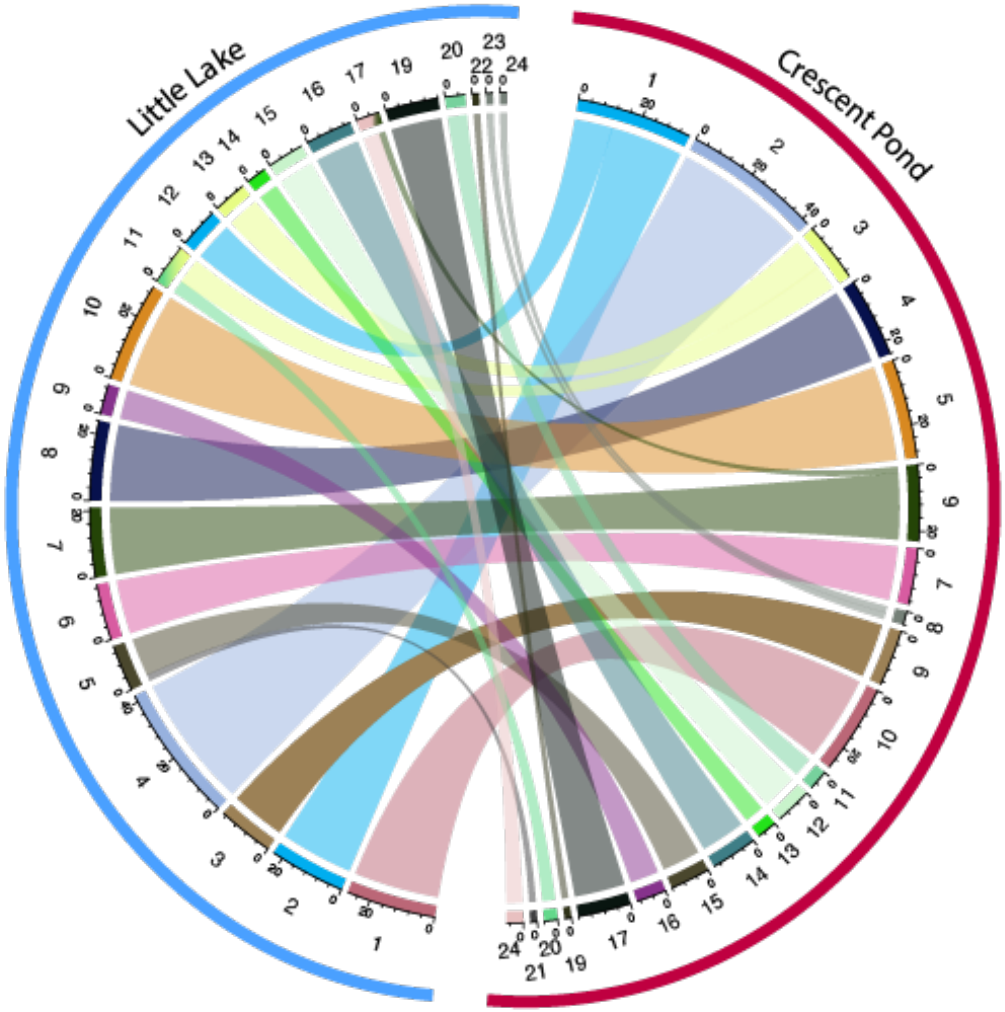

Figure 3 Circos plot depicting the relationship between the Crescent Pond (red) and Little Lake linkage maps (blue), which share 324 markers within 10 kbp of one another. Numbers surrounding each semi-circle represent linkage group numbers in each lake. Markers that are shared across lakes are connected via the colored lines.

Figure 4.

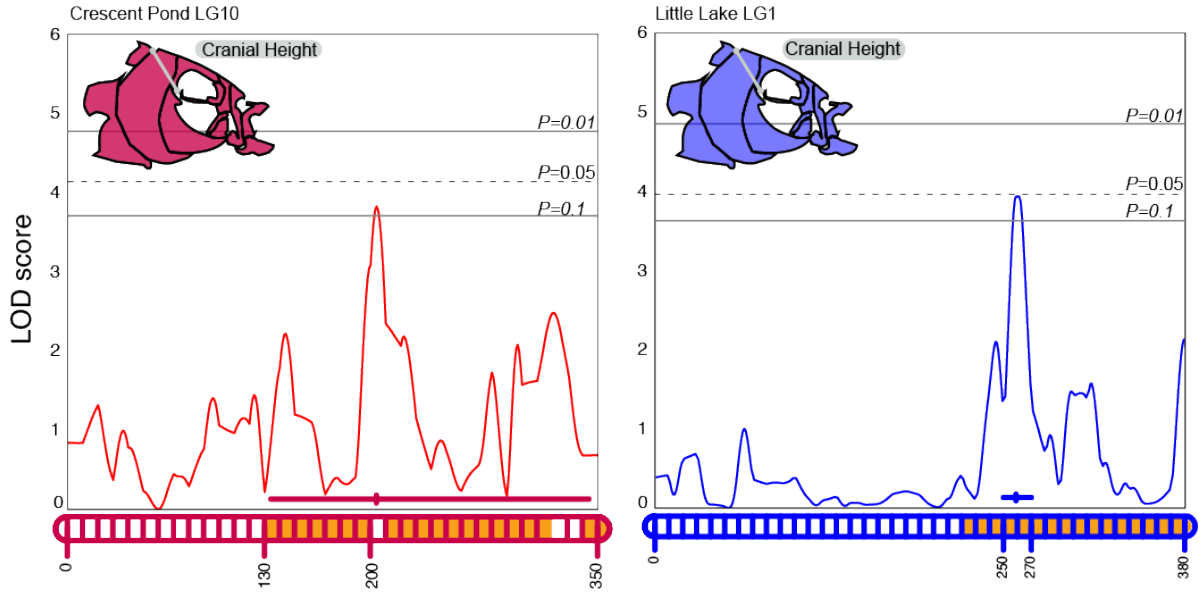

Figure 4 LOD profile for cranial height in Crescent Pond (red) and Little Lake (blue) F2 hybrids. LOD profiles were estimated by a Haley-Knott regression and are plotted relative to the position along the implicated linkage group (LG 10 for Crescent Pond, LG 1 for Little Lake) which are represented along the X-axis. Genome wide significance levels of P = 0.1, 0.05, and 0.01 are shown by the grey horizontal lines. Linkage groups along the X-axis also show the position of maximum LOD along with 95% Bayesian credible intervals. The orange fill color within the linkage groups corresponds to overlapping regions of scaffold 33 between crosses.

Figure 5.

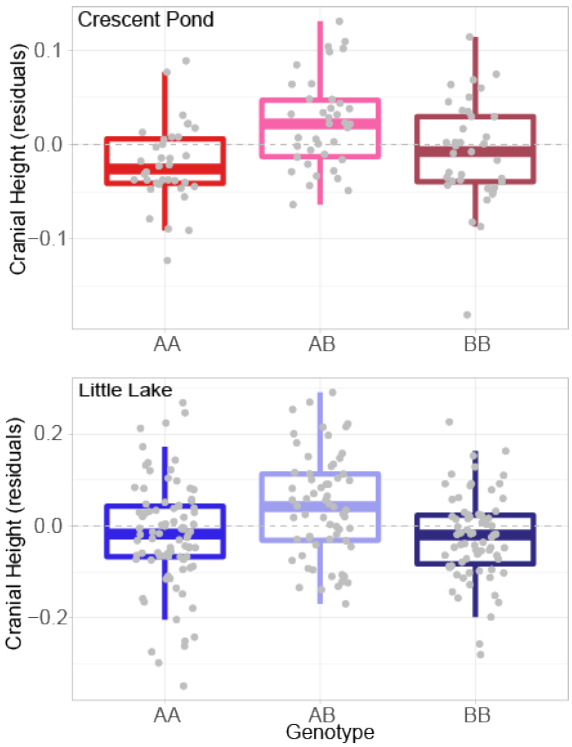

Figure 5 Cranial height phenotypes (size-corrected residuals) for each genotype in Crescent Pond (red) and Little Lake (blue). Both lakes show that heterozygotes (AB) exhibit greater cranial heights than homozygous parental genotypes.

Supplemental Materials

Supplemental tables

Table S1. List of genes that fall within or partially within significant QTL regions.

Trait	Gene	Scaffold	Pop.
Adductor Mandibulae Height	abca4	HiC_scaffold_11	CP
Adductor Mandibulae Height	agrp	HiC_scaffold_11	CP
Adductor Mandibulae Height	ahrr	HiC_scaffold_11	CP
Adductor Mandibulae Height	arhgap29	HiC_scaffold_11	CP
Adductor Mandibulae Height	b2m	HiC_scaffold_11	CP
Adductor Mandibulae Height	bco1	HiC_scaffold_11	CP
Adductor Mandibulae Height	bloc1s5	HiC_scaffold_11	CP
Adductor Mandibulae Height	brpf3	HiC_scaffold_11	CP
Adductor Mandibulae Height	ccdc63	HiC_scaffold_11	CP
Adductor Mandibulae Height	cebpe	HiC_scaffold_11	CP
Adductor Mandibulae Height	cngb3	HiC_scaffold_11	CP
Adductor Mandibulae Height	col11a1	HiC_scaffold_11	CP
Adductor Mandibulae Height	cpne3	HiC_scaffold_11	CP
Adductor Mandibulae Height	dcaf11	HiC_scaffold_11	CP
Adductor Mandibulae Height	dph2	HiC_scaffold_11	CP
Adductor Mandibulae Height	eef1e1	HiC_scaffold_11	CP
Adductor Mandibulae Height	emp3	HiC_scaffold_11	CP
Adductor Mandibulae Height	fam168b	HiC_scaffold_11	CP
Adductor Mandibulae Height	fam83e	HiC_scaffold_11	CP
Adductor Mandibulae Height	fen1	HiC_scaffold_11	CP
Adductor Mandibulae Height	fitm1	HiC_scaffold_11	CP
Adductor Mandibulae Height	foxj3	HiC_scaffold_11	CP
Adductor Mandibulae Height	garem1	HiC_scaffold_11	CP
Adductor Mandibulae Height	glyctk	HiC_scaffold_11	CP
Adductor Mandibulae Height	hbp1	HiC_scaffold_11	CP
Adductor Mandibulae Height	hmcn2	HiC_scaffold_11	CP
Adductor Mandibulae Height	kazn	HiC_scaffold_11	CP
Adductor Mandibulae Height	kazna	HiC_scaffold_11	CP
Adductor Mandibulae Height	kbp	HiC_scaffold_11	CP
Adductor Mandibulae Height	kif20a	HiC_scaffold_11	CP
Adductor Mandibulae Height	mag	HiC_scaffold_11	CP
Adductor Mandibulae Height	mak	HiC_scaffold_11	CP
Adductor Mandibulae Height	mcur1	HiC_scaffold_11	CP
Adductor Mandibulae Height	mon1b	HiC_scaffold_11	CP
Adductor Mandibulae Height	myh6	HiC_scaffold_11	CP
Adductor Mandibulae Height	myh7	HiC_scaffold_11	CP

Adductor Mandibulae Height	ngdn	HiC_scaffold_11	CP
Adductor Mandibulae Height	nrros	HiC_scaffold_11	CP
Adductor Mandibulae Height	ntng1	HiC_scaffold_11	CP
Adductor Mandibulae Height	olfm3	HiC_scaffold_11	CP
Adductor Mandibulae Height	pabpn1	HiC_scaffold_11	CP
Adductor Mandibulae Height	pck2	HiC_scaffold_11	CP
Adductor Mandibulae Height	pdcd6	HiC_scaffold_11	CP
Adductor Mandibulae Height	phldb2	HiC_scaffold_11	CP
Adductor Mandibulae Height	pigm	HiC_scaffold_11	CP
Adductor Mandibulae Height	pkia	HiC_scaffold_11	CP
Adductor Mandibulae Height	plch2	HiC_scaffold_11	CP
Adductor Mandibulae Height	plcxd2	HiC_scaffold_11	CP
Adductor Mandibulae Height	pomp	HiC_scaffold_11	CP
Adductor Mandibulae Height	ppcs	HiC_scaffold_11	CP
Adductor Mandibulae Height	prdm2	HiC_scaffold_11	CP
Adductor Mandibulae Height	prkdc	HiC_scaffold_11	CP
Adductor Mandibulae Height	prmt6	HiC_scaffold_11	CP
Adductor Mandibulae Height	psme1	HiC_scaffold_11	CP
Adductor Mandibulae Height	ramp3	HiC_scaffold_11	CP
Adductor Mandibulae Height	rec8	HiC_scaffold_11	CP
Adductor Mandibulae Height	rgs9bp-b	HiC_scaffold_11	CP
Adductor Mandibulae Height	rmdn1	HiC_scaffold_11	CP
Adductor Mandibulae Height	rnpc3	HiC_scaffold_11	CP
Adductor Mandibulae Height	rps20	HiC_scaffold_11	CP
Adductor Mandibulae Height	serpinb1	HiC_scaffold_11	CP
Adductor Mandibulae Height	serpinb10	HiC_scaffold_11	CP
Adductor Mandibulae Height	serpinb1b	HiC_scaffold_11	CP
Adductor Mandibulae Height	serpinb6	HiC_scaffold_11	CP
Adductor Mandibulae Height	sh3glb1	HiC_scaffold_11	CP
Adductor Mandibulae Height	siglec1	HiC_scaffold_11	CP
Adductor Mandibulae Height	siglec10	HiC_scaffold_11	CP
Adductor Mandibulae Height	siglec13	HiC_scaffold_11	CP
Adductor Mandibulae Height	siglec14	HiC_scaffold_11	CP
Adductor Mandibulae Height	siglec9	HiC_scaffold_11	CP
Adductor Mandibulae Height	ski	HiC_scaffold_11	CP
Adductor Mandibulae Height	slc22a17	HiC_scaffold_11	CP
Adductor Mandibulae Height	slc35b3	HiC_scaffold_11	CP
Adductor Mandibulae Height	snx16	HiC_scaffold_11	CP
Adductor Mandibulae Height	tecr	HiC_scaffold_11	CP
Adductor Mandibulae Height	tfap2a	HiC_scaffold_11	CP
Adductor Mandibulae Height	thap6	HiC_scaffold_11	CP

Adductor Mandibulae Height	thtpa	HiC_scaffold_11	CP
Adductor Mandibulae Height	tm9sf1	HiC_scaffold_11	CP
Adductor Mandibulae Height	tmem14c	HiC_scaffold_11	CP
Adductor Mandibulae Height	tmem51	HiC_scaffold_11	CP
Adductor Mandibulae Height	tmem56-b	HiC_scaffold_11	CP
Adductor Mandibulae Height	txndc5	HiC_scaffold_11	CP
Adductor Mandibulae Height	utp3	HiC_scaffold_11	CP
Adductor Mandibulae Height	vav3	HiC_scaffold_11	CP
Adductor Mandibulae Height	wdr19	HiC_scaffold_11	CP
Adductor Mandibulae Height	wdr37	HiC_scaffold_11	CP
Adductor Mandibulae Height	wwp1	HiC_scaffold_11	CP
Adductor Mandibulae Height	zc2hc1a	HiC_scaffold_11	CP
Adductor Mandibulae Height	zfhx4	HiC_scaffold_11	CP
Cranial Height	aak1	HiC_scaffold_33	CP
Cranial Height	acacb	HiC_scaffold_33	CP
Cranial Height	acdh-11	HiC_scaffold_33	CP
Cranial Height	adra1a	HiC_scaffold_33	CP
Cranial Height	adrb4c	HiC_scaffold_33	CP
Cranial Height	aebp1	HiC_scaffold_33	CP
Cranial Height	aifm3	HiC_scaffold_33	CP
Cranial Height	akr1a1a	HiC_scaffold_33	CP
Cranial Height	aldh3b1	HiC_scaffold_33	CP
Cranial Height	amy2	HiC_scaffold_33	CP
Cranial Height	ank1	HiC_scaffold_33	CP
Cranial Height	ank1	HiC_scaffold_33	LL
Cranial Height	ankrd13a	HiC_scaffold_33	CP
Cranial Height	ankrd39	HiC_scaffold_33	CP
Cranial Height	antxr1	HiC_scaffold_33	CP
Cranial Height	aopep	HiC_scaffold_39	CP
Cranial Height	ap1b1	HiC_scaffold_33	CP
Cranial Height	ap1b1	HiC_scaffold_33	LL
Cranial Height	aqp3	HiC_scaffold_33	CP
Cranial Height	arl6ip4	HiC_scaffold_33	CP
Cranial Height	arl6ip4	HiC_scaffold_33	LL
Cranial Height	arrdc3	HiC_scaffold_33	CP
Cranial Height	arsk	HiC_scaffold_33	CP
Cranial Height	asb6	HiC_scaffold_33	CP
Cranial Height	atp6v0a2	HiC_scaffold_33	CP
Cranial Height	atp6v0a2	HiC_scaffold_33	LL
Cranial Height	bag4	HiC_scaffold_33	CP
Cranial Height	bco2	HiC_scaffold_33	CP

Cranial Height	bin3	HiC_scaffold_33	CP
Cranial Height	bmp1	HiC_scaffold_33	CP
Cranial Height	bri3bp	HiC_scaffold_33	CP
Cranial Height	bri3bp	HiC_scaffold_33	LL
Cranial Height	c2cd4cc2cd4_family	HiC_scaffold_33	CP
Cranial Height	c2cd4cc2cd4_family	HiC_scaffold_33	LL
Cranial Height	c9orf78	HiC_scaffold_33	CP
Cranial Height	carnmt1	HiC_scaffold_33	CP
Cranial Height	ccdc117	HiC_scaffold_33	CP
Cranial Height	ccdc117	HiC_scaffold_33	LL
Cranial Height	ccdc157	HiC_scaffold_33	CP
Cranial Height	ccdc92	HiC_scaffold_33	CP
Cranial Height	ccnh	HiC_scaffold_33	CP
Cranial Height	cemip2	HiC_scaffold_33	CP
Cranial Height	ciao1a	HiC_scaffold_33	CP
Cranial Height	cldn22	HiC_scaffold_33	CP
Cranial Height	clip1	HiC_scaffold_33	CP
Cranial Height	cmlkr1	HiC_scaffold_33	CP
Cranial Height	coe2	HiC_scaffold_33	CP
Cranial Height	coe2	HiC_scaffold_33	LL
Cranial Height	cox7c	HiC_scaffold_33	CP
Cranial Height	crat	HiC_scaffold_33	CP
Cranial Height	ctrc	HiC_scaffold_33	CP
Cranial Height	dao	HiC_scaffold_33	CP
Cranial Height	dbn1	HiC_scaffold_33	CP
Cranial Height	dbnl	HiC_scaffold_33	CP
Cranial Height	ddr2	HiC_scaffold_33	CP
Cranial Height	dguok	HiC_scaffold_33	CP
Cranial Height	dguok	HiC_scaffold_33	LL
Cranial Height	disp3	HiC_scaffold_33	CP
Cranial Height	dnajb5	HiC_scaffold_33	CP
Cranial Height	dnm1l	HiC_scaffold_33	CP
Cranial Height	dpysl2	HiC_scaffold_33	CP
Cranial Height	dusp18	HiC_scaffold_33	CP
Cranial Height	dusp26	HiC_scaffold_33	CP
Cranial Height	ehd1	HiC_scaffold_33	CP
Cranial Height	eif4ebp1	HiC_scaffold_33	CP
Cranial Height	eif4ebp1	HiC_scaffold_33	LL
Cranial Height	elac1	HiC_scaffold_39	CP

Cranial Height	elmod3	HiC_scaffold_33	CP
Cranial Height	elovl7	HiC_scaffold_39	CP
Cranial Height	emid1	HiC_scaffold_33	CP
Cranial Height	emid1	HiC_scaffold_33	LL
Cranial Height	epx	HiC_scaffold_33	CP
Cranial Height	epx	HiC_scaffold_33	LL
Cranial Height	erap2	HiC_scaffold_33	CP
Cranial Height	ercc8	HiC_scaffold_39	CP
Cranial Height	es1	HiC_scaffold_33	CP
Cranial Height	ewsr1	HiC_scaffold_33	CP
Cranial Height	ewsr1	HiC_scaffold_33	LL
Cranial Height	f2r	HiC_scaffold_33	CP
Cranial Height	fabp1	HiC_scaffold_39	CP
Cranial Height	fam173b	HiC_scaffold_39	CP
Cranial Height	fam219a	HiC_scaffold_33	CP
Cranial Height	fam222a	HiC_scaffold_33	CP
Cranial Height	fancg	HiC_scaffold_33	CP
Cranial Height	fgfr1a	HiC_scaffold_33	CP
Cranial Height	ficd	HiC_scaffold_33	CP
Cranial Height	foxb2	HiC_scaffold_33	CP
Cranial Height	foxb2	HiC_scaffold_33	LL
Cranial Height	foxd5-a	HiC_scaffold_39	CP
Cranial Height	foxn4	HiC_scaffold_33	CP
Cranial Height	fzd10-a	HiC_scaffold_33	CP
Cranial Height	gal3st1	HiC_scaffold_33	CP
Cranial Height	gas2l1	HiC_scaffold_33	CP
Cranial Height	gas2l1	HiC_scaffold_33	LL
Cranial Height	gatc	HiC_scaffold_33	CP
Cranial Height	gcnt1	HiC_scaffold_33	CP
Cranial Height	gfra2	HiC_scaffold_33	CP
Cranial Height	gimap2	HiC_scaffold_33	CP
Cranial Height	gimap4	HiC_scaffold_33	CP
Cranial Height	gimap7	HiC_scaffold_33	CP
Cranial Height	gimap8	HiC_scaffold_33	CP
Cranial Height	gins4	HiC_scaffold_33	CP
Cranial Height	git2	HiC_scaffold_33	CP
Cranial Height	gltp	HiC_scaffold_33	CP
Cranial Height	gna14	HiC_scaffold_33	CP
Cranial Height	gna14	HiC_scaffold_33	LL
Cranial Height	gnaq	HiC_scaffold_33	CP
Cranial Height	gnaq	HiC_scaffold_33	LL

Cranial Height	gnrh1	HiC_scaffold_33	CP
Cranial Height	gpat4	HiC_scaffold_33	CP
Cranial Height	gramd2b	HiC_scaffold_33	CP
Cranial Height	grk5	HiC_scaffold_33	CP
Cranial Height	gtf2h3	HiC_scaffold_33	CP
Cranial Height	hapln1	HiC_scaffold_33	CP
Cranial Height	hcar2	HiC_scaffold_33	CP
Cranial Height	hcar2	HiC_scaffold_33	LL
Cranial Height	hip1r	HiC_scaffold_33	CP
Cranial Height	hip1r	HiC_scaffold_33	LL
Cranial Height	homer1	HiC_scaffold_33	CP
Cranial Height	hspb11	HiC_scaffold_33	CP
Cranial Height	ier5l	HiC_scaffold_33	CP
Cranial Height	igsf9	HiC_scaffold_33	CP
Cranial Height	ine	HiC_scaffold_33	CP
Cranial Height	ine	HiC_scaffold_33	LL
Cranial Height	iqgap1	HiC_scaffold_33	CP
Cranial Height	iscu	HiC_scaffold_33	CP
Cranial Height	jmy	HiC_scaffold_33	CP
Cranial Height	kansl3	HiC_scaffold_33	CP
Cranial Height	kctd10	HiC_scaffold_33	CP
Cranial Height	kctd9	HiC_scaffold_33	CP
Cranial Height	kiaa0825	HiC_scaffold_33	CP
Cranial Height	kif24	HiC_scaffold_33	CP
Cranial Height	kin14e	HiC_scaffold_33	CP
Cranial Height	klf9	HiC_scaffold_33	CP
Cranial Height	klhl10	HiC_scaffold_33	CP
Cranial Height	klhl10	HiC_scaffold_33	LL
Cranial Height	kmt5aa	HiC_scaffold_33	CP
Cranial Height	kmt5aa	HiC_scaffold_33	LL
Cranial Height	kntc1	HiC_scaffold_33	CP
Cranial Height	koza	HiC_scaffold_33	CP
Cranial Height	lgi3	HiC_scaffold_33	CP
Cranial Height	limk2	HiC_scaffold_33	CP
Cranial Height	limk2	HiC_scaffold_33	LL
Cranial Height	lix1	HiC_scaffold_33	CP
Cranial Height	lox	HiC_scaffold_33	CP
Cranial Height	loxhd1	HiC_scaffold_39	CP
Cranial Height	lsm1	HiC_scaffold_33	CP
Cranial Height	lysmd3	HiC_scaffold_33	CP
Cranial Height	lztr1	HiC_scaffold_33	CP

Cranial Height	lzts1	HiC_scaffold_33	CP
Cranial Height	mapk4	HiC_scaffold_39	CP
Cranial Height	mblac2	HiC_scaffold_33	CP
Cranial Height	mctp1	HiC_scaffold_33	CP
Cranial Height	me2	HiC_scaffold_39	CP
Cranial Height	med22	HiC_scaffold_33	CP
Cranial Height	mfsd3	HiC_scaffold_33	CP
Cranial Height	mier3	HiC_scaffold_39	CP
Cranial Height	mlxip	HiC_scaffold_33	CP
Cranial Height	mmab	HiC_scaffold_33	CP
Cranial Height	mn1	HiC_scaffold_33	CP
Cranial Height	mob1a	HiC_scaffold_33	CP
Cranial Height	mob1a	HiC_scaffold_33	LL
Cranial Height	morc2a	HiC_scaffold_33	CP
Cranial Height	mspa	HiC_scaffold_33	CP
Cranial Height	mthfd2	HiC_scaffold_33	CP
Cranial Height	mthfd2	HiC_scaffold_33	LL
Cranial Height	mtx3	HiC_scaffold_33	CP
Cranial Height	mvk	HiC_scaffold_33	CP
Cranial Height	myo1h	HiC_scaffold_33	CP
Cranial Height	ncs1	HiC_scaffold_33	CP
Cranial Height	ndufaf2	HiC_scaffold_39	CP
Cranial Height	nefh	HiC_scaffold_33	CP
Cranial Height	nefl	HiC_scaffold_33	CP
Cranial Height	neurl3	HiC_scaffold_33	CP
Cranial Height	nfu1	HiC_scaffold_33	CP
Cranial Height	nkx2-6	HiC_scaffold_33	CP
Cranial Height	nkx6-3	HiC_scaffold_33	CP
Cranial Height	nodal	HiC_scaffold_33	CP
Cranial Height	nodal	HiC_scaffold_33	LL
Cranial Height	nol6	HiC_scaffold_33	CP
Cranial Height	nono	HiC_scaffold_33	CP
Cranial Height	npc1l1	HiC_scaffold_33	CP
Cranial Height	npy1r	HiC_scaffold_33	CP
Cranial Height	omg	HiC_scaffold_33	CP
Cranial Height	osbp2	HiC_scaffold_33	CP
Cranial Height	osbp2	HiC_scaffold_33	LL
Cranial Height	p2rx2	HiC_scaffold_33	CP
Cranial Height	p2ry14	HiC_scaffold_33	CP
Cranial Height	p2ry14	HiC_scaffold_33	LL
Cranial Height	pcsk5	HiC_scaffold_33	CP

Cranial Height	pde4d	HiC_scaffold_39	CP
Cranial Height	pdlim2	HiC_scaffold_33	CP
Cranial Height	pebp4	HiC_scaffold_33	CP
Cranial Height	pes1	HiC_scaffold_33	CP
Cranial Height	pgbd3	HiC_scaffold_33	CP
Cranial Height	pgbd3	HiC_scaffold_33	LL
Cranial Height	pgm5	HiC_scaffold_39	CP
Cranial Height	phyhip	HiC_scaffold_33	CP
Cranial Height	pik3ip1	HiC_scaffold_33	CP
Cranial Height	pik3ip1	HiC_scaffold_33	LL
Cranial Height	pip5k1b	HiC_scaffold_33	CP
Cranial Height	pitpnb	HiC_scaffold_33	CP
Cranial Height	pitpnm2	HiC_scaffold_33	CP
Cranial Height	pitpnm2	HiC_scaffold_33	LL
Cranial Height	pla2g3	HiC_scaffold_33	CP
Cranial Height	plcl1	HiC_scaffold_33	CP
Cranial Height	plekha2	HiC_scaffold_33	CP
Cranial Height	plk2	HiC_scaffold_39	CP
Cranial Height	pole	HiC_scaffold_33	CP
Cranial Height	polr3d	HiC_scaffold_33	CP
Cranial Height	polr3g	HiC_scaffold_33	CP
Cranial Height	ppp1r3c	HiC_scaffold_33	CP
Cranial Height	prlhr	HiC_scaffold_33	CP
Cranial Height	prune2	HiC_scaffold_33	CP
Cranial Height	prune2	HiC_scaffold_33	LL
Cranial Height	psap	HiC_scaffold_33	CP
Cranial Height	psap	HiC_scaffold_33	LL
Cranial Height	psbp1	HiC_scaffold_33	CP
Cranial Height	psmd9	HiC_scaffold_33	CP
Cranial Height	ptch1	HiC_scaffold_39	CP
Cranial Height	ptger4	HiC_scaffold_39	CP
Cranial Height	pxmp2	HiC_scaffold_33	CP
Cranial Height	rab11fip1	HiC_scaffold_33	CP
Cranial Height	rab3c	HiC_scaffold_39	CP
Cranial Height	rabgef1	HiC_scaffold_33	CP
Cranial Height	rasa1	HiC_scaffold_33	CP
Cranial Height	rasl10b	HiC_scaffold_33	CP
Cranial Height	rasl10b	HiC_scaffold_33	LL
Cranial Height	rfesd	HiC_scaffold_33	CP
Cranial Height	rflna	HiC_scaffold_33	CP
Cranial Height	rgmb	HiC_scaffold_33	CP

Cranial Height	rhbdd3	HiC_scaffold_33	CP
Cranial Height	rhbdd3	HiC_scaffold_33	LL
Cranial Height	rilpl1	HiC_scaffold_33	CP
Cranial Height	rilpl1	HiC_scaffold_33	LL
Cranial Height	rilpl2	HiC_scaffold_33	CP
Cranial Height	rilpl2	HiC_scaffold_33	LL
Cranial Height	rimbp2	HiC_scaffold_33	CP
Cranial Height	riok2	HiC_scaffold_33	CP
Cranial Height	rnf214	HiC_scaffold_33	CP
Cranial Height	rnf223	HiC_scaffold_33	CP
Cranial Height	rorb	HiC_scaffold_33	CP
Cranial Height	rph3a	HiC_scaffold_33	CP
Cranial Height	rsrc2	HiC_scaffold_33	CP
Cranial Height	rtkn	HiC_scaffold_33	CP
Cranial Height	sart3	HiC_scaffold_33	CP
Cranial Height	sds	HiC_scaffold_33	CP
Cranial Height	seca	HiC_scaffold_33	CP
Cranial Height	setbp1	HiC_scaffold_33	CP
Cranial Height	sgsm1	HiC_scaffold_33	CP
Cranial Height	slc15a4	HiC_scaffold_33	CP
Cranial Height	slc25a37	HiC_scaffold_33	CP
Cranial Height	slc2a11	HiC_scaffold_33	CP
Cranial Height	slc2a8	HiC_scaffold_33	CP
Cranial Height	slc6a4	HiC_scaffold_33	CP
Cranial Height	slc7a4	HiC_scaffold_33	CP
Cranial Height	slc8b1	HiC_scaffold_33	CP
Cranial Height	slf1	HiC_scaffold_33	CP
Cranial Height	smim15	HiC_scaffold_39	CP
Cranial Height	smn1	HiC_scaffold_33	CP
Cranial Height	smtn	HiC_scaffold_33	CP
Cranial Height	smtn	HiC_scaffold_33	LL
Cranial Height	smtnl1	HiC_scaffold_33	CP
Cranial Height	smtnl1	HiC_scaffold_33	LL
Cranial Height	smyd1	HiC_scaffold_39	CP
Cranial Height	snrnp200	HiC_scaffold_33	CP
Cranial Height	snx2	HiC_scaffold_33	CP
Cranial Height	sorbs3	HiC_scaffold_33	CP
Cranial Height	srrd	HiC_scaffold_33	CP
Cranial Height	ssbp2	HiC_scaffold_33	CP
Cranial Height	ssh1	HiC_scaffold_33	CP
Cranial Height	star	HiC_scaffold_33	CP

Cranial Height	stx2	HiC_scaffold_33	CP
Cranial Height	sv2c	HiC_scaffold_33	CP
Cranial Height	svop	HiC_scaffold_33	CP
Cranial Height	tacc1	HiC_scaffold_33	CP
Cranial Height	tbx5	HiC_scaffold_33	CP
Cranial Height	tcf7l1a	HiC_scaffold_33	CP
Cranial Height	tchp	HiC_scaffold_33	CP
Cranial Height	tcn2	HiC_scaffold_33	CP
Cranial Height	tcn2	HiC_scaffold_33	LL
Cranial Height	tctn2	HiC_scaffold_33	CP
Cranial Height	tctn2	HiC_scaffold_33	LL
Cranial Height	tent2	HiC_scaffold_33	CP
Cranial Height	tfip11	HiC_scaffold_33	CP
Cranial Height	thbs4b	HiC_scaffold_33	CP
Cranial Height	thoc5	HiC_scaffold_33	CP
Cranial Height	tmem119	HiC_scaffold_33	CP
Cranial Height	tmem127	HiC_scaffold_33	CP
Cranial Height	tmem132c	HiC_scaffold_33	CP
Cranial Height	tmem132d	HiC_scaffold_33	CP
Cranial Height	tmem161b	HiC_scaffold_33	CP
Cranial Height	tmem167a	HiC_scaffold_33	CP
Cranial Height	tmem230	HiC_scaffold_33	CP
Cranial Height	tmem248	HiC_scaffold_33	CP
Cranial Height	tnks	HiC_scaffold_33	CP
Cranial Height	tpcn1	HiC_scaffold_33	CP
Cranial Height	trafd1	HiC_scaffold_33	CP
Cranial Height	trafd1	HiC_scaffold_33	LL
Cranial Height	trpm3	HiC_scaffold_33	CP
Cranial Height	trpm6	HiC_scaffold_33	CP
Cranial Height	tspan36	HiC_scaffold_39	CP
Cranial Height	ttc28	HiC_scaffold_33	CP
Cranial Height	ttc37	HiC_scaffold_33	CP
Cranial Height	tutl	HiC_scaffold_33	CP
Cranial Height	ube3b	HiC_scaffold_33	CP
Cranial Height	ubl4aa	HiC_scaffold_33	CP
Cranial Height	ulk1	HiC_scaffold_33	CP
Cranial Height	unc45b	HiC_scaffold_33	CP
Cranial Height	usp30	HiC_scaffold_33	CP
Cranial Height	usp39	HiC_scaffold_33	CP
Cranial Height	usp39	HiC_scaffold_33	LL
Cranial Height	vcp	HiC_scaffold_33	CP

Cranial Height	vegt	HiC_scaffold_33	CP
Cranial Height	vps13c	HiC_scaffold_33	CP
Cranial Height	vps33a	HiC_scaffold_33	CP
Cranial Height	wdr31	HiC_scaffold_33	CP
Cranial Height	wdr31	HiC_scaffold_33	LL
Cranial Height	wdr66	HiC_scaffold_33	CP
Cranial Height	wscd2	HiC_scaffold_33	CP
Cranial Height	xrcc4	HiC_scaffold_33	CP
Cranial Height	zfand5	HiC_scaffold_33	CP
Cranial Height	znf180	HiC_scaffold_33	CP
Cranial Height	znf366	HiC_scaffold_39	CP
Cranial Height	znf608	HiC_scaffold_33	CP
Dentigerous Arm Depth	abca4	HiC_scaffold_11	CP
Dentigerous Arm Depth	abhd10	HiC_scaffold_11	CP
Dentigerous Arm Depth	abi1	HiC_scaffold_11	CP
Dentigerous Arm Depth	acad11	HiC_scaffold_11	CP
Dentigerous Arm Depth	acbd5a	HiC_scaffold_11	CP
Dentigerous Arm Depth	ackr4	HiC_scaffold_11	CP
Dentigerous Arm Depth	adamts12	HiC_scaffold_5	LL
Dentigerous Arm Depth	adamts7	HiC_scaffold_5	LL
Dentigerous Arm Depth	adgrg4	HiC_scaffold_11	CP
Dentigerous Arm Depth	agrp	HiC_scaffold_11	CP
Dentigerous Arm Depth	agtr1	HiC_scaffold_11	CP
Dentigerous Arm Depth	ahrr	HiC_scaffold_11	CP
Dentigerous Arm Depth	akap13	HiC_scaffold_5	LL
Dentigerous Arm Depth	amer2	HiC_scaffold_11	CP
Dentigerous Arm Depth	ankh	HiC_scaffold_11	CP
Dentigerous Arm Depth	ankrd33b	HiC_scaffold_11	CP
Dentigerous Arm Depth	ano9	HiC_scaffold_5	LL
Dentigerous Arm Depth	ap2a2	HiC_scaffold_5	LL
Dentigerous Arm Depth	apod	HiC_scaffold_11	CP
Dentigerous Arm Depth	arfgef1	HiC_scaffold_11	CP
Dentigerous Arm Depth	arhgap21	HiC_scaffold_11	CP
Dentigerous Arm Depth	arhgap29	HiC_scaffold_11	CP
Dentigerous Arm Depth	armc1	HiC_scaffold_11	CP
Dentigerous Arm Depth	arpp19	HiC_scaffold_5	LL
Dentigerous Arm Depth	arx	HiC_scaffold_11	CP
Dentigerous Arm Depth	asap1	HiC_scaffold_11	CP
Dentigerous Arm Depth	atp8a2	HiC_scaffold_11	CP
Dentigerous Arm Depth	b2m	HiC_scaffold_11	CP
Dentigerous Arm Depth	b4galt1	HiC_scaffold_11	CP

Dentigerous Arm Depth	bbs4	HiC_scaffold_5	LL
Dentigerous Arm Depth	bco1	HiC_scaffold_11	CP
Dentigerous Arm Depth	bdh1	HiC_scaffold_11	CP
Dentigerous Arm Depth	bhlhe22	HiC_scaffold_11	CP
Dentigerous Arm Depth	bloc1s5	HiC_scaffold_11	CP
Dentigerous Arm Depth	boc	HiC_scaffold_11	CP
Dentigerous Arm Depth	brpf3	HiC_scaffold_11	CP
Dentigerous Arm Depth	c1qtnf9	HiC_scaffold_11	CP
Dentigerous Arm Depth	c8g	HiC_scaffold_11	CP
Dentigerous Arm Depth	ca1	HiC_scaffold_11	CP
Dentigerous Arm Depth	cacnb2	HiC_scaffold_11	CP
Dentigerous Arm Depth	calml4	HiC_scaffold_5	LL
Dentigerous Arm Depth	caprin2	HiC_scaffold_11	CP
Dentigerous Arm Depth	cbln2	HiC_scaffold_11	CP
Dentigerous Arm Depth	ccdc106	HiC_scaffold_11	CP
Dentigerous Arm Depth	ccdc58	HiC_scaffold_11	CP
Dentigerous Arm Depth	ccdc63	HiC_scaffold_11	CP
Dentigerous Arm Depth	ccl20	HiC_scaffold_11	CP
Dentigerous Arm Depth	ccne1	HiC_scaffold_5	LL
Dentigerous Arm Depth	ccr1	HiC_scaffold_11	CP
Dentigerous Arm Depth	cct5	HiC_scaffold_11	CP
Dentigerous Arm Depth	cd226	HiC_scaffold_11	CP
Dentigerous Arm Depth	cd276	HiC_scaffold_5	LL
Dentigerous Arm Depth	cd38	HiC_scaffold_11	CP
Dentigerous Arm Depth	cd81	HiC_scaffold_5	LL
Dentigerous Arm Depth	cdh10	HiC_scaffold_11	CP
Dentigerous Arm Depth	cdh12	HiC_scaffold_11	CP
Dentigerous Arm Depth	cdh18	HiC_scaffold_11	CP
Dentigerous Arm Depth	cdh20	HiC_scaffold_11	CP
Dentigerous Arm Depth	cdh6	HiC_scaffold_11	CP
Dentigerous Arm Depth	cdh7	HiC_scaffold_11	CP
Dentigerous Arm Depth	cdk13	HiC_scaffold_11	CP
Dentigerous Arm Depth	cdk8	HiC_scaffold_11	CP
Dentigerous Arm Depth	cdv3	HiC_scaffold_11	CP
Dentigerous Arm Depth	cebpe	HiC_scaffold_11	CP
Dentigerous Arm Depth	cela2a	HiC_scaffold_11	CP
Dentigerous Arm Depth	chmp4c	HiC_scaffold_11	CP
Dentigerous Arm Depth	chmp5	HiC_scaffold_11	CP
Dentigerous Arm Depth	chrna7	HiC_scaffold_5	LL
Dentigerous Arm Depth	chst2	HiC_scaffold_11	CP
Dentigerous Arm Depth	cldn15	HiC_scaffold_5	LL

Dentigerous Arm Depth	cln6	HiC_scaffold_5	LL
Dentigerous Arm Depth	clul1	HiC_scaffold_11	CP
Dentigerous Arm Depth	cmbl	HiC_scaffold_11	CP
Dentigerous Arm Depth	cngb3	HiC_scaffold_11	CP
Dentigerous Arm Depth	col11a1	HiC_scaffold_11	CP
Dentigerous Arm Depth	colec12	HiC_scaffold_11	CP
Dentigerous Arm Depth	cops5	HiC_scaffold_11	CP
Dentigerous Arm Depth	cpa6	HiC_scaffold_11	CP
Dentigerous Arm Depth	cpb1	HiC_scaffold_11	CP
Dentigerous Arm Depth	cpeb1	HiC_scaffold_5	LL
Dentigerous Arm Depth	cpne3	HiC_scaffold_11	CP
Dentigerous Arm Depth	crh	HiC_scaffold_11	CP
Dentigerous Arm Depth	crispld1	HiC_scaffold_11	CP
Dentigerous Arm Depth	cry-dash	HiC_scaffold_11	CP
Dentigerous Arm Depth	csnk1g1	HiC_scaffold_5	LL
Dentigerous Arm Depth	csrnp1	HiC_scaffold_11	CP
Dentigerous Arm Depth	cstb	HiC_scaffold_11	CP
Dentigerous Arm Depth	dcaf11	HiC_scaffold_11	CP
Dentigerous Arm Depth	dhcr7	HiC_scaffold_5	LL
Dentigerous Arm Depth	dlec1	HiC_scaffold_11	CP
Dentigerous Arm Depth	dnajb6	HiC_scaffold_11	CP
Dentigerous Arm Depth	dnajc13	HiC_scaffold_11	CP
Dentigerous Arm Depth	dok6	HiC_scaffold_11	CP
Dentigerous Arm Depth	dph2	HiC_scaffold_11	CP
Dentigerous Arm Depth	dpp6	HiC_scaffold_11	CP
Dentigerous Arm Depth	drd3	HiC_scaffold_11	CP
Dentigerous Arm Depth	drosha	HiC_scaffold_11	CP
Dentigerous Arm Depth	dsel	HiC_scaffold_11	CP
Dentigerous Arm Depth	dusp28	HiC_scaffold_5	LL
Dentigerous Arm Depth	eef1e1	HiC_scaffold_11	CP
Dentigerous Arm Depth	ell2	HiC_scaffold_5	LL
Dentigerous Arm Depth	eloc	HiC_scaffold_11	CP
Dentigerous Arm Depth	emc9	HiC_scaffold_11	CP
Dentigerous Arm Depth	emilin2	HiC_scaffold_11	CP
Dentigerous Arm Depth	emp3	HiC_scaffold_11	CP
Dentigerous Arm Depth	erya	HiC_scaffold_11	CP
Dentigerous Arm Depth	esyt2	HiC_scaffold_11	CP
Dentigerous Arm Depth	eya1	HiC_scaffold_11	CP
Dentigerous Arm Depth	f13a1	HiC_scaffold_11	CP
Dentigerous Arm Depth	f13e9.13	HiC_scaffold_5	LL
Dentigerous Arm Depth	fam168b	HiC_scaffold_11	CP

Dentigerous Arm Depth	fam214a	HiC_scaffold_5	LL
Dentigerous Arm Depth	fam49b	HiC_scaffold_11	CP
Dentigerous Arm Depth	fam83e	HiC_scaffold_11	CP
Dentigerous Arm Depth	fastkd3	HiC_scaffold_11	CP
Dentigerous Arm Depth	fbxl7	HiC_scaffold_11	CP
Dentigerous Arm Depth	fen1	HiC_scaffold_11	CP
Dentigerous Arm Depth	fitm1	HiC_scaffold_11	CP
Dentigerous Arm Depth	flt3	HiC_scaffold_11	CP
Dentigerous Arm Depth	foxh1	HiC_scaffold_11	CP
Dentigerous Arm Depth	foxj3	HiC_scaffold_11	CP
Dentigerous Arm Depth	gabarapl2	HiC_scaffold_5	LL
Dentigerous Arm Depth	gad2	HiC_scaffold_11	CP
Dentigerous Arm Depth	garem1	HiC_scaffold_11	CP
Dentigerous Arm Depth	gars	HiC_scaffold_11	CP
Dentigerous Arm Depth	gdap1	HiC_scaffold_11	CP
Dentigerous Arm Depth	ggh	HiC_scaffold_11	CP
Dentigerous Arm Depth	gimap4	HiC_scaffold_11	CP
Dentigerous Arm Depth	gli3	HiC_scaffold_11	CP
Dentigerous Arm Depth	glyctk	HiC_scaffold_11	CP
Dentigerous Arm Depth	gnb5b	HiC_scaffold_5	LL
Dentigerous Arm Depth	gnrhr2	HiC_scaffold_5	LL
Dentigerous Arm Depth	gorasp1	HiC_scaffold_11	CP
Dentigerous Arm Depth	gpr12	HiC_scaffold_11	CP
Dentigerous Arm Depth	gpr141	HiC_scaffold_11	CP
Dentigerous Arm Depth	gpr17	HiC_scaffold_11	CP
Dentigerous Arm Depth	gpt2l	HiC_scaffold_11	CP
Dentigerous Arm Depth	gramd1c	HiC_scaffold_11	CP
Dentigerous Arm Depth	gramd2a	HiC_scaffold_5	LL
Dentigerous Arm Depth	gtf3a	HiC_scaffold_11	CP
Dentigerous Arm Depth	hacd1	HiC_scaffold_11	CP
Dentigerous Arm Depth	hbp1	HiC_scaffold_11	CP
Dentigerous Arm Depth	hgd	HiC_scaffold_11	CP
Dentigerous Arm Depth	hhatl	HiC_scaffold_11	CP
Dentigerous Arm Depth	hmcn2	HiC_scaffold_11	CP
Dentigerous Arm Depth	hnf4g	HiC_scaffold_11	CP
Dentigerous Arm Depth	idh2	HiC_scaffold_5	LL
Dentigerous Arm Depth	il20rb	HiC_scaffold_5	LL
Dentigerous Arm Depth	impa1	HiC_scaffold_11	CP
Dentigerous Arm Depth	insig1	HiC_scaffold_11	CP
Dentigerous Arm Depth	insy1	HiC_scaffold_5	LL
Dentigerous Arm Depth	itga11	HiC_scaffold_5	LL

Dentigerous Arm Depth	jph1	HiC_scaffold_11	CP
Dentigerous Arm Depth	kazn	HiC_scaffold_11	CP
Dentigerous Arm Depth	kazna	HiC_scaffold_11	CP
Dentigerous Arm Depth	kbp	HiC_scaffold_11	CP
Dentigerous Arm Depth	kbtbd2	HiC_scaffold_11	CP
Dentigerous Arm Depth	kcnb2	HiC_scaffold_11	CP
Dentigerous Arm Depth	kif13b	HiC_scaffold_5	LL
Dentigerous Arm Depth	kif20a	HiC_scaffold_11	CP
Dentigerous Arm Depth	klhl40b	HiC_scaffold_11	CP
Dentigerous Arm Depth	kpna1	HiC_scaffold_11	CP
Dentigerous Arm Depth	limd2	HiC_scaffold_11	CP
Dentigerous Arm Depth	lnx2	HiC_scaffold_11	CP
Dentigerous Arm Depth	loxl1	HiC_scaffold_5	LL
Dentigerous Arm Depth	lpin2	HiC_scaffold_11	CP
Dentigerous Arm Depth	lsm5	HiC_scaffold_11	CP
Dentigerous Arm Depth	lypla1	HiC_scaffold_11	CP
Dentigerous Arm Depth	lztfl1	HiC_scaffold_11	CP
Dentigerous Arm Depth	maf1	HiC_scaffold_11	CP
Dentigerous Arm Depth	mag	HiC_scaffold_11	CP
Dentigerous Arm Depth	mak	HiC_scaffold_11	CP
Dentigerous Arm Depth	map3k15	HiC_scaffold_11	CP
Dentigerous Arm Depth	mastl	HiC_scaffold_11	CP
Dentigerous Arm Depth	mc4r	HiC_scaffold_11	CP
Dentigerous Arm Depth	mcl1	HiC_scaffold_5	LL
Dentigerous Arm Depth	mcur1	HiC_scaffold_11	CP
Dentigerous Arm Depth	med1	HiC_scaffold_11	CP
Dentigerous Arm Depth	mesd	HiC_scaffold_5	LL
Dentigerous Arm Depth	mettl4	HiC_scaffold_11	CP
Dentigerous Arm Depth	mllt10	HiC_scaffold_11	CP
Dentigerous Arm Depth	mon1b	HiC_scaffold_11	CP
Dentigerous Arm Depth	mrc1	HiC_scaffold_11	CP
Dentigerous Arm Depth	mrpl15	HiC_scaffold_11	CP
Dentigerous Arm Depth	mrpl46	HiC_scaffold_5	LL
Dentigerous Arm Depth	msc	HiC_scaffold_11	CP
Dentigerous Arm Depth	msrb2	HiC_scaffold_11	CP
Dentigerous Arm Depth	mtfr1	HiC_scaffold_11	CP
Dentigerous Arm Depth	mtmr6	HiC_scaffold_11	CP
Dentigerous Arm Depth	mtrr	HiC_scaffold_11	CP
Dentigerous Arm Depth	mtss1l	HiC_scaffold_5	LL
Dentigerous Arm Depth	mup20	HiC_scaffold_11	CP
Dentigerous Arm Depth	mybl1	HiC_scaffold_11	CP

Dentigerous Arm Depth	myd88	HiC_scaffold_11	CP
Dentigerous Arm Depth	myh6	HiC_scaffold_11	CP
Dentigerous Arm Depth	myh7	HiC_scaffold_11	CP
Dentigerous Arm Depth	myo5a	HiC_scaffold_5	LL
Dentigerous Arm Depth	myo9a	HiC_scaffold_5	LL
Dentigerous Arm Depth	naa50	HiC_scaffold_11	CP
Dentigerous Arm Depth	ncapg2	HiC_scaffold_11	CP
Dentigerous Arm Depth	nck1	HiC_scaffold_11	CP
Dentigerous Arm Depth	ncoa2	HiC_scaffold_11	CP
Dentigerous Arm Depth	neto1	HiC_scaffold_11	CP
Dentigerous Arm Depth	nfi1	HiC_scaffold_11	CP
Dentigerous Arm Depth	nfx1	HiC_scaffold_11	CP
Dentigerous Arm Depth	ngdn	HiC_scaffold_11	CP
Dentigerous Arm Depth	nlrc3	HiC_scaffold_11	CP
Dentigerous Arm Depth	nlrp1	HiC_scaffold_11	CP
Dentigerous Arm Depth	nlrp12	HiC_scaffold_5	LL
Dentigerous Arm Depth	nom1	HiC_scaffold_11	CP
Dentigerous Arm Depth	nrn1	HiC_scaffold_11	CP
Dentigerous Arm Depth	nrros	HiC_scaffold_11	CP
Dentigerous Arm Depth	ntng1	HiC_scaffold_11	CP
Dentigerous Arm Depth	ntrk3	HiC_scaffold_5	LL
Dentigerous Arm Depth	nup58	HiC_scaffold_11	CP
Dentigerous Arm Depth	olfm3	HiC_scaffold_11	CP
Dentigerous Arm Depth	onecut1	HiC_scaffold_5	LL
Dentigerous Arm Depth	oplah	HiC_scaffold_11	CP
Dentigerous Arm Depth	oprk1	HiC_scaffold_11	CP
Dentigerous Arm Depth	otol1	HiC_scaffold_5	LL
Dentigerous Arm Depth	otulin	HiC_scaffold_11	CP
Dentigerous Arm Depth	oxsr1	HiC_scaffold_11	CP
Dentigerous Arm Depth	pabpn1	HiC_scaffold_11	CP
Dentigerous Arm Depth	pan3	HiC_scaffold_11	CP
Dentigerous Arm Depth	pck2	HiC_scaffold_11	CP
Dentigerous Arm Depth	pcolce2	HiC_scaffold_11	CP
Dentigerous Arm Depth	pdcd6	HiC_scaffold_11	CP
Dentigerous Arm Depth	pde7a	HiC_scaffold_11	CP
Dentigerous Arm Depth	pdia4	HiC_scaffold_11	CP
Dentigerous Arm Depth	pdk3	HiC_scaffold_11	CP
Dentigerous Arm Depth	pdpr	HiC_scaffold_5	LL
Dentigerous Arm Depth	pdx1	HiC_scaffold_11	CP
Dentigerous Arm Depth	pex2	HiC_scaffold_11	CP
Dentigerous Arm Depth	pgbd2	HiC_scaffold_11	CP

Dentigerous Arm Depth	phex	HiC_scaffold_11	CP
Dentigerous Arm Depth	phldb2	HiC_scaffold_11	CP
Dentigerous Arm Depth	pi15a	HiC_scaffold_11	CP
Dentigerous Arm Depth	pigm	HiC_scaffold_11	CP
Dentigerous Arm Depth	pign	HiC_scaffold_11	CP
Dentigerous Arm Depth	pim2	HiC_scaffold_11	CP
Dentigerous Arm Depth	pkia	HiC_scaffold_11	CP
Dentigerous Arm Depth	pkp3	HiC_scaffold_5	LL
Dentigerous Arm Depth	pks15/1	HiC_scaffold_11	CP
Dentigerous Arm Depth	plcd1	HiC_scaffold_11	CP
Dentigerous Arm Depth	plch2	HiC_scaffold_11	CP
Dentigerous Arm Depth	plcxd2	HiC_scaffold_11	CP
Dentigerous Arm Depth	plod2	HiC_scaffold_11	CP
Dentigerous Arm Depth	plscr2	HiC_scaffold_11	CP
Dentigerous Arm Depth	pnoc	HiC_scaffold_5	LL
Dentigerous Arm Depth	pola1	HiC_scaffold_11	CP
Dentigerous Arm Depth	polr1d	HiC_scaffold_11	CP
Dentigerous Arm Depth	pomp	HiC_scaffold_11	CP
Dentigerous Arm Depth	pop4	HiC_scaffold_5	LL
Dentigerous Arm Depth	pou6f2	HiC_scaffold_11	CP
Dentigerous Arm Depth	ppcs	HiC_scaffold_11	CP
Dentigerous Arm Depth	ppp1r16a	HiC_scaffold_11	CP
Dentigerous Arm Depth	ppp1r42	HiC_scaffold_11	CP
Dentigerous Arm Depth	prdm14	HiC_scaffold_11	CP
Dentigerous Arm Depth	prdm2	HiC_scaffold_11	CP
Dentigerous Arm Depth	prex2	HiC_scaffold_11	CP
Dentigerous Arm Depth	prkdc	HiC_scaffold_11	CP
Dentigerous Arm Depth	prlh	HiC_scaffold_11	CP
Dentigerous Arm Depth	prmt6	HiC_scaffold_11	CP
Dentigerous Arm Depth	proc	HiC_scaffold_5	LL
Dentigerous Arm Depth	prpf4b	HiC_scaffold_11	CP
Dentigerous Arm Depth	prtfdc1	HiC_scaffold_11	CP
Dentigerous Arm Depth	psma4	HiC_scaffold_5	LL
Dentigerous Arm Depth	psme1	HiC_scaffold_11	CP
Dentigerous Arm Depth	psme2	HiC_scaffold_11	CP
Dentigerous Arm Depth	ptprn2	HiC_scaffold_11	CP
Dentigerous Arm Depth	puf60	HiC_scaffold_11	CP
Dentigerous Arm Depth	qtrt2	HiC_scaffold_11	CP
Dentigerous Arm Depth	rala	HiC_scaffold_11	CP
Dentigerous Arm Depth	ralyl	HiC_scaffold_11	CP
Dentigerous Arm Depth	ramp3	HiC_scaffold_11	CP

Dentigerous Arm Depth	rbm33	HiC_scaffold_11	CP
Dentigerous Arm Depth	rbpms2	HiC_scaffold_5	LL
Dentigerous Arm Depth	rdh10a	HiC_scaffold_11	CP
Dentigerous Arm Depth	rdh12	HiC_scaffold_11	CP
Dentigerous Arm Depth	rec8	HiC_scaffold_11	CP
Dentigerous Arm Depth	relch	HiC_scaffold_11	CP
Dentigerous Arm Depth	rgs20	HiC_scaffold_11	CP
Dentigerous Arm Depth	rgs9bp-b	HiC_scaffold_11	CP
Dentigerous Arm Depth	rmdn1	HiC_scaffold_11	CP
Dentigerous Arm Depth	rnf152	HiC_scaffold_11	CP
Dentigerous Arm Depth	rnf6	HiC_scaffold_11	CP
Dentigerous Arm Depth	rnh1	HiC_scaffold_11	CP
Dentigerous Arm Depth	rnh1	HiC_scaffold_5	LL
Dentigerous Arm Depth	rnpc3	HiC_scaffold_11	CP
Dentigerous Arm Depth	rp1	HiC_scaffold_11	CP
Dentigerous Arm Depth	rpl21	HiC_scaffold_11	CP
Dentigerous Arm Depth	rpl7	HiC_scaffold_11	CP
Dentigerous Arm Depth	rps17	HiC_scaffold_5	LL
Dentigerous Arm Depth	rps20	HiC_scaffold_11	CP
Dentigerous Arm Depth	rrs1	HiC_scaffold_11	CP
Dentigerous Arm Depth	rxfp3	HiC_scaffold_5	LL
Dentigerous Arm Depth	sag	HiC_scaffold_5	LL
Dentigerous Arm Depth	sbspon	HiC_scaffold_11	CP
Dentigerous Arm Depth	scamp2	HiC_scaffold_5	LL
Dentigerous Arm Depth	scamp5-a	HiC_scaffold_5	LL
Dentigerous Arm Depth	scrib	HiC_scaffold_11	CP
Dentigerous Arm Depth	sec22c	HiC_scaffold_11	CP
Dentigerous Arm Depth	sec61g	HiC_scaffold_11	CP
Dentigerous Arm Depth	sema4b	HiC_scaffold_5	LL
Dentigerous Arm Depth	sema5a	HiC_scaffold_11	CP
Dentigerous Arm Depth	senp8	HiC_scaffold_5	LL
Dentigerous Arm Depth	serpinb1	HiC_scaffold_11	CP
Dentigerous Arm Depth	serpinb10	HiC_scaffold_11	CP
Dentigerous Arm Depth	serpinb1b	HiC_scaffold_11	CP
Dentigerous Arm Depth	serpinb6	HiC_scaffold_11	CP
Dentigerous Arm Depth	sgk3	HiC_scaffold_11	CP
Dentigerous Arm Depth	sh3glb1	HiC_scaffold_11	CP
Dentigerous Arm Depth	sh3kbp1	HiC_scaffold_11	CP
Dentigerous Arm Depth	shhb	HiC_scaffold_11	CP
Dentigerous Arm Depth	shisa2	HiC_scaffold_11	CP

Dentigerous Arm Depth	si:ch211-238a12.2	HiC_scaffold_5	LL
Dentigerous Arm Depth	siglec1	HiC_scaffold_11	CP
Dentigerous Arm Depth	siglec10	HiC_scaffold_11	CP
Dentigerous Arm Depth	siglec13	HiC_scaffold_11	CP
Dentigerous Arm Depth	siglec14	HiC_scaffold_11	CP
Dentigerous Arm Depth	siglec9	HiC_scaffold_11	CP
Dentigerous Arm Depth	ski	HiC_scaffold_11	CP
Dentigerous Arm Depth	skida1	HiC_scaffold_11	CP
Dentigerous Arm Depth	slc22a13	HiC_scaffold_11	CP
Dentigerous Arm Depth	slc22a17	HiC_scaffold_11	CP
Dentigerous Arm Depth	slc35b3	HiC_scaffold_11	CP
Dentigerous Arm Depth	slc35g2	HiC_scaffold_11	CP
Dentigerous Arm Depth	slc39a12	HiC_scaffold_11	CP
Dentigerous Arm Depth	slc4a2	HiC_scaffold_11	CP
Dentigerous Arm Depth	slc51a	HiC_scaffold_11	CP
Dentigerous Arm Depth	slco5a1	HiC_scaffold_11	CP
Dentigerous Arm Depth	smarcd3	HiC_scaffold_11	CP
Dentigerous Arm Depth	smchd1	HiC_scaffold_11	CP
Dentigerous Arm Depth	snx1	HiC_scaffold_5	LL
Dentigerous Arm Depth	snx16	HiC_scaffold_11	CP
Dentigerous Arm Depth	socs6	HiC_scaffold_11	CP
Dentigerous Arm Depth	sox17a	HiC_scaffold_11	CP
Dentigerous Arm Depth	spag16	HiC_scaffold_11	CP
Dentigerous Arm Depth	spata13	HiC_scaffold_11	CP
Dentigerous Arm Depth	spice1	HiC_scaffold_11	CP
Dentigerous Arm Depth	sppl2a	HiC_scaffold_5	LL
Dentigerous Arm Depth	st14	HiC_scaffold_11	CP
Dentigerous Arm Depth	stard5	HiC_scaffold_5	LL
Dentigerous Arm Depth	sun3	HiC_scaffold_5	LL
Dentigerous Arm Depth	sv2b	HiC_scaffold_5	LL
Dentigerous Arm Depth	tagln3	HiC_scaffold_11	CP
Dentigerous Arm Depth	tcf24	HiC_scaffold_11	CP
Dentigerous Arm Depth	tecr	HiC_scaffold_11	CP
Dentigerous Arm Depth	terf1	HiC_scaffold_11	CP
Dentigerous Arm Depth	tfap2a	HiC_scaffold_11	CP
Dentigerous Arm Depth	tfrc	HiC_scaffold_11	CP
Dentigerous Arm Depth	thap6	HiC_scaffold_11	CP
Dentigerous Arm Depth	thtpa	HiC_scaffold_11	CP
Dentigerous Arm Depth	tlnrd1	HiC_scaffold_5	LL
Dentigerous Arm Depth	tm9sf1	HiC_scaffold_11	CP

Dentigerous Arm Depth	tmem14c	HiC_scaffold_11	CP
Dentigerous Arm Depth	tmem236	HiC_scaffold_11	CP
Dentigerous Arm Depth	tmem51	HiC_scaffold_11	CP
Dentigerous Arm Depth	tmem56-b	HiC_scaffold_11	CP
Dentigerous Arm Depth	tmprss7	HiC_scaffold_11	CP
Dentigerous Arm Depth	tnk2	HiC_scaffold_11	CP
Dentigerous Arm Depth	topbp1-a	HiC_scaffold_11	CP
Dentigerous Arm Depth	tph1	HiC_scaffold_5	LL
Dentigerous Arm Depth	tram1l1	HiC_scaffold_11	CP
Dentigerous Arm Depth	trim55	HiC_scaffold_11	CP
Dentigerous Arm Depth	trim69	HiC_scaffold_5	LL
Dentigerous Arm Depth	trip4	HiC_scaffold_5	LL
Dentigerous Arm Depth	trp53inp1	HiC_scaffold_5	LL
Dentigerous Arm Depth	trpa1	HiC_scaffold_11	CP
Dentigerous Arm Depth	trpc1	HiC_scaffold_11	CP
Dentigerous Arm Depth	trpm7	HiC_scaffold_5	LL
Dentigerous Arm Depth	tshz3	HiC_scaffold_5	LL
Dentigerous Arm Depth	tssc4	HiC_scaffold_5	LL
Dentigerous Arm Depth	tssk1b	HiC_scaffold_11	CP
Dentigerous Arm Depth	tstd3	HiC_scaffold_11	CP
Dentigerous Arm Depth	txndc5	HiC_scaffold_11	CP
Dentigerous Arm Depth	tyms	HiC_scaffold_11	CP
Dentigerous Arm Depth	u2surp	HiC_scaffold_11	CP
Dentigerous Arm Depth	ube2w	HiC_scaffold_11	CP
Dentigerous Arm Depth	ube3c	HiC_scaffold_11	CP
Dentigerous Arm Depth	ubl7	HiC_scaffold_5	LL
Dentigerous Arm Depth	urad	HiC_scaffold_11	CP
Dentigerous Arm Depth	usf3	HiC_scaffold_11	CP
Dentigerous Arm Depth	usp12	HiC_scaffold_11	CP
Dentigerous Arm Depth	utp3	HiC_scaffold_11	CP
Dentigerous Arm Depth	vav3	HiC_scaffold_11	CP
Dentigerous Arm Depth	vcpip1	HiC_scaffold_5	LL
Dentigerous Arm Depth	vil1	HiC_scaffold_11	CP
Dentigerous Arm Depth	vipr1	HiC_scaffold_11	CP
Dentigerous Arm Depth	vps35	HiC_scaffold_5	LL
Dentigerous Arm Depth	vstm2a	HiC_scaffold_11	CP
Dentigerous Arm Depth	wasf3	HiC_scaffold_11	CP
Dentigerous Arm Depth	wdr19	HiC_scaffold_11	CP
Dentigerous Arm Depth	wdr37	HiC_scaffold_11	CP
Dentigerous Arm Depth	wdr60	HiC_scaffold_11	CP
Dentigerous Arm Depth	wwp1	HiC_scaffold_11	CP

Dentigerous Arm Depth	xcc-b100_1894	HiC_scaffold_11	CP
Dentigerous Arm Depth	xkr9	HiC_scaffold_11	CP
Dentigerous Arm Depth	yes1	HiC_scaffold_11	CP
Dentigerous Arm Depth	yme1l1	HiC_scaffold_11	CP
Dentigerous Arm Depth	ythdf2	HiC_scaffold_11	CP
Dentigerous Arm Depth	zc2hc1a	HiC_scaffold_11	CP
Dentigerous Arm Depth	zdhhc23	HiC_scaffold_11	CP
Dentigerous Arm Depth	zfand1	HiC_scaffold_11	CP
Dentigerous Arm Depth	zfhx4	HiC_scaffold_11	CP
Dentigerous Arm Depth	zic1	HiC_scaffold_11	CP
Dentigerous Arm Depth	zkscan5	HiC_scaffold_5	LL
Dentigerous Arm Depth	znf235	HiC_scaffold_11	CP
Dentigerous Arm Depth	znf25	HiC_scaffold_5	LL
Dentigerous Arm Depth	znf45	HiC_scaffold_5	LL
Dentigerous Arm Depth	znf507	HiC_scaffold_5	LL
Dentigerous Arm Depth	znf569	HiC_scaffold_5	LL
Dentigerous Arm Depth	znf609	HiC_scaffold_5	LL
Dentigerous Arm Depth	znf652	HiC_scaffold_11	CP
Dentigerous Arm Depth	znf710	HiC_scaffold_5	LL
Dentigerous Arm Width	abca1	HiC_scaffold_24	LL
Dentigerous Arm Width	abca4	HiC_scaffold_24	LL
Dentigerous Arm Width	abca7	HiC_scaffold_24	LL
Dentigerous Arm Width	abr	HiC_scaffold_24	LL
Dentigerous Arm Width	acadvl	HiC_scaffold_24	LL
Dentigerous Arm Width	acan	HiC_scaffold_24	LL
Dentigerous Arm Width	acbp4	HiC_scaffold_24	LL
Dentigerous Arm Width	acy3.2	HiC_scaffold_24	LL
Dentigerous Arm Width	adamtsl1	HiC_scaffold_24	LL
Dentigerous Arm Width	adcy2	HiC_scaffold_24	LL
Dentigerous Arm Width	adgra3	HiC_scaffold_24	LL
Dentigerous Arm Width	adgrl3	HiC_scaffold_24	LL
Dentigerous Arm Width	agfg1	HiC_scaffold_24	LL
Dentigerous Arm Width	alpk1	HiC_scaffold_58	LL
Dentigerous Arm Width	ami	HiC_scaffold_24	LL
Dentigerous Arm Width	arap2	HiC_scaffold_24	LL
Dentigerous Arm Width	arhgef11	HiC_scaffold_24	LL
Dentigerous Arm Width	arl2	HiC_scaffold_24	LL
Dentigerous Arm Width	atp6ap1	HiC_scaffold_24	LL
Dentigerous Arm Width	b3gat3	HiC_scaffold_24	LL
Dentigerous Arm Width	bad	HiC_scaffold_24	LL

Dentigerous Arm Width	bank1	HiC_scaffold_24	LL
Dentigerous Arm Width	bcl6b	HiC_scaffold_24	LL
Dentigerous Arm Width	brms1la	HiC_scaffold_24	LL
Dentigerous Arm Width	btn2a1	HiC_scaffold_24	LL
Dentigerous Arm Width	btn2a2	HiC_scaffold_24	LL
Dentigerous Arm Width	c1ql4	HiC_scaffold_24	LL
Dentigerous Arm Width	cabp4	HiC_scaffold_24	LL
Dentigerous Arm Width	capg	HiC_scaffold_24	LL
Dentigerous Arm Width	card6	HiC_scaffold_24	LL
Dentigerous Arm Width	cbln1	HiC_scaffold_24	LL
Dentigerous Arm Width	ccdc149b	HiC_scaffold_24	LL
Dentigerous Arm Width	cct7	HiC_scaffold_24	LL
Dentigerous Arm Width	cd48	HiC_scaffold_24	LL
Dentigerous Arm Width	cdca9	HiC_scaffold_24	LL
Dentigerous Arm Width	chordc1	HiC_scaffold_24	LL
Dentigerous Arm Width	chrnb1	HiC_scaffold_24	LL
Dentigerous Arm Width	chst12	HiC_scaffold_24	LL
Dentigerous Arm Width	clcn5	HiC_scaffold_24	LL
Dentigerous Arm Width	cldn7a	HiC_scaffold_24	LL
Dentigerous Arm Width	cldnd1	HiC_scaffold_24	LL
Dentigerous Arm Width	clec10a	HiC_scaffold_24	LL
Dentigerous Arm Width	clec12b	HiC_scaffold_24	LL
Dentigerous Arm Width	clec20a	HiC_scaffold_24	LL
Dentigerous Arm Width	cmas	HiC_scaffold_24	LL
Dentigerous Arm Width	cnpy3	HiC_scaffold_24	LL
Dentigerous Arm Width	coro1b	HiC_scaffold_24	LL
Dentigerous Arm Width	cpras1	HiC_scaffold_24	LL
Dentigerous Arm Width	cpz	HiC_scaffold_24	LL
Dentigerous Arm Width	ctdnep1a	HiC_scaffold_24	LL
Dentigerous Arm Width	cyld	HiC_scaffold_24	LL
Dentigerous Arm Width	cyp26b1	HiC_scaffold_24	LL
Dentigerous Arm Width	dctn1	HiC_scaffold_24	LL
Dentigerous Arm Width	dctn6	HiC_scaffold_24	LL
Dentigerous Arm Width	ddit4l	HiC_scaffold_24	LL
Dentigerous Arm Width	dennd4c	HiC_scaffold_24	LL
Dentigerous Arm Width	dgkd	HiC_scaffold_24	LL
Dentigerous Arm Width	dmrta1	HiC_scaffold_24	LL
Dentigerous Arm Width	dnai2	HiC_scaffold_24	LL
Dentigerous Arm Width	dok1	HiC_scaffold_24	LL
Dentigerous Arm Width	dok7	HiC_scaffold_24	LL
Dentigerous Arm Width	dtx4	HiC_scaffold_24	LL

Dentigerous Arm Width	dysf	HiC_scaffold_24	LL
Dentigerous Arm Width	eif5a	HiC_scaffold_24	LL
Dentigerous Arm Width	elavl2	HiC_scaffold_24	LL
Dentigerous Arm Width	elp5	HiC_scaffold_24	LL
Dentigerous Arm Width	emc4	HiC_scaffold_24	LL
Dentigerous Arm Width	endod1	HiC_scaffold_24	LL
Dentigerous Arm Width	epd	HiC_scaffold_58	LL
Dentigerous Arm Width	epd2	HiC_scaffold_58	LL
Dentigerous Arm Width	epo	HiC_scaffold_24	LL
Dentigerous Arm Width	ern1	HiC_scaffold_24	LL
Dentigerous Arm Width	etnppl	HiC_scaffold_24	LL
Dentigerous Arm Width	fabp2	HiC_scaffold_24	LL
Dentigerous Arm Width	fcgr2	HiC_scaffold_24	LL
Dentigerous Arm Width	fn1	HiC_scaffold_24	LL
Dentigerous Arm Width	fxr1	HiC_scaffold_58	LL
Dentigerous Arm Width	g0s2	HiC_scaffold_24	LL
Dentigerous Arm Width	gab1	HiC_scaffold_24	LL
Dentigerous Arm Width	gabarap	HiC_scaffold_24	LL
Dentigerous Arm Width	gba3	HiC_scaffold_24	LL
Dentigerous Arm Width	gdi1	HiC_scaffold_24	LL
Dentigerous Arm Width	gimap3	HiC_scaffold_24	LL
Dentigerous Arm Width	gimap4	HiC_scaffold_24	LL
Dentigerous Arm Width	gimap5	HiC_scaffold_24	LL
Dentigerous Arm Width	gimap6	HiC_scaffold_24	LL
Dentigerous Arm Width	gimap7	HiC_scaffold_24	LL
Dentigerous Arm Width	gimap8	HiC_scaffold_24	LL
Dentigerous Arm Width	gpha2	HiC_scaffold_24	LL
Dentigerous Arm Width	gpr12	HiC_scaffold_24	LL
Dentigerous Arm Width	gpr26	HiC_scaffold_24	LL
Dentigerous Arm Width	gpr4	HiC_scaffold_24	LL
Dentigerous Arm Width	gps2	HiC_scaffold_24	LL
Dentigerous Arm Width	gvin1	HiC_scaffold_24	LL
Dentigerous Arm Width	haus4	HiC_scaffold_58	LL
Dentigerous Arm Width	hdlbp	HiC_scaffold_24	LL
Dentigerous Arm Width	hgfac	HiC_scaffold_24	LL
Dentigerous Arm Width	hmx1	HiC_scaffold_24	LL
Dentigerous Arm Width	hmx2	HiC_scaffold_24	LL
Dentigerous Arm Width	hnrnpc	HiC_scaffold_24	LL
Dentigerous Arm Width	hspa12b	HiC_scaffold_24	LL
Dentigerous Arm Width	htr2a	HiC_scaffold_24	LL
Dentigerous Arm Width	irs1-b	HiC_scaffold_24	LL

Dentigerous Arm Width	itih6	HiC_scaffold_24	LL
Dentigerous Arm Width	kcnip4	HiC_scaffold_24	LL
Dentigerous Arm Width	kdm6b	HiC_scaffold_24	LL
Dentigerous Arm Width	kirrel1	HiC_scaffold_58	LL
Dentigerous Arm Width	klhl33	HiC_scaffold_24	LL
Dentigerous Arm Width	lgi2	HiC_scaffold_24	LL
Dentigerous Arm Width	lpcat4	HiC_scaffold_24	LL
Dentigerous Arm Width	lrfn2	HiC_scaffold_24	LL
Dentigerous Arm Width	ltb4r	HiC_scaffold_24	LL
Dentigerous Arm Width	ltb4r2	HiC_scaffold_24	LL
Dentigerous Arm Width	lurap1l	HiC_scaffold_24	LL
Dentigerous Arm Width	majin	HiC_scaffold_24	LL
Dentigerous Arm Width	mark2	HiC_scaffold_24	LL
Dentigerous Arm Width	mb21d2	HiC_scaffold_24	LL
Dentigerous Arm Width	mpdz	HiC_scaffold_24	LL
Dentigerous Arm Width	mrc1	HiC_scaffold_24	LL
Dentigerous Arm Width	mrc2	HiC_scaffold_24	LL
Dentigerous Arm Width	mrpl48	HiC_scaffold_58	LL
Dentigerous Arm Width	msantd1	HiC_scaffold_24	LL
Dentigerous Arm Width	msmeg_2408	HiC_scaffold_24	LL
Dentigerous Arm Width	mus81	HiC_scaffold_24	LL
Dentigerous Arm Width	myadm	HiC_scaffold_24	LL
Dentigerous Arm Width	myoz2	HiC_scaffold_24	LL
Dentigerous Arm Width	n4bp1	HiC_scaffold_24	LL
Dentigerous Arm Width	naa40	HiC_scaffold_24	LL
Dentigerous Arm Width	nagk	HiC_scaffold_24	LL
Dentigerous Arm Width	ndrg2	HiC_scaffold_24	LL
Dentigerous Arm Width	ndufs2	HiC_scaffold_58	LL
Dentigerous Arm Width	nectin4	HiC_scaffold_58	LL
Dentigerous Arm Width	neurl4	HiC_scaffold_24	LL
Dentigerous Arm Width	nfib	HiC_scaffold_24	LL
Dentigerous Arm Width	nlgn4x	HiC_scaffold_24	LL
Dentigerous Arm Width	nlrc3	HiC_scaffold_24	LL
Dentigerous Arm Width	nlrp1	HiC_scaffold_24	LL
Dentigerous Arm Width	nwd2	HiC_scaffold_24	LL
Dentigerous Arm Width	obscn	HiC_scaffold_24	LL
Dentigerous Arm Width	oga	HiC_scaffold_24	LL
Dentigerous Arm Width	or131-2	HiC_scaffold_24	LL
Dentigerous Arm Width	osbp	HiC_scaffold_24	LL
Dentigerous Arm Width	ostc	HiC_scaffold_24	LL

Dentigerous Arm Width	otub1	HiC_scaffold_58	LL
Dentigerous Arm Width	ovol1	HiC_scaffold_24	LL
Dentigerous Arm Width	p2ry1	HiC_scaffold_24	LL
Dentigerous Arm Width	paip2b	HiC_scaffold_24	LL
Dentigerous Arm Width	parp14	HiC_scaffold_24	LL
Dentigerous Arm Width	parp15	HiC_scaffold_24	LL
Dentigerous Arm Width	parp9	HiC_scaffold_24	LL
Dentigerous Arm Width	pcdh7	HiC_scaffold_24	LL
Dentigerous Arm Width	pced1a	HiC_scaffold_24	LL
Dentigerous Arm Width	pcolce2	HiC_scaffold_24	LL
Dentigerous Arm Width	pea15	HiC_scaffold_58	LL
Dentigerous Arm Width	per1	HiC_scaffold_24	LL
Dentigerous Arm Width	pfkfb1	HiC_scaffold_24	LL
Dentigerous Arm Width	phf23b	HiC_scaffold_24	LL
Dentigerous Arm Width	pla2r1	HiC_scaffold_24	LL
Dentigerous Arm Width	plac8l1	HiC_scaffold_24	LL
Dentigerous Arm Width	plin2	HiC_scaffold_24	LL
Dentigerous Arm Width	plscr2	HiC_scaffold_24	LL
Dentigerous Arm Width	polr2a	HiC_scaffold_24	LL
Dentigerous Arm Width	pop7	HiC_scaffold_24	LL
Dentigerous Arm Width	ppargc1a	HiC_scaffold_24	LL
Dentigerous Arm Width	ppp1r14b	HiC_scaffold_24	LL
Dentigerous Arm Width	ppp2r5b	HiC_scaffold_24	LL
Dentigerous Arm Width	ppp3ca	HiC_scaffold_24	LL
Dentigerous Arm Width	prox1	HiC_scaffold_24	LL
Dentigerous Arm Width	prss27	HiC_scaffold_24	LL
Dentigerous Arm Width	prss8	HiC_scaffold_24	LL
Dentigerous Arm Width	ptprd	HiC_scaffold_24	LL
Dentigerous Arm Width	rab38	HiC_scaffold_24	LL
Dentigerous Arm Width	rab39b	HiC_scaffold_24	LL
Dentigerous Arm Width	rasgrp2-b	HiC_scaffold_58	LL
Dentigerous Arm Width	rbm4b	HiC_scaffold_58	LL
Dentigerous Arm Width	rbpms	HiC_scaffold_24	LL
Dentigerous Arm Width	rcor2	HiC_scaffold_24	LL
Dentigerous Arm Width	ripk4	HiC_scaffold_24	LL
Dentigerous Arm Width	rnf183	HiC_scaffold_24	LL
Dentigerous Arm Width	rnf223	HiC_scaffold_24	LL
Dentigerous Arm Width	rpl34	HiC_scaffold_24	LL
Dentigerous Arm Width	sec24d	HiC_scaffold_24	LL
Dentigerous Arm Width	sema4f	HiC_scaffold_24	LL
Dentigerous Arm Width	sgcz	HiC_scaffold_24	LL

Dentigerous Arm Width	shbg	HiC_scaffold_24	LL
Dentigerous Arm Width	slamf9	HiC_scaffold_24	LL
Dentigerous Arm Width	slc12a3	HiC_scaffold_24	LL
Dentigerous Arm Width	slc12a6	HiC_scaffold_24	LL
Dentigerous Arm Width	slc14a2	HiC_scaffold_24	LL
Dentigerous Arm Width	slc16a13	HiC_scaffold_24	LL
Dentigerous Arm Width	slc2a4	HiC_scaffold_24	LL
Dentigerous Arm Width	slc8a1	HiC_scaffold_24	LL
Dentigerous Arm Width	sned1	HiC_scaffold_24	LL
Dentigerous Arm Width	snx15	HiC_scaffold_24	LL
Dentigerous Arm Width	spag17	HiC_scaffold_24	LL
Dentigerous Arm Width	stk26	HiC_scaffold_24	LL
Dentigerous Arm Width	supt16h	HiC_scaffold_24	LL
Dentigerous Arm Width	synpo2	HiC_scaffold_24	LL
Dentigerous Arm Width	syt4	HiC_scaffold_24	LL
Dentigerous Arm Width	taf8	HiC_scaffold_24	LL
Dentigerous Arm Width	tdrd7b	HiC_scaffold_24	LL
Dentigerous Arm Width	tgas006m08.1	HiC_scaffold_24	LL
Dentigerous Arm Width	tkfc	HiC_scaffold_24	LL
Dentigerous Arm Width	tmem151b	HiC_scaffold_24	LL
Dentigerous Arm Width	tmem179b	HiC_scaffold_24	LL
Dentigerous Arm Width	tmem55bb	HiC_scaffold_24	LL
Dentigerous Arm Width	tmem88	HiC_scaffold_24	LL
Dentigerous Arm Width	tmprss15	HiC_scaffold_24	LL
Dentigerous Arm Width	tnc	HiC_scaffold_24	LL
Dentigerous Arm Width	tnfsf10	HiC_scaffold_24	LL
Dentigerous Arm Width	tnk2	HiC_scaffold_24	LL
Dentigerous Arm Width	tox4-b	HiC_scaffold_24	LL
Dentigerous Arm Width	tp53	HiC_scaffold_24	LL
Dentigerous Arm Width	trbv2	HiC_scaffold_58	LL
Dentigerous Arm Width	trim27	HiC_scaffold_24	LL
Dentigerous Arm Width	trim39	HiC_scaffold_24	LL
Dentigerous Arm Width	trip6	HiC_scaffold_24	LL
Dentigerous Arm Width	trmt44	HiC_scaffold_24	LL
Dentigerous Arm Width	tyrp1	HiC_scaffold_24	LL
Dentigerous Arm Width	ufsp1	HiC_scaffold_24	LL
Dentigerous Arm Width	ugt2b20	HiC_scaffold_24	LL
Dentigerous Arm Width	ugt2c1	HiC_scaffold_24	LL
Dentigerous Arm Width	urgcp	HiC_scaffold_24	LL
Dentigerous Arm Width	vangl2	HiC_scaffold_24	LL

Dentigerous Arm Width	vbp1	HiC_scaffold_24	LL
Dentigerous Arm Width	wasf3	HiC_scaffold_24	LL
Dentigerous Arm Width	ybx1	HiC_scaffold_24	LL
Dentigerous Arm Width	zbtb38	HiC_scaffold_24	LL
Dentigerous Arm Width	zdhhc21	HiC_scaffold_24	LL
Dentigerous Arm Width	zdhhc3	HiC_scaffold_24	LL
Dentigerous Arm Width	znf638	HiC_scaffold_24	LL
Jaw closing In-Lever	a1cf	HiC_scaffold_8	LL
Jaw closing In-Lever	abcc3	HiC_scaffold_8	LL
Jaw closing In-Lever	acadsb	HiC_scaffold_8	LL
Jaw closing In-Lever	adam12	HiC_scaffold_8	LL
Jaw closing In-Lever	adap1	HiC_scaffold_8	LL
Jaw closing In-Lever	ado	HiC_scaffold_8	LL
Jaw closing In-Lever	amdhd2	HiC_scaffold_8	LL
Jaw closing In-Lever	antxr1	HiC_scaffold_8	LL
Jaw closing In-Lever	aqp8	HiC_scaffold_8	LL
Jaw closing In-Lever	arf1	HiC_scaffold_8	LL
Jaw closing In-Lever	arhgap17	HiC_scaffold_8	LL
Jaw closing In-Lever	arhgap24	HiC_scaffold_8	LL
Jaw closing In-Lever	asb12	HiC_scaffold_8	LL
Jaw closing In-Lever	atp6v0a1	HiC_scaffold_8	LL
Jaw closing In-Lever	atpaf2	HiC_scaffold_8	LL
Jaw closing In-Lever	baiap2l1	HiC_scaffold_8	LL
Jaw closing In-Lever	bbs1	HiC_scaffold_8	LL
Jaw closing In-Lever	bccip	HiC_scaffold_8	LL
Jaw closing In-Lever	bms1	HiC_scaffold_8	LL
Jaw closing In-Lever	bricd5	HiC_scaffold_8	LL
Jaw closing In-Lever	btbd17	HiC_scaffold_8	LL
Jaw closing In-Lever	bub3	HiC_scaffold_8	LL
Jaw closing In-Lever	cacna1g	HiC_scaffold_8	LL
Jaw closing In-Lever	cavin1	HiC_scaffold_8	LL
Jaw closing In-Lever	cbx7	HiC_scaffold_8	LL
Jaw closing In-Lever	cd163	HiC_scaffold_8	LL
Jaw closing In-Lever	cdr2l	HiC_scaffold_8	LL
Jaw closing In-Lever	chadl	HiC_scaffold_8	LL
Jaw closing In-Lever	chrm3	HiC_scaffold_8	LL
Jaw closing In-Lever	chst15	HiC_scaffold_8	LL
Jaw closing In-Lever	coe3	HiC_scaffold_8	LL
Jaw closing In-Lever	col14a1	HiC_scaffold_8	LL
Jaw closing In-Lever	cox19	HiC_scaffold_8	LL
Jaw closing In-Lever	cpped1	HiC_scaffold_8	LL

Jaw closing In-Lever	cpxm2	HiC_scaffold_8	LL
Jaw closing In-Lever	cxcr6	HiC_scaffold_8	LL
Jaw closing In-Lever	cybc1	HiC_scaffold_8	LL
Jaw closing In-Lever	d7ertd443e	HiC_scaffold_8	LL
Jaw closing In-Lever	dhrs7ca	HiC_scaffold_8	LL
Jaw closing In-Lever	dnah9	HiC_scaffold_8	LL
Jaw closing In-Lever	dpysl2	HiC_scaffold_8	LL
Jaw closing In-Lever	egr2b	HiC_scaffold_8	LL
Jaw closing In-Lever	elovl6	HiC_scaffold_8	LL
Jaw closing In-Lever	endod1	HiC_scaffold_8	LL
Jaw closing In-Lever	ep300	HiC_scaffold_8	LL
Jaw closing In-Lever	ercc4	HiC_scaffold_8	LL
Jaw closing In-Lever	exoc6	HiC_scaffold_8	LL
Jaw closing In-Lever	fads6	HiC_scaffold_8	LL
Jaw closing In-Lever	fam13a	HiC_scaffold_8	LL
Jaw closing In-Lever	fam171a2	HiC_scaffold_8	LL
Jaw closing In-Lever	fam53b	HiC_scaffold_8	LL
Jaw closing In-Lever	fasn	HiC_scaffold_8	LL
Jaw closing In-Lever	fdxr	HiC_scaffold_8	LL
Jaw closing In-Lever	fmnl1	HiC_scaffold_8	LL
Jaw closing In-Lever	foxj1b	HiC_scaffold_8	LL
Jaw closing In-Lever	foxk2	HiC_scaffold_8	LL
Jaw closing In-Lever	foxl1	HiC_scaffold_8	LL
Jaw closing In-Lever	frmpd2	HiC_scaffold_8	LL
Jaw closing In-Lever	galk1	HiC_scaffold_8	LL
Jaw closing In-Lever	galr2	HiC_scaffold_8	LL
Jaw closing In-Lever	gas7	HiC_scaffold_8	LL
Jaw closing In-Lever	gdf10	HiC_scaffold_8	LL
Jaw closing In-Lever	get4	HiC_scaffold_8	LL
Jaw closing In-Lever	gid4	HiC_scaffold_8	LL
Jaw closing In-Lever	gimap4	HiC_scaffold_8	LL
Jaw closing In-Lever	glp2r	HiC_scaffold_8	LL
Jaw closing In-Lever	gpr142	HiC_scaffold_8	LL
Jaw closing In-Lever	gpr26	HiC_scaffold_8	LL
Jaw closing In-Lever	gprc5c	HiC_scaffold_8	LL
Jaw closing In-Lever	grb10	HiC_scaffold_8	LL
Jaw closing In-Lever	grid2ip	HiC_scaffold_8	LL
Jaw closing In-Lever	grn	HiC_scaffold_8	LL
Jaw closing In-Lever	gsg1l	HiC_scaffold_8	LL
Jaw closing In-Lever	hba1	HiC_scaffold_8	LL
Jaw closing In-Lever	hbb1	HiC_scaffold_8	LL

Jaw closing In-Lever	hexd	HiC_scaffold_8	LL
Jaw closing In-Lever	hhex	HiC_scaffold_8	LL
Jaw closing In-Lever	hid1	HiC_scaffold_8	LL
Jaw closing In-Lever	hmx3b	HiC_scaffold_8	LL
Jaw closing In-Lever	hpdl	HiC_scaffold_8	LL
Jaw closing In-Lever	hs3st3a1	HiC_scaffold_8	LL
Jaw closing In-Lever	hs3st3b1	HiC_scaffold_8	LL
Jaw closing In-Lever	itgb4	HiC_scaffold_8	LL
Jaw closing In-Lever	jakmip3	HiC_scaffold_8	LL
Jaw closing In-Lever	jmjd8	HiC_scaffold_8	LL
Jaw closing In-Lever	kcnj16	HiC_scaffold_8	LL
Jaw closing In-Lever	kcnj2	HiC_scaffold_8	LL
Jaw closing In-Lever	kdelr2	HiC_scaffold_8	LL
Jaw closing In-Lever	kif20b	HiC_scaffold_8	LL
Jaw closing In-Lever	lcmt1	HiC_scaffold_8	LL
Jaw closing In-Lever	lect2	HiC_scaffold_8	LL
Jaw closing In-Lever	lhpp	HiC_scaffold_8	LL
Jaw closing In-Lever	llgl2	HiC_scaffold_8	LL
Jaw closing In-Lever	lmf1	HiC_scaffold_8	LL
Jaw closing In-Lever	lrrc45	HiC_scaffold_8	LL
Jaw closing In-Lever	map2k4	HiC_scaffold_8	LL
Jaw closing In-Lever	map2k6	HiC_scaffold_8	LL
Jaw closing In-Lever	map3k14	HiC_scaffold_8	LL
Jaw closing In-Lever	mapk8b	HiC_scaffold_8	LL
Jaw closing In-Lever	mbtd1	HiC_scaffold_8	LL
Jaw closing In-Lever	meiob	HiC_scaffold_8	LL
Jaw closing In-Lever	mettl9	HiC_scaffold_8	LL
Jaw closing In-Lever	mfap4	HiC_scaffold_8	LL
Jaw closing In-Lever	mlst8	HiC_scaffold_8	LL
Jaw closing In-Lever	mmp21	HiC_scaffold_8	LL
Jaw closing In-Lever	mms19	HiC_scaffold_8	LL
Jaw closing In-Lever	mprip	HiC_scaffold_8	LL
Jaw closing In-Lever	mrpl27	HiC_scaffold_8	LL
Jaw closing In-Lever	mrpl38	HiC_scaffold_8	LL
Jaw closing In-Lever	mrtfa	HiC_scaffold_8	LL
Jaw closing In-Lever	mrtfb	HiC_scaffold_8	LL
Jaw closing In-Lever	mtfr1l	HiC_scaffold_8	LL
Jaw closing In-Lever	mtr	HiC_scaffold_8	LL
Jaw closing In-Lever	myh16	HiC_scaffold_8	LL
Jaw closing In-Lever	myh7	HiC_scaffold_8	LL
Jaw closing In-Lever	myo15a	HiC_scaffold_8	LL

Jaw closing In-Lever	myo15b	HiC_scaffold_8	LL
Jaw closing In-Lever	myocd	HiC_scaffold_8	LL
Jaw closing In-Lever	narf	HiC_scaffold_8	LL
Jaw closing In-Lever	ndufaf4	HiC_scaffold_8	LL
Jaw closing In-Lever	nme2	HiC_scaffold_8	LL
Jaw closing In-Lever	noxo1	HiC_scaffold_8	LL
Jaw closing In-Lever	nploc4	HiC_scaffold_8	LL
Jaw closing In-Lever	nptx2	HiC_scaffold_8	LL
Jaw closing In-Lever	nrbf2	HiC_scaffold_8	LL
Jaw closing In-Lever	nt5m	HiC_scaffold_8	LL
Jaw closing In-Lever	oat	HiC_scaffold_8	LL
Jaw closing In-Lever	pgp	HiC_scaffold_8	LL
Jaw closing In-Lever	phf5a	HiC_scaffold_8	LL
Jaw closing In-Lever	phyhipl	HiC_scaffold_8	LL
Jaw closing In-Lever	pim3	HiC_scaffold_8	LL
Jaw closing In-Lever	plau	HiC_scaffold_8	LL
Jaw closing In-Lever	plcd3a	HiC_scaffold_8	LL
Jaw closing In-Lever	plcxd1	HiC_scaffold_8	LL
Jaw closing In-Lever	polr3d	HiC_scaffold_8	LL
Jaw closing In-Lever	ppp1r3cb	HiC_scaffold_8	LL
Jaw closing In-Lever	prkg1	HiC_scaffold_8	LL
Jaw closing In-Lever	prss8	HiC_scaffold_8	LL
Jaw closing In-Lever	pstk	HiC_scaffold_8	LL
Jaw closing In-Lever	pts	HiC_scaffold_8	LL
Jaw closing In-Lever	rab37	HiC_scaffold_8	LL
Jaw closing In-Lever	rab3gap1	HiC_scaffold_8	LL
Jaw closing In-Lever	ramp1	HiC_scaffold_8	LL
Jaw closing In-Lever	rangap1	HiC_scaffold_8	LL
Jaw closing In-Lever	rasd1	HiC_scaffold_8	LL
Jaw closing In-Lever	rbp3	HiC_scaffold_8	LL
Jaw closing In-Lever	reep3	HiC_scaffold_8	LL
Jaw closing In-Lever	rhbdf1	HiC_scaffold_8	LL
Jaw closing In-Lever	sap30bp	HiC_scaffold_8	LL
Jaw closing In-Lever	sbk1	HiC_scaffold_8	LL
Jaw closing In-Lever	shisa6	HiC_scaffold_8	LL
Jaw closing In-Lever	shisa9	HiC_scaffold_8	LL
Jaw closing In-Lever	shisa9a	HiC_scaffold_8	LL
Jaw closing In-Lever	slc16a12b	HiC_scaffold_8	LL
Jaw closing In-Lever	slc2a11	HiC_scaffold_8	LL
Jaw closing In-Lever	slc9a3r1	HiC_scaffold_8	LL
Jaw closing In-Lever	snx29	HiC_scaffold_8	LL

Jaw closing In-Lever	sox8	HiC_scaffold_8	LL
Jaw closing In-Lever	spag9	HiC_scaffold_8	LL
Jaw closing In-Lever	srcin1	HiC_scaffold_8	LL
Jaw closing In-Lever	sstr2	HiC_scaffold_8	LL
Jaw closing In-Lever	st6galnac2	HiC_scaffold_8	LL
Jaw closing In-Lever	stat5b	HiC_scaffold_8	LL
Jaw closing In-Lever	sult2b1	HiC_scaffold_8	LL
Jaw closing In-Lever	tcerg1l	HiC_scaffold_8	LL
Jaw closing In-Lever	tdrkh	HiC_scaffold_8	LL
Jaw closing In-Lever	tex2	HiC_scaffold_8	LL
Jaw closing In-Lever	tgas113e22.1	HiC_scaffold_8	LL
Jaw closing In-Lever	thap10	HiC_scaffold_8	LL
Jaw closing In-Lever	tmem130	HiC_scaffold_8	LL
Jaw closing In-Lever	tmem238	HiC_scaffold_8	LL
Jaw closing In-Lever	tmem94	HiC_scaffold_8	LL
Jaw closing In-Lever	tmprss5	HiC_scaffold_8	LL
Jaw closing In-Lever	tnfrsf13b	HiC_scaffold_8	LL
Jaw closing In-Lever	tom1l2	HiC_scaffold_8	LL
Jaw closing In-Lever	trim16	HiC_scaffold_8	LL
Jaw closing In-Lever	trim39	HiC_scaffold_8	LL
Jaw closing In-Lever	trim65	HiC_scaffold_8	LL
Jaw closing In-Lever	trrap	HiC_scaffold_8	LL
Jaw closing In-Lever	trub1	HiC_scaffold_8	LL
Jaw closing In-Lever	tuba1c	HiC_scaffold_8	LL
Jaw closing In-Lever	tvp23b	HiC_scaffold_8	LL
Jaw closing In-Lever	ubald1	HiC_scaffold_8	LL
Jaw closing In-Lever	ubtd1	HiC_scaffold_8	LL
Jaw closing In-Lever	ugt2c1	HiC_scaffold_8	LL
Jaw closing In-Lever	unc13d	HiC_scaffold_8	LL
Jaw closing In-Lever	unk	HiC_scaffold_8	LL
Jaw closing In-Lever	uros	HiC_scaffold_8	LL
Jaw closing In-Lever	ush1g	HiC_scaffold_8	LL
Jaw closing In-Lever	usp22	HiC_scaffold_8	LL
Jaw closing In-Lever	uts2r	HiC_scaffold_8	LL
Jaw closing In-Lever	wbp2	HiC_scaffold_8	LL
Jaw closing In-Lever	wfikkn2	HiC_scaffold_8	LL
Jaw closing In-Lever	xrcc6	HiC_scaffold_8	LL
Jaw closing In-Lever	zc3h7b	HiC_scaffold_8	LL
Jaw closing In-Lever	znf235	HiC_scaffold_8	LL
Jaw closing In-Lever	znf569	HiC_scaffold_8	LL

Jaw closing In-Lever	znf84	HiC_scaffold_8	LL
Jaw closing In-Lever	zranb1	HiC_scaffold_8	LL
Maxillary Head Protrusion	sep7	HiC_scaffold_53	LL
Maxillary Head Protrusion	abcb1	HiC_scaffold_53	LL
Maxillary Head Protrusion	abhd16a	HiC_scaffold_53	LL
Maxillary Head Protrusion	acan	HiC_scaffold_53	LL
Maxillary Head Protrusion	adam22	HiC_scaffold_53	LL
Maxillary Head Protrusion	adamts16	HiC_scaffold_53	LL
Maxillary Head Protrusion	adar	HiC_scaffold_53	LL
Maxillary Head Protrusion	adcy2	HiC_scaffold_53	LL
Maxillary Head Protrusion	agmo	HiC_scaffold_53	LL
Maxillary Head Protrusion	ago1	HiC_scaffold_53	LL
Maxillary Head Protrusion	ago3	HiC_scaffold_53	LL
Maxillary Head Protrusion	aicda	HiC_scaffold_53	LL
Maxillary Head Protrusion	aif1l	HiC_scaffold_53	LL
Maxillary Head Protrusion	alg2	HiC_scaffold_53	LL
Maxillary Head Protrusion	ankib1	HiC_scaffold_53	LL
Maxillary Head Protrusion	ankmy2	HiC_scaffold_53	LL
Maxillary Head Protrusion	ankrd28	HiC_scaffold_53	LL
Maxillary Head Protrusion	apoa1	HiC_scaffold_53	LL
Maxillary Head Protrusion	apoa4	HiC_scaffold_53	LL
Maxillary Head Protrusion	apoeb	HiC_scaffold_53	LL
Maxillary Head Protrusion	apoh	HiC_scaffold_53	LL
Maxillary Head Protrusion	aqp10	HiC_scaffold_53	LL
Maxillary Head Protrusion	arhgef1	HiC_scaffold_53	LL
Maxillary Head Protrusion	arid1a	HiC_scaffold_53	LL
Maxillary Head Protrusion	arnt	HiC_scaffold_53	LL
Maxillary Head Protrusion	atg12	HiC_scaffold_53	LL
Maxillary Head Protrusion	atp1a3	HiC_scaffold_53	LL
Maxillary Head Protrusion	atp6v1c1a	HiC_scaffold_53	LL
Maxillary Head Protrusion	atp8b2	HiC_scaffold_53	LL
Maxillary Head Protrusion	atxn1	HiC_scaffold_53	LL
Maxillary Head Protrusion	azi2	HiC_scaffold_53	LL
Maxillary Head Protrusion	azin1	HiC_scaffold_53	LL
Maxillary Head Protrusion	baiap2	HiC_scaffold_53	LL
Maxillary Head Protrusion	bcam	HiC_scaffold_53	LL
Maxillary Head Protrusion	bckdhb	HiC_scaffold_53	LL
Maxillary Head Protrusion	bcl3	HiC_scaffold_53	LL
Maxillary Head Protrusion	brd2	HiC_scaffold_53	LL
Maxillary Head Protrusion	brd9	HiC_scaffold_53	LL
Maxillary Head Protrusion	btg4	HiC_scaffold_53	LL

Maxillary Head Protrusion	c1orf232	HiC_scaffold_53	LL
Maxillary Head Protrusion	c1ra	HiC_scaffold_53	LL
Maxillary Head Protrusion	c3ar1	HiC_scaffold_53	LL
Maxillary Head Protrusion	c4	HiC_scaffold_53	LL
Maxillary Head Protrusion	c7orf31	HiC_scaffold_53	LL
Maxillary Head Protrusion	c8orf76	HiC_scaffold_53	LL
Maxillary Head Protrusion	c8orf88	HiC_scaffold_53	LL
Maxillary Head Protrusion	ca14	HiC_scaffold_53	LL
Maxillary Head Protrusion	cacng6	HiC_scaffold_53	LL
Maxillary Head Protrusion	cacng7	HiC_scaffold_53	LL
Maxillary Head Protrusion	cacng8	HiC_scaffold_53	LL
Maxillary Head Protrusion	carmil1	HiC_scaffold_53	LL
Maxillary Head Protrusion	casp2	HiC_scaffold_53	LL
Maxillary Head Protrusion	ccdc106	HiC_scaffold_53	LL
Maxillary Head Protrusion	ccr3	HiC_scaffold_53	LL
Maxillary Head Protrusion	ccr4	HiC_scaffold_53	LL
Maxillary Head Protrusion	ccr5	HiC_scaffold_53	LL
Maxillary Head Protrusion	cd22	HiC_scaffold_53	LL
Maxillary Head Protrusion	cd2ap	HiC_scaffold_53	LL
Maxillary Head Protrusion	cd33	HiC_scaffold_53	LL
Maxillary Head Protrusion	cd4	HiC_scaffold_53	LL
Maxillary Head Protrusion	cd40	HiC_scaffold_53	LL
Maxillary Head Protrusion	cd79a	HiC_scaffold_53	LL
Maxillary Head Protrusion	cdc42	HiC_scaffold_53	LL
Maxillary Head Protrusion	cdc42ep5	HiC_scaffold_53	LL
Maxillary Head Protrusion	cdca3	HiC_scaffold_53	LL
Maxillary Head Protrusion	cdh17	HiC_scaffold_53	LL
Maxillary Head Protrusion	ceacam1	HiC_scaffold_53	LL
Maxillary Head Protrusion	ceacam2	HiC_scaffold_53	LL
Maxillary Head Protrusion	ceacam5	HiC_scaffold_53	LL
Maxillary Head Protrusion	celf3	HiC_scaffold_53	LL
Maxillary Head Protrusion	cep72	HiC_scaffold_53	LL
Maxillary Head Protrusion	cers2	HiC_scaffold_53	LL
Maxillary Head Protrusion	cgn	HiC_scaffold_53	LL
Maxillary Head Protrusion	chrna7	HiC_scaffold_53	LL
Maxillary Head Protrusion	chrnb2	HiC_scaffold_53	LL
Maxillary Head Protrusion	ciart	HiC_scaffold_53	LL
Maxillary Head Protrusion	cic	HiC_scaffold_53	LL
Maxillary Head Protrusion	cited3	HiC_scaffold_53	LL
Maxillary Head Protrusion	cldn12	HiC_scaffold_53	LL
Maxillary Head Protrusion	clec3b	HiC_scaffold_53	LL

Maxillary Head Protrusion	clk2	HiC_scaffold_53	LL
Maxillary Head Protrusion	clptm1l	HiC_scaffold_53	LL
Maxillary Head Protrusion	clstn3	HiC_scaffold_53	LL
Maxillary Head Protrusion	cmc1	HiC_scaffold_53	LL
Maxillary Head Protrusion	cmlkr1	HiC_scaffold_53	LL
Maxillary Head Protrusion	cnfn	HiC_scaffold_53	LL
Maxillary Head Protrusion	cnot3	HiC_scaffold_53	LL
Maxillary Head Protrusion	cnp-1	HiC_scaffold_53	LL
Maxillary Head Protrusion	cnr2	HiC_scaffold_53	LL
Maxillary Head Protrusion	col14a1	HiC_scaffold_53	LL
Maxillary Head Protrusion	coq3	HiC_scaffold_53	LL
Maxillary Head Protrusion	cox6b1	HiC_scaffold_53	LL
Maxillary Head Protrusion	cpq	HiC_scaffold_53	LL
Maxillary Head Protrusion	cpvl	HiC_scaffold_53	LL
Maxillary Head Protrusion	crabp2	HiC_scaffold_53	LL
Maxillary Head Protrusion	creb5	HiC_scaffold_53	LL
Maxillary Head Protrusion	crot	HiC_scaffold_53	LL
Maxillary Head Protrusion	CP	HiC_scaffold_53	LL
Maxillary Head Protrusion	csmd3	HiC_scaffold_53	LL
Maxillary Head Protrusion	csnk2a1	HiC_scaffold_53	LL
Maxillary Head Protrusion	csnk2b	HiC_scaffold_53	LL
Maxillary Head Protrusion	cspg5	HiC_scaffold_53	LL
Maxillary Head Protrusion	cthrc1	HiC_scaffold_53	LL
Maxillary Head Protrusion	ctrl	HiC_scaffold_53	LL
Maxillary Head Protrusion	cxcr3	HiC_scaffold_53	LL
Maxillary Head Protrusion	cxcr3.2	HiC_scaffold_53	LL
Maxillary Head Protrusion	cxcr4-b	HiC_scaffold_53	LL
Maxillary Head Protrusion	cyp21a2	HiC_scaffold_53	LL
Maxillary Head Protrusion	cyp4b1	HiC_scaffold_53	LL
Maxillary Head Protrusion	cyth2	HiC_scaffold_53	LL
Maxillary Head Protrusion	cyth3	HiC_scaffold_53	LL
Maxillary Head Protrusion	d215	HiC_scaffold_53	LL
Maxillary Head Protrusion	dbi	HiC_scaffold_53	LL
Maxillary Head Protrusion	dcaf13	HiC_scaffold_53	LL
Maxillary Head Protrusion	dcbld1	HiC_scaffold_53	LL
Maxillary Head Protrusion	ddr1	HiC_scaffold_53	LL
Maxillary Head Protrusion	dedd2	HiC_scaffold_53	LL
Maxillary Head Protrusion	dennd3	HiC_scaffold_53	LL
Maxillary Head Protrusion	depdc1b	HiC_scaffold_53	LL
Maxillary Head Protrusion	deptor	HiC_scaffold_53	LL
Maxillary Head Protrusion	derl1	HiC_scaffold_53	LL

Maxillary Head Protrusion	dgat1	HiC_scaffold_53	LL
Maxillary Head Protrusion	dgkb	HiC_scaffold_53	LL
Maxillary Head Protrusion	dnah11	HiC_scaffold_53	LL
Maxillary Head Protrusion	dnali1	HiC_scaffold_53	LL
Maxillary Head Protrusion	dop1a	HiC_scaffold_53	LL
Maxillary Head Protrusion	dpy19l1	HiC_scaffold_53	LL
Maxillary Head Protrusion	dpys	HiC_scaffold_53	LL
Maxillary Head Protrusion	dscc1	HiC_scaffold_53	LL
Maxillary Head Protrusion	e2f3	HiC_scaffold_53	LL
Maxillary Head Protrusion	ebag9	HiC_scaffold_53	LL
Maxillary Head Protrusion	ecm1	HiC_scaffold_53	LL
Maxillary Head Protrusion	edn1	HiC_scaffold_53	LL
Maxillary Head Protrusion	efhb	HiC_scaffold_53	LL
Maxillary Head Protrusion	efna1	HiC_scaffold_53	LL
Maxillary Head Protrusion	efna3	HiC_scaffold_53	LL
Maxillary Head Protrusion	eif3e	HiC_scaffold_53	LL
Maxillary Head Protrusion	emc2	HiC_scaffold_53	LL
Maxillary Head Protrusion	emg1	HiC_scaffold_53	LL
Maxillary Head Protrusion	entpd3	HiC_scaffold_53	LL
Maxillary Head Protrusion	epb41	HiC_scaffold_53	LL
Maxillary Head Protrusion	ephb5	HiC_scaffold_53	LL
Maxillary Head Protrusion	epn1	HiC_scaffold_53	LL
Maxillary Head Protrusion	erf	HiC_scaffold_53	LL
Maxillary Head Protrusion	erp44	HiC_scaffold_53	LL
Maxillary Head Protrusion	esrp1	HiC_scaffold_53	LL
Maxillary Head Protrusion	etfb	HiC_scaffold_53	LL
Maxillary Head Protrusion	ethe1	HiC_scaffold_53	LL
Maxillary Head Protrusion	etv1	HiC_scaffold_53	LL
Maxillary Head Protrusion	eva1b	HiC_scaffold_53	LL
Maxillary Head Protrusion	fabp4	HiC_scaffold_53	LL
Maxillary Head Protrusion	fam110c	HiC_scaffold_53	LL
Maxillary Head Protrusion	fam131b	HiC_scaffold_53	LL
Maxillary Head Protrusion	fam189b	HiC_scaffold_53	LL
Maxillary Head Protrusion	fam83a	HiC_scaffold_53	LL
Maxillary Head Protrusion	fam8a1	HiC_scaffold_53	LL
Maxillary Head Protrusion	faxc	HiC_scaffold_53	LL
Maxillary Head Protrusion	fbxl4	HiC_scaffold_53	LL
Maxillary Head Protrusion	fbxw7	HiC_scaffold_53	LL
Maxillary Head Protrusion	fcgbp	HiC_scaffold_53	LL
Maxillary Head Protrusion	fdps	HiC_scaffold_53	LL
Maxillary Head Protrusion	fez2	HiC_scaffold_53	LL

Maxillary Head Protrusion	ffar2	HiC_scaffold_53	LL
Maxillary Head Protrusion	ffar3	HiC_scaffold_53	LL
Maxillary Head Protrusion	fhl3	HiC_scaffold_53	LL
Maxillary Head Protrusion	fhod3	HiC_scaffold_53	LL
Maxillary Head Protrusion	fkbp14	HiC_scaffold_53	LL
Maxillary Head Protrusion	flcn	HiC_scaffold_53	LL
Maxillary Head Protrusion	flot1	HiC_scaffold_53	LL
Maxillary Head Protrusion	foxj2	HiC_scaffold_53	LL
Maxillary Head Protrusion	foxo3	HiC_scaffold_53	LL
Maxillary Head Protrusion	frrs1l	HiC_scaffold_53	LL
Maxillary Head Protrusion	fsbp	HiC_scaffold_53	LL
Maxillary Head Protrusion	fxyd1	HiC_scaffold_53	LL
Maxillary Head Protrusion	fzd6	HiC_scaffold_53	LL
Maxillary Head Protrusion	galnt1	HiC_scaffold_53	LL
Maxillary Head Protrusion	galr1	HiC_scaffold_53	LL
Maxillary Head Protrusion	gapdh	HiC_scaffold_53	LL
Maxillary Head Protrusion	gba	HiC_scaffold_53	LL
Maxillary Head Protrusion	gdf6a	HiC_scaffold_53	LL
Maxillary Head Protrusion	gem	HiC_scaffold_53	LL
Maxillary Head Protrusion	glcci1	HiC_scaffold_53	LL
Maxillary Head Protrusion	glipr2	HiC_scaffold_53	LL
Maxillary Head Protrusion	gmeb1	HiC_scaffold_53	LL
Maxillary Head Protrusion	gnb3	HiC_scaffold_53	LL
Maxillary Head Protrusion	gnl2	HiC_scaffold_53	LL
Maxillary Head Protrusion	gpatch3	HiC_scaffold_53	LL
Maxillary Head Protrusion	gpn2	HiC_scaffold_53	LL
Maxillary Head Protrusion	gpr20	HiC_scaffold_53	LL
Maxillary Head Protrusion	gpr42	HiC_scaffold_53	LL
Maxillary Head Protrusion	grb10	HiC_scaffold_53	LL
Maxillary Head Protrusion	grik3	HiC_scaffold_53	LL
Maxillary Head Protrusion	grik5	HiC_scaffold_53	LL
Maxillary Head Protrusion	grina	HiC_scaffold_53	LL
Maxillary Head Protrusion	grwd1	HiC_scaffold_53	LL
Maxillary Head Protrusion	gsdme	HiC_scaffold_53	LL
Maxillary Head Protrusion	gsg1l	HiC_scaffold_53	LL
Maxillary Head Protrusion	gsk3a	HiC_scaffold_53	LL
Maxillary Head Protrusion	gstk1	HiC_scaffold_53	LL
Maxillary Head Protrusion	gtpbp10	HiC_scaffold_53	LL
Maxillary Head Protrusion	h2-eb1	HiC_scaffold_53	LL
Maxillary Head Protrusion	hacl1	HiC_scaffold_53	LL
Maxillary Head Protrusion	hamp	HiC_scaffold_53	LL

Maxillary Head Protrusion	hamp1	HiC_scaffold_53	LL
Maxillary Head Protrusion	has1	HiC_scaffold_53	LL
Maxillary Head Protrusion	has2	HiC_scaffold_53	LL
Maxillary Head Protrusion	hcn4	HiC_scaffold_53	LL
Maxillary Head Protrusion	hdac9b	HiC_scaffold_53	LL
Maxillary Head Protrusion	hepacam2	HiC_scaffold_53	LL
Maxillary Head Protrusion	herpud2	HiC_scaffold_53	LL
Maxillary Head Protrusion	hey1	HiC_scaffold_53	LL
Maxillary Head Protrusion	hibadh	HiC_scaffold_53	LL
Maxillary Head Protrusion	hivep3	HiC_scaffold_53	LL
Maxillary Head Protrusion	hlf	HiC_scaffold_53	LL
Maxillary Head Protrusion	hoxa10b	HiC_scaffold_53	LL
Maxillary Head Protrusion	hoxa11b	HiC_scaffold_53	LL
Maxillary Head Protrusion	hoxa9b	HiC_scaffold_53	LL
Maxillary Head Protrusion	hspa8	HiC_scaffold_53	LL
Maxillary Head Protrusion	hspb6	HiC_scaffold_53	LL
Maxillary Head Protrusion	iffo1	HiC_scaffold_53	LL
Maxillary Head Protrusion	iglon5	HiC_scaffold_53	LL
Maxillary Head Protrusion	il16	HiC_scaffold_53	LL
Maxillary Head Protrusion	il20ra	HiC_scaffold_53	LL
Maxillary Head Protrusion	il6r	HiC_scaffold_53	LL
Maxillary Head Protrusion	ing4	HiC_scaffold_53	LL
Maxillary Head Protrusion	ino80c	HiC_scaffold_53	LL
Maxillary Head Protrusion	invs	HiC_scaffold_53	LL
Maxillary Head Protrusion	iqcg	HiC_scaffold_53	LL
Maxillary Head Protrusion	irgc	HiC_scaffold_53	LL
Maxillary Head Protrusion	irx2	HiC_scaffold_53	LL
Maxillary Head Protrusion	irx4	HiC_scaffold_53	LL
Maxillary Head Protrusion	isoc2	HiC_scaffold_53	LL
Maxillary Head Protrusion	ispd	HiC_scaffold_53	LL
Maxillary Head Protrusion	itga10	HiC_scaffold_53	LL
Maxillary Head Protrusion	jazf1	HiC_scaffold_53	LL
Maxillary Head Protrusion	josd2	HiC_scaffold_53	LL
Maxillary Head Protrusion	kcnj2	HiC_scaffold_53	LL
Maxillary Head Protrusion	kcnk5	HiC_scaffold_53	LL
Maxillary Head Protrusion	kdf1	HiC_scaffold_53	LL
Maxillary Head Protrusion	khdc4	HiC_scaffold_53	LL
Maxillary Head Protrusion	kirrel1	HiC_scaffold_53	LL
Maxillary Head Protrusion	klf10	HiC_scaffold_53	LL
Maxillary Head Protrusion	krtcap2	HiC_scaffold_53	LL
Maxillary Head Protrusion	lag3	HiC_scaffold_53	LL

Maxillary Head Protrusion	laptm4b	HiC_scaffold_53	LL
Maxillary Head Protrusion	lars2	HiC_scaffold_53	LL
Maxillary Head Protrusion	lenep	HiC_scaffold_53	LL
Maxillary Head Protrusion	leng1	HiC_scaffold_53	LL
Maxillary Head Protrusion	leng8	HiC_scaffold_53	LL
Maxillary Head Protrusion	leng9	HiC_scaffold_53	LL
Maxillary Head Protrusion	lim2	HiC_scaffold_53	LL
Maxillary Head Protrusion	limd1	HiC_scaffold_53	LL
Maxillary Head Protrusion	lin37	HiC_scaffold_53	LL
Maxillary Head Protrusion	lipe	HiC_scaffold_53	LL
Maxillary Head Protrusion	lmtk3	HiC_scaffold_53	LL
Maxillary Head Protrusion	lpcat1	HiC_scaffold_53	LL
Maxillary Head Protrusion	lsr	HiC_scaffold_53	LL
Maxillary Head Protrusion	m6pr	HiC_scaffold_53	LL
Maxillary Head Protrusion	macc1	HiC_scaffold_53	LL
Maxillary Head Protrusion	mag	HiC_scaffold_53	LL
Maxillary Head Protrusion	maip1	HiC_scaffold_53	LL
Maxillary Head Protrusion	mal2	HiC_scaffold_53	LL
Maxillary Head Protrusion	malsu1	HiC_scaffold_53	LL
Maxillary Head Protrusion	mamu-dra	HiC_scaffold_53	LL
Maxillary Head Protrusion	man1c1	HiC_scaffold_53	LL
Maxillary Head Protrusion	maneal	HiC_scaffold_53	LL
Maxillary Head Protrusion	map7d1	HiC_scaffold_53	LL
Maxillary Head Protrusion	matn4	HiC_scaffold_53	LL
Maxillary Head Protrusion	mboat1	HiC_scaffold_53	LL
Maxillary Head Protrusion	mboat7	HiC_scaffold_53	LL
Maxillary Head Protrusion	mbp	HiC_scaffold_53	LL
Maxillary Head Protrusion	mcam	HiC_scaffold_53	LL
Maxillary Head Protrusion	mdc1	HiC_scaffold_53	LL
Maxillary Head Protrusion	me1	HiC_scaffold_53	LL
Maxillary Head Protrusion	mecr	HiC_scaffold_53	LL
Maxillary Head Protrusion	med18	HiC_scaffold_53	LL
Maxillary Head Protrusion	megf8	HiC_scaffold_53	LL
Maxillary Head Protrusion	meox2	HiC_scaffold_53	LL
Maxillary Head Protrusion	mep1b	HiC_scaffold_53	LL
Maxillary Head Protrusion	mindy3	HiC_scaffold_53	LL
Maxillary Head Protrusion	mios	HiC_scaffold_53	LL
Maxillary Head Protrusion	mlf2	HiC_scaffold_53	LL
Maxillary Head Protrusion	mms22l	HiC_scaffold_53	LL
Maxillary Head Protrusion	mpp6	HiC_scaffold_53	LL
Maxillary Head Protrusion	mpra	HiC_scaffold_53	LL

Maxillary Head Protrusion	mpv17l	HiC_scaffold_53	LL
Maxillary Head Protrusion	mrc1	HiC_scaffold_53	LL
Maxillary Head Protrusion	mrpl13	HiC_scaffold_53	LL
Maxillary Head Protrusion	mrpl17	HiC_scaffold_53	LL
Maxillary Head Protrusion	mrpl51	HiC_scaffold_53	LL
Maxillary Head Protrusion	mrps15	HiC_scaffold_53	LL
Maxillary Head Protrusion	mrs2	HiC_scaffold_53	LL
Maxillary Head Protrusion	mrtfb	HiC_scaffold_53	LL
Maxillary Head Protrusion	msh5	HiC_scaffold_53	LL
Maxillary Head Protrusion	mtdh	HiC_scaffold_53	LL
Maxillary Head Protrusion	mtf1	HiC_scaffold_53	LL
Maxillary Head Protrusion	mtss1	HiC_scaffold_53	LL
Maxillary Head Protrusion	mycbp	HiC_scaffold_53	LL
Maxillary Head Protrusion	myh10	HiC_scaffold_53	LL
Maxillary Head Protrusion	mypop	HiC_scaffold_53	LL
Maxillary Head Protrusion	nacad	HiC_scaffold_53	LL
Maxillary Head Protrusion	nat14	HiC_scaffold_53	LL
Maxillary Head Protrusion	ncapd2	HiC_scaffold_53	LL
Maxillary Head Protrusion	ndufa3	HiC_scaffold_53	LL
Maxillary Head Protrusion	ndufv1	HiC_scaffold_53	LL
Maxillary Head Protrusion	necap1	HiC_scaffold_53	LL
Maxillary Head Protrusion	nectin1	HiC_scaffold_53	LL
Maxillary Head Protrusion	nectin2	HiC_scaffold_53	LL
Maxillary Head Protrusion	nek10	HiC_scaffold_53	LL
Maxillary Head Protrusion	nfatc1	HiC_scaffold_53	LL
Maxillary Head Protrusion	ngfr	HiC_scaffold_53	LL
Maxillary Head Protrusion	nhlrc1	HiC_scaffold_53	LL
Maxillary Head Protrusion	nkd2l	HiC_scaffold_53	LL
Maxillary Head Protrusion	nmt2	HiC_scaffold_53	LL
Maxillary Head Protrusion	nop2	HiC_scaffold_53	LL
Maxillary Head Protrusion	notch1	HiC_scaffold_53	LL
Maxillary Head Protrusion	nov	HiC_scaffold_53	LL
Maxillary Head Protrusion	nphs1	HiC_scaffold_53	LL
Maxillary Head Protrusion	nptx2	HiC_scaffold_53	LL
Maxillary Head Protrusion	nr0b2	HiC_scaffold_53	LL
Maxillary Head Protrusion	nr1d2	HiC_scaffold_53	LL
Maxillary Head Protrusion	nr4a3	HiC_scaffold_53	LL
Maxillary Head Protrusion	nrsn1	HiC_scaffold_53	LL
Maxillary Head Protrusion	nxph1	HiC_scaffold_53	LL
Maxillary Head Protrusion	oprd1	HiC_scaffold_53	LL
Maxillary Head Protrusion	osbpl3	HiC_scaffold_53	LL

Maxillary Head Protrusion	oscp1	HiC_scaffold_53	LL
Maxillary Head Protrusion	osgin2	HiC_scaffold_53	LL
Maxillary Head Protrusion	oxr1	HiC_scaffold_53	LL
Maxillary Head Protrusion	p3h3	HiC_scaffold_53	LL
Maxillary Head Protrusion	pafah1b3	HiC_scaffold_53	LL
Maxillary Head Protrusion	pde11a	HiC_scaffold_53	LL
Maxillary Head Protrusion	pdp1	HiC_scaffold_53	LL
Maxillary Head Protrusion	pex5	HiC_scaffold_53	LL
Maxillary Head Protrusion	phactr4b	HiC_scaffold_53	LL
Maxillary Head Protrusion	phc1	HiC_scaffold_53	LL
Maxillary Head Protrusion	phldb3	HiC_scaffold_53	LL
Maxillary Head Protrusion	pigv	HiC_scaffold_53	LL
Maxillary Head Protrusion	pim2	HiC_scaffold_53	LL
Maxillary Head Protrusion	pip5k1a	HiC_scaffold_53	LL
Maxillary Head Protrusion	pitpnc1	HiC_scaffold_53	LL
Maxillary Head Protrusion	plcl2	HiC_scaffold_53	LL
Maxillary Head Protrusion	plec	HiC_scaffold_53	LL
Maxillary Head Protrusion	plekhg4b	HiC_scaffold_53	LL
Maxillary Head Protrusion	plekhg6	HiC_scaffold_53	LL
Maxillary Head Protrusion	pnisr	HiC_scaffold_53	LL
Maxillary Head Protrusion	pon2	HiC_scaffold_53	LL
Maxillary Head Protrusion	pop1	HiC_scaffold_53	LL
Maxillary Head Protrusion	pou2f2	HiC_scaffold_53	LL
Maxillary Head Protrusion	pou3f1	HiC_scaffold_53	LL
Maxillary Head Protrusion	pou3f2	HiC_scaffold_53	LL
Maxillary Head Protrusion	ppp1r8	HiC_scaffold_53	LL
Maxillary Head Protrusion	prdm9	HiC_scaffold_53	LL
Maxillary Head Protrusion	prkca	HiC_scaffold_53	LL
Maxillary Head Protrusion	proser3	HiC_scaffold_53	LL
Maxillary Head Protrusion	prpf3	HiC_scaffold_53	LL
Maxillary Head Protrusion	prpf31	HiC_scaffold_53	LL
Maxillary Head Protrusion	prss35	HiC_scaffold_53	LL
Maxillary Head Protrusion	psenen	HiC_scaffold_53	LL
Maxillary Head Protrusion	psmd4	HiC_scaffold_53	LL
Maxillary Head Protrusion	ptdss1	HiC_scaffold_53	LL
Maxillary Head Protrusion	ptk2	HiC_scaffold_53	LL
Maxillary Head Protrusion	ptp4a3	HiC_scaffold_53	LL
Maxillary Head Protrusion	ptpn3	HiC_scaffold_53	LL
Maxillary Head Protrusion	ptpn6	HiC_scaffold_53	LL
Maxillary Head Protrusion	ptpru	HiC_scaffold_53	LL
Maxillary Head Protrusion	ptx2	HiC_scaffold_53	LL

Maxillary Head Protrusion	pxn1	HiC_scaffold_53	LL
Maxillary Head Protrusion	rab5a	HiC_scaffold_53	LL
Maxillary Head Protrusion	rabac1	HiC_scaffold_53	LL
Maxillary Head Protrusion	racgap1	HiC_scaffold_53	LL
Maxillary Head Protrusion	rad54b	HiC_scaffold_53	LL
Maxillary Head Protrusion	rapgef5	HiC_scaffold_53	LL
Maxillary Head Protrusion	rarb	HiC_scaffold_53	LL
Maxillary Head Protrusion	rasip1	HiC_scaffold_53	LL
Maxillary Head Protrusion	rbfox1l	HiC_scaffold_53	LL
Maxillary Head Protrusion	rbm12b	HiC_scaffold_53	LL
Maxillary Head Protrusion	rbm24	HiC_scaffold_53	LL
Maxillary Head Protrusion	rbp1	HiC_scaffold_53	LL
Maxillary Head Protrusion	rcc1	HiC_scaffold_53	LL
Maxillary Head Protrusion	rec8	HiC_scaffold_53	LL
Maxillary Head Protrusion	rft2	HiC_scaffold_53	LL
Maxillary Head Protrusion	rhbdl2	HiC_scaffold_53	LL
Maxillary Head Protrusion	rims2	HiC_scaffold_53	LL
Maxillary Head Protrusion	rnf144b	HiC_scaffold_53	LL
Maxillary Head Protrusion	rnf41	HiC_scaffold_53	LL
Maxillary Head Protrusion	rpa2	HiC_scaffold_53	LL
Maxillary Head Protrusion	rpp38	HiC_scaffold_53	LL
Maxillary Head Protrusion	rps19	HiC_scaffold_53	LL
Maxillary Head Protrusion	rps27l	HiC_scaffold_53	LL
Maxillary Head Protrusion	rps9	HiC_scaffold_53	LL
Maxillary Head Protrusion	rragc	HiC_scaffold_53	LL
Maxillary Head Protrusion	rsph4a	HiC_scaffold_53	LL
Maxillary Head Protrusion	rspo1	HiC_scaffold_53	LL
Maxillary Head Protrusion	rt1-b	HiC_scaffold_53	LL
Maxillary Head Protrusion	rundc3b	HiC_scaffold_53	LL
Maxillary Head Protrusion	rusc1	HiC_scaffold_53	LL
Maxillary Head Protrusion	rxrba	HiC_scaffold_53	LL
Maxillary Head Protrusion	s100a1	HiC_scaffold_53	LL
Maxillary Head Protrusion	s100a16	HiC_scaffold_53	LL
Maxillary Head Protrusion	s100a6	HiC_scaffold_53	LL
Maxillary Head Protrusion	s100g	HiC_scaffold_53	LL
Maxillary Head Protrusion	sall3	HiC_scaffold_53	LL
Maxillary Head Protrusion	sbk2	HiC_scaffold_53	LL
Maxillary Head Protrusion	scgn	HiC_scaffold_53	LL
Maxillary Head Protrusion	scrt2	HiC_scaffold_53	LL
Maxillary Head Protrusion	sdc2-b	HiC_scaffold_53	LL
Maxillary Head Protrusion	serinc1	HiC_scaffold_53	LL

Maxillary Head Protrusion	setdb1b	HiC_scaffold_53	LL
Maxillary Head Protrusion	shc1	HiC_scaffold_53	LL
Maxillary Head Protrusion	she	HiC_scaffold_53	LL
Maxillary Head Protrusion	shisa7	HiC_scaffold_53	LL
Maxillary Head Protrusion	siglec1	HiC_scaffold_53	LL
Maxillary Head Protrusion	siglec14	HiC_scaffold_53	LL
Maxillary Head Protrusion	siglec5	HiC_scaffold_53	LL
Maxillary Head Protrusion	slc25a32	HiC_scaffold_53	LL
Maxillary Head Protrusion	slc25a40	HiC_scaffold_53	LL
Maxillary Head Protrusion	slc2a3	HiC_scaffold_53	LL
Maxillary Head Protrusion	slc40a1	HiC_scaffold_53	LL
Maxillary Head Protrusion	slc50a1	HiC_scaffold_53	LL
Maxillary Head Protrusion	slc6a3	HiC_scaffold_53	LL
Maxillary Head Protrusion	smarcc1	HiC_scaffold_53	LL
Maxillary Head Protrusion	smg9	HiC_scaffold_53	LL
Maxillary Head Protrusion	smp	HiC_scaffold_53	LL
Maxillary Head Protrusion	smpd5	HiC_scaffold_53	LL
Maxillary Head Protrusion	snip1	HiC_scaffold_53	LL
Maxillary Head Protrusion	snx27	HiC_scaffold_53	LL
Maxillary Head Protrusion	sostdc1	HiC_scaffold_53	LL
Maxillary Head Protrusion	sox11	HiC_scaffold_53	LL
Maxillary Head Protrusion	sp8b	HiC_scaffold_53	LL
Maxillary Head Protrusion	spaca6	HiC_scaffold_53	LL
Maxillary Head Protrusion	sphk2	HiC_scaffold_53	LL
Maxillary Head Protrusion	spire1	HiC_scaffold_53	LL
Maxillary Head Protrusion	spsb1	HiC_scaffold_53	LL
Maxillary Head Protrusion	sqle	HiC_scaffold_53	LL
Maxillary Head Protrusion	st14	HiC_scaffold_53	LL
Maxillary Head Protrusion	steap4	HiC_scaffold_53	LL
Maxillary Head Protrusion	stk40	HiC_scaffold_53	LL
Maxillary Head Protrusion	stmn2	HiC_scaffold_53	LL
Maxillary Head Protrusion	sybu	HiC_scaffold_53	LL
Maxillary Head Protrusion	taf12	HiC_scaffold_53	LL
Maxillary Head Protrusion	tap1	HiC_scaffold_53	LL
Maxillary Head Protrusion	tarsl2	HiC_scaffold_53	LL
Maxillary Head Protrusion	tbc1d15	HiC_scaffold_53	LL
Maxillary Head Protrusion	tbc1d31	HiC_scaffold_53	LL
Maxillary Head Protrusion	tbrg4	HiC_scaffold_53	LL
Maxillary Head Protrusion	tcea3	HiC_scaffold_53	LL
Maxillary Head Protrusion	tent4a	HiC_scaffold_53	LL
Maxillary Head Protrusion	tent5a	HiC_scaffold_53	LL

Maxillary Head Protrusion	tex10	HiC_scaffold_53	LL
Maxillary Head Protrusion	tfpt	HiC_scaffold_53	LL
Maxillary Head Protrusion	them4	HiC_scaffold_53	LL
Maxillary Head Protrusion	themis2	HiC_scaffold_53	LL
Maxillary Head Protrusion	thsd4	HiC_scaffold_53	LL
Maxillary Head Protrusion	tlr13	HiC_scaffold_53	LL
Maxillary Head Protrusion	tmc7	HiC_scaffold_53	LL
Maxillary Head Protrusion	tmem106b	HiC_scaffold_53	LL
Maxillary Head Protrusion	tmem107	HiC_scaffold_53	LL
Maxillary Head Protrusion	tmem158	HiC_scaffold_53	LL
Maxillary Head Protrusion	tmem222	HiC_scaffold_53	LL
Maxillary Head Protrusion	tmem238	HiC_scaffold_53	LL
Maxillary Head Protrusion	tmem244	HiC_scaffold_53	LL
Maxillary Head Protrusion	tmem245	HiC_scaffold_53	LL
Maxillary Head Protrusion	tmem65	HiC_scaffold_53	LL
Maxillary Head Protrusion	tmem67	HiC_scaffold_53	LL
Maxillary Head Protrusion	tmem74	HiC_scaffold_53	LL
Maxillary Head Protrusion	tmprss6	HiC_scaffold_53	LL
Maxillary Head Protrusion	tnc	HiC_scaffold_53	LL
Maxillary Head Protrusion	tnfrsf11b	HiC_scaffold_53	LL
Maxillary Head Protrusion	tnfrsf1a	HiC_scaffold_53	LL
Maxillary Head Protrusion	tnfrsf6b	HiC_scaffold_53	LL
Maxillary Head Protrusion	tpbg	HiC_scaffold_53	LL
Maxillary Head Protrusion	tpi1b	HiC_scaffold_53	LL
Maxillary Head Protrusion	tppp	HiC_scaffold_53	LL
Maxillary Head Protrusion	trhr	HiC_scaffold_53	LL
Maxillary Head Protrusion	trim16	HiC_scaffold_53	LL
Maxillary Head Protrusion	trim25	HiC_scaffold_53	LL
Maxillary Head Protrusion	trim46	HiC_scaffold_53	LL
Maxillary Head Protrusion	trio	HiC_scaffold_53	LL
Maxillary Head Protrusion	trip13	HiC_scaffold_53	LL
Maxillary Head Protrusion	trp3	HiC_scaffold_53	LL
Maxillary Head Protrusion	trpv5	HiC_scaffold_53	LL
Maxillary Head Protrusion	tshz1	HiC_scaffold_53	LL
Maxillary Head Protrusion	tstd3	HiC_scaffold_53	LL
Maxillary Head Protrusion	ttk	HiC_scaffold_53	LL
Maxillary Head Protrusion	ttyh1	HiC_scaffold_53	LL
Maxillary Head Protrusion	tuft1	HiC_scaffold_53	LL
Maxillary Head Protrusion	twist1	HiC_scaffold_53	LL
Maxillary Head Protrusion	tyrobp	HiC_scaffold_53	LL
Maxillary Head Protrusion	ube2s	HiC_scaffold_53	LL

Maxillary Head Protrusion	ubxn11	HiC_scaffold_53	LL
Maxillary Head Protrusion	upp1	HiC_scaffold_53	LL
Maxillary Head Protrusion	usf2	HiC_scaffold_53	LL
Maxillary Head Protrusion	utp11	HiC_scaffold_53	LL
Maxillary Head Protrusion	uts2r	HiC_scaffold_53	LL
Maxillary Head Protrusion	vamp1	HiC_scaffold_53	LL
Maxillary Head Protrusion	vars	HiC_scaffold_53	LL
Maxillary Head Protrusion	vim	HiC_scaffold_53	LL
Maxillary Head Protrusion	virma	HiC_scaffold_53	LL
Maxillary Head Protrusion	vmo1	HiC_scaffold_53	LL
Maxillary Head Protrusion	vsig10l	HiC_scaffold_53	LL
Maxillary Head Protrusion	vwde	HiC_scaffold_53	LL
Maxillary Head Protrusion	wdtc1	HiC_scaffold_53	LL
Maxillary Head Protrusion	wnt4	HiC_scaffold_53	LL
Maxillary Head Protrusion	xrcc1	HiC_scaffold_53	LL
Maxillary Head Protrusion	yqjl	HiC_scaffold_53	LL
Maxillary Head Protrusion	yrdc	HiC_scaffold_53	LL
Maxillary Head Protrusion	zadh2	HiC_scaffold_53	LL
Maxillary Head Protrusion	zbtb7b	HiC_scaffold_53	LL
Maxillary Head Protrusion	zc3h12a	HiC_scaffold_53	LL
Maxillary Head Protrusion	zdhhc11	HiC_scaffold_53	LL
Maxillary Head Protrusion	zdhhc18	HiC_scaffold_53	LL
Maxillary Head Protrusion	zhx2	HiC_scaffold_53	LL
Maxillary Head Protrusion	znf208	HiC_scaffold_53	LL
Maxillary Head Protrusion	znf226	HiC_scaffold_53	LL
Maxillary Head Protrusion	znf236	HiC_scaffold_53	LL
Maxillary Head Protrusion	znf282	HiC_scaffold_53	LL
Maxillary Head Protrusion	znf385d	HiC_scaffold_53	LL
Maxillary Head Protrusion	znf436	HiC_scaffold_53	LL
Maxillary Head Protrusion	znf516	HiC_scaffold_53	LL
Maxillary Head Protrusion	znf524	HiC_scaffold_53	LL
Maxillary Head Protrusion	znf574	HiC_scaffold_53	LL
Maxillary Head Protrusion	znf585b	HiC_scaffold_53	LL
Maxillary Head Protrusion	znf628	HiC_scaffold_53	LL
Maxillary Head Protrusion	znf687a	HiC_scaffold_53	LL
Maxillary Head Protrusion	znf737	HiC_scaffold_53	LL
Maxillary Head Protrusion	znf79	HiC_scaffold_53	LL
Maxillary Head Protrusion	znf865	HiC_scaffold_53	LL

Supplemental figures
Figure S1.

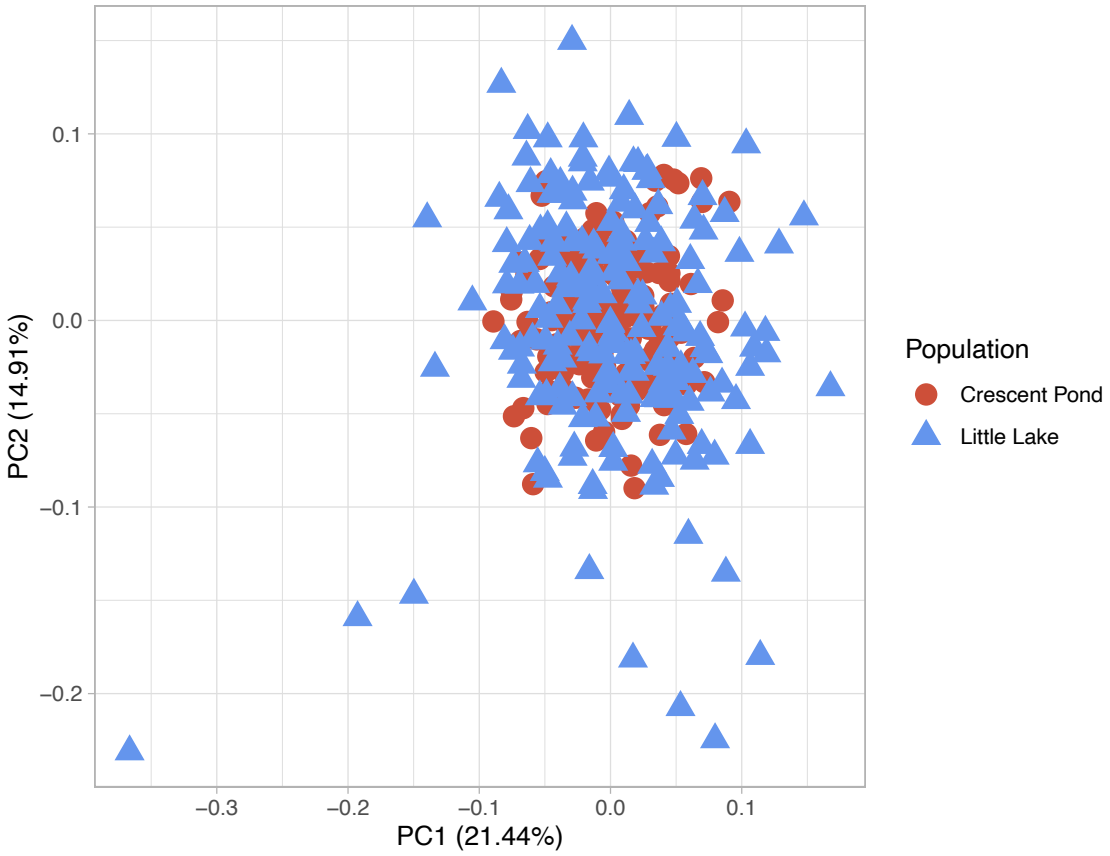

Figure S1 Principal component analysis depicting phenotypic variation across 28 size corrected skeletal traits for Crescent Pond F2 hybrids (red circles) and Little Lake F2 hybrids (blue triangles). Skeletal traits were calculated as the mean from two lateral photographs from each individual. There was no significant difference between Crescent Pond and Little Lake individuals (MANOVA, df = 28, approximate F-value= 0.34, *P* = 1).

Figure S2.

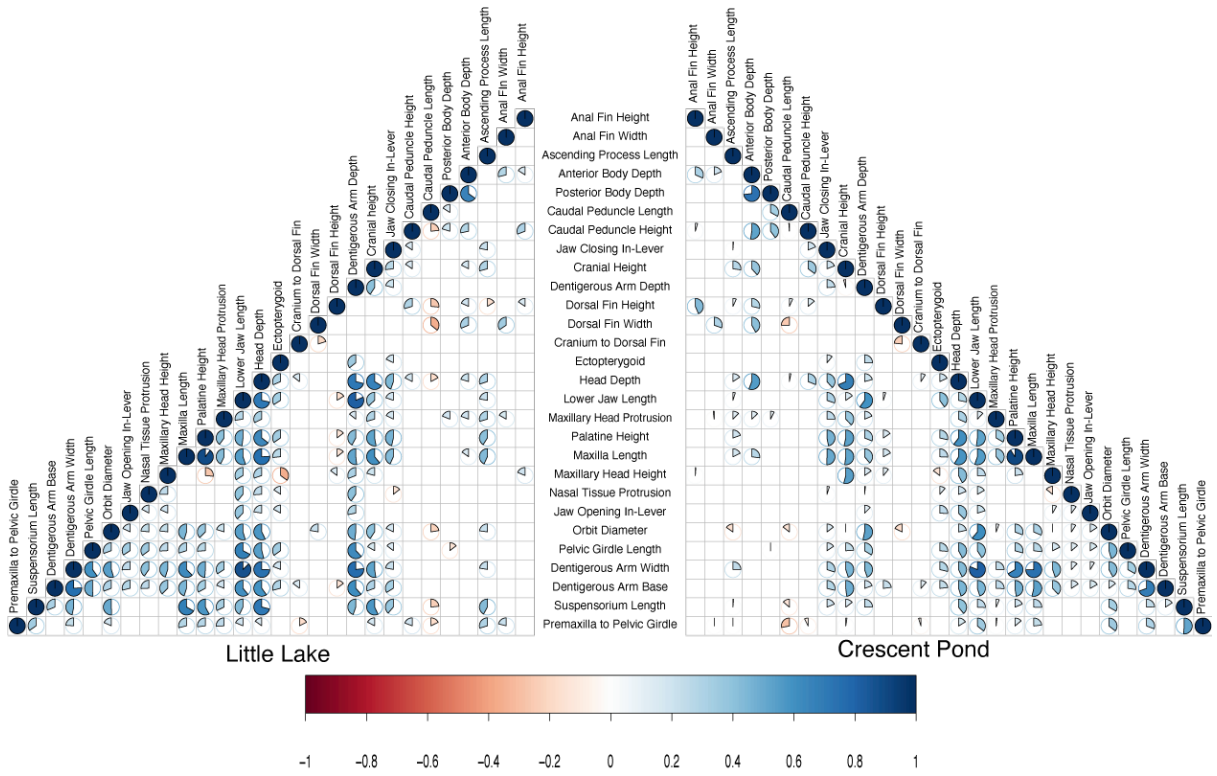

Supplemental Figure S2 Correlation matrices depicting the relationship between phenotypic traits in Little Lake and Crescent Pond. Visualized pie charts represent relationships that are significant at the $P < 0.05$ level. Red pie charts represent negative relationships and blue pie charts represent positive relationships.

Dissertation Conclusion

My dissertation work explores the multivariate nature of evolutionary novelty using the pupfish system and suggests that shifts in behavioral phenotypes are necessary for occupying novel ecological niches. The unique integration of behavioral, morphological, and genomic data in my work has revealed a new pattern— that for some ecological niches, shifts in behavioral phenotypes are sufficient for a successful transition, but for other potentially rarer niches, shifts across multiple phenotypic axes are crucial. Additionally, this work provides empirical data to further inform hypotheses and predictions regarding the origins of evolutionary novelty.

The ecological opportunity hypothesis predicts that novel phenotypes should be adaptive for performance in an organism's ecological niche. In line with this hypothesis, in Chapter One I showed a relationship between increased aggression and specialist niches, which may suggest that increased aggression is needed for consuming snails and scales. It should be noted, however, that this chapter did not directly measure whether increased aggression improves an individual's feeding performance and future work is needed to directly assess whether increased aggression is adaptive for snail- and scale-eating. Chapter Two provides a more direct line of support for the ecological opportunity hypothesis by linking novel traits to feeding performance. Scale-eating pupfish exhibit novel morphologies, such as their extremely large jaws, and novel behaviors, such as their unique feeding kinematics, and this research directly ties these novelties to increased bite performance.

The third chapter of my dissertation, however, shows that new ecological opportunity is not always sufficient for explaining the evolution of novelty. Instead, the novel nasal protrusion— which is unique to the snail-eating pupfish species—does not provide an additional advantage for consuming more or larger snails. Furthermore, intermediate snail-eating hybrids and even generalist pupfish species from San Salvador Island consumed statistically similar numbers of snails. In the context of the ecological opportunity hypothesis, these results suggest that novelties need not be directly tied to performance in an organism's ecological niche. Together, these chapters suggest that shifts in behavioral phenotypes may be sufficient for moving into new ecological niches, that morphological novelty may refine performance in said niche, or that some examples of novelty may be unrelated to an organism's ecological niche.

Alternatively, other hypotheses focus on the underlying developmental and genetic process that may produce novelty, predicting that only new mechanisms can produce novel phenotypes. My dissertation provides mixed support for this hypothesis.
In chapter one I found that 30% of differentially expressed genes in aggression related pathways were shared between snail-eaters and scale-eaters, suggesting that a single genetic mechanism could be responsible for several instances of novelty. On the other hand, scale-eaters showed additional and unique differential expression patterns that were not observed in the snail-eater suggesting that perhaps these additional and unique differential expression patterns are what is responsible for scale-eating novelty. Similarly, chapter four shows that many of the genomic regions associated with

adaptive phenotypes for both snail- and scale-eating are frequently reused to produce variation in several different traits. This may suggest that a single genomic region can contribute to several phenotypic novelties. On the other hand, the nature of this this QTL study required regions of interested to be alternatively fixed between parental populations (i.e., snail-eaters and scale-eaters) meaning that this data may be better suited to comparing the effects of unique alleles instead of unique genes or genomic regions.

While the allelic differences in this study are unique to either snail- or scale-eaters in our QTL mapping population, many of these alleles exist in pupfish populations outside of San Salvador Island. In fact, genomic regions associated with adaptive phenotypes for snail- and scale-eating contained more introgressed single nucleotide polymorphisms than expected by chance indicating that introgression from other pupfish populations may have facilitated the evolution of novelty on San Salvador Island. Ultimately, results from my dissertation research highlight that predictions about the genetic mechanisms that produce novelty may be highly dependent on the biological level being examined.

Finally, hypotheses considering evolutionary novelty from the viewpoint of movement across a fitness landscape predict that novel peaks are far from the ancestral peak and that there must be a steep fitness valley separating the two. However, my dissertation research shows that these predictions may be dependent on the degree of novelty being examined. For example, scale-eating hybrids and non-scale-eating pupfish species exhibited low bite performance, implying that they would, likely fall into the predicted fitness valley between peaks. This pattern, however, was not present for the snail-feeding niche. Instead, snail-eating hybrids and even some generalist pupfish populations were able to easily consume snails. This may suggest that the snail-eater fitness peak is close to the ancestral peak, as hybrids and generalists with ongoing gene flow with snail-eaters are able to avoid the predicted fitness valley. Theory also predicts that jumping between fitness peaks, especially if they are quite distant are likely to involve few large effect loci, however, results from chapter four show that genomic regions associated with both snail-eating and scale-eating phenotypes have small or moderate effects. Results from this thesis suggest that novelty does not necessarily require large movements across the fitness valley.

In conclusion, my chapters highlight the need to examine evolutionary novelty across many biological levels including behavior, morphology, and genomics. The data generated from this research suggests that evolutionary novelty is multivariate, yet current hypotheses only consider variation along a single axis, limiting our ability to accurately predict the processes that produce novelty or the processes that lead to the success of evolutionary novelty. Future research into the complex relationships between biological levels may provide this necessary insight and ultimately improve our understanding of diversification.

References

Alachiotis, N., A. Stamatakis, and P. Pavlidis. 2012. OmegaPlus: A scalable tool for rapid detection of selective sweeps in whole-genome datasets. Bioinformatics 28:2274–2275. Oxford Academic.

Albert, A. Y. K., S. Sawaya, T. H. Vines, A. K. Knecht, C. T. Miller, B. R. Summers, S. Balabhadra, D. M. Kingsley, and D. Schluter. 2008. The genetics of adaptive shape shift in stickleback: pleiotropy and effect size. Evolution 62:76–85.

Andersson, M. 1994. Sexual Selection. Princeton University Press.

Araújo, M. S., P. R. Guimarães, R. Svanbäck, A. Pinheiro, P. Guuimarães, S. F. Dos Reis, and D. I. Bolnick. 2008. Network analysis reveals contrasting effects of intraspecific competition on individual vs. population diets. Ecology 89:1981–1993.

Arias-Rodriguez, L., M. Tobler, M. Palacios, F. J. García de León, D. Bierbach, M. Mateos, I. Mitrofanov, M. Plath, and L. J. Chapman. 2011. Evolution in extreme environments: replicated phenotypic differentiation in livebearing fish inhabiting sulfidic springs. Evolution (N. Y). 65:2213–2228.

Arnold, M. L. 1992. Natural Hybridization as an Evolutionary Process. Annu. Rev. Ecol. Syst. 23:237–261.

Arnold, S. J. 1983. Morphology, Performance and Fitness. Am. Zool. 23:347–361.

Arnold, S. J. 2003. Performance Surfaces and Adaptive Landscapes. Integr. Comp. Biol. 43:367–375.

Arnott, G., E. Beattie, and R. W. Elwood. 2016. To breathe or fight? Siamese fighting fish differ when facing a real opponent or mirror image. Behav. Processes 129:11–17.

Ashburner, M., C. A. Ball, J. A. Blake, D. Botstein, H. Butler, J. M. Cherry, A. P. Davis, K. Dolinski, S. S. Dwight, J. T. Eppig, M. A. Harris, D. P. Hill, L. Issel-Tarver, A. Kasarskis, S. Lewis, J. C. Matese, J. E. Richardson, M. Ringwald, G. M. Rubin, and G. Sherlock. 2000. Gene Ontology: tool for the unification of biology. Nat. Genet. 25:25–29.

Ashton, D. T., P. A. Ritchie, and M. Wellenreuther. 2017. Fifteen years of quantitative trait loci studies in fish: challenges and future directions. Mol. Ecol. 26:1465–1476.

Aubin-Horth, N., J. K. Desjardins, Y. M. Martei, S. Balshine, and H. A. Hofmann. 2007. Masculinized dominant females in a cooperatively breeding species. Mol. Ecol. 16:1349–1358.

Bailey, N. W., B. Gray, and M. Zuk. 2010. Acoustic Experience Shapes Alternative Mating Tactics and Reproductive Investment in Male Field Crickets. Curr. Biol. 20:845–849.

Balzarini, V., M. Taborsky, S. Wanner, F. Koch, and J. G. Frommen. 2014. Mirror, mirror on the wall: the predictive value of mirror tests for measuring aggression in fish. Behav. Ecol. Sociobiol. 68:871–878.

Barton, N., and L. Partridge. 2000. Limits to natural selection. Bioessays 22:1075–84.

Bates, D., M. Mächler, B. Bolker, and S. Walker. 2014. Fitting Linear Mixed-Effects Models using lme4. J. Stat. Softw. 67:1–48.

Beavis, W. D. 1998. QTL analyses: power, precision, and accuracy. Pp. 145–162 *in* Molecular dissection of complex traits. CRC press.

Benkman, C. W. 2003. Divergent selection drives the adaptive radiation of crossbills. Evolution (N. Y). 57:1176–1181.
Bewick, V., L. Cheek, and J. Ball. 2004. Statistics review 12: survival analysis. Crit. Care 8:389–94.
Blowes, S. A., M. S. Pratchett, and S. R. Connolly. 2013. Heterospecific Aggression and Dominance in a Guild of Coral-Feeding Fishes: The Roles of Dietary Ecology and Phylogeny. Am. Nat. 182:157–168.
Boileau, N., F. Cortesi, B. Egger, M. Muschick, A. Indermaur, A. Theis, H. H. Büscher, and W. Salzburger. 2015. A complex mode of aggressive mimicry in a scale-eating cichlid fish. Biol. Lett. 11:20150521.
Bolnick, D. I., R. D. H. Barrett, K. B. Oke, D. J. Rennison, and Y. E. Stuart. 2018. (Non)Parallel evolution.
Bolnick, D. I., R. Svanbäck, J. A. Fordyce, L. H. Yang, J. M. Davis, C. D. Hulsey, and M. L. Forister. 2003. The ecology of individuals: incidence and implications of individual specialization. Am. Nat. 161:1–28.
Bowman, R. I., and S. L. Billeb. 1965. Blood-eating in a Galápagos finch. Living Bird 4:29–44.
Braasch, I., W. Salzburger, and A. Meyer. 2006. Asymmetric evolution in two fish-specifically duplicated receptor tyrosine kinase paralogons involved in teleost coloration. Mol. Biol. Evol. 23:1192–1202.
Broman, K. W., D. M. Gatti, P. Simecek, N. A. Furlotte, P. Prins, Ś. Sen, B. S. Yandell, and G. A. Churchill. 2019. R/qtl2: Software for mapping quantitative trait loci with high-dimensional data and multiparent populations. Genetics 211:495–502.
Broman, K. W., H. Wu, Ś. Sen, and G. A. Churchill. 2003. R/qtl: QTL mapping in experimental crosses. Bioinformatics 19:889–890.
Brown, C., F. Jones, and V. Braithwaite. 2005. In situ examination of boldness-shyness traits in the tropical poeciliid, Brachyraphis episcopi. Anim. Behav. 70:1003–1009.
Buckland, S. T., A. C. Davison, and D. V. Hinkley. 1998. Bootstrap Methods and Their Application. Biometrics 54:795.
Budaev, S. V. 1997. Alternative styles in the European wrasse, Symphodus ocellatus: Boldness-related schooling tendency. Environ. Biol. Fishes 49:71–78.
Burnham, K. P., and D. R. Anderson. 2002. Model selection and multimodel inference: a practical information-theoretic approach. Springer New York, New York, NY.
Buston, P. M., and M. A. Cant. 2006. A new perspective on size hierarchies in nature: Patterns, causes, and consequences. Oecologia 149:362–372.
Canty, A., and B. Ripley. 2017. boot: Bootstrap R (S-Plus) Functions. R package version 1.3-20.
Canty, A., and B. D. Ripley. 2021. boot: Bootstrap R (S-Plus) Functions. R Packag. version 1.3-28.
Carbon, S., A. Ireland, C. J. Mungall, S. Shu, B. Marshall, and S. Lewis. 2009. AmiGO: online access to ontology and annotation data. Bioinforma. Appl. NOTE 25:288–28910.
Carlborg, Ö., L. Jacobsson, P. Åhgren, P. Siegel, and L. Andersson. 2006. Epistasis and the release of genetic variation during long-term selection. Nat. Genet. 38:418–420.
Chan, Y. F., M. E. Marks, F. C. Jones, G. Villarreal, M. D. Shapiro, S. D. Brady, A. M.

Southwick, D. M. Absher, J. Grimwood, J. Schmutz, R. M. Myers, D. Petrov, B. Jónsson, D. Schluter, M. A. Bell, and D. M. Kingsley. 2010. Adaptive evolution of pelvic reduction in sticklebacks by recurrent deletion of a pitxl enhancer. Science (80-.). 327:302–305.
Chen, L., A. L. Devries, and C. H. C. Cheng. 1997. Convergent evolution of antifreeze glycoproteins in Antarctic notothenioid fish and Arctic cod. Proc. Natl. Acad. Sci. U. S. A. 94:3817–3822.
China, V., L. Levy, A. Liberzon, T. Elmaliach, and R. Holzman. 2017. Hydrodynamic regime determines the feeding success of larval fish through the modulation of strike kinematics. Proc. R. Soc. B Biol. Sci. 284:20170235.
Chubaty, A. M., B. O. Ma, R. W. Stein, D. R. Gillespie, L. M. Henry, C. Phelan, E. Palsson, F. W. Simon, and B. D. Roitberg. 2014. On the evolution of omnivory in a community context. Ecol. Evol. 4:251–265.
Clark, P. U., A. S. Dyke, J. D. Shakun, A. E. Carlson, J. Clark, B. Wohlfarth, J. X. Mitrovica, S. W. Hostetler, and A. M. McCabe. 2009. The Last Glacial Maximum. Science (80-.). 325:710–714.
Clutton-Brock, T. H., and G. A. Parker. 1992. Potential Reproductive Rates and the Operation of Sexual Selection. Q. Rev. Biol. 67:437–456.
Colosimo, P. F., C. L. Peichel, K. Nereng, B. K. Blackman, M. D. Shapiro, D. Schluter, and D. M. Kingsley. 2004. The genetic architecture of parallel armor plate reduction in threespine sticklebacks. PLoS Biol. 2:e109. Public Library of Science.
Cone, R. D. 2005. Anatomy and regulation of the central melanocortin system. Nat. Neurosci. 8:571–8.
Conith, M. R., A. J. Conith, and R. C. Albertson. 2019. Evolution of a soft-tissue foraging adaptation in African cichlids: Roles for novelty, convergence, and constraint. Evolution (N. Y). 73:2072–2084.
Conith, M. R., Y. Hu, A. J. Conith, M. A. Maginnis, J. F. Webb, and R. Craig Albertson. 2018. Genetic and developmental origins of a unique foraging adaptation in a Lake Malawi cichlid genus. Proc. Natl. Acad. Sci. U. S. A. 115:7063–7068.
Conte, G. L., M. E. Arnegard, C. L. Peichel, and D. Schluter. 2012. The probability of genetic parallelism and convergence in natural populations. Proc. R. Soc. B Biol. Sci. 279:5039–5047.
Cortesi, F., Z. Musilová, S. M. Stieb, N. S. Hart, U. E. Siebeck, M. Malmstrøm, O. K. Tørresen, S. Jentoft, K. L. Cheney, N. J. Marshall, K. L. Carleton, and W. Salzburger. 2015. Ancestral duplications and highly dynamic opsin gene evolution in percomorph fishes. Proc. Natl. Acad. Sci. 112:1493–1498.
Cresko, W. A., A. Amores, C. Wilson, J. Murphy, M. Currey, P. Phillips, M. A. Bell, C. B. Kimmel, and J. H. Postlethwait. 2004. Parallel genetic basis for repeated evolution of armor loss in Alaskan threespine stickleback populations. Proc. Natl. Acad. Sci. U. S. A. 101:6050–6055.
Cullen, J. A., T. Maie, H. L. Schoenfuss, and R. W. Blob. 2013. Evolutionary Novelty versus Exaptation: Oral Kinematics in Feeding versus Climbing in the Waterfall-Climbing Hawaiian Goby Sicyopterus stimpsoni. PLoS One 8:e53274.
Curry, R. L., and D. J. Anderson. 2012. Interisland Variation in Blood Drinking by Galápagos Mockingbirds. Auk 104:517–521.
Dalquen, D. A., and C. Dessimoz. 2013. Bidirectional Best Hits Miss Many Orthologs in

Duplication-Rich Clades such as Plants and Animals. Genome Biol. Evol. 5:1800–1806.
Davis, A. L., M. H. Babb, M. C. Lowe, A. T. Yeh, B. T. Lee, and C. H. Martin. 2018. Testing Darwin's Hypothesis about the Wonderful Venus Flytrap: Marginal Spikes Form a "Horrid Prison" for Moderate-Sized Insect Prey. Am. Nat. 193:309–317.
De Visser, J., and C. D. N. Barel. 1996. Architectonic constraints on the hyoid's optimal starting position for suction feeding of fish. J. Morphol. 228:1–18.
Demartini, E. E., and J. A. Coyer. 1981. Cleaning and Scale-Eating in Juveniles of the Kyphosid Fishes, Hermosilla azurea and Girella nigricans. Copeia 785–789.
Depristo, M. A., E. Banks, R. Poplin, K. V Garimella, J. R. Maguire, C. Hartl, A. A. Philippakis, G. Del Angel, M. A. Rivas, M. Hanna, A. McKenna, T. J. Fennell, A. M. Kernytsky, A. Y. Sivachenko, K. Cibulskis, S. B. Gabriel, D. Altshuler, and M. J. Daly. 2011. A framework for variation discovery and genotyping using next-generation DNA sequencing data. Nat. Genet. 43:491–501.
Ding, N., H. Zhou, P. O. Esteve, H. G. Chin, S. Kim, X. Xu, S. M. Joseph, M. J. Friez, C. E. Schwartz, S. Pradhan, and T. G. Boyer. 2008. Mediator Links Epigenetic Silencing of Neuronal Gene Expression with X-Linked Mental Retardation. Mol. Cell 31:347–359.
Dingerkus, G., and L. D. Uhler. 1977. Enzyme clearing of alcian blue stained whole small vertebrates for demonstration of cartilage. Biotech. Histochem. 52:229–232.
Donley, J. M., C. A. Sepulveda, P. Konstantinidis, S. Gemballa, and R. E. Shadwick. 2004. Convergent evolution in mechanical design of lamnid sharks and tunas. Nature 429:61–65.
Douard, V., F. Brunet, B. Boussau, I. Ahrens-Fath, V. Vlaeminck-Guillem, B. Haendler, V. Laudet, and Y. Guiguen. 2008. The fate of the duplicated androgen receptor in fishes: a late neofunctionalization event? BMC Evol. Biol. 8:336.
Duckworth, R. A. 2006. Aggressive behaviour affects selection on morphology by influencing settlement patterns in a passerine bird. Proc. R. Soc. B Biol. Sci. 273:1789–1795.
Ducrest, A.-L., L. Keller, and A. Roulin. 2008. Pleiotropy in the melanocortin system, coloration and behavioural syndromes. Trends Ecol. Evol. 23:502–10.
Echelle, A. A., and A. E. Echelle. 2020. Cyprinodontidae : Pupfishes. Pp. 609–673 *in* Freshwater Fishes of North America. The Johns Hopkins University Press.
Elwood, R. W., V. Stoilova, A. McDonnell, R. L. Earley, and G. Arnott. 2014. Do mirrors reflect reality in agonistic encounters? A test of mutual cooperation in displays. Anim. Behav. 97:63–67.
Erickson, P. A., A. M. Glazer, E. E. Killingbeck, R. M. Agoglia, J. Baek, S. M. Carsanaro, A. M. Lee, P. A. Cleves, D. Schluter, and C. T. Miller. 2016. Partially repeatable genetic basis of benthic adaptation in threespine sticklebacks. Evolution (N. Y). 70:887–902.
Erwin, D. H. 2021. A conceptual framework of evolutionary novelty and innovation. Biol. Rev. 96:1–15.
Erwin, D. H. 2015. Novelty and Innovation in the History of Life. Curr. Biol. 25:R930–R940.
Erwin, D. H. 2019. Prospects for a General Theory of Evolutionary Novelty. J. Comput. Biol. 26:735–744.

Erwin, D. H., M. Laflamme, S. M. Tweedt, E. A. Sperling, D. Pisani, and K. J. Peterson. 2011. The Cambrian conundrum: Early divergence and later ecological success in the early history of animals. Science (80-.). 334:1091–1097.
Ewels, P., M. Magnusson, S. Lundin, and M. Käller. 2016. MultiQC: Summarize analysis results for multiple tools and samples in a single report. Bioinformatics 32:3047–3048.
Feldman, C. R., E. D. Brodie, E. D. Brodie, and M. E. Pfrender. 2009. The evolutionary origins of beneficial alleles during the repeated adaptation of garter snakes to deadly prey. Proc. Natl. Acad. Sci. U. S. A. 106:13415–13420.
Felsenstein, J. 1985. Phylogenies and the Comparative Method. Am. Nat. 125:1–15.
Ferry-Graham, L. A. 2002. Using Functional Morphology to Examine the Ecology and Evolution of Specialization. Integr. Comp. Biol. 42:265–277.
Ferry-Graham, L. A., L. P. Hernandez, A. C. Gibb, and C. Pace. 2010. Unusual kinematics and jaw morphology associated with piscivory in the poeciliid, Belonesox belizanus. Zoology 113:140–147.
Ferry-Graham, L. A., P. C. Wainwright, C. Darrin Hulsey, and D. R. Bellwood. 2001. Evolution and mechanics of long jaws in butterflyfishes (Family Chaetodontidae). J. Morphol. 248:120–143.
Feulner, P. G. D., F. J. J. Chain, M. Panchal, C. Eizaguirre, M. Kalbe, T. L. Lenz, M. Mundry, I. E. Samonte, M. Stoll, M. Milinski, T. B. H. Reusch, and E. Bornberg-Bauer. 2013. Genome-wide patterns of standing genetic variation in a marine population of three-spined sticklebacks. Mol. Ecol. 22:635–649.
Francis, R. C. 2010. Temperament in a Fish: A Longitudinal Study of the Development of Individual Differences in Aggression and Social Rank in the Midas Cichlid. Ethology 86:311–325.
Fraser, D. F., J. F. Gilliam, M. J. Daley, A. N. Le, and G. T. Skalski. 2001. Explaining Leptokurtic Movement Distributions: Intrapopulation Variation in Boldness and Exploration. Am. Nat. 158:124–135.
Fryer, G., P. H. Greenwood, and E. Trewavas. 1955. Scale-eating Habits of African Cichlid Fishes. Nature 175:1089–1090.
Fryer, G., and T. D. Iles. 1972. The cichlid fishes of the Great Lakes of Africa: Their biology and evolution. Vol. 23. Oliver & Boyd, Croythron House.
Futuyman, D. J. 1986. Evolutionary Biology. 2d ed. Sinauer, Sunderland, Mass.
Futuyman, D. J., and G. Moreno. 1988. The Evolution of Ecological Specialization. Annu. Rev. Ecol. Syst. 19:207–233.
Gardner, K. M., and R. G. Latta. 2007. Shared quantitative trait loci underlying the genetic correlation between continuous traits. Mol. Ecol. 16:4195–4209.
Genner, M. J., G. F. Turner, and S. J. Hawkins. 1999. Resource control by territorial male cichlid fish in Lake Malawi. J. Anim. Ecol. 68:522–529.
Gidmark, N. J., N. Konow, E. LoPresti, and E. L. Brainerd. 2013. Bite force is limited by the force–length relationship of skeletal muscle in black carp, Mylopharyngodon piceus. Biol. Lett. 9:20121181.
Gidmark, N. J., C. Taylor, E. Lopresti, and E. Brainerd. 2015. Functional morphology of durophagy in black carp, Mylopharyngodon piceus. J. Morphol. 276:1422–1432.
Grant, P. R., and B. R. Grant. 2002. Adaptive radiation of Darwin's finches: Recent data help explain how this famous group of Galápagos birds evolved, although gaps in

our understanding remain. Am. Sci. 90:130–139.
Grant, P. R., B. R. Grant, J. A. Markert, L. F. Keller, and K. Petren. 2004. Convergent evolution of Darwin's finches caused by introgressive hybridization and selection. Evolution (N. Y). 58:1588–1599.
Greenwood, P. H. 1965. Two new species of Haplochromis (Pisces, Cichlidae) from Lake Victoria. J. Nat. Hist. Ser. 13 8:303–318.
Gruber, J., G. Brown, M. J. Whiting, and R. Shine. 2017. Geographic divergence in dispersal-related behaviour in cane toads from range-front versus range-core populations in Australia. Behav. Ecol. Sociobiol. 71:38.
Grubich, J. 2003. Morphological convergence of pharyngeal jaw structure in durophagous perciform fish. Biol. J. Linn. Soc. 80:147–165.
Gumm, J. M. 2012. Sex recognition of female-like sneaker males in the Comanche Springs pupfish, Cyprinodon elegans. Anim. Behav. 83:1421–1426.
Haenel, Q., M. Roesti, D. Moser, A. D. C. MacColl, and D. Berner. 2019. Predictable genome-wide sorting of standing genetic variation during parallel adaptation to basic versus acidic environments in stickleback fish. Evol. Lett. 3:28–42. Wiley.
Hagey, F. M., and J. E. Mylroie. 1995. Pleistocene lake and lagoon deposits, San Salvador island, Bahamas. Spec. Pap. Soc. Am. 77–90.
Haley, C. S., and S. A. Knott. 1992. A simple regression method for mapping quantitative trait loci in line crosses using flanking markers. Heredity (Edinb). 69:315–324.
Hall, B. D., R. G. Cadle, S. M. Morrill-Cornelius, and C. A. Bay. 2007. Phakomatosis pigmentovascularis: Implications for severity with special reference to Mongolian spots associated with Sturge-Weber and Klippel-Trenaunay syndromes. Pp. 3047–3053 *in* American Journal of Medical Genetics, Part A.
Hallgrímsson, B., H. A. Jamniczky, N. M. Young, C. Rolian, U. Schmidt-Ott, and R. S. Marcucio. 2012. The generation of variation and the developmental basis for evolutionary novelty.
Hankison, S. J., and M. R. Morris. 2003. Avoiding a compromise between sexual selection and species recognition: Female swordtail fish assess multiple species-specific cues. Behav. Ecol. 14:282–287.
Harmon, L. J., J. B. Losos, T. J. Davies, R. G. Gillespie, J. L. Gittleman, W. B. Jennings, K. H. Kozak, M. A. McPeek, F. Moreno-Roark, T. J. Near, A. Purvis, R. E. Ricklefs, D. Schluter, J. A. Schulte, O. Seehausen, B. L. Sidlauskas, O. Torres-Carvajal, J. T. Weir, and A. Ø. Mooers. 2010. Early bursts of body size and shape evolution are rare in comparative data. Evolution 64:2385–2396.
Hashikawa, K., Y. Hashikawa, A. Falkner, and D. Lin. 2016. The neural circuits of mating and fighting in male mice. Curr. Opin. Neurobiol. 38:27–37.
Hata, H., M. Yasugi, and M. Hori. 2011. Jaw Laterality and Related Handedness in the Hunting Behavior of a Scale-Eating Characin, Exodon paradoxus. PLoS One 6:e29349.
Hatfield, T., and D. Schluter. 1999. Ecological Speciation in Sticklebacks: Environment-Dependent Hybrid Fitness. Evolution (N. Y). 53:866.
Haukoos, J. S., and R. J. Lewis. 2005. Advanced Statistics: Bootstrapping Confidence Intervals for Statistics with '"Difficult"' Distributions. Acad. Emerg. Med. 12.4:360–365.

Hedrick, P. W. 2013. Adaptive introgression in animals: Examples and comparison to new mutation and standing variation as sources of adaptive variation.
Hedrick, T. L. 2008. Software techniques for two- and three-dimensional kinematic measurements of biological and biomimetic systems. Bioinspir. Biomim. 3:034001.
Henning, F., G. Machado-Schiaffino, L. Baumgarten, and A. Meyer. 2017. Genetic dissection of adaptive form and function in rapidly speciating cichlid fishes. Evolution (N. Y). 71:1297–1312.
Hernandez, L. P., D. Adriaens, C. H. Martin, P. C. Wainwright, B. Masschaele, and M. Dierick. 2018. Building trophic specializations that result in substantial niche partitioning within a young adaptive radiation. J. Anat. 232:173–185.
Hernandez, P. L., A. C. Gibb, and L. Ferry-Graham. 2009. Trophic apparatus in cyprinodontiform fishes: Functional specializations for picking and scraping behaviors. J. Morphol. 270:645–661.
Higham, T. E., S. M. Rogers, R. B. Langerhans, H. A. Jamniczky, G. V Lauder, W. J. Stewart, C. H. Martin, and D. N. Reznick. 2016. Speciation through the lens of biomechanics : locomotion , prey capture and reproductive isolation. Proc. R. Soc. B Biol. Sci. 283:20161294.
Höjesjö, J., M. Axelsson, R. Dahy, L. Gustavsson, and J. I. Johnsson. 2015. Sight or smell? Behavioural and heart rate responses in subordinate rainbow trout exposed to cues from dominant fish. PeerJ 3:e1169.
Holbrook, S. J., and R. J. Schmitt. 1992. Causes and Consequences of Dietary Specialization in Surfperches : Patch Choice and Intraspecific Competition. Ecology 73:402–412.
Holtmeier, C. L. 2001. Heterochrony, maternal effects, and phenotypic variation among sympatric pupfishes. Evolution 55:330–8.
Holzman, R., S. W. Day, R. S. Mehta, and P. C. Wainwright. 2008. Jaw protrusion enhances forces exerted on prey by suction feeding fishes. J. R. Soc. Interface 5:1445–1457.
Holzman, R., and P. C. Wainwright. 2009. How to surprise a copepod: Strike kinematics reduce hydrodynamic disturbance and increase stealth of suction-feeding fish. Limnol. Oceanogr. 54:2201–2212.
Hopkins, C. D. 1995. Convergent designs for electrogenesis and electroreception. Curr. Opin. Neurobiol. 5:769–777.
Horton, B. M., Y. Hu, C. L. Martin, B. P. Bunke, B. S. Matthews, I. T. Moore, J. W. Thomas, and D. L. Maney. 2013. Behavioral Characterization of a White-Throated Sparrow Homozygous for the ZAL2m Chromosomal Rearrangement. Behav. Genet. 43:60–70.
Horton, B. M., W. H. Hudson, E. A. Ortlund, S. Shirk, J. W. Thomas, E. R. Young, W. M. Zinzow-Kramer, and D. L. Maney. 2014. Estrogen receptor polymorphism in a species with alternative behavioral phenotypes. Proc. Natl. Acad. Sci. 111:1443–1448.
Hu, Y., N. Nelson-Maney, and P. S. L. Anderson. 2017. Common evolutionary trends underlie the four-bar linkage systems of sunfish and mantis shrimp. Evolution (N. Y). 71:1397–1405.
Hubbs, C. L. 1955. Hybridization between Fish Species in Nature. Syst. Biol. 4.1:1–20.
Huey, R. B., P. E. Hertz, and B. Sinervo. 2003. Behavioral Drive versus Behavioral

Inertia in Evolution: A Null Model Approach. Am. Nat. 161:357–366.
Hulsey, C. D., R. J. Roberts, A. S. P. Lin, R. Guldberg, and J. T. Streelman. 2008. Convergence in a mechanically complex phenotype: Detecting structural adaptations for crushing in cichlid fish. Evolution (N. Y). 62:1587–1599.
James, M. E., M. J. Wilkinson, H. L. North, J. Engelstädter, and D. Ortiz-Barrientos. 2020. A framework to quantify phenotypic and genotypic parallel evolution. BioRxiv.
Janovetz, J. 2005a. Functional morphology of feeding in the scale-eating specialist Catoprion mento. J. Exp. Biol. 208:4757–4768.
Janovetz, J. 2005b. Functional morphology of feeding in the scale-eating specialist Catoprion mento. J. Exp. Biol. 208:4757–4768.
Jennions, M. D., and M. Petrie. 2007. Variation in mate choice and mating preferences: a review of causes and consequences. Biol. Rev. 72:283–327.
Jones, F. C., M. G. Grabherr, Y. F. Chan, P. Russell, E. Mauceli, J. Johnson, R. Swofford, M. Pirun, M. C. Zody, S. White, E. Birney, S. Searle, J. Schmutz, J. Grimwood, M. C. Dickson, R. M. Myers, C. T. Miller, B. R. Summers, A. K. Knecht, S. D. Brady, H. Zhang, A. A. Pollen, T. Howes, C. Amemiya, J. Baldwin, T. Bloom, D. B. Jaffe, R. Nicol, J. Wilkinson, E. S. Lander, F. Di Palma, K. Lindblad-Toh, and D. M. Kingsley. 2012. The genomic basis of adaptive evolution in threespine sticklebacks. Nature 484:55–61.
Jost, M. C., D. M. Hillis, Y. Lu, J. W. Kyle, H. A. Fozzard, and H. H. Zakon. 2008. Toxin-resistant sodium channels: Parallel adaptive evolution across a complete gene family. Mol. Biol. Evol. 25:1016–1024.
Juenger, T. E., S. Sen, K. A. Stowe, and E. L. Simms. 2005. Epistasis and genotype-environment interaction for quantitative trait loci affecting flowering time in Arabidopsis thaliana. Pp. 87–105 *in* Genetica.
Kang, H. Y., S. Yeh, N. Fujimoto, and C. Chang. 1999. Cloning and characterization of human prostate coactivator ARA54, a novel protein that associates with the androgen receptor. J. Biol. Chem. 274:8570–6.
Katz, P. S. 2006. Comparative Neurophysiology: An Electric Convergence in Fish. Curr. Biol. 16:R327–R330.
Katzir, G. 1981. Aggression by the damselfish Dascyllus aruanus L. Towards conspecifics and heterospecifics. Anim. Behav. 29:835–841.
Kodric-Brown, A., and J. H. Brown. 1984. Truth in advertising: the kinds of traits favored by sexual selection. Am. Nat. 124:309–323.
Kodric-Brown, A., R. M. Sibly, and J. H. Brown. 2006. The allometry of ornaments and weapons. Proc. Natl. Acad. Sci. U. S. A. 103:8733–8738.
Kolmann, M. A., J. M. Huie, K. Evans, and A. P. Summers. 2018. Specialized specialists and the narrow niche fallacy : a tale of scale-feeding fishes. R. Soc. Open Sci. 5.1:171581.
Konings, A. 2007. Malawi cichlids in their natural habitat 4th Edition.
Kowalko, J. E., N. Rohner, T. A. Linden, S. B. Rompani, W. C. Warren, R. Borowsky, C. J. Tabin, W. R. Jeffery, and M. Yoshizawa. 2013. Convergence in feeding posture occurs through different genetic loci in independently evolved cave populations of Astyanax mexicanus. Proc. Natl. Acad. Sci. U. S. A. 110:16933–16938.
Kuhn, M. 2008. Building predictive models in R using the caret package. J. Stat. Softw. 1–26.

Labandeira, C. 2007. The origin of herbivory on land: Initial patterns of plant tissue consumption by arthropods. Insect Sci. 14:259–275.
Lander, E., and L. Kruglyak. 1995. Genetic dissection of complex traits: Guidelines for interpreting and reporting linkage results. Nat. Genet. 11:241–247.
Lander, E. S., and S. Botstein. 1989. Mapping mendelian factors underlying quantitative traits using RFLP linkage maps. Genetics 121:185.
Lauder, G. V. 1983. Functional and morphological bases of trophic specialization in sunfishes (Teleostei, centrarchidae). J. Morphol. 178:1–21.
Lencer, E. S., W. C. Warren, R. Harrison, and A. R. McCune. 2017. The Cyprinodon variegatus genome reveals gene expression changes underlying differences in skull morphology among closely related species. BMC Genomics 18:424.
Lenski, R. E., and M. Travisano. 1994. Dynamics of adaptation and diversification: a 10,000-generation experiment with bacterial populations. Proc. Natl. Acad. Sci. U. S. A. 91:6808–14.
Liao, Y., G. K. Smyth, and W. Shi. 2013. The Subread aligner: fast, accurate and scalable read mapping by seed-and-vote. Nucleic Acids Res. 41:e108.
Liem, K. F. 1980. Adaptive significance of intra- and interspecific differences in the feeding repertoires of cichlid fishes. Integr. Comp. Biol. 20:295–314.
Liem, K. F. 1973. Evolutionary Strategies and Morphological Innovations: Cichlid Pharyngeal Jaws. Syst. Zool. 22:425.
Liem, K. F. 1978. Modulatory multiplicity in the functional repertoire of the feeding mechanism in cichlid fishes. I. Piscivores. J. Morphol. 158:323–360.
Linnen, C. R., Y. P. Poh, B. K. Peterson, R. D. H. Barrett, J. G. Larson, J. D. Jensen, and H. E. Hoekstra. 2013. Adaptive evolution of multiple traits through multiple mutations at a single gene. Science (80-.). 339:1312–1316.
Liu, J., M. Aoki, I. Illa, C. Wu, M. Fardeau, C. Angelini, C. Serrano, J. Andoni Urtizberea, F. Hentati, M. Ben Hamida, S. Bohlega, E. J. Culper, A. A. Amato, K. Bossie, J. Oeltjen, K. Bejaoui, D. McKenna-Yasek, B. A. Hosler, E. Schurr, K. Arahata, P. J. De Jong, and R. H. Brown. 1998. Dysferlin, a novel skeletal muscle gene, is mutated in Miyoshi myopathy and limb girdle muscular dystrophy. Nat. Genet. 20:31–36.
Liu, R. K., and A. A. Echelle. 2013. Behavior of the Catarina pupfish (cyprinodontidae: Megupsilon aporus), a severely imperiled species. Southwest. Nat. 58:1–7.
Longo, S. J., T. Goodearly, and P. C. Wainwright. 2018. Extremely fast feeding strikes are powered by elastic recoil in a seahorse relative, the snipefish, Macroramphosus scolopax. Proc. R. Soc. B Biol. Sci. 285:20181078.
Losey, G. S. 1979. Fish cleaning symbiosis: proximate causes of host behavior. Anim. Behav. 27:669–685.
Losey, G. S. 1972. The ecological importance of cleaning symbiosis. Copeia 820–833.
Losos, J. B. 2010. Adaptive Radiation, Ecological Opportunity, and Evolutionary Determinism. Am. Nat. 175:623–639.
Losos, J. B., T. W. Schoener, R. B. Langerhans, and D. A. Spiller. 2006. Rapid temporal reversal in predator-driven natural selection. Science (80-.). 314:1111.
Losos, J. B., T. W. Schoener, and D. A. Spiller. 2004. Predator-induced behaviour shifts and natural selection in field-experimental lizard populations. Nature 432:505–508.
Love, M. I., W. Huber, and S. Anders. 2014. Moderated estimation of fold change and

dispersion for RNA-seq data with DESeq2. Genome Biol. 15:550.
Lundeba, M., J. S. Likongwe, H. Madsen, and J. R. Stauffer. 2011. Oral shelling of Bulinus spp. (Mollusca: Planorbidae) by the Lake Malaŵi cichlid, Metriaclima lanisticola (Pisces: Cichlidae). J. Freshw. Ecol. 26:593–597.
Lynch, M., and B. Walsh. 1998. Genetics and Analysis of Quantitative Traits. Vol. 1. Sinauer Associates, Sunderland, MA, Sunderland, MA.
Madsen, H., K. C. J. Kamanga, J. R. Stauffer, and J. Likongwe. 2010. Biology of the Molluscivorous Fish Trematocranus placodon (Pisces: Cichlidae) from Lake Malaŵi. J. Freshw. Ecol. 25:449–455.
Marsden, C. D., Y. Lee, K. Kreppel, A. Weakley, A. Cornel, H. M. Ferguson, E. Eskin, and G. C. Lanzaro. 2014. Diversity, differentiation, and linkage disequilibrium: Prospects for association mapping in the malaria vector anopheles arabiensis. G3 Genes, Genomes, Genet. 4:121–131.
Martin, C. H. 2016. The cryptic origins of evolutionary novelty: 1000-fold faster trophic diversification rates without increased ecological opportunity or hybrid swarm. Evolution (N. Y). 70:2504–2519.
Martin, C. H., J. E. Crawford, B. J. Turner, and L. H. Simons. 2016. Diabolical survival in Death Valley: recent pupfish colonization, gene flow and genetic assimilation in the smallest species range on earth. Proc. R. Soc. B Biol. Sci. 283:20152334.
Martin, C. H., J. S. Cutler, J. P. Friel, C. Dening Touokong, G. Coop, and P. C. Wainwright. 2015. Complex histories of repeated gene flow in Cameroon crater lake cichlids cast doubt on one of the clearest examples of sympatric speciation. Evolution (N. Y). 69:1406–1422.
Martin, C. H., P. A. Erickson, and C. T. Miller. 2017. The genetic architecture of novel trophic specialists: larger effect sizes are associated with exceptional oral jaw diversification in a pupfish adaptive radiation. Mol. Ecol. 26:624–638.
Martin, C. H., and L. C. Feinstein. 2014. Novel trophic niches drive variable progress towards ecological speciation within an adaptive radiation of pupfishes. Mol. Ecol. 23:1846–1862.
Martin, C. H., and M. J. Genner. 2009. High niche overlap between two successfully coexisting pairs of Lake Malawi cichlid fishes. Can. J. Fish. Aquat. Sci. 66:579–588.
Martin, C. H., J. A. McGirr, E. J. Richards, and M. E. St. John. 2019. How to Investigate the Origins of Novelty: Insights Gained from Genetic, Behavioral, and Fitness Perspectives. Integr. Org. Biol. 1:obz018.
Martin, C. H., and P. C. Wainwright. 2013a. A Remarkable Species Flock of Cyprinodon Pupfishes Endemic to San Salvador Island, Bahamas. Bull. Peabody Museum Nat. Hist. 54:231–241.
Martin, C. H., and P. C. Wainwright. 2013b. Multiple fitness peaks on the adaptive landscape drive adaptive radiation in the wild. Science 339:208–11.
Martin, C. H., and P. C. Wainwright. 2013c. On the Measurement of Ecological Novelty: Scale-Eating Pupfish Are Separated by 168 my from Other Scale-Eating Fishes. PLoS One 8:e71164.
Martin, C. H., and P. C. Wainwright. 2011. Trophic novelty is linked to exceptional rates of morphological diversification in two adaptive radiations of cyprinodon pupfish. Evolution (N. Y). 65:2197–2212.
Martyn, A. C., E. Choleris, D. J. Gillis, J. N. Armstrong, T. R. Amor, A. R. R.

McCluggage, P. V Turner, G. Liang, K. Cai, and R. Lu. 2012. Luman/CREB3 Recruitment Factor Regulates Glucocorticoid Receptor Activity and Is Essential for Prolactin-Mediated Maternal Instinct. Mol. Cell. Biol. 32:5140–5150. American Society for Microbiology (ASM).
Matthews, D. G., and R. C. Albertson. 2017. Effect of craniofacial genotype on the relationship between morphology and feeding performance in cichlid fishes. Evolution (N. Y). 71:2050–2061.
Mayr, E. 1963. Animal Species and Evolution. Harvard University Press; London: Oxford University Press.
Mayr, E. 1960. The emergence of evolutionary novelties. Pp. 349–380 *in* The Evolution of Life. University of Chicago Press, Chicago, IL.
McGee, M. D., D. Schluter, and P. C. Wainwright. 2013. Functional basis of ecological divergence in sympatric stickleback. BMC Evol. Biol. 13:277.
McGhee, K. E., R. C. Fuller, and J. Travis. 2007. Male competition and female choice interact to determine mating success in the bluefin killifish. Behav. Ecol. 18:822–830.
McGirr, J. A., and C. H. Martin. 2020. Ecological divergence in sympatry causes gene misexpression in hybrids. Mol. Ecol. 29:2707–2721.
McGirr, J. A., and C. H. Martin. 2021. Few Fixed Variants between Trophic Specialist Pupfish Species Reveal Candidate Cis-Regulatory Alleles Underlying Rapid Craniofacial Divergence. Mol. Biol. Evol. 38:405–423.
McGirr, J. A., and C. H. Martin. 2016. Novel candidate genes underlying extreme trophic specialization in Caribbean pupfishes. Mol. Biol. Evol. 34:msw286.
McGirr, J. A., and C. H. Martin. 2018. Parallel evolution of gene expression between trophic specialists despite divergent genotypes and morphologies. Evol. Lett., doi: 10.1002/evl3.41.
McGraw, K.J., Dale, J., Mackillop, E. A. 2003. Social environment during molt and the expression of melanin-based plumage pigmentation in male house sparrows (Passer domesticus). Behav. Ecol. Sociobiol. 53:116–122.
McKaye, K. R., and A. Marsh. 1983. Food switching by two specialized algae-scraping cichlid fishes in Lake Malawi, Africa. Oecologia 56:245–248.
Michael, D., S. Soi, J. Cabera-Perez, M. Weller, S. Alexander, I. Alevizos, G. G. Illei, and J. A. Chiorini. 2011. Microarray analysis of sexually dimorphic gene expression in human minor salivary glands. Oral Dis. 17:653–661.
Miller, M. J. 2006. The Ecology and Functional Morphology of Feeding of North American Sturgeon and Paddlefish. Pp. 87–102 *in* Sturgeons and Paddlefish of North America. Kluwer Academic Publishers, Dordrecht.
Morjan, C. L., and L. H. Rieseberg. 2004. How species evolve collectively: implications of gene flow and selection for the spread of advantageous alleles. Mol. Ecol. 13:1341–1356. John Wiley & Sons, Ltd.
Moyer, K. E. 1971. The physiology of hostility. Oxford, England: Markham.
Nelson, J. S., T. C. Grande, and M. V. H. Wilson. 2016. Fishes of the World. John Wiley & Sons, Inc, Hoboken, NJ.
Nelson, R. J., and S. Chiavegatto. 2001. Molecular basis of aggression. Trends Neurosci. 24:713–719.
Nelson, R. J., and B. C. Trainor. 2007. Neural mechanisms of aggression. Nat. Rev.

Neurosci. 8:536–546.
Nelson, T. C., and W. A. Cresko. 2018. Ancient genomic variation underlies repeated ecological adaptation in young stickleback populations. Evol. Lett. 2:9–21.
Nicolakakis, N., and L. Lefebvre. 2000. Forebrain size and innovation rate in European birds: Feeding, nesting and confounding variables. Behaviour 137:1415–1429.
Novakowski, G. C., R. Fugi, and N. S. Hahn. 2004. Diet and dental development of three species of Roeboides (Characiformes: Characidae). Neotrop. Ichthyol. 2:157–162.
Nshombo, M., Y. Yanagisawa, and M. Nagoshi. 1985. Scale-Eating in Perissodus microlepis (Cichlidae) and of Its Food Habits with Growth. Japanese J. Ichthyol. 32:66–73.
Nyholt, D. R. 2000. All LODs are not created equal. Am. J. Hum. Genet. 67:282–288.
O'Brown, N. M., B. R. Summers, F. C. Jones, S. D. Brady, and D. M. Kingsley. 2015. A recurrent regulatory change underlying altered expression and Wnt response of the stickleback armor plates gene EDA. Elife 4:e05290.
O'Neill, M. W., and A. C. Gibb. 2013. Does Feeding Behavior Facilitate Trophic Niche Partitioning in Two Sympatric Sucker Species from the American Southwest? Physiol. Biochem. Zool. 87:65–76.
Orr, H. A. 2006. The distribution of fitness effects among beneficial mutations in Fisher's geometric model of adaptation. J. Theor. Biol. 238:279–285.
Overington, S. E., J. Morand-Ferron, N. J. Boogert, and L. Lefebvre. 2009. Technical innovations drive the relationship between innovativeness and residual brain size in birds. Anim. Behav. 78:1001–1010.
Paaby, A. B., and M. V. Rockman. 2013. The many faces of pleiotropy. Trends Genet. 29:66–73.
Parsons, T. E., S. M. Weinberg, K. Khaksarfard, R. N. Howie, M. Elsalanty, J. C. Yu, and J. J. Cray. 2014. Craniofacial Shape Variation in Twist1 +/− Mutant Mice. Anat. Rec. 297:826–833.
Patek, S. N., J. E. Baio, B. L. Fisher, and A. V Suarez. 2006. Multifunctionality and mechanical origins: Ballistic jaw propulsion in trap-jaw ants. Proc. Natl. Acad. Sci. U. S. A. 103:12787–12792.
Patton, A. H., E. J. Richards, K. J. Gould, L. K. Buie, and C. H. Martin. 2022. Hybridization alters the shape of the genotypic fitness landscape, increasing access to novel fitness peaks during adaptive radiation. Elife 11:e72905.
Pauers, M. J., J. M. Kapfer, C. E. Fendos, and C. S. Berg. 2008. Aggressive biases towards similarly coloured males in Lake Malawi cichlid fishes. Biol. Lett. 4:156–159.
Pavlidis, P., D. Živković, A. Stamatakis, and N. Alachiotis. 2013. SweeD: Likelihood-based detection of selective sweeps in thousands of genomes. Mol. Biol. Evol. 30:2224–2234.
Peiman, K. S., and B. W. Robinson. 2010. Ecology and Evolution of Resource-Related Heterospecific Aggression. Q. Rev. Biol. 85:133–158.
Perry, S., B. Kiragasi, D. Dickman, and A. Ray. 2017. The Role of Histone Deacetylase 6 in Synaptic Plasticity and Memory. Cell Rep. 18:1337–1345.
Peterson, C. C., and P. McIntyre. 1998. Ontogenetic diet shifts in Roeboides affinis with morphological comparisons. Environ. Biol. Fishes 53:105–110.

Peterson, C. C., and K. O. Winemiller. 1997. Ontogenic diet shifts and scale-eating in Roeboides dayi, a Neotropical characid. Environ. Biol. Fishes 49:111–118.
Philibert, R. A., and A. Madan. 2007. Role of MED12 in transcription and human behavior. Pharmacogenomics 8:909–916.
Pickrell, J. K., and J. K. Pritchard. 2012. Inference of Population Splits and Mixtures from Genome-Wide Allele Frequency Data. PLoS Genet. 8:e1002967.
Pigliucci, M. 2008. What, if Anything, Is an Evolutionary Novelty? Philos. Sci. 75:887–898.
Price, A., C. Weadick, J. Shim, and F. Helen Rodd. 2008. Pigments, Patterns, and Fish Behavior. Zebrafish 5:297–307.
Pyke, G. H. 1984. Optimal foraging theory: a critical review. Annu. Rev. Ecol. Syst. Vol. 15 15:523–575.
R Core Team. 2018. R: A Language and Environment for Statistical Computing. Vienna, Austria.
Ralston, K. R., and P. C. Wainwright. 1997. Functional consequences of trophic specialization in pufferfishes. Funct. Ecol. 11:43–52.
Rand, A. S., and E. E. Williams. 1970. An estimation of redundancy and information content of anole dewlaps. Am. Nat. 104:99–103.
Rehage, J. S., and A. Sih. 2004. Dispersal behavior, boldness, and the link to invasiveness: A comparison of four gambusia species. Biol. Invasions 6:379–391.
Ribbink, A. J., B. A. Marsh, A. C. Marsh, A. C. Ribbink, and B. J. Sharp. 1983. A preliminary survey of the cichlid fishes of rocky habitats in Lake Malawi. South African J. Zool. 18:149–310.
Rich, J. T., J. G. Neely, R. C. Paniello, C. C. J. Voelker, B. Nussenbaum, and E. W. Wang. 2010. A practical guide to understanding Kaplan-Meier curves. Otolaryngol. Neck Surg. 143:331–336.
Richards, E. J., and C. H. Martin. 2017. Adaptive introgression from distant Caribbean islands contributed to the diversification of a microendemic adaptive radiation of trophic specialist pupfishes. PLoS Genet. 13:e1006919.
Richards, E. J., J. A. McGirr, J. R. Wang, M. E. St. John, J. W. Poelstra, M. J. Solano, D. C. O'Connell, B. J. Turner, and C. H. Martin. 2021. A vertebrate adaptive radiation is assembled from an ancient and disjunct spatiotemporal landscape. Proc. Natl. Acad. Sci. 118:e2011811118.
Richards, E. J., M. R. Servedio, and C. H. Martin. 2019. Searching for Sympatric Speciation in the Genomic Era. BioEssays 41:1900047.
Risch, N. 1990. Linkage strategies for genetically complex traits. I. Multilocus models. Am. J. Hum. Genet. 46:222–228.
Risheg, H., J. M. Graham, R. D. Clark, R. C. Rogers, J. M. Opitz, J. B. Moeschler, A. P. Peiffer, M. May, S. M. Joseph, J. R. Jones, R. E. Stevenson, C. E. Schwartz, and M. J. Friez. 2007. A recurrent mutation in MED12 leading to R961W causes Opitz-Kaveggia syndrome. Nat. Genet. 39:451–453.
Robinson, B. W., and D. S. Wilson. 1998. Optimal foraging, specialization, and a solution to Liem's paradox. Am. Nat. 151:223–235.
Rosenberg, M. S. 2002. Fiddler crab claw shape variation: A geometric morphometric analysis across the genus Uca (Crustacea: Brachyura: Ocypodidae). Biol. J. Linn. Soc. 75:147–162.

Rosenblum, E. B., C. E. Parent, and E. E. Brandt. 2014. The molecular basis of phenotypic convergence. Annu. Rev. Ecol. Evol. Syst. 45:203–226.
Rosenthal, G. G., and C. S. Evans. 1998. Female preference for swords in Xiphophorus helleri reflects a bias for large apparent size. Proc. Natl. Acad. Sci. U. S. A. 95:4431–4436.
Rosvall, K. A. 2013. Proximate perspectives on the evolution of female aggression: good for the gander, good for the goose? Philos. Trans. R. Soc. B Biol. Sci. 368:20130083.
Rowland, W. J. 1989. The effects of body size, aggression and nuptial coloration on competition for territories in male threespine sticklebacks, Gasterosteus aculeatus. Anim. Behav. 37:282–289.
Russello, M. A., M. D. Waterhouse, P. D. Etter, and E. A. Johnson. 2015. From promise to practice: pairing non-invasive sampling with genomics in conservation. PeerJ 3:e1106.
Sazima, I. 1983. Scale-eating in characoids and other fishes. Environ. Biol. Fishes 9:87–101.
Sazima, I., and F. A. Machado. 1990. Underwater observations of piranhas in western Brazil. Environ. Biol. Fishes 28:17–31.
Schindelin, J., I. Arganda-Carreras, E. Frise, V. Kaynig, M. Longair, T. Pietzsch, S. Preibisch, C. Rueden, S. Saalfeld, B. Schmid, J. Y. Tinevez, D. J. White, V. Hartenstein, K. Eliceiri, P. Tomancak, and A. Cardona. 2012. Fiji: An open-source platform for biological-image analysis. Nat. Methods 9:676–682.
Schluter, D. 1993. Adaptive radiation in sticklebacks: size, shape, and habitat use efficiency. Ecology 74:699–709.
Schluter, D. 1995. Adaptive Radiation in Sticklebacks: Trade-Offs in Feeding Performance and Growth. Ecology 76:82–90.
Schluter, D., E. A. Clifford, M. Nemethy, and J. S. McKinnon. 2004. Parallel Evolution and Inheritance of Quantitative Traits. Am. Nat. 163:809–822.
Schluter, D., and P. R. Grant. 1984. Determinants of morphological patterns in communities of Darwin's finches. Am. Nat. 123:175–196.
Sebé-Pedrós, A., E. Chomsky, K. Pang, D. Lara-Astiaso, F. Gaiti, Z. Mukamel, I. Amit, A. Hejnol, B. M. Degnan, and A. Tanay. 2018. Early metazoan cell type diversity and the evolution of multicellular gene regulation. Nat. Ecol. Evol. 2:1176–1188.
Seehausen, O. 2006. African cichlid fish: a model system in adaptive radiation research. Proc. R. Soc. B Biol. Sci. 273:1987–1998.
Sen, Ś., J. M. Satagopan, K. W. Broman, and G. A. Churchill. 2007. R/qtlDesign: Inbred line cross experimental design. Mamm. Genome 18:87–93.
Shah, N., M. G. Nute, T. Warnow, and M. Pop. 2019. Misunderstood parameter of NCBI BLAST impacts the correctness of bioinformatics workflows. Bioinformatics 35:1613–1614.
Shibuya, A., J. Zuanon, and M. R. de Carvalho. 2020. Neuromast distribution and its relevance to feeding in Neotropical freshwater stingrays (Elasmobranchii: Potamotrygonidae). Zoomorphology 139:61–69.
Shingleton, A. W., and W. A. Frankino. 2013. New perspectives on the evolution of exaggerated traits. BioEssays 35:100–107.
Shirley, M. D., H. Tang, C. J. Gallione, J. D. Baugher, L. P. Frelin, B. Cohen, P. E.

North, D. A. Marchuk, A. M. Comi, and J. Pevsner. 2013. Sturge–Weber Syndrome and Port-Wine Stains Caused by Somatic Mutation in GNAQ. N. Engl. J. Med. 368:1971–1979.
Sih, A., A. M. Bell, J. C. Johnson, and R. E. Ziemba. 2004. Behavioral Syndromes: An Integrative Overview. Q. Rev. Biol. 79:241–277.
Simmons, L. W., and J. L. Tomkins. 1996. Sexual selection and the allometry of earwig forceps. Evol. Ecol. 10:97–104.
Simpson, G. G. 1953. The Major Features of Evolution. Columbia University press, New York.
Slootweg, R. 1987. Prey selection by molluscivorous cichlids foraging on a schistosomiasis vector snail, Biomphalaria glabrata. Oecologia 74:193–202.
Sol, D., and L. Lefebvre. 2000. Behavioural flexibility predicts invasion success in birds introduced to New Zealand. Oikos 90:599–605.
Sommerfeld, N., and R. Holzman. 2019. The interaction between suction feeding performance and prey escape response determines feeding success in larval fish. J. Exp. Biol. 222:jeb204834.
St. John, M. E., K. Dixon, and C. H. Martin. 2020a. Oral shelling within an adaptive radiation of pupfishes: testing the adaptive function of novel nasal protrusion and behavioral preference. J. Fish Biol. 1–9.
St. John, M. E., R. Holzman, and C. H. Martin. 2020b. Rapid adaptive evolution of scale-eating kinematics to a novel ecological niche. J. Exp. Biol. jeb.217570.
St. John, M. E., J. A. McGirr, and C. H. Martin. 2019. The behavioral origins of novelty: did increased aggression lead to scale-eating in pupfishes? Behav. Ecol. 30:557–569.
Stayton, C. T. 2019. Performance in three shell functions predicts the phenotypic distribution of hard-shelled turtles. Evolution (N. Y). 73:720–734. John Wiley & Sons, Ltd (10.1111).
Stern, D. L. 2011. Evolution, Development, & the Predictable Genome. Roberts and Company Publishers, Greenwood Village, CO.
Stern, D. L. 2013. The genetic causes of convergent evolution. Nat. Rev. Genet. 14:751–764.
Stern, D. L., and V. Orgogozo. 2008. The loci of evolution: How predictable is genetic evolution? Evolution (N. Y). 62:2155–2177.
Stevenson, M. M. 1981. Karyomorphology of Several Species of Cyprinodon. Copeia 1981:494.
Strömberg, C. A. E. 2005. Decoupled taxonomic radiation and ecological expansion of open-habitat grasses in the Cenozoic of North America. Proc. Natl. Acad. Sci. U. S. A. 102:11980–11984.
Stuart, Y. E., T. Veen, J. N. Weber, D. Hanson, M. Ravinet, B. K. Lohman, C. J. Thompson, T. Tasneem, A. Doggett, R. Izen, N. Ahmed, R. D. H. Barrett, A. P. Hendry, C. L. Peichel, and D. I. Bolnick. 2017. Contrasting effects of environment and genetics generate a continuum of parallel evolution. Nat. Ecol. Evol. 1:0158.
Surget-Groba, Y. 2011. Lizards in an Evolutionary Tree: Ecology and Adaptive Radiation of Anoles. Amphibia-Reptilia 32:141–142. Berkeley.
Svanbäck, R., and D. I. Bolnick. 2005. Intraspecific competition affects the strength of individual specialization: An optimal diet theory method. Evol. Ecol. Res. 7:993–

1012.
Svanbäck, R., and D. I. Bolnick. 2007. Intraspecific competition drives increased resource use diversity within a natural population. Proc. R. Soc. B Biol. Sci. 274:839–844.
Svanbäck, R., P. C. Wainwright, and L. A. Ferry-Graham. 2002. Linking Cranial Kinematics, Buccal Pressure, and Suction Feeding Performance in Largemouth Bass. Physiol. Biochem. Zool. 75:532–543.
Takeuchi, Y., M. Hori, and Y. Oda. 2012. Lateralized kinematics of predation behavior in a Lake Tanganyika scale-eating cichlid fish. PLoS One 7:e29272.
Taylor, J., and D. Butler. 2017. R package ASMap: Efficient genetic linkage map construction and diagnosis. J. Stat. Softw., doi: 10.18637/jss.v079.i06.
Taylor, R. S., M. Manseau, R. L. Horn, S. Keobouasone, G. B. Golding, and P. J. Wilson. 2020. The role of introgression and ecotypic parallelism in delineating intraspecific conservation units. Mol. Ecol. 29:2793–2809. Blackwell Publishing Ltd.
Tebbich, S., K. Sterelny, and I. Teschke. 2010. The tale of the finch: Adaptive radiation and behavioural flexibility. Philos. Trans. R. Soc. B Biol. Sci. 365:1099–1109.
Teng, C. S., M. C. Ting, D. T. Farmer, M. Brockop, R. E. Maxson, and J. G. Crump. 2018. Altered bone growth dynamics prefigure craniosynostosis in a zebrafish model of Saethre-Chotzen syndrome. Elife 7:e37024.
The Gene Ontology Consortium. 2017. Expansion of the Gene Ontology knowledgebase and resources. Nucleic Acids Res. 45:D331–D338.
Therneau, T. M. 2016. A Package for Survival Analysis in S. version 2.38.
Thompson, K. A., M. M. Osmond, and D. Schluter. 2019. Parallel genetic evolution and speciation from standing variation. Evol. Lett. 3:129–141. Wiley.
Tinghitella, R. M., and M. Zuk. 2009. Asymmetric mating preferences accommodated the rapid evolutionary loss of a sexual signal. Evolution (N. Y). 63:2087–2098.
Tobler, M., J. L. Kelley, M. Plath, and R. Riesch. 2018. Extreme environments and the origins of biodiversity: Adaptation and speciation in sulphide spring fishes. Mol. Ecol. 27:843–859.
Tobler, M., R. Riesch, and M. Plath. 2015. Extremophile Fishes: An Integrative Synthesis. Pp. 279–296 *in* Extremophile Fishes. Springer International Publishing, Cham.
Trewavas, E. 1947. An Example of ‘Mimicry’ in Fishes. Nature 160:120–120.
Trivers, R. L. 1972. Parental investment and sexual selection. Cambridge, MA Biol. Lab. Harvard Univ. Vol. 136.
TURNER, B. J., D. D. DUVERNELL, T. M. BUNT, and M. G. BARTON. 2008. Reproductive isolation among endemic pupfishes (Cyprinodon) on San Salvador Island, Bahamas: microsatellite evidence. Biol. J. Linn. Soc. 95:566–582.
Tuttle, E. M. 2003. Alternative reproductive strategies in the white-throated sparrow: Behavioral and genetic evidence. Behav. Ecol. 14:425–432.
Van Wassenbergh, S., T. Lieben, A. Herrel, F. Huysentruyt, T. Geerinckx, D. Adriaens, and P. Aerts. 2008. Kinematics of benthic suction feeding in Callichthyidae and Mochokidae, with functional implications for the evolution of food scraping in catfishes. J. Exp. Biol. 212:116–125.
Vøllestad, L. A., and T. P. Quinn. 2003. Trade-off between growth rate and aggression in juvenile coho salmon, Oncorhynchus kisutch. Anim. Behav. 66:561–568.

Vranken, N., M. Van Steenberge, and J. Snoeks. 2019. Similar ecology, different morphology: Three new species of oral-mollusc shellers from Lake Edward. J. Fish Biol. jfb.14107.
Vulto-Van Silfhout, A. T., B. B. A. De Vries, B. W. M. Van Bon, A. Hoischen, M. Ruiterkamp-Versteeg, C. Gilissen, F. Gao, M. Van Zwam, C. L. Harteveld, A. J. Van Essen, B. C. J. Hamel, T. Kleefstra, M. A. A. P. Willemsen, H. G. Yntema, H. Van Bokhoven, H. G. Brunner, T. G. Boyer, and A. P. M. De Brouwer. 2013. Mutations in MED12 cause X-linked ohdo syndrome. Am. J. Hum. Genet. 92:401–406.
Wagner, G. P., J. P. Kenney-Hunt, M. Pavlicev, J. R. Peck, D. Waxman, and J. M. Cheverud. 2008. Pleiotropic scaling of gene effects and the 'cost of complexity.' Nature 452:470–472.
Wainwright, P. C. 1987. Biomechanical limits to ecological performance: mollusc-crushing by the Caribbean hogfish, Lachnolaimus maximus (Labridae). J. Zool. 213:283–297.
Wainwright, P. C. 1991. Ecomorphology: Experimental functional anatomy for ecological problems. Integr. Comp. Biol. 31:680–693.
Ward, A. J. W., and T. Mehner. 2010. Multimodal mixed messages: the use of multiple cues allows greater accuracy in social recognition and predator detection decisions in the mosquitofish, Gambusia holbrooki. Behav. Ecol. 21:1315–1320.
Werner, T. K., and T. W. Sherry. 1987. Behavioral feeding specialization in Pinaroloxias inornata, the "Darwin's Finch" of Cocos Island, Costa Rica. Proc. Natl. Acad. Sci. 84:5506–5510.
Whitford, M. D., G. A. Freymiller, T. E. Higham, and R. W. Clark. 2019. Determinants of predation success: How to survive an attack from a rattlesnake. Funct. Ecol. 33:1099–1109.
Wilson, A. D. M., and J. G. J. Godin. 2009. Boldness and behavioral syndromes in the bluegill sunfish, Lepomis macrochirus. Behav. Ecol. 20:231–237.
Winterbottom, R. 1974. The familial phylogeny of the Tetraodontiformes (Acanthopterygii: Pisces) as evidenced by their comparative myology. Smithson. Contrib. to Zool. 1–201.
Wittkopp, P. J., B. L. Williams, J. E. Selegue, and S. B. Carroll. 2003. Drosophila pigmentation evolution: Divergent genotypes underlying convergent phenotypes. Proc. Natl. Acad. Sci. 100:1808–1813.
Wood, S. N. 2011. Fast stable restricted maximum likelihood and marginal likelihood estimation of semiparametric generalized linear models. J. R. Stat. Soc. Ser. B Stat. Methodol. 73:3–36.
Wueringer, B. E., L. Squire, S. M. Kajiura, N. S. Hart, and S. P. Collin. 2012. The function of the sawfish's saw. Curr. Biol. 22:R150–R151.
Xie, K. T., G. Wang, A. C. Thompson, J. I. Wucherpfennig, T. E. Reimchen, A. D. C. MacColl, D. Schluter, M. A. Bell, K. M. Vasquez, and D. M. Kingsley. 2019. DNA fragility in the parallel evolution of pelvic reduction in stickleback fish. Science (80-.). 363:81–84.
Yang, J., N. A. Zaitlen, M. E. Goddard, P. M. Visscher, and A. L. Price. 2014. Advantages and pitfalls in the application of mixed-model association methods. Nat. Genet. 46:100–106.

Yu, J., G. Pressoir, W. H. Briggs, I. Vroh Bi, M. Yamasaki, J. F. Doebley, M. D. McMullen, B. S. Gaut, D. M. Nielsen, J. B. Holland, S. Kresovich, and E. S. Buckler. 2006. A unified mixed-model method for association mapping that accounts for multiple levels of relatedness. Nat. Genet. 38:203–208.

Zamani, N., P. Russell, H. Lantz, M. P. Hoeppner, J. R. Meadows, N. Vijay, E. Mauceli, F. di Palma, K. Lindblad-Toh, P. Jern, and M. G. Grabherr. 2013. Unsupervised genome-wide recognition of local relationship patterns. BMC Genomics 14:1–11.

Zuk, M., J. T. Rotenberry, and R. M. Tinghitella. 2006. Silent night: adaptive disappearance of a sexual signal in a parasitized population of field crickets. Biol. Lett. 2:521–524.